

**Prion infections and tauopathy in animal models:  
disease progression and proteolysis**

by

Ghazaleh Eskandari-Sedighi

A thesis submitted in partial fulfillment of the requirements for the degree of

Doctor of Philosophy

Department of Biochemistry

University of Alberta

© Ghazaleh Eskandari-Sedighi, 2020

# Abstract

Neurodegenerative diseases are a rising concern worldwide. Currently 10% of people aged 65 or more are diagnosed with a neurodegenerative disease and this number is predicted to triplicate by 2050. In developed societies approximately one percent of the global gross domestic product is allocated to the cost of care of affected patients. Aggregation and deposition of misfolded protein species is the common feature in almost all these diseases, hence the name protein misfolding diseases. With lack of any mechanism-based therapeutics, understanding the detailed molecular events contributing to disease pathogenesis is extremely important towards finding an efficient cure for these diseases.

Herein, I have applied biochemical techniques to study different aspects of protein misfolding diseases caused by two well-known proteins, tau and the cellular prion protein, in cell and animal models:

- 1) Using a transgenic animal model of tauopathy, I have analyzed the role of different conformations of misfolded protein species in disease pathogenesis and phenotypic heterogeneities observed amongst different patients.
- 2) I have investigated the molecular transition of scrapie prion protein in a prion disease mouse model. And I have assessed disease-associated symptoms at different timepoints to identify the misfolded protein species in charge of triggering pathogenesis.
- 3) I have investigated the cell and biochemical details of a proteolytic processing event that targets a mutant allele of the prion protein with higher tendency than the wildtype form, with the aim to validate this model as a reliable platform to study the enzymology of this processing event.

In summary, the projects discussed in this thesis entail biochemical analysis of disease pathogenesis in tauopathies and prion diseases, with a focus on the impact of proteolytic processing in health and disease conditions.

## Preface

The literature review in chapter 1 is my original work. Parts of chapter 1 are in press as Eskandari-Sedighi, G., Westaway, D. (2020) Murine models of tauopathies: a platform to study neurodegenerative diseases associated with aging. *Molecular Neurobiology of Aging Part 2*, Elsevier. This review was written by me and edited by DW.

A modified version of chapter 2 has been published as Eskandari-Sedighi, G., Daude, N., Yang, J., Gapesina, H., Sanders, D., Shi, B., Ghetti, B., Diamond, M.I., Janus, C., Westaway, D. (2017) The CNS in inbred transgenic models of 4-repeat tauopathy develops consistent tau seeding capacity yet focal and diverse patterns of protein deposition. *Molecular Neurodegeneration*. 12, 72. <https://doi.org/10.1186/s13024-017-0215-7>

A few experiments presented in chapter 2 is published at as Daude, N., Kim, C. Kang, S.G.\*, Eskandari-Sedighi, G.\*... Westaway, D. (2020) Diverse, evolving conformer populations drive distinct phenotypes in frontotemporal lobar degeneration caused by the same MAPT-P301L mutation. *Acta Neuropathologica*. <https://doi.org/10.1007/s00401-020-02148-4>. (\*co-second author). The LC/MS/MS analysis experiments were performed in Dr. Olivier Julien's lab with the help of Erik Gomez Cardona.

Chapter 3 in under review in journal of "*Molecular Neurobiology*" as Eskandari-Sedighi, G., Cortez, L., Yang, J., Daude, N., Shmeit, K., Sim, V., Westaway, D. (2020) Quaternary structure changes for PrP<sup>Sc</sup> predate PrP<sup>C</sup> down-regulation and neuronal death during progression of experimental scrapie disease. The asymmetric-flow field flow fractionation and RT-QuIC assays on the brain homogenates in this chapter were done by Dr. Leonardo Cortez.

All histology experiments were performed by Hristina Gapesina and Dr. Nathalie Daude.

The experiments presented in chapter 4 are all my original work, except for the capillary western blot analysis of my sample lysates which was performed by Dr. Andrew Castle.

The conclusive remarks discussed in chapter 5 is my original work.

All animal studies described herein were performed in accordance with Canadian Council on Animal Care (CCAC) guidelines, with specific protocols approved by the animal care use

committee for Health Sciences Laboratory Animal Services at the University of Alberta  
(protocols AUP00000356 and AUP00000357).

# **Dedication**

To my lovely parents.

For their unconditional love, and for giving me everything I needed to pursue my dreams

## Acknowledgements

I would like to start by thanking my dear supervisor, Dr. David Westaway, for all his help and support throughout my time in his lab. His patience, knowledge and caring makes him one of the best mentors I have ever had, and I could have not asked for a better supervisor for my PhD studies.

I am also thankful to my supervisory committee members Drs. Joanne Lemieux and Satyabrata Kar for their advice and stimulating discussions.

I would also like to thank all Westaway lab members: Charles Mays, Robert C.C Mercer, Kerry Ko, Hristina Gapeshtina, Stephanie Brown (past members), Serene Wohlgemuth, Jing Yang, Nathalie Daude, Andrew Castle, Sangyung Kang, Zelin Fu, Luis Arce and George Han. Their continuous help and support, as well as their precious friendship was a great source of joy and happiness for me.

The Centre for Prions and Protein Folding is a great environment in which I had the privilege of enhancing both my scientific and social skills. For this I am grateful to all primary investigators in this center, Drs. Debbie McKenzie, Sue-Ann Mok, Valerie Sim, Satyabrata Kar, Holger Wille, Judd Aiken and Ted Allison as well as their group members, especially my dear friends Maria Carmen Garza-Garcia, Ilaria Vanni (past members), Leonardo Cortez, Klinton Shmeit, Andrew Schmaus, Razieh Kamali-Jamil and Sara Amidian for their help and support, as well as their valuable friendship throughout the years.

I would like to thank all Department of Biochemistry past and present members, especially Olivier Julien and Erik Gomez for the tremendous amount of help and support they provided me with for the mass spectrometry experiments in my projects. I would also like to thank Dr. David Stuart for his continuous help and support as the graduate program coordinator and, Dr. Charles Holmes as the department chair for putting up such great environment for trainees. Lastly, I cannot thank enough the amazing graduate program advisors throughout the years I have been a student Ms. Kimberly Arndt, Ms. Kelsey Robertson and Ms. Lisa Dublin.

Lastly, I want to acknowledge my lovely family; my mom and dad who always supported me to pursue my dreams. I greatly appreciate all they have done for me and hope I can be as great as

them as a parent. I also thank my dear husband Mohammad Hossein for being the most supporting and understanding companion I could have asked for. I have been a graduate student ever since we started our relationship, and he has never been anything but helpful. And the newest member of my family, my sweet little girl Niki Rose who has brought charm and joy into our lives.

# Table of Contents

Abstract .....	ii
Preface .....	iv
Dedication .....	vi
Acknowledgements .....	vii
Table of Contents .....	ix
List of Figures .....	xv
List of Tables.....	xviii
List of Abbreviations .....	xix
<b>Chapter 1: Introduction</b> .....	<b>1</b>
1.1 Biochemistry of protein misfolding.....	2
1.2 Protein misfolding and neurodegeneration .....	2
1.2.1 The replication and spreading of misfolded protein aggregates.....	3
1.2.1.1 Templated assembly model.....	4
1.2.1.2 Monomer-directed conversion (heterodimer model).....	4
1.2.1.3 Non-catalytic nucleated polymerization model.....	5
1.2.1.4 Nucleated conformational conversion model .....	5
1.3 Mechanism(s) of neurotoxicity of misfolded protein species: .....	8
1.3.1 Inflammation and microgliosis: .....	8
1.3.2 The unfolded protein response (UPR):.....	9
1.3.3 Autophagy and mitophagy.....	11
1.3.4 Other mechanisms: .....	13
1.3.4.2 Disruption of cellular/axonal transport:.....	13
1.3.4.3 Formation of pores in the plasma membrane:.....	14

1.4 Studying neurodegenerative diseases: the impact of animal models.....	14
1.4.1 Assessment of neurodegeneration in animal models .....	17
1.5 Tau and tauopathies .....	19
1.5.1 Tau, from gene to protein .....	19
1.5.2 Post translational modifications (PTMs) of tau protein .....	22
1.5.3 Tau protein in neurodegenerative diseases .....	24
1.5.4 Animal models of tauopathies .....	25
1.6 PrP <sup>C</sup> and prion diseases.....	27
1.6.1 PrP <sup>C</sup> , from gene to protein .....	27
1.7 The “strain” phenomenon in prion diseases .....	31
1.8 The “prion” concept in other proteinopathies .....	31
1.8.1 Formation of amyloid fibrils:.....	32
1.8.2 Generation of protease resistant aggregates: .....	32
1.8.3 Presence of different conformers (strains) of misfolded protein species: .....	33
1.8.4 Phenotypic diversity:.....	33
1.8.5 Seeding and spreading of the misfolded proteins throughout the CNS: .....	33
1.9 Role of proteolytic processing in protein misfolding diseases.....	34
1.9.1 Proteolytic processing of tau protein in health and disease .....	34
1.9.2 Proteolytic processing of PrP <sup>C</sup> in health and disease .....	37
1.10 Thesis objectives and goals: .....	41
<b>Chapter 2: The CNS in inbred transgenic models of 4-repeat Tauopathy develops</b>	
<b>consistent Tau seeding capacity yet focal and diverse patterns of protein deposition .....</b>	<b>42</b>
2.1 Introduction .....	43
2.2 Experimental Procedures .....	45
2.2.1 Animals.....	45

2.2.2 Genotyping and genome-wide analysis of SNPs .....	46
2.2.3 Evaluation of disease-related symptoms in aged mice.....	46
2.2.4 Quantification of phosphorylated and total Tau protein.....	47
2.2.5 Extraction of phosphorylated Tau protein .....	47
2.2.6 Western blots .....	48
2.2.7 Trypsin digestion of sarkosyl-insoluble Tau extracts.....	49
2.2.8 Immunohistochemistry:.....	49
2.2.9 Homogenate and lysate preparation: .....	50
2.2.10 Negative stain electron microscopy: .....	50
2.2.11 Cell culture:.....	51
2.2.12 Transduction of homogenates into Clone 1 cells: .....	51
2.2.13 Confocal analysis of seeded Clone 1 cells:.....	51
2.2.14 Data analysis .....	52
2.2.15 Trypsin digestion of sarkosyl-insoluble Tau extracts and in-gel analysis:.....	52
2.2.16 Mass spectrometry:.....	53
2.2.17 Dephosphorylation of phospho-tau by lambda phosphor-protein phosphatase (lambda PP):.....	54
2.3 RESULTS .....	54
2.3.1 Genetic profiles and Tau expression in sublines of TgTau <sup>P301L</sup> mice. ....	54
2.3.2 Neurologic symptoms and Tau species in aged Tg mice. ....	58
2.3.3 Quantification of neuronal loss in aged TgTau <sup>P301L</sup> mice. ....	61
2.3.4 Heterogeneity in Tau pathologies. ....	64
2.3.5 Variable Tau pathology versus transgene expression effects. ....	90
2.3.6 Biochemical analyses of Tau species in Different Pathology Classes. ....	93
2.3.7 Electron microscopic analysis of Tau filaments. ....	100

2.3.8 Seeding activity in brains from aged Tau <sup>P301L</sup> mice.....	100
2.3.9 Presence of a 25 kDa fragment in the soluble fraction of TgTau <sup>P301L</sup> mice suggest potential cleavage of tau by calpain.....	106
2.4 DISCUSSION.....	109
2.4.1 Phenotypic variation and classes in P301L Tauopathy. ....	109
2.4.2 Signatures of uniform expression and protein misfolding in TgTau <sup>P301L</sup> mice. ....	109
2.4.3 Tau proteolysis, classes of Pathology and Tau spreading. ....	111
2.4.4 Pathological heterogeneity and Tau strains. ....	112
2.4.5 Origins of variegated Tau pathology in inbred mice.....	114
2.6 CONCLUSIONS. ....	116
<b>Chapter 3: Quaternary structure changes for PrP<sup>Sc</sup> predate PrP<sup>C</sup> down-regulation and neuronal death during progression of experimental scrapie disease .....</b>	<b>117</b>
3.1 Introduction. ....	118
3.2 Experimental procedures.....	119
3.2.1 Animals:.....	119
3.2.2 Brain homogenization: .....	119
3.2.3 Quantification of brain cells using Isotropic fractionator:.....	120
3.2.4 Immunohistochemistry: .....	121
3.2.5 Western Blotting: .....	121
3.2.6 Data Analysis: .....	121
3.2.7 Proteinase-K digestion:.....	122
3.2.8 Asymmetric Flow field-flow fractionation (AF4):.....	122
3.2.9 Expression and Purification of mouse PrP: .....	123
3.2.10 Real-time quaking-induced conversion (RT-QuIC) assay: .....	124
3.3 Results:.....	124

3.3.1 Quantitative and qualitative changes in brain cell populations during the course of infection with the RML scrapie prion isolate. ....	124
3.3.2 Pathological changes in the brain can be detected at 90 DPI, close to the appearance of clinical symptoms .....	127
3.3.3 Molecular transitions of PrP: decrease at PrP <sup>C</sup> levels and presence of high-molecular-weight species at early stages of the disease .....	132
3.3.4 Polymeric assemblies of PrP have distinct protease resistance characteristics .....	137
3.4 Discussion: .....	140
3.4.1 Downregulation of the cellular prion protein precedes neuronal loss.....	140
3.4.2 Molecular transition of prion protein and formation of prion assemblies is initiated at early stages of the disease .....	141
<b>Chapter 4: Cell and molecular studies on proteolytic processing of an octarepeat mutant allele of prion protein with increased C2 fragmentation, PrPS3 .....</b>	<b>143</b>
4.1 Introduction .....	144
4.2 Experimental Procedures .....	148
4.2.1 Cell Culture.....	148
4.2.2 Cell treatment with Cyclohexamide .....	148
4.2.3 Cell treatment with lysosomotropic agents (ammonium chloride and chloroquine) ..	148
4.2.4 Acridine Orange assay .....	149
4.2.5 Cell treatment with thapsigargin .....	149
4.2.6 Plasmid constructs.....	149
4.2.7 Cell conditioned media preparation .....	150
4.2.8 <i>In vitro</i> proteolysis of recombinant PrPS3.....	150
4.2.9 De-glycosylation of prion protein by PNGase-F .....	151
4.2.10 Western blotting .....	151
4.2.11 Capillary western blotting (WES) .....	151

4.3 Results .....	152
4.3.1 Fragments of prion protein have different half-lives .....	152
4.3.2 C2-fragmentation of PrPS3 can be inhibited by protease inhibitors <i>in vitro</i> .....	155
4.3.3 Inhibition of lysosomal proteolysis does not have an impact on C2-fragmentation of PrPS3.....	157
4.3.4 Induction of endoplasmic reticulum-stress does not affect C2-fragmentation.....	157
4.3.5 Absence of GPI-anchor affects both C1 and C2 fragmentation of both prion protein alleles, PrP <sup>Wt</sup> and PrPS3 .....	160
4.4 Discussion .....	162
<b>Chapter 5: Conclusions and Future directions.....</b>	<b>164</b>
5.1 Generation and validation of <i>in vivo</i> and <i>ex vivo</i> models for studying protein misfolding diseases .....	165
5.2 Distinct conformers of tau in FTLD- <i>MAPT</i> animal model.....	165
5.2.2 Tau fragmentation and aggregation: the cause or a side effect?.....	167
5.3 Molecular evolution of PrP <sup>Sc</sup> during prion disease progression.....	168
5.4 PrPS3 as a model to study proteolytic processing of cellular prion protein (PrP <sup>C</sup> ) .....	169
5.4.1 The importance of PrP <sup>C</sup> proteolytic processing in prion diseases .....	169
<b>Cumulative Bibliography .....</b>	<b>171</b>

## List of Figures

Figure 1-1. Four major kinetic models of misfolded protein replication .....	7
Figure 1-2. A schematic representing pathways that are activated upon initiation of UPR and the final outcome for each pathway.....	11
Figure 1-3. A spectrum representing reductionism-based and holism-based models in biology..	16
Figure 1-4. Tau from gene to protein.....	21
Figure 1-5. A schematic of phosphorylation sites on 2N4R tau protein.....	23
Figure 1-6. PrP <sup>C</sup> from gene to protein.....	28
Figure 1-7. A schematic of PrP <sup>C</sup> presenting different regions within the molecule.....	30
Figure 1-8. A schematic of proteolytic processing of PrP <sup>C</sup> . The cleavage site and subsequent fragments generated for each cleavage are presented.....	40
Figure 2-1. Total human Tau and total phosphorylated Tau in 3 congenic strains of TgTauP301L mice.....	57
Figure 2-2. Presence of phosphorylated Tau species in fractioned brain of 90- and 240-days old mice from 3 genetic backgrounds.....	59
Figure 2-3. Appearance of disease-associated symptoms in TgTauP301L mice three genetic backgrounds.....	60
Figure 2-4. Quantification of neurons in whole brain of aged TgTauP301L and non-Tg littermate mice.....	63
Figure 2-5. Class I Tau pathology.....	67
Figure 2-6. Class II Tau pathology.....	68
Figure 2-7. Class III Tau pathology.....	69
Figure 2-8. Class IV Tau pathology.....	70
Figure 2-9. Class V Tau pathology.....	71
Figure 2-10. Focal staining in aged TgTauP301L mice.....	72
Figure 2-11. MC1 staining in class I mice.....	73
Figure 2-12. CP27 staining in class I mice.....	74
Figure 2-13. RZ3 staining in class I mice.....	75
Figure 2-14. PHF1 staining in class I mice.....	76

Figure 2-15. MC1 staining in Class II mice. ....	77
Figure 2-16. CP27 staining in class II mice. ....	78
Figure 2-17. RZ3 staining in class II mice. ....	79
Figure 2-18. PHF1 staining in class II mice. ....	80
Figure 2-19. MC1 staining in class III mice. ....	81
Figure 2-20. CP27 staining in class III mice. ....	82
Figure 2-21. RZ3 staining in class III mice. ....	83
Figure 2-22. PHF1 staining in Class III mice. ....	84
Figure 2-23. MC1 staining in class IV mice. ....	85
Figure 2-24. CP27 staining in class IV mice. ....	86
Figure 2-25. RZ3 staining in class IV mice. ....	87
Figure 2-26. PHF1 staining in class IV mice. ....	88
Figure 2-27. CP27, RZ3 and PHF1 staining in class V mice. ....	89
Figure 2-28. Transgene-encoded human Tau is not expressed in a focal pattern in areas subject to focal staining in aged mice. ....	91
Figure 2-29. Presence of Tau protein in aged Tg animals with negative pathology. ....	92
Figure 2-30. Insoluble Tau species in the brains of aged TgTauP301L mice. ....	94
Figure 2-31. Pathology in aged Tg mice assessed for insoluble Tau species. ....	95
Figure 2-32. Undigested P3 fraction assessed with CP13 and PHF1 antibodies. ....	96
Figure 2-33. Trypsin-resistance of sarkosyl-insoluble Tau fractions. ....	98
Figure 2-34. The protein sequence of trypsin-resistant core of TgTauP301L mice identified by LC/MS/MS. ....	99
Figure 2-35. Negative stain electron microscopy of insoluble Tau fractions. ....	102
Figure 2-36. Clones used for fluorescence microscopy assays. ....	104
Figure 2-37. Assessment of Tau strains in a cell-based seeding assay. ....	105
Figure 2-38. The 25 kDa fragment in the soluble fraction of TgTauP301L mice. ....	107
Figure 2-39. In-gel digestion and LC/MS/MS of the 25 kDa fragment in SUP1 of TgTauP301L mice. ....	108
Figure 3-1. Quantification of brain cells by isotropic fractionator ....	126
Figure 3-2. H and E staining of brain sections from RML and NBH inoculated animals at different timepoints during disease progression. ....	128

Figure 3-3. PrP <sup>Sc</sup> immunostaining of brain sections from RML and NBH inoculated animals at different timepoints .....	129
Figure 3-4. GFAP immunostaining of brain slices from RML and NBH inoculated animals ....	130
Figure 3-5. Assessment of inflammatory and synaptic health markers' changes at different timepoints during disease progression. ....	131
Figure 3-6. PrP <sup>C</sup> levels in brain homogenate of RML-inoculated animals at different timepoints .....	134
Figure 3-7. AF4 analysis of solubilized brain homogenate of RML-infected animals at different timepoints during disease progression. ....	135
Figure 3-8. PK-resistant PrP <sup>Sc</sup> in fractionated brain of RML-inoculated animals at different timepoints .....	138
Figure 3-9. Seeding activity of total brain homogenate of RML-inoculated animals at different timepoints .....	139
Figure 4-1. A schematic of different major fragmentation events that target PrP <sup>C</sup> with generated fragments. ....	147
Figure 4-2. Cyclohexamide (CHX) treatment of cells expressing PrPWt or PrPS3 .....	154
Figure 4-3. Inhibition of C2-fragmentation of recPrPS3 by cell lysate by addition of protease inhibitors in vitro.....	156
Figure 4-4. Incubating RK13 cells expressing PrPWt or PrPS3 with lysomotropic agents did not have any impact on C1 or C2 fragmentation. ....	158
Figure 4-5. Induction of ER stress with thapsigargin did not affect C1 or C2 fragmentation in PrPWt or PrPS3 expressing cells. ....	159
Figure 4-6. Absence of GPI anchor impacts C1 and C2 fragmentation of both PrPWt and PrPS3 alleles.....	161

## List of Tables

Table 1-1 A list of some identified proteolysis events that tau protein can go through. ....	36
Table 2-1. Single Nucleotide Polymorphism (SNP) profiling of congenic and incipient congenic lines. ....	56
Table 2-2. Pathology classes were based upon the location of AT8 antibody immunostaining. ..	66
Table 2-3. Categorization of individual Tau filaments according to pathology classification and genetic background. ....	103
Table 3-1. Full-length PrP molecules per oligomer as a function of $R_H$ .....	136

## List of Abbreviations

**A $\beta$** : Amyloid beta protein

**AD**: Alzheimer's disease

**Chr**: Chromosome

**CNS**: Central nervous system

**FL**: Full length protein

**FTLD-*MAPT***: Frontotemporal lobar degeneration associated with *MAPT* gene

**GFTs**: gliofibrillary tangles (deposits of tau protein formed in glial cells rather than neurons)

**H-tau**: Human tau protein

**LC/MS/MS** : Liquid chromatography-mass spectrometry

**MAPT**: Microtubule associated protein tau

***MAPT***: Tau gene

**MT**: Microtubule protein

**NBH**: Normal brain homogenate

**NFTs**: Neurofibrillary tangles

**OR**: Octapeptide repeat region of the prion protein

**PHF**: Paired helical filaments

**PK**: Proteinase K

**PrP**: Prion protein

**PrP<sup>C</sup>**: Cellular prion protein

**PrP<sup>Sc</sup>**: Scrapie prion protein (a term used for the misfolded, infectious prion protein)

**PrP<sup>res</sup>**: PK-resistant prion protein

**PrPWt:** The Wt form of cellular prion protein

**PrPS3:** A mutant allele of PrP, with amino acid substitutions in the octapeptide repeat region

**PTMs:** Post translational modifications

**p-Tau:** Phosphorylated tau

**RD:** tau repeat domain

**RML:** Rocky Mountain lab strain (a mouse-adapted ovine scrapie prion strain)

**Tg:** Transgenic

**TgTau<sup>P301L</sup>:** transgenic mice expressing longest form of h-tau protein with P301L mutation.

**UPR:** Unfolded protein response

**WT/Wt:** Wild type

**YFP:** Yellow fluorescent protein

# **Chapter 1: Introduction**

## **1.1 Biochemistry of protein misfolding**

There are an estimated 20,000-25,000 protein-coding genes identified in the human genome (Piovesan, Antonaros et al. 2019). This is while human proteome consists of approximately 100,000 proteins, some of which with functions that have yet to be identified (Wang, Li et al. 2006).

Proteins are involved in almost all events critical to an organism's survival: catalysis of reactions, structural subunits of the organism (from individual cells, to tissue and organs) and replication of genetic information, are just a few examples of fundamental functions of proteins. The fact that such variety of functions can be delivered by polymers made up of only 20 residues relies heavily on the 3-dimensional structure of these molecules. The process through which a protein obtains the proper "conformation", which enables it to perform a very specific task is called "protein folding" (Dobson 2003). Proper folding is such a crucial aspect of an organism's survival that there are several control systems specifically assigned for its maintenance. It is thus not surprising that defective protein folding may induce huge catastrophic consequences which are manifested in various human diseases (Araki and Nagata 2011, Xu and Ng 2015).

Protein misfolding can often result in two scenarios: a misfolded protein can lose its original function, and the loss of function will then cause disease-associated complexities. Some examples include diseases such as cystic fibrosis and cancers caused due to unmasking of recessive oncogene mutations. Under some circumstances though, apart from the loss of function, there is a "gain of function" for the misfolded protein. In these cases, the unnatural conformation can have toxic effects on the system that then results in cell death and disease development. Protein misfolding diseases of the central nervous system (CNS), also known as neurodegenerative diseases are considered one of the unfortunate outcomes of protein misfolding events in the brain (Winklhofer, Tatzelt et al. 2008).

## **1.2 Protein misfolding and neurodegeneration**

Neurodegenerative diseases are a rising issue worldwide, especially in developed societies where they are amongst the most expensive health issues affecting a vast percentage of population

(Hardy 1999, Iqbal, Liu et al. 2016). A common feature in most of these diseases is the aggregation and deposition of misfolded protein species in brain, followed by pathological consequences including cognitive decline and dementia (Taylor, Hardy et al. 2002, Ross and Poirier 2004). Currently, there are several proteins that can undergo misfolding and aggregation, followed by disease development and neurodegeneration in humans. Amyloid-beta ( $A\beta$ ), tau, the cellular prion protein ( $PrP^C$ ) and alpha-synuclein are a few examples.

None of these proteins share any obvious similarities in terms of sequence, size, structure, expression level, or function. However, they all have one common feature regarding their role in neurodegenerative diseases: misfolding from their native states to form intermolecular  $\beta$ -sheet-rich structures known as “amyloids”, ranging from small oligomers to large fibrillar aggregates. Amyloids are defined as highly ordered aggregates of protein, 100–200 Å in diameter, with consistent X-ray diffraction pattern and high affinity for certain dyes such as Congo red or thioflavin (Soto and Pritzkow 2018). Initially, large aggregated deposits were thought to be the most neurotoxic species in the brain, but further studies indicated that small and soluble oligomers are the most toxic assemblies in most neurodegenerative diseases. But the molecular structure responsible for the toxicity of amyloid and amyloid intermediates is not fully understood yet. (Jucker and Walker 2013, Kraus, Groveman et al. 2013).

### **1.2.1 The replication and spreading of misfolded protein aggregates**

In early stages of the protein misfolding diseases, the pathological changes, including aggregated protein accumulation and neurological dysfunctions are restricted to confined regions of the nervous system. However, as the disease progresses such alterations spread throughout the CNS, suggesting the presence of a spreading mechanism for misfolded protein species (Polymenidou and Cleveland 2012). There are four major kinetic models that have been developed to explain the mechanism of misfolded protein aggregates' replication and spreading: 1) The templated assembly model; 2) The monomer-directed conversion model, 3) The non-catalytic nucleated polymerization model and 4) The nucleated conformational conversion model (**Fig 1.1**) (Stroylova, Kiselev et al. 2014). These models are fundamentally different in the role that they propose for pre-existing polymers of the misfolded protein species in the process of converting

the folded monomeric forms (Serio, Cashikar et al. 2000). The mechanisms proposed in these models were mostly developed to explain prion replication, but they can be expanded to the replication and spreading of other prion-like proteins (Polymenidou and Cleveland 2012).

### **1.2.1.1 Templated assembly model**

According to the “templated assembly model”, the misfolded protein complexes present in the system act as templates for conformational conversion of the native, folded proteins. In this model, the conversion of native or partially unfolded protein to the misfolded form is considered the rate-limiting step which is enhanced by the presence of pre-existing polymeric misfolded species acting as the template and, the energy barrier for conversion is lowered through an interaction between “misfolded” and “native” protein. According to this model, the assembly of misfolded protein is a consequence, not a cause of conversion (Serio, Cashikar et al. 2000, Polymenidou and Cleveland 2012, Stroylova, Kiselev et al. 2014).

### **1.2.1.2 Monomer-directed conversion (heterodimer model)**

The heterodimer model postulates that instead of the polymeric assembly of misfolded protein, a single monomer acts as the template. Herein, the monomeric misfolded protein binds to the native partially unfolded protein in the solution, forming a heterodimer. The misfolded monomer then guides the folding of the partially unfolded protein to the amyloid state. After this interaction, the newly formed misfolded protein may act as a catalyst of more native monomers refolding into the infectious form (Serio, Cashikar et al. 2000). According to this hypothesis, a high activation energy barrier does not usually allow this process to occur spontaneously with any significant rate. But the formation of the heterodimeric complex decreases the activation energy on the way towards the formation of new misfolded protein, thus increasing the rate of conversion (Serio, Cashikar et al. 2000, Stroylova, Kiselev et al. 2014).

### **1.2.1.3 Non-catalytic nucleated polymerization model**

According to the “non-catalytic nucleated polymerization model” the transition between native protein and misfolded one is a reversible thermodynamically driven equilibrium, but with a strong shift towards the formation of the folded form. The less stable misfolded form can be stabilized through forming structurally ordered aggregates. The appearance of such assembly in the environment initiates the process of recruiting the new forming misfolded monomers to the growing fibril; and all these in turn shifts the equilibrium towards the formation of more misfolded proteins. Thus, in the framework of this hypothesis, the process of protein misfolding consists of a slow and thermodynamically unfavorable nucleation phase through which stable seed or nucleus of polymerized protein aggregates are formed, followed by a rapid elongation stage where seeds grow by incorporating monomeric proteins into the polymer (Jarrett and Lansbury Jr 1993, Soto and Pritzkow 2018). The large polymers of misfolded protein could fragment and generate new seeds, and this would accelerate the propagation of misfolded aggregates (Jarrett and Lansbury Jr 1993, Jucker and Walker 2013, Soto and Pritzkow 2018).

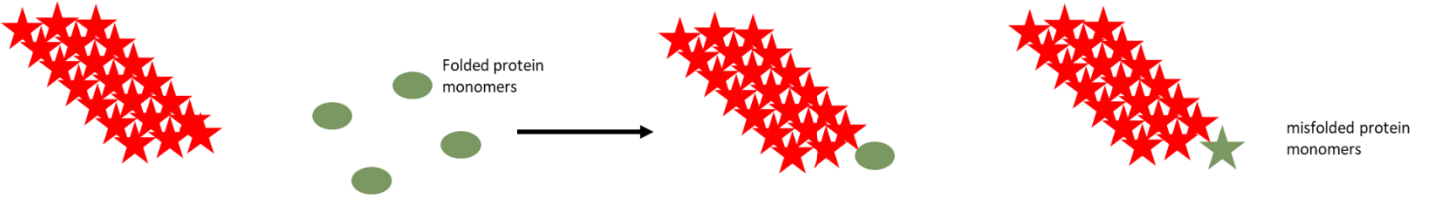
### **1.2.1.4 Nucleated conformational conversion model**

According to the “nucleated conformational conversion model”, the stable superstructure of the misfolded protein aggregates is achieved through formation of an intermediate assembly of structurally flexible oligomers. The oligomeric species then act as a growing unit for the formation of stable misfolded fibrils, forming amyloid nuclei inside their irregular structure (in the case of the sporadic forms of the disease), or by interacting with the already preformed amyloid structures (Kelly 2000, Bhak, Choe et al. 2009).

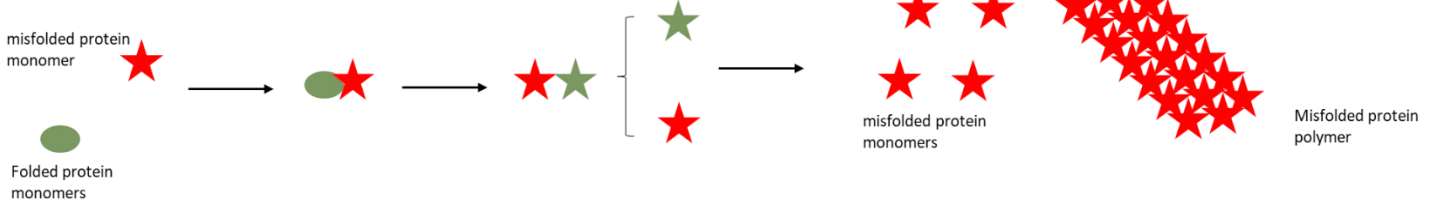
From a biophysical perspective, the process of protein misfolding and aggregation involves re-arrangement of the structure of the native protein into a series of  $\beta$ -strands which are stabilized by hydrogen bonding and hydrophobic interactions (Jarrett and Lansbury Jr 1993, Kraus, Groveman et al. 2013, Soto and Pritzkow 2018). Although the primary scaffold of the

misfolded aggregates is similar, the individual molecules can adopt many quite varied structures, which give rise to the possibility of conformational strains, as discussed in upcoming sections (Serio, Cashikar et al. 2000, Bhak, Choe et al. 2009, Polymenidou and Cleveland 2012).

### Templated assembly model



### Monomer-directed conversion (heterodimer) model



### Non-catalytic nucleated polymerization model



### Nucleated conformational conversion model

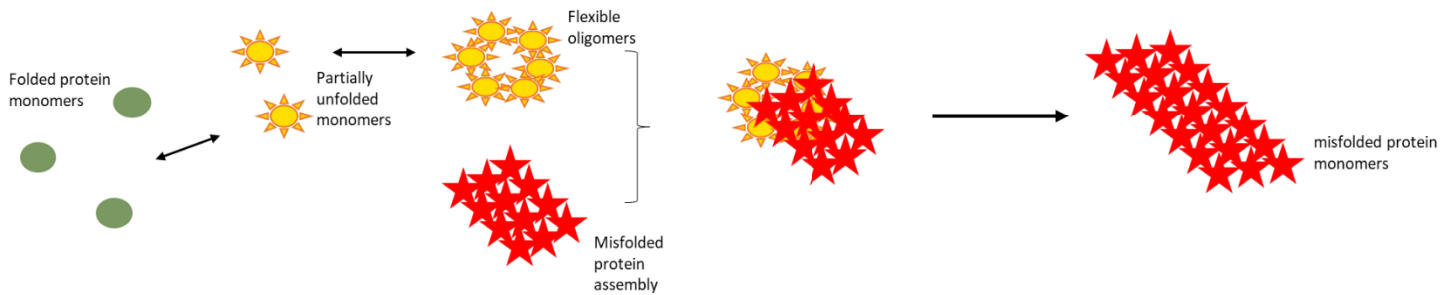


**Figure 1-1. Four major kinetic models of misfolded protein replication**

The templated assembly model, the monomer-directed conversion model, the non-catalytic nucleated polymerization model and, the nucleated conformational conversion model. These models are fundamentally different in the role that they propose for pre-existing polymers of the misfolded protein species in the process of converting the folded monomeric forms

### **1.3 Mechanism(s) of neurotoxicity of misfolded protein species:**

Although results obtained from numerous studies indicate that misfolded protein aggregates are toxic to neurons *in vitro* and *in vivo*, the molecular mechanism through which they induce their toxicity is not well established. This is partially due to the fact that the population of aggregated and misfolded proteins are usually very heterogenous and misfolded proteins can exist in several distinct forms with different features and characteristics. Amorphous aggregates, detergent soluble oligomers and detergent insoluble fibrils are just a few examples of different forms of misfolded protein that can co-exist at the same time, and they can each induce neurotoxicity in their own unique ways.

#### **1.3.1 Inflammation and microgliosis:**

Microglia and astrocytes are the main effector cells of the innate immune response in the CNS, and they are strongly activated during disease progression in various neurodegenerative diseases, producing an array of inflammatory mediators and fulfilling phagocytic functions. Several factors could contribute to inflammation in neurodegenerative disorders: accumulation of protein aggregate species, molecules released from or associated with injured neurons or synapses, and dysregulation of inflammatory control mechanisms. The resulting inflammatory responses may modulate neurodegenerative pathways in either a beneficial or a deleterious fashion. Given the multiple functions of inflammatory factors, such as cytokines and chemokines, it is often difficult to determine their roles in specific pathophysiological situations. The fact that neurons carry receptors for many cytokines and chemokines, suggest an active crosstalk between the immune and nervous system in health and disease (Wyss-Coray and Mucke 2002).

Several studies in transgenic mouse models of CNS diseases suggest that altered expression of specific inflammatory factors may trigger or enhance the development of neurodegenerative disease. For example, astroglial overexpression of TNF- $\alpha$ , interferon- $\alpha$ , or interleukin-6 resulted in neurodegeneration, gliosis, and progressive neurological disease (Campbell, Abraham et al. 1993). Development of more severe pathological phenotypes in TNF- $\alpha$  transgenic mice that lacked mature T or B lymphocytes, suggest that microglia/macrophages are responsible for the

pathogenic inflammatory process (Stalder, Carson et al. 1998). However, other reports suggest that the network of the CNS and the immune system is more complicated than this and it is not a one-to-one interaction. As an example, a study on the impact of depleted immune system on brain health show that transgenic mice lacking TNF- $\alpha$  receptors are more susceptible to ischemia and excitotoxic injury, underlining how difficult it might be to predict the outcome of therapeutic manipulations aimed at these molecules (Bruce, Boling et al. 1996, Sullivan, Bruce-Keller et al. 1999, Wyss-Coray and Mucke 2002).

Despite all the ambiguities, it is well established that inflammation and gliosis play a critical role in neurodegenerative diseases. However, to tackle down the mechanistic details of this phenomenon, more research is required.

### **1.3.2 The unfolded protein response (UPR):**

In the dynamic environment of a cell, the homeostasis of proteins -also known as “proteostasis”- is critical and highly regulated. This process consists of dynamic coordination of efficient folding of newly synthesized proteins, as well as regulation of degradative mechanisms to reduce the load of unfolded and misfolded proteins and prevent accumulation of abnormal protein aggregates (Hetz and Mollereau 2014). Under conditions of cellular and endoplasmic reticulum (ER) stress, such as rising levels of misfolded proteins and, in an attempt to restore proteostasis, cells activate a dynamic signaling network known as the unfolded protein response (UPR). From a molecular perspective, the UPR could be summarized as a signal transduction pathway that involves two main components: 1) stress sensors at the ER membrane, and 2) downstream transcription factors that re-program gene expression toward stress mitigation or the induction of apoptosis. These target genes could vary depending on the tissue context and the type of physiological perturbation that causes the ER stress (Hetz and Saxena 2017). The cascade of events that occur upon UPR activation include: a) production of chaperone proteins to prevent protein aggregation and facilitate correct protein folding, b) temporary reduction of protein translation to lower the amount of proteins present in the ER, c) stimulation of lipid synthesis to increase ER volume, and d) induction of unfolded proteins degradation by activating the

endoplasmic reticulum-associated protein degradation (ERAD) pathway (Halliday and Mallucci 2014, Hetz and Saxena 2017). **Fig 1.2** summarizes the key role players of UPR, and the cascade of events triggered by them. Activation of UPR has been associated with several neurodegenerative diseases including, but not limited to, AD, Parkinson's disease (PD), Huntington's disease and prion diseases (Halliday and Mallucci 2014, Hetz and Mollereau 2014, Hetz and Saxena 2017). This wide range of consistency suggests a central and conserved role for ER stress in the pathogenic neuronal response. Despite the initial protective and adaptive nature of downstream pathways of UPR, long-term ER stress over-rides the adaptive responses and can induce apoptosis, which eventually causes neuronal loss. Moreover, chronic inhibition of protein synthesis has a negative impact on synaptic health and, thus, would result in synaptic dysfunction and axonal degeneration. It is hence fair to suggest that UPR can have very different outputs regarding cell-fate, depending on which pathways are initiated and how long they remain activated (Hetz and Papa 2018).

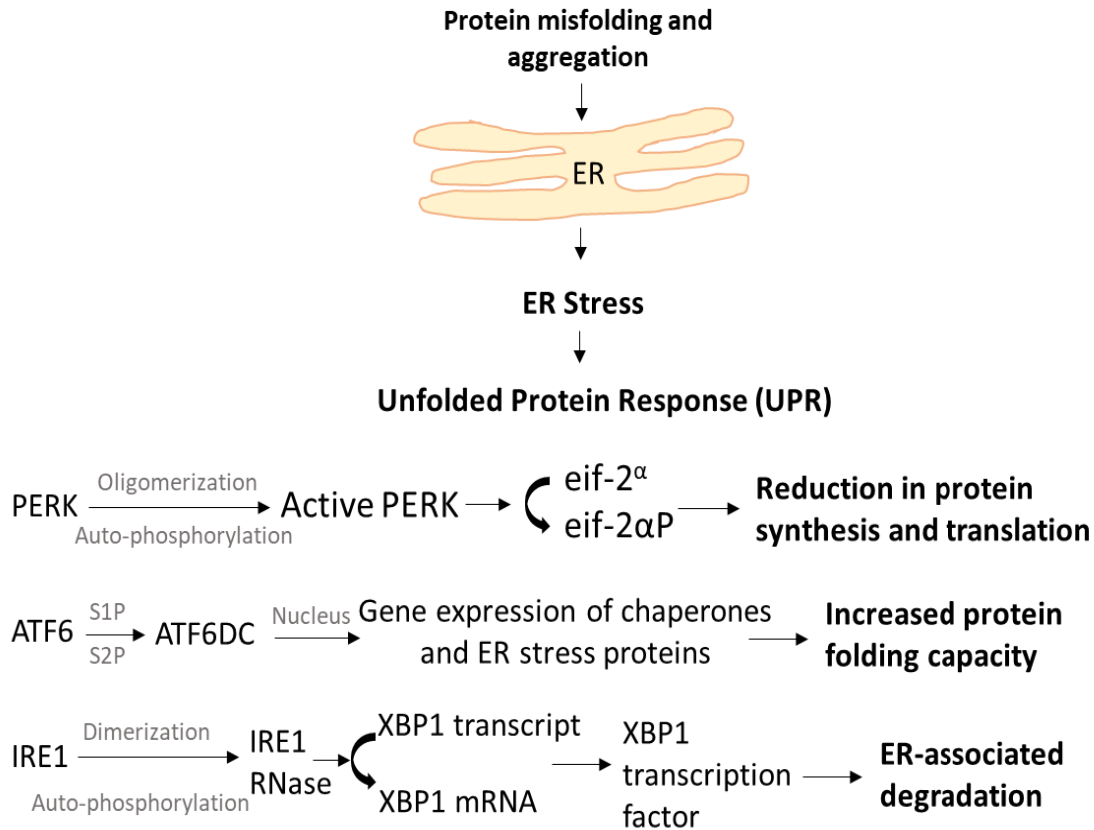


**Figure 1-2. A schematic representing pathways that are activated upon initiation of UPR and the final outcome for each pathway.**

Three major pathways presented here are activated upon UPR and result in temporary reduction of protein translation to lower the amount of proteins present in the ER, production of chaperone proteins to prevent protein aggregation and facilitate correct protein folding, and induction of unfolded proteins degradation by activating the endoplasmic reticulum-associated protein degradation (ERAD) pathway

### 1.3.3 Autophagy and mitophagy

Autophagy is a self-degradative process in cells which, aside from its role in balancing sources of energy at critical times of nutrient stress, has a housekeeping function in removing damaged organelles or misfolded and aggregated proteins (Fivenson, Lautrup et al. 2017, Yu, Chen et al. 2018). Autophagy could be subdivided to: 1) chaperone-mediated autophagy restricted to soluble, small misfolded proteins that can be unfolded, 2) microautophagy and 3) macroautophagy, which is broadly involved in removal of protein aggregates by formation of organelles called “autophagosome” (Chu 2019). Through the process of macroautophagy, proteins are detected and engulfed by (through binding to a receptor lysosome associated membrane protein), and translocated into the lysosomal lumen where they get degraded (Jellinger 2010). Over the last decade, it has been revealed that ubiquitination not only controls proteosomal degradation, but also plays a critical regulatory role for selective autophagy. Autophagy is therefore considered a major regulatory system for degradation of protein aggregates, especially in conditions where the proteosomal system fails to keep up with proper removal of misfolded proteins (Yu, Chen et al. 2018, Chu 2019).

“Mitophagy” is a type of autophagy which selectively targets removal of damaged and superfluous mitochondrion in order to maintain mitochondrial homeostasis (Fivenson, Lautrup et al. 2017). One of the most studied pathways in mitophagy in mammalian cells is the PINK1/Parkin pathway. This pathway plays critical role in several neurodegenerative diseases, and its defect has been reported in various animal models of protein misfolding diseases. PINK1-Parkin-dependent mitophagy is initiated when a decrease in mitochondrial membrane potential caused by mitochondrial damage leads to the stabilization of the ubiquitin kinase (PTEN)-induced kinase 1 (PINK1) on the outer mitochondrial membrane, where it phosphorylates ubiquitin, leading to the recruitment of the E3 ubiquitin ligase Parkin. Parkin is then phosphorylated and activated by PINK1, and polyubiquitinates mitochondrial proteins, leading to their association with the ubiquitin-binding domains of autophagy receptors and the formation of the autophagosome. The autophagosome then fuses with the lysosome, leading to degradation of the mitochondria (Lazarou, Sliter et al. 2015).

Compelling evidence supports the importance of selective autophagy and mitophagy for neuronal health. Mutations in proteins required for autophagy or mitophagy including PINK1, Parkin, etc. leads to neurodegeneration, hence indicating the impact that these pathways have on maintaining neuronal function (Holzbaur 2017).

#### **1.3.4 Other mechanisms:**

Aside from the discussed major mechanisms, there are some other less prominent mechanisms through which misfolded protein species can induce neurotoxicity and neuronal cell death. Some of these reported mechanisms are as follows.

##### **1.3.4.1 Oxidative stress:**

Oxidative stress occurs under conditions when the production of free radicals or their products are in excess of the cellular antioxidant defense mechanisms. This then leads to increased levels of oxidative damage to DNA, lipids and proteins, followed by initiation of a cascade of events, including excitotoxicity, dysfunction of mitochondrial respiration system, and a fatal rise in cytosolic calcium leading to cellular dysfunction together with formation of nitric oxide and reactive nitrogen species (Jellinger 2010).

##### **1.3.4.2 Disruption of cellular/axonal transport:**

Growing evidence suggests that defective neuronal and axonal transport due to early axonal dysfunction could play an important role in most neurodegenerative diseases. Motor protein mutations are observed in human kindred of neurodegenerative diseases and the presence of these mutations in cell and animal models induces disrupted cell/axonal transport that then leads to slow neuronal degeneration and loss of connectivity. Despite all this information, whether misregulation of axonal transport has a direct role in the pathogenesis of these disorders or is a secondary phenomenon remains to be elucidated.

### 1.3.4.3 Formation of pores in the plasma membrane:

Formation of amyloid pores are one of the other mechanisms proposed for neurotoxicity of misfolded protein species. So far, toxic amyloid oligomers of A $\beta$ ,  $\alpha$ -synuclein, and some forms of prion protein (106-126) have been shown to form membrane pores that are capable of contributing to cell death (Last and Miranker 2013, Walsh, Vanderlee et al. 2014). From a structural point of view, amyloid pores consist of spherical, surface-active oligomers that are prone to form pore-like assemblies in the plasma membrane of cells. These structures can then behave as Ca<sup>2+</sup> selective channels and induce dysregulated entry of Ca<sup>2+</sup> into the cytoplasm, which eventually leads to apoptosis and cell death (Di Scala, Yahi et al. 2016).

### 1.4 Studying neurodegenerative diseases: the impact of animal models

Biological systems are sophisticated and extremely dynamic (Walleczek 2006). Thus, an inevitable aspect of studying them would be the development and usage of appropriate models (Ahn, Tewari et al. 2006). Reductionism-based models are considered useful tools and stepping-stones in medical research, providing us with some fundamental information in easy, reproducible and affordable systems. Nevertheless, such models lack the detailed complications required for understanding complex biological systems and have limitations, which are most severe when studying human physiology, where molecular and cellular systems interact to elicit a net response (**Fig.1.2**). Thus it is fair to propose that one of the most valuable models in studying human biology are *in vivo* models, since they are the closest we can get to the complicated network of thousands of genes and proteins, and millions of cells interacting with each other in the human body (Palsson 2000)

Animal models provide a platform to monitor disease progression within a controlled system, with presence of scientific controls, and the possibility to monitor different aspects of disease at various timepoints during disease progression. Understanding detailed molecular mechanisms contributing to disease progression, assessment of various factors contributing to symptoms development in patients and discovering reliable biomarkers for pre-clinical diagnosis of disease are a few examples of points that could be achieved by using animal models.

Generation of high-quality animal models, which can recapitulate the disease as observed in human kindreds, is thus a fundamental step towards studying disease mechanism and development of mechanism-based therapeutics.

The observation that age-related neurodegenerative diseases are largely restricted to humans adds to the challenge (Janus and Welzl 2010, Jucker 2010). Most animal models generated in the field of neurodegenerative diseases are genetically engineered to express proteins with familial disease mutations. However, with regards to humans, familial cases have a prevalence rate of only 5-10%, and most human cases of neurodegenerative diseases are sporadic and therefore of unknown etiology. Moreover, most common neurodegenerative diseases show “comorbidity” with other chronic medical disorders which adds to the complexity of pathological symptoms in human systems (Janus and Welzl 2010, Jucker 2010). It is thus not surprising to have limitations in reiterating the specific and complex pathophysiology of the disease entities observed by neurologists in a specific model. Despite the limitations though, there has been tremendous success in designing reliable animal models in the field of neurodegenerative diseases.

## Reductionism vs. Holism

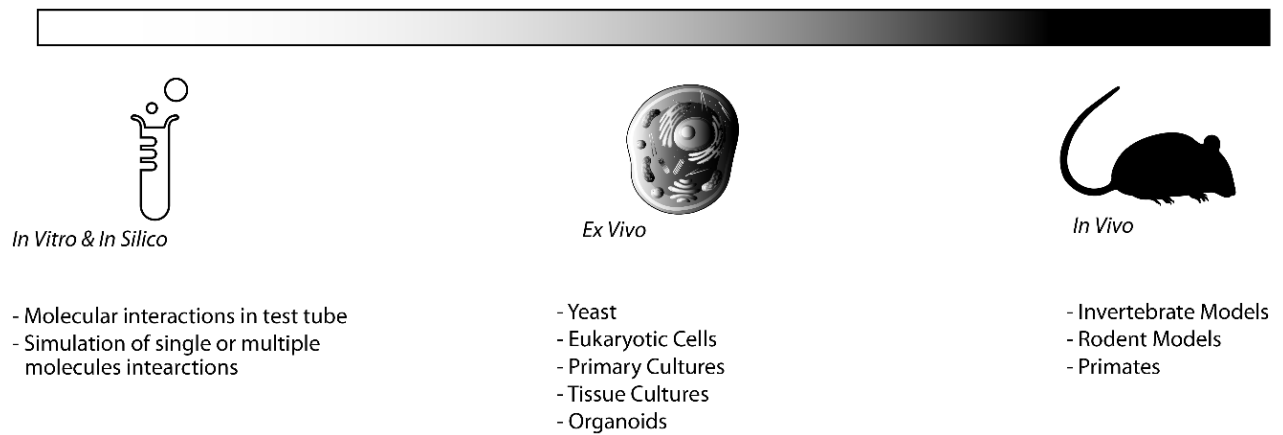


**Figure 1-3. A spectrum representing reductionism-based and holism-based models in biology**

Although reductionism-based models are considered great tools in medical research that can provide some fundamental information in easy, reproducible and affordable systems, they mostly lack the detailed complications in holism-based models. Holism-based models are hence useful for studying complex biological systems where molecular and cellular systems interact to elicit a total synchronized response.

### **1.4.1 Assessment of neurodegeneration in animal models**

Assessment of the mechanisms underlying neurodegeneration and brain injury are crucial aspects in studying protein misfolding diseases. To assess brain injury and quantify the damage caused to the cells, and to understand the impact of neurological insults or neurodegenerative disease progression in animal models, accurate quantification of absolute neuron counts in various brain regions is essential (Golub, Brewer et al. 2015). This information is also essential to confirm the relevance of observed biological changes in the animal model (such as protein aggregation and inflammation) to neurodegeneration. Moreover, to be able to verify the impact of therapeutics in animal models of neurodegenerative disease, quantification of changes in the number of neurons and identification of the timepoint when neurodegeneration begins, are of great importance.

Scientists have employed several techniques throughout time, to elucidate different cellular populations in different brain areas. One of the oldest techniques developed for this purpose is “direct enumeration”, in which brain tissue is homogenized and the density of cell nuclei in re-suspended fluid samples is determined (Nurnberger and Gordon 1957, Brizzee 1973). The main disadvantage of this technique is potential damage to the cells during homogenization. But an even more serious issue would be the lack of any molecular marker to verify specific cells types, such as neurons, glia etc. Later on, stereological methods were developed to provide researchers with unparalleled quantitative data from tissue samples (Glaser and Glaser 2000). Stereological analysis has specifically been of widespread success in part because of the ability to employ immunohistochemical protocols to tag neurons as well as histological procedures to visualize cells, including the Nissl staining, and neurotransmitter biomarkers, such as acetylcholinesterase in adjacent brain slices (Mullen, Buck et al. 1992, Miller, Duka et al. 2012). However, applying stereological techniques requires specific training and elaborate sampling strategies and, as a result, is considered a rather time-consuming and expensive technique.

The most recent addition to the techniques developed for quantification of brain cells population would be “Isotropic fractionator” (IF). Isotropic fractionator is a fast, easy and reliable technique for quantification of changes in brain cells population, as well as tracking neuronal loss (Herculano-Houzel and Lent 2005, Herculano-Houzel, von Bartheld et al. 2015). This technique is the product of combining “direct enumeration” with immunohistochemistry to investigate the

number of neuronal and non-neuronal cells in a tissue sample. Herein, neuronal cells are characterized by the presence of NeuN- a neuronal-cell specific marker on the surface of the nuclei. By immunostaining the nuclei with NeuN antibodies, the neuronal cell population can be separated from other cells in the tissue.

Accuracy and reliability of data obtained from isotropic fractionator have been validated using several other techniques such as unbiased stereology, flow cytometry and cell numbers calculation using extracted DNA (Collins, Young et al. 2010, Bahney and von Bartheld 2014, Miller, Balaram et al. 2014). Since developed and introduced to the field, isotropic fractionator has been vastly used to answer some fundamental questions in various aspects of neuroscience. In evolutionary neuroscience, IF has been used to address questions regarding correlation of brain size, brain cell number and intelligence in different species, or the balance of neurons vs. non-neural cells in primate brains (Azevedo, Carvalho et al. 2009, Herculano-Houzel 2014, Herculano-Houzel, Messeder et al. 2015, Herculano-Houzel 2016). IF has also been applied in studies focusing on neurodegeneration, where it's been used for quantification of neuronal loss in different animal models of neurodegenerative diseases to confirm neural cell death, or to compare different animal models (Brautigam, Steele et al. 2012, Eskandari-Sedighi, Daude et al. 2017). As mentioned earlier, stereological analysis of brain slices can provide great anatomical details, however the preparation of histological sections is time-consuming and adequately sampling brain tissue can be challenging. IF is as accurate as unbiased stereology and faster than stereological techniques, as it requires no elaborate histological processing or sampling paradigms, providing reliable estimates in a few days rather than many weeks (Miller, Balaram et al. 2014). Tissue shrinkage is also not an issue, since the estimates provided are independent of tissue volume and are normalized to the volume of homogenate. The main disadvantage of IF, however, is that it necessarily destroys the tissue analyzed and thus provides no spatial information on the cellular composition of biological regions of interest (Herculano-Houzel, von Bartheld et al. 2015). However, despite being destroyed, the tissues used in IF are not lost; the suspension, or aliquots of it, can be stored in an anti-freeze solution and kept frozen for years for later re-analysis (for instance, when new antibodies become available) with little loss of immunoreactivity (Herculano-Houzel 2011, Herculano-Houzel, von Bartheld et al. 2015). Moreover, similar to "direct enumeration", tissue homogenization could cause some damage to the cell nuclei in the suspension, affecting the final outcome. But this problem could be mostly avoided by practice and adequate training. The biggest

shortage of IF is the lack of a nuclei marker for cells other than neurons (i.e. glia, astrocytes, etc.), due to which these cells cannot be specifically and individually quantified.

The work in this thesis has focused on three different experimental paradigms in lab mice designed to study several aspects of neurodegenerative diseases and the pathophysiology of precursor proteins. The projects discussed entail two well-known proteins, tau and PrP<sup>C</sup>, which are key role players in neurodegenerative diseases known as “tauopathies” and “prion diseases” respectively. I will hence provide a brief review of biochemical features of both these proteins in the following sections.

## **1.5 Tau and tauopathies**

Tauopathies are a group of neurodegenerative diseases with the common feature of tau protein aggregation and deposition in the brain. Biochemistry of tau and its role in these class of neurodegenerative diseases are discussed in the following sections.

### **1.5.1 Tau, from gene to protein**

Tau is a microtubule associated protein (MAP), encoded by a single gene, *MAPT*, located on chromosome 17 of the human genome. Tau mRNA can go through various splicing events that upon translation generates 6 different isoforms in adult human brain (Buée, Bussi re et al. 2000, Guo, Noble et al. 2017). These isoforms differ from each other by the presence or absence of exons 2, 3 and 10. Isoforms resulting from mRNA that include exon 10, which encodes an additional microtubule-binding motif, are commonly referred to as four-repeat (4R) tau isoforms, whereas isoforms that exclude exon 10 are referred to as three-repeat (3R) tau isoforms (**Fig.1.3**) (Bu e, Bussi re et al. 2000, Mandelkow and Mandelkow 2012). All isoforms of the tau protein are mainly expressed in neurons, where they have several important functions, such as maintenance and stabilization of microtubule (MT) assembly, DNA/RNA protection and interaction of MT with other proteins (Cleveland, Hwo et al. 1977, Avila, Lucas et al. 2004,

Goedert and Spillantini 2011, Mandelkow and Mandelkow 2012). Neuronal expression of tau is believed to be achieved by interaction of neural specific factors with DNA sequences upstream of the *MAPT* gene, however, presence of possible silencer elements in nonneural cells could also contribute to this matter (Avila, Lucas et al. 2004). Despite its many reported functions in neurons, absence of tau in mice has no severe consequences and, despite a few minor phenotypes, *MAPT* knock-outs develop normally and do not display any overt histological abnormalities, possibly due to the rescue effects of tau function by other MAPs (Harada, Oguchi et al. 1994, Dawson, Ferreira et al. 2001).

Tau protein is a hydrophilic protein, with two major domains: the projection domain consisting of the amino-terminal of the protein and the microtubule-binding domain containing the carboxy-terminal (Lee, Cowan et al. 1988, Friedhoff, von Bergen et al. 2000). The N-terminal domain of the protein is primarily involved in its interactions with other tau interactors (i.e. other proteins, cell membrane and nuclear membrane etc.). The repeat domains in the C-terminal are important for tau interactions with MT protein, but they can also interact with other proteins (Buée, Bussièrè et al. 2000, Avila, Lucas et al. 2004, Mandelkow and Mandelkow 2012).

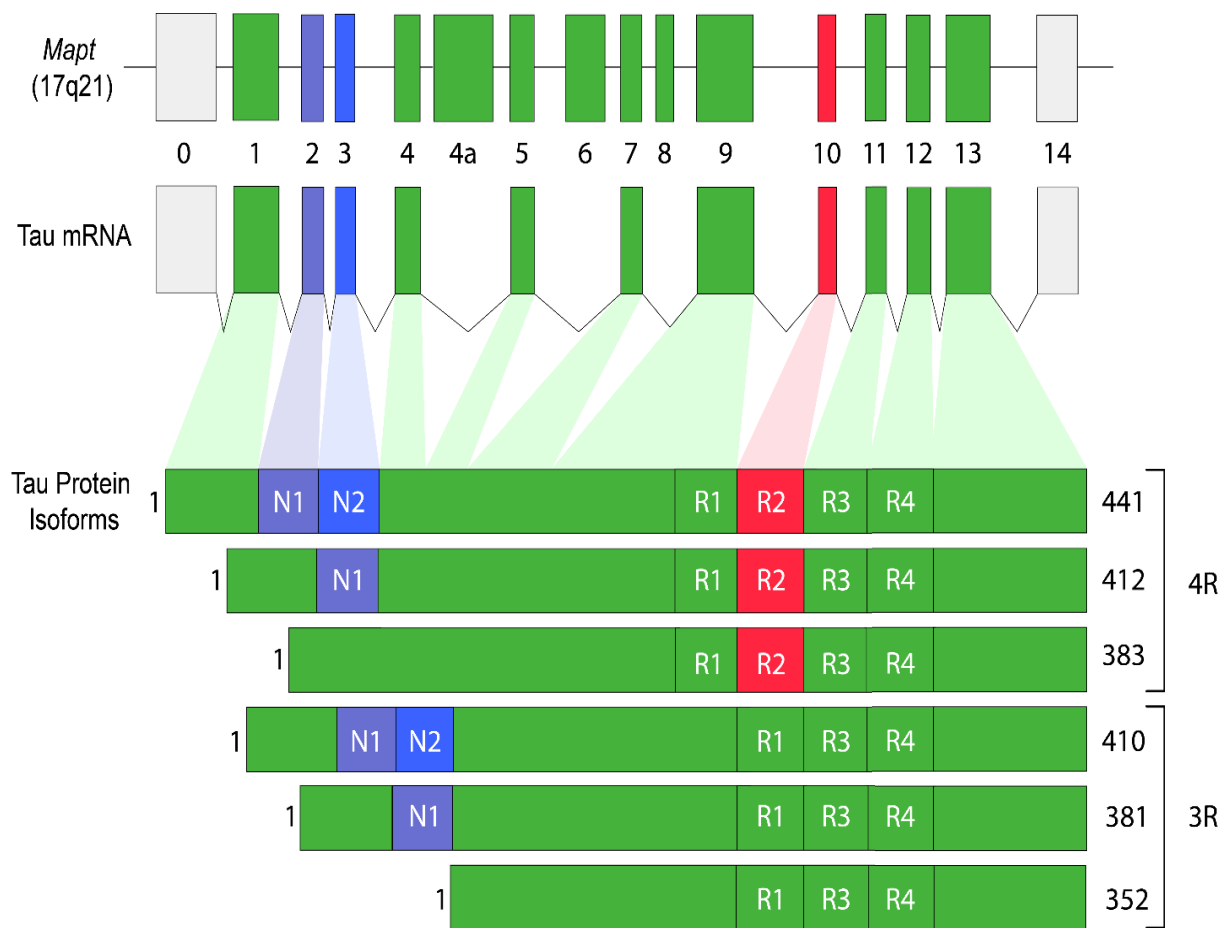


**Figure 1-4. Tau from gene to protein.**

A schematic of the *MAPT* gene, transcribed mRNA and 6 spliced protein isoforms. Tau mRNA can go through various splicing events that upon translation generates 6 different isoforms in adult human brain. These isoforms differ from each other by the presence or absence of exons 2, 3 and 10. Isoforms resulting from mRNA that include exon 10, which encodes an additional microtubule-binding motif, are commonly referred to as four-repeat (4R) tau isoforms, whereas isoforms that exclude exon 10 are referred to as three-repeat (3R) tau isoforms

### 1.5.2 Post translational modifications (PTMs) of tau protein

Tau can undergo multiple post translational modifications (PTMs). Some of these modifications potentially contribute to tau misfolding and aggregation in tauopathies. Glycation, acetylation, oxidation, polyamination, proteolysis and ubiquitylation are just a few examples of PTMs that tau protein can go through (Avila, Lucas et al. 2004, Mandelkow and Mandelkow 2012, Guo, Noble et al. 2017, Quinn, Corbett et al. 2018).

Phosphorylation is arguably one of the most common PTMs of tau, and due to a long-established link between abnormal phosphorylation and self-aggregation of tau, it is one of the most well-studied PTMs of this protein. With over 80 potential phosphorylation sites in the protein sequence (79 Ser/Thr and 5 Tyr residues), the tau protein is a great target for several kinases and phosphatases (**Fig 1.4**) (Tenreiro, Eckermann et al. 2014, Guo, Noble et al. 2017).

Phosphorylation regulates different roles of tau protein: Interaction with MT network and MT assembly, modulation of cell polarity and axonogenesis, cell localization and modulation of neuronal morphology during developmental stages of life (Buée, Bussièrè et al. 2000, Dujardin, Colin et al. 2015). However, aside from its regular function, phosphorylation also plays a major role in tau aggregation and neurotoxicity (Friedhoff, von Bergen et al. 2000, Tenreiro, Eckermann et al. 2014, Irwin 2016).

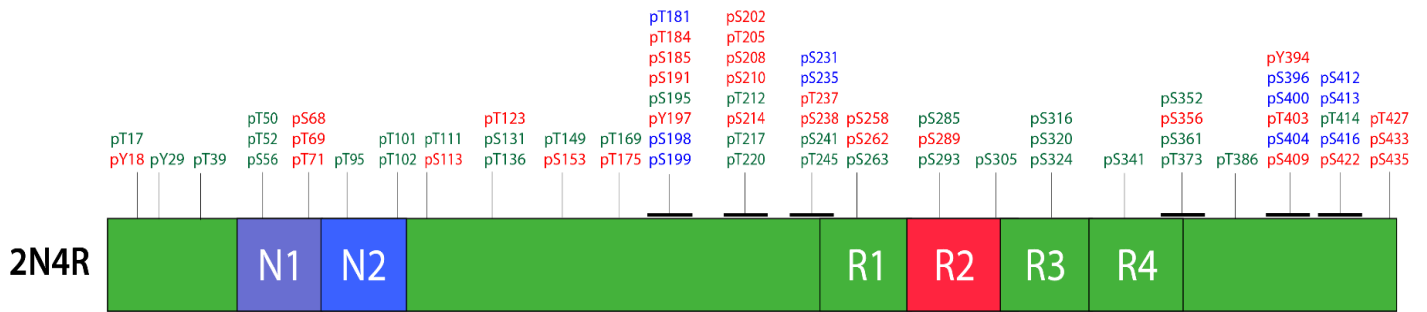


**Figure 1-5. A schematic of phosphorylation sites on 2N4R tau protein.**

The longest form of human tau protein with phosphorylation sites observed in normal brain (green), AD brain (red) or both (blue).

Normal tau is phosphorylated on two or three residues, and the underphosphorylated form is a more efficient MT network stabilizer. Hyperphosphorylated tau is usually phosphorylated at least eight residues, has less interaction with microtubule proteins, and is thus more prone to misfolding and aggregation (Cairns, Bigio et al. 2007, Tenreiro, Eckermann et al. 2014). Other mechanisms that could contribute to hyperphosphorylated tau aggregation and neurotoxicity include tau mis-sorting from axons to somatodendritic compartment, disruption of intracellular degradation routes of the protein and disturbance in tau functions mostly by influencing its protein-protein interactions (Dickey, Kamal et al. 2007, Hanger, Anderton et al. 2009, Hoover, Reed et al. 2010, Gilley, Ando et al. 2016). It must be taken into account that despite the long list of harmful consequences listed for hyperphosphorylated tau, some phosphorylation sites are believed to have protective effects and inhibit the formation of toxic species (Ittner, Chua et al. 2016).

Tauopathies are generally categorized into two subgroups: primary and secondary. In primary tauopathies, mutations in the *MAPT* gene leads to tau protein misfolding and aggregation, driving the pathogenesis of the disease. Some examples include Frontotemporal Dementia, Pick's disease and Cerebral Nuclear palsy (Hardy 1999). In secondary tauopathies, there are no mutations in the *MAPT* gene. It is the aggregation of other proteins that initiates the pathogenesis of disease which then leads to co-aggregation of tau as a secondary event. Alzheimer's disease (AD), amyotrophic lateral sclerosis (ALS) and Gerstmann-Straussler-Scheinker syndrome (GSS) are a few examples of secondary tauopathies (Hardy 1999, Irwin 2016, Lebouvier, Pasquier et al. 2017)

### **1.5.3 Tau protein in neurodegenerative diseases**

Despite being an intrinsically disordered protein, tau forms insoluble filamentous aggregates in disease conditions, followed by diverse synaptic loss, gliosis and neuronal cell death. The most well-studied filamentous tau structure is paired helical filaments (PHFs), the principal constituent of the neurofibrillary tangles (NFTs) in AD patients. These filaments consist of two structurally distinct parts: an external "fuzzy coat" comprised of the N and C-terminal region of the protein, that can be removed by treatment with the broad-spectrum protease pronase and a distinct

pronase-resistant core that is made up of the tandem microtubule binding repeats (Goedert and Spillantini 2011).

Tau aggregation and deposition in brain is the common event in all tauopathies. This class of neurodegenerative diseases is generally categorized into two subgroups: primary and secondary tauopathies. Primary tauopathies are the diseases in which tau aggregation plays a key role in disease pathogenesis; some examples include Frontotemporal Dementia with Parkinsonism (FTLD-MAPT), Pick's disease and Cerebral Nuclear palsy. In secondary tauopathies, the disease is fueled by defects of other proteins, which could then lead to co-aggregation of tau as a secondary event. Alzheimer's disease (AD), amyotrophic lateral sclerosis (ALS) and the inherited prion disease Gerstmann–Sträussler–Scheinker syndrome (GSS) are examples of secondary tauopathies (Irwin 2016).

Despite the established role of tau protein in all these diseases, the mechanism connecting tau dysfunction to its toxicity is not yet well understood. There are several hypotheses based on clinical evidence with disrupted axonal transport, cellular toxicity of hyperphosphorylated and aggregated tau protein, nuclear toxicity and inflammation being a few examples (Hanger, Anderton et al. 2009, Gilley, Seereeram et al. 2012, Iqbal, Liu et al. 2016, Guo, Noble et al. 2017). These hypotheses have been tested in different *ex vivo* and *in vivo* models, as well as in post-mortem human samples. Most researchers agree that the disease pathogenesis in humans is due to a combination of these factors and that no single event can contribute to all the phenotypes observed in patients (Goedert and Spillantini 2011, Iqbal, Liu et al. 2016).

#### **1.5.4 Animal models of tauopathies**

Most animal models generated in the field of neurodegenerative diseases are genetically engineered to express proteins with familial disease mutations. However, in the human setting, familial cases have a prevalence rate of only 5-10%, and the majority of human cases of neurodegenerative diseases are sporadic and therefore of unknown etiology. Moreover, most common neurodegenerative diseases show “comorbidity” with other chronic medical disorders, and this adds to the complexity of pathological symptoms in human systems (Janus and Welzl 2010, Jucker 2010). It is thus not surprising to have limitations in reiterating the specific and

complex pathophysiology of the disease entities observed by neurologists, especially since some animal model of tauopathy will have been designed to test specific hypotheses, and hence mimicking only certain compartmentalized aspects of the full pathological landscape.

Transgenic (Tg) mouse models are one of the most prevalent model organisms used in the generation of tauopathy animal models. These model animals are considered standard yet powerful tools to elucidate protein activity and potential influence of genetic mutations in health and disease. Transgenic technologies can be divided into a) embryo-mediated, where genetic modifications are introduced into an embryo; and b) cell-mediated approaches where genetic modifications are introduced to an individual cell, usually embryonic stem cells (ESCs). The latter approach has the advantage of full characterization of genetic modifications prior to generation of the Tg animal (Laible 2018).

Over 100 Tg mouse models reported to capture some aspects of human tauopathies but, to date, no mouse model is a faithful reproduction of idiopathic (sporadic) disease cases. Despite such limitations, transgenic animals can be useful tools when properly matched to the experimental questions being studied.

In chapter 2 of this thesis, disease pathogenesis and biochemistry of tau protein aggregates have been investigated in an animal model of genetic tauopathy that was previously generated by our group (Murakami, Paitel et al. 2006).

## 1.6 PrP<sup>C</sup> and prion diseases

Prion diseases are a class of neurodegenerative diseases also known as transmissible spongiform encephalopathies and caused primarily by misfolding and aggregation of the cellular prion protein (PrP<sup>C</sup>) to a protease resistant conformation referred to as PrP<sup>Sc</sup> (Colby and Prusiner 2011). The biochemistry and function of PrP<sup>C</sup> will be reviewed in the following section.

### 1.6.1 PrP<sup>C</sup>, from gene to protein

The cellular prion protein is a glycoprotein, anchored to the outer leaflet of the plasma membrane via a glycosylphosphatidylinositol (GPI) anchor. The *PRNP* gene coding for the protein is located on chromosome 20 in humans and chromosome 2 of mice and is strongly conserved amongst mammals. The gene consists of 3 exons and the entire open reading frame (ORF) encoding the protein is encompassed within exon 3 (Watts and Westaway 2007) (**Fig. 1.5**).

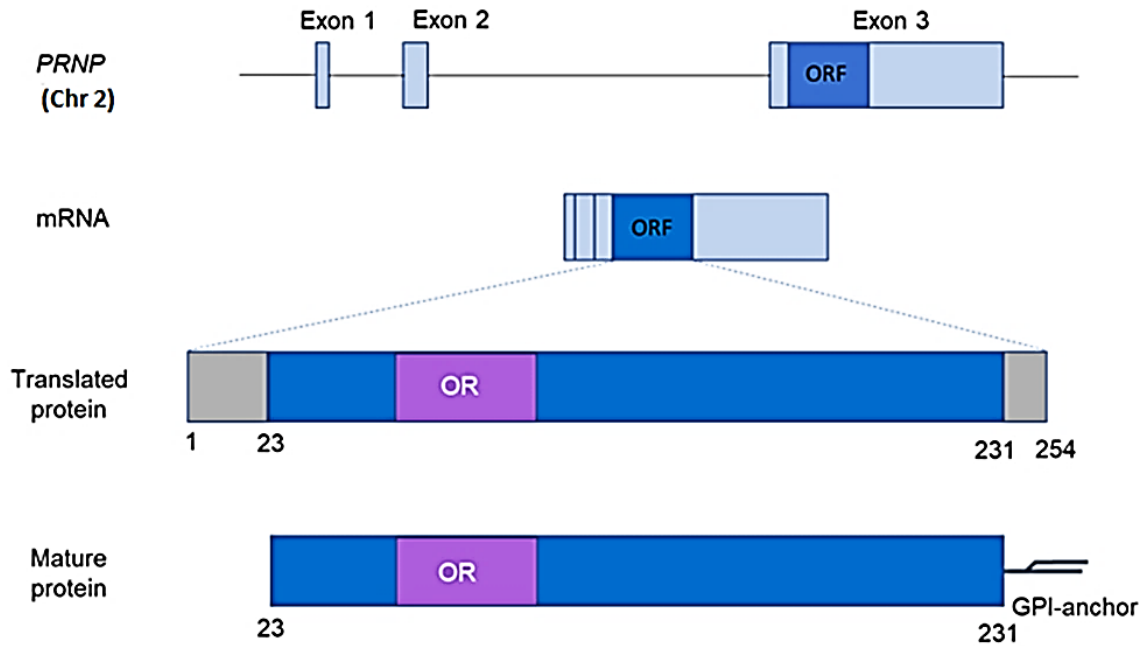


**Figure 1-6. PrP<sup>C</sup> from gene to protein.**

A schematic of murine *PRNP* gene located on chromosome 2 of mouse genome, its transcribed mRNA, the translated protein and mature PrP<sup>C</sup> protein. The mature protein is a glycosylphosphatidylinositol (GPI) anchored protein and entails residues 23-231.

Polymorphisms within the *PRNP* gene and their impact on susceptibility to prion diseases have been well studied and characterized, with the polymorphism at position 129 (M or V) being one of the strongest, influencing the pathogenesis of several prion diseases in humans. Mutations within *PRNP* can cause genetic forms of prion diseases such as Gerstmann–Sträussler–Scheinker syndrome (GSS). There are two paralogs of *PRNP* in mammals, *PRND* and *SPRN*, encoding for proteins known as doppel and shadoo respectively.

PrP<sup>C</sup> is expressed in several tissues such as heart, lung and spleen, but the highest level of expression is in muscle tissue and the central nervous system (CNS). Despite being highly conserved in mammals, no critical function has yet been defined for this protein as *PRNP* knock out animals survive without any major defects. Throughout decades of research attempting to understand the main role of PrP<sup>C</sup>, several potential functions have been identified for this protein; neuroprotective roles, involvement in copper homeostasis, signal transduction and myelin maintenance are some of the proposed functions of PrP<sup>C</sup>. However, PrP<sup>C</sup> is still mostly known for its direct role in prion diseases, where it undergoes a conformational change from a mainly alpha-helical structure to a beta-sheet rich conformation of the protein.

From a structural point of view, PrP<sup>C</sup> is composed of a flexible N-terminal region (including a charged patch), two hexarepeats, five tandem repeats of eight amino acid residues forming an octarepeat region (OR), a hydrophobic linker region sometimes referred to as the “HD” (hydrophobic domain) and a C-terminal globular domain. The C-terminal is composed of mostly alpha helices ( $\alpha A$ ,  $\alpha B$  and  $\alpha C$ ) and two small beta sheets ( $\beta 1$  and  $\beta 2$ ).

Upon synthesis in the endoplasmic reticulum (ER), PrP<sup>C</sup> goes through several post-translational modifications. Throughout the synthesis, the protein goes through N-glycosylation on two Asn residues in the C-terminal region (Asn181 and Asn 197). A disulfide bond is formed amongst two Cys residues in  $\alpha B$  and  $\alpha C$ . Moreover, through the maturation process, the first 22 amino acid residues of the protein are removed from the N-terminal. Also 23 residues from the C-terminal of the protein which act as glycosylphosphatidylinositol (GPI) anchor signal are removed and replaced by a GPI anchor (**Fig 1.4**).

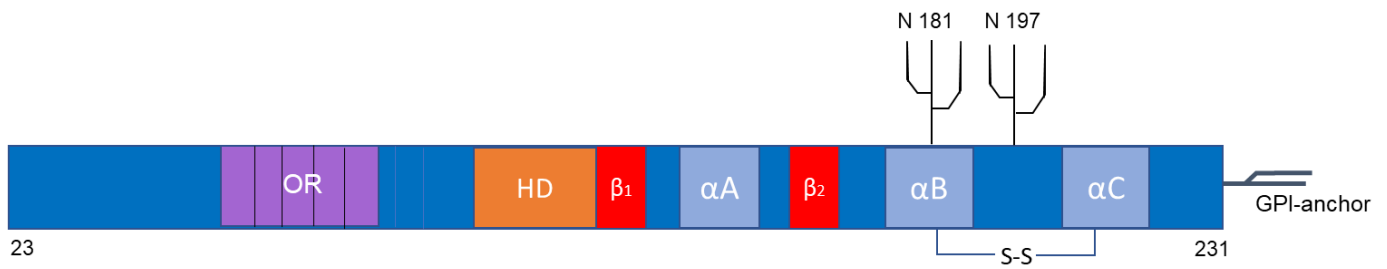


**Figure 1-7. A schematic of PrP<sup>C</sup> presenting different regions within the molecule.**

Mature cellular prion protein consists of 23-231 amino acid residues. The N-terminal domain is naturally disordered and include the octapeptide repeat (OR) region and hydrophobic core (HD). The C-terminal globular domain consists of glycosylation sites, as well as the disulfide bond amongst two Cys residues.

## 1.7 The “strain” phenomenon in prion diseases

In microbiology, a strain is classically defined as a genetic variant of a microorganism or a virus, with distinguishable surface markers and unique pathogenesis features. The term “strain” has been introduced and well-accepted in the field of prions and protein misfolding diseases, albeit with a different definition; in the field of proteinopathies, a strain is recognized as an isolate that, upon introduction into distinct host environments, causes disease with distinct and consistent patterns of clinical and biochemical characteristics. And these phenotypic traits of a strain typically persist upon serial transmission (Aguzzi, Heikenwalder et al. 2007). Prion strains can be classified by different parameters; The main *in vivo* characteristics that can be used to differentiate prion strains are a) incubation periods, b) profile of histological damage and c) clinical signs (Morales, Abid et al. 2007). Albeit it is important to consider that not all strains present differences in each of these parameters and sometimes two different strains could present identical incubation period, or clinical signs. In addition to the *in vivo* differences, each prion strain possesses some distinct biochemical characteristics in the infectious protein that could be used to distinguish it from other strains. Some of the most common biochemical phenotypes for distinguishing prion strains are a) the electrophoretic mobility of proteinase K (PK)-resistant PrP, b) glycosylation pattern of PrP<sup>Sc</sup>, c) the extent of PrP<sup>Sc</sup> PK resistance, d) sedimentation assays and e) resistance to denaturation by chaotropic agents (Morales, Abid et al. 2007).

Presence of different prion strains can pose unprecedented challenge to prion research. However, understanding the molecular mechanism of *de novo* strain development, and the correlation between disease pathogenesis and strains, could result in fundamental changes in our understanding of prion diseases, and, potentially other protein misfolding diseases.

## 1.8 The “prion” concept in other proteinopathies

As discussed earlier, the term prion was originally generated to refer to a specific group of proteinopathies caused by misfolding of the cellular prion protein. However, throughout the years more proteins were discovered that have the ability undergo the same process. Today, several proteins such as A $\beta$ , tau,  $\alpha$ -synuclein and TAR DNA-binding protein 43 (TDP-43) are

known to have the ability to go through prion-like templated protein misfolding and aggregation, and cause neurodegeneration. Today, the prion paradigm, according to which a fundamental cause of specific disorders is the misfolding and seeded aggregation of specific proteins, is more of a unifying molecular principle for the pathogenesis of many age-related neurodegenerative diseases (Walker and Jucker 2015). Proteins with such behavior are thus referred to as “prion-like” (or “prions” in some literature). The common features observed in proteins with prion-like behavior are briefly summarized in the following section.

### **1.8.1 Formation of amyloid fibrils:**

Misfolded protein species are usually rich in  $\beta$ -sheets, and it's through intermolecular interactions amongst these  $\beta$ -sheets that they can form amyloids (Westermarck and Westermarck 2010). Amyloids are defined as highly ordered aggregates of proteins characterized by high  $\beta$ -sheet content, typical appearance under the electron microscope, consistent X-ray diffraction pattern and high affinity for certain dyes such as Congo red or thioflavin (Soto and Pritzkow 2018). Amyloid formation is a nucleation-dependent event, and the formation of the nucleus is the energetically unfavorable and hence rate-limiting step. The formed nucleus then expands rapidly by recruiting new molecules of the same biochemical nature to form amyloid fibrils (Soto, Estrada et al. 2006, Westermarck and Westermarck 2010).

### **1.8.2 Generation of protease resistant aggregates:**

A unique feature of prion diseases is the conversion of soluble, protease-sensitive PrP<sup>C</sup> to insoluble, protease-resistant PrP<sup>Sc</sup> aggregates. Several other proteins involved in proteinopathies share this feature with prions, and form relatively protease-resistant aggregates.

### **1.8.3 Presence of different conformers (strains) of misfolded protein species:**

As discussed earlier in this chapter, the strain phenomenon in prion disease is a unique concept that has given rise to several questions in the field. Compelling evidence suggest the existence of conformational strains for misfolded aggregates composed of several prion-like proteins such as A $\beta$ , tau,  $\alpha$ -Syn and etc. (Soto and Pritzkow 2018).

### **1.8.4 Phenotypic diversity:**

Similar to prion diseases, several diseases caused by prion-like proteins present diverse phenotypes involving both the CNS and peripheral nervous system (PNS) and exhibit distinct rates of progression during disease formation (Frost and Diamond 2010). The molecular mechanism contributing to this phenomenon is believed to be presence of different strains and conformation of misfolded protein species.

### **1.8.5 Seeding and spreading of the misfolded proteins throughout the CNS:**

Neurodegenerative diseases present deposits of aggregated proteins and neurobiological dysfunction in a discrete region whereas, at later stages of the disease, deposition of aggregated proteins involve much larger areas of the brain. For each disease, the pathology often occurs in certain neural networks and progresses in a predictable manner (Fivenson, Lautrup et al. 2017).

It must be noted that despite the common features listed here, the transmissibility and infectious nature of prion diseases is a unique feature which has not been reported for any of the other neurodegenerative diseases caused by “prion-like” proteins. This difference is one of the rationales behind hesitance in categorizing prion-like proteins such as A $\beta$ , tau,  $\alpha$ -synuclein as “prions”.

## **1.9 Role of proteolytic processing in protein misfolding diseases**

Proteases are enzymes that catalyze the hydrolysis of the peptide bond of peptide substrates and proteins. They were primarily considered simple destructive enzymes necessary for protein catabolism and the generation of amino acids in primitive organisms. And thus, for many years, studies on proteases have focused on their role in protein degradation. However, it has now become clear that proteases are more than protein degradation tools and they have multiple important functions in cells: modulating enzyme activity, regulating membrane function, altering receptor channel properties, transcription control, cell cycle regulation and reproduction, etc. Hence, it is not surprising that disturbances in proteolytic homeostasis can result in severe consequences and induce several disease conditions.

An important aspect of proteolytic processing in protein misfolding diseases is the impact of proteolysis on a protein's half-life. Fragments could behave differently compared to the full-length protein regarding 1) conformation, 2) solubility, 3) stability and half-life, 4) cell localization and 5) interacting molecules and proteins. Proteolytic processing of proteins is thus considered a critical event in protein misfolding diseases. Proteolysis has turned out to be a critical step in disease progression in almost all the proteins involved in protein misfolding diseases. Proteolytic processing of tau and prion protein will be discussed in more details in the upcoming sections.

### **1.9.1 Proteolytic processing of tau protein in health and disease**

Proteolytic processing is one of the several PTMs that tau protein can go through. Under normal circumstances, tau is only targeted for proteolysis for recycling of the protein. However, in disease conditions, tau can become the target of several proteases and break into fragments of different sizes, that could be detected in cerebrospinal fluid (CSF) and plasma of patients with different tauopathies. Although tau proteolysis could be beneficial for the cell, via clearance and depletion of the protein, the main reason it has sparked much research interest is because of its ability to aggravate tau aggregation. This is likely due to two major consequences: 1) an initial

disruption of the primary structure of tau and 2) the generation of neurotoxic tau fragments (Quinn, Corbett et al. 2018).

As discussed earlier, fragments of a protein could manifest different behavior compared to the full-length molecule. In the case of the tau protein, there are some fragments that are more prone to aggregation relative to the full-length tau and, hence, their generation could disrupt the system by generating seeds of aggregated protein which can then recruit full length tau and enhance its aggregation. Overt generation of these types of fragments have been correlated with disease progression and accumulation of pathologic tau in several animal models, as well as post-mortem tissue extracted from tauopathy patients. Some of the proteases that have been identified to cleave tau, and the characteristics of the subsequent fragments generated, are listed in Table 1.1.

<b>cleavage site</b>	<b>Identified fragment</b>	<b>Protease</b>	<b>The impact of cleavage on disease pathogenesis</b>	<b>Reference</b>
D25-Q26 and R230-T231	26–230 (20-22kDa)	Caspase 3	Exacerbating mitochondrial dysfunction. Caused NMDAR-mediated cell death in rat CGCs	(Amadoro, Ciotti et al. 2006)
D314-L315, ( <i>In vitro</i> D421-S422)	1–314 ( $\Delta$ tau314)	Caspase 2	Lower propensity to aggregate compared to tau441. Impaired synaptic transmission and drives hippocampal neuronal loss.	(Zhao, Kotilinek et al. 2016)
N368-K369	1-368	Asparagine Endopeptidase	Reduced ability to induce MT polymerization, triggered apoptosis, The C-terminal fragment has increased propensity to aggregate into PHFs compared to tau441	(Zhang, Song et al. 2014)
A152-T153	153–441 (Tau-A)	ADAM10	Found in serum from patients with AD and inversely correlates with cognitive test scores	(Henriksen, Wang et al. 2013)
R242-L243	243–441 (Tau-CTF24)	Calpain-1	Accelerates intracellular propagation of tau and has reduced capacity for promoting MT assembly compared to tau441	(Matsumoto, Motoi et al. 2015)

**Table 1-1 A list of some identified proteolysis events that tau protein can go through.**

Some of the most well-characterized fragments of tau, as well as their impact on disease pathogenesis have been presented.

## 1.9.2 Proteolytic processing of PrP<sup>C</sup> in health and disease

Unlike tau protein, PrP<sup>C</sup> undergo several proteolytic processing events in normal conditions; alpha-cleavage, beta-cleavage, gamma-cleavage and shedding are the known proteolytic events that can target PrP<sup>C</sup> (Lewis, Johanssen et al. 2016). The subsequent fragments produced upon each fragmentation process have unique, yet potentially different characteristics. Fragmentation of PrP<sup>C</sup> could impact the protein fate in both health and disease conditions.

### 1.9.2.1 Alpha cleavage:

The most prominent proteolytic processing that targets full-length PrP<sup>C</sup> is  $\alpha$ -cleavage, which breaks the molecule to two distinct fragments: a) N1 which is a 10 kDa soluble fragment consisting of residues 23-110 (in the mouse, or residues 23-111 in humans) from the N-terminal of the protein, and b) C1 fragment which is a membrane-attached counterpart of approximately 16 kDa molecular weight (Altmeppen, Puig et al. 2012, Castle and Gill 2017) (**Fig.1.8**). As mentioned earlier,  $\alpha$ -cleavage is the main proteolytic processing event targeting PrP<sup>C</sup>, and C1 fragment can make up to 50% of total PrP<sup>C</sup> in some cell lines. Some reports have indicated that the  $\alpha$ -cleavage event produces biologically active fragments, with C1 being pro-apoptotic and N1 being protective against staurosporine treatment in a p53-dependent manner (Sunyach, Cisse et al. 2007, Guillot-Sestier, Sunyach et al. 2009).

Several cellular compartments have been proposed as the site of  $\alpha$ -cleavage, but recent evidence from several studies suggest that this event takes place while PrP<sup>C</sup> is traversing through the late secretory pathway (Zhao, Klingeborn et al. 2006, Walmsley, Watt et al. 2009).

### 1.9.2.2 Beta-cleavage:

A less prominent cleavage of PrP<sup>C</sup> is  $\beta$ -cleavage which takes place upstream of the  $\alpha$ -cleavage site, at the end of the octapeptide repeat region (residue 90 approximately). This cleavage produces a soluble N2 fragment of 8 kDa and a membrane bound C2 fragment of 18 kDa (Altmeppen, Puig et al. 2012).  $\beta$ -cleavage is one of the more obscured proteolytic processing

routes that PrP<sup>C</sup> will go through under physiological conditions. However, in disease conditions, there is tremendous increase in a fragment with similar molecular weight to C2 (Yadavalli, Guttmann et al. 2004). However, it is still not clear whether this fragment is identical to the C2 fragment generated by  $\beta$ -cleavage of PrP<sup>C</sup> in physiological conditions (Watt, Taylor et al. 2005). Interestingly, similar to N1, N2 is not as easily detectable as its C-termini counterpart.

For quite some time,  $\beta$ -cleavage was believed to be a chemical reaction driven by reactive oxygen species (ROS), localized to the octapeptide repeat domain by copper ions (Cu<sup>2+</sup>) bound to His residues in this region. However, a combination of work by several research groups eliminated this theory, suggesting that  $\beta$ -cleavage is in fact a proteolytic processing event (Lau, McDonald et al. 2015).

### **1.9.2.3 Gamma-cleavage:**

A third proteolytic processing of PrP<sup>C</sup> that was reported just recently is  $\gamma$ -cleavage (Lewis, Johanssen et al. 2016). As a result of this proteolysis, the protein breaks into a 20 kDa N-terminal fragment called N3 and a small C-terminal fragment referred as C3.  $\gamma$ -cleavage is believed to occur late in the secretory pathway, preferentially from an unglycosylated substrate (Lewis, Johanssen et al. 2016). There are not many physiological functions defined for N3 and C3, and this could partially be due to the fact that they have been discovered quite recently. Whether products of  $\gamma$ -cleavage are bioactive or not will be clarified in the future, but what is known for now is that this specific proteolysis event could have a negative impact on PrP<sup>Sc</sup> replication, since the sequence necessary for PrP<sup>C</sup> transition is absent in both N3 and C3.

### **1.9.2.4 Shedding:**

A fourth physiological cleavage of PrP<sup>C</sup> occurs in close proximity to its GPI-anchor and results in the release of the almost full-length protein from the plasma membrane. It must be noted that this proteolytic processing is different from cleavage of the GPI anchor by phospholipases and is driven by A Disintegrin and Metalloprotease 10 (ADAM 10) at residue 228 (mouse numbering) (Altmepfen, Puig et al. 2012, Altmepfen, Prox et al. 2013). Since shedding results in the release

of PrP<sup>C</sup>, from the plasma membrane, it is considered a physiological mechanism to regulate PrP<sup>C</sup> levels at the plasma membrane. This is of great importance regarding the multiple functions discussed for PrP<sup>C</sup>, but more importantly in the course of prion diseases since shed prion protein could contribute to propagation and spreading of infectivity.

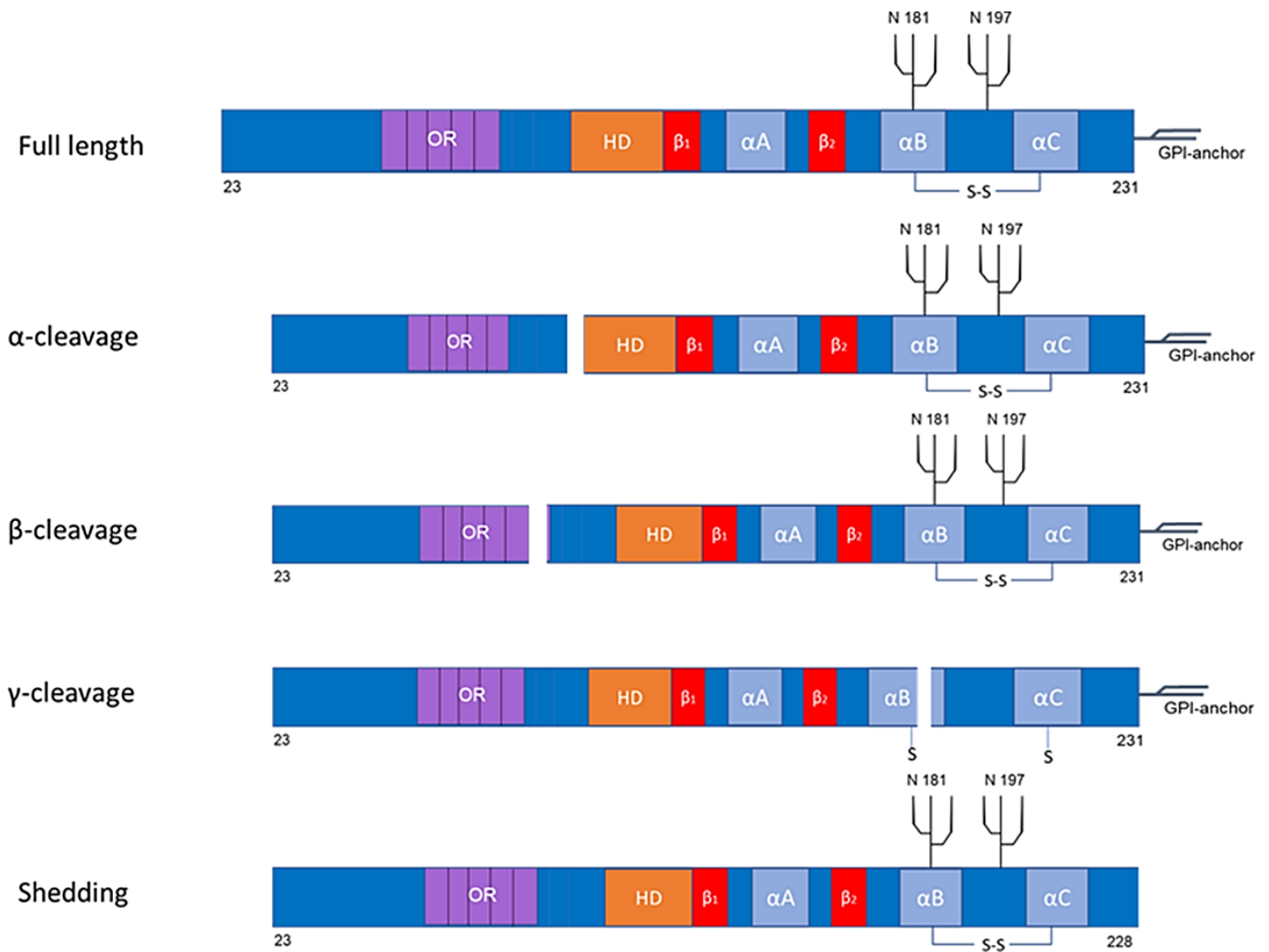


**Figure 1-8. A schematic of proteolytic processing events that have been identified to date.**

PrP<sup>C</sup> (and potentially PrP<sup>Sc</sup>) can go through up to four fragmentation events:  $\alpha$ -cleavage,  $\beta$ -cleavage,  $\gamma$ -cleavage and shedding. The cleavage site and subsequent fragments generated for each cleavage are presented. Residue numberings are based on mouse PrP<sup>C</sup> sequence. Fragmentation of PrP<sup>C</sup> could impact the protein fate in both health and disease conditions. The subsequent fragments produced upon each fragmentation process have different characteristics.

### **1.10 Thesis objectives and goals:**

The common aim of the projects presented in this thesis is application of *in vivo* and *ex vivo* models to study biochemistry of two major proteins involved in proteinopathies of the nervous system, tau and prion protein, in health and disease. In chapter 2, using a series of experiments, I have analyzed the biochemical characteristics of tau species extracted from the brain of a previously developed animal model of genetic tauopathies, with the goal to validate this model as a unique tool to study phenotypic heterogeneities observed in human patients. In chapter 3, using a well-established prion disease animal model, I have assessed the prion protein molecular transition events throughout disease progression, to characterize the key role players in triggering clinical symptoms development. And finally, in chapter 4, I have characterized cellular and molecular details of proteolytic processing of a mutant PrP allele with overt C2-fragmentation, with the goal to use it as a model to study  $\beta$ -cleavage of PrP<sup>C</sup>.

**Chapter 2:** The CNS in inbred transgenic models of 4-repeat Tauopathy develops consistent Tau seeding capacity yet focal and diverse patterns of protein deposition

## 2.1 Introduction

Major questions in neurodegenerative disease research include the origins of sporadic disease, the time-lag before germline mutations in central nervous system (CNS)-expressed genes produce neurological symptoms and the degree of impact of prion-like effects upon CNS dysfunction. All of these issues are germane to diagnostic and therapeutic strategies and all occur in the literature of diseases involving the Tau protein. Primary Tauopathies refer to syndromes with aberrant forms of Tau, a microtubule-associated cytoplasmic protein. While primary Tauopathies include corticobasal degeneration and progressive supranuclear palsy, cases with germline mutations in the Tau gene (*MAPT*) are also notable. These were originally detected in the context of a clinical syndrome referred to as FTLD-*MAPT* (Frontotemporal lobar degeneration linked to *MAPT* gene) (Foster, Wilhelmsen et al. 1997). These *MAPT* mutations included missense mutations in the coding sequence or intronic alterations that shifted the WT steady-state ratio of 3-repeat to 4-repeat spliced forms to lead to more 4R Tau (Hutton, Lendon et al. 1998, Spillantini, Murrell et al. 1998). The term "Tauopathy" has been used as a descriptor for any neurologic syndrome that feature abnormal forms of this protein; for example, Alzheimer's disease (AD) can be considered a secondary Tauopathy where neurofibrillary tangles (NFTs) containing hyperphosphorylated forms of Tau are a hallmark feature, yet where *MAPT* is free of mutations that alter protein structure or spliced forms.

Animal models based on mutated proteins can guide our understanding of pathogenic events and mutant forms of Tau have already been used for over 15 years to create rodent models of neurodegenerative disease (Lewis, McGowan et al. 2000, Götz, Chen et al. 2001). These mice have pathologies that recapitulate those seen in human disease and have been used extensively in preliminary tests of therapies (Phinney, Horne et al. 2003, Gotz, Deters et al. 2007, Li, Ebrahimi et al. 2013). With regards to accuracy in modeling of pathophysiological processes, most neurodegenerative diseases - and specifically frontotemporal dementia (FTD) are not congenital and instead occur with onset in mid to late life. On the other hand, overexpression of transgenes, while convenient to attain fast onset of pathology and shortened durations for experimental studies, can lead to changes in the CNS of adolescents rather than individuals with aged nervous and immune systems. The use of low-expressor mice has been applied to A $\beta$ -related pathologies (Kulnane and Lamb 2001, Saito, Matsuba et al. 2014) and is also of interest in the context of Tau

(Bondulich, Guo et al. 2016). In this vein, we created transgenic (Tg) mice expressing a P301L mutant version of the longest spliced form of human Tau, 2N, 4R [“TgTau(P301L)23027 mice”] at low levels (1.7x endogenous full-length Tau (Murakami, Paitel et al. 2006)]. Because the transgene construct is based on a cDNA clone and lacks introns between protein coding exons, simultaneous production of human 3R and 4R Tau mRNA is eliminated as an operational variable in this model. Denoted for brevity as TgTau<sup>P301L</sup>, these mice develop, albeit slowly, pre-tangles and also a number of florid pathologies including numerous granofibrillary tangles ("GFTs", used to describe accumulations of Tau in astrocytes) and NFT-like structures in the CNS. Besides immunohistochemistry, Tau inclusions in these mice were visualized with Thioflavin S, Gallyas-Braak and Bielschowsky staining procedures (Murakami, Paitel et al. 2006). Notably, motor defects present in some other Tau Tg mice (due to extensive Tau deposition in the spinal cord) are absent in our model. Cell death was noted in TgTau<sup>P301L</sup> mice in the temporal and hippocampal formations thus paralleling cell death widely reported amongst TgTau models (Brion, Ando et al. 2010).

Interestingly, in the original description of this TgTau<sup>P301L</sup> transgenic line, the time of onset of clinical disease differed between Tg colonies derived from the same founder stock yet maintained at different laboratory sites (Okayama and Toronto). Moreover, heterogeneity also existed within cohorts of age-matched Tg mice of the same colony with regards to levels of insoluble Tau and memory function (Murakami, Paitel et al. 2006). Given that phenotypic variation occurs in patients carrying the same P301L mutation (Foster, Wilhelmsen et al. 1997, Mirra, Murrell et al. 1999, van Swieten, Stevens et al. 1999, Tacik, Sanchez-Contreras et al. 2016), we extrapolated that the TgTau<sup>P301L</sup> line might be manifesting a related biological effect and, ultimately, might allow us to understand parameters that dictate phenotypic diversity (Bird, Nochlin et al. 1999).

In studies presented here we have considered two alternative hypotheses to account for this effect. First, that phenotypic heterogeneity reflects the action of genetic modifier loci and can be exacerbated by moving the transgene onto different inbred backgrounds (**Fig. 2.1A**). Second, that phenotypic variations in TgTau<sup>P301L</sup> mice do not reflect the genetic modifier loci but rather reflect stochastic cell biological events and/or environmental inputs. To explore these two hypotheses, we imposed constraints on the original transgenic system wherein the TgTau<sup>P301L(T)</sup>

founder stock was used to create three inbred derivatives. Our studies defined variations in Tau deposition shared between (and independent of) the three inbred genetic backgrounds, thus suggesting the action of extrinsic disease modifiers to trigger stochastic events. Moreover, different biochemical signatures associated with different pathologies strongly imply that these inbred animal models can generate distinct Tau strains.

## **2.2 Experimental Procedures**

### **2.2.1 Animals**

TgTau<sup>P301L</sup> mice and their non-Tg littermates have been previously derived by injections into oocytes from 129/SvEvTac x FVB/J F<sub>1</sub> mice and the Tg offspring bred to 129/SvEvTac mice to enrich for this genetic background. For the studies here, starting with mice sourced from the University of Toronto, back-crosses were continued with 129/SvEvTac mice (N11) to make a congenic derivative (Green 1966, Crusio, Goldowitz et al. 2009). Crosses were also carried out to make an FVB/J congenic derivative (N12). Lastly, we attempted to make a fully congenic derivative using C57BL/6Tac mice but, due to lower fecundity encountered in this background, we achieved an enriched stock after N8 backcrosses. Animals were maintained in ventilated racks (Tecniplast, Green Line) and fed irradiated chow (LabDiets, 5053). They were housed with a 12 hr/12 hr light/dark cycle. Cage environmental enrichment comprised 5 cm diameter plastic tubes and nesting material ("Nestlets", Ancare Inc.). All animal experiments were performed in accordance with local and CCAC guidelines.

For the collection of brains for analysis by the isotropic fractionator technique, animals were anesthetized by isoflurane inhalation, perfused with 25 mL phosphate saline then 25 mL 4% phosphate-buffered paraformaldehyde (PFA) both at a flow rate of 4-5 mL/min. For western blot experiments, mice were sacrificed by cervical dislocation to exclude post-mortem phosphorylation artefacts due to anesthesia-induced temperature changes (Planel, Krishnamurthy et al. 2008). Tissue was immediately extracted, frozen on dry ice and kept at -80 °C until use.

### **2.2.2 Genotyping and genome-wide analysis of SNPs**

For routine genotyping of litters, tail-derived genomic DNA was amplified with primers 1572 = 5'. TGGATCTTAGCAACGTCCAGTCC.3' and Primer 1587 = 5'. CTCTCCTCTCCACAATTATTGACCG.3'. PCR cycle conditions were 94°C 3 min (94°C 20 sec, 55°C 20 sec, 72°C 30 sec) x35, 72°C 7 min, 4°C hold, yielding a diagnostic fragment of 521 bp. For genome-wide analysis of single nucleotide polymorphisms (SNPs), genomic DNA from brain of representative Tg animals of the three backgrounds (backcross numbers indicated as above) were genotyped at 384 dimorphic SNP loci positioned, on average, every 7 Mbp across the mouse genome (Charles River Genome Testing Services, Wilmington, MA). Results are reported as overall divergence and divergence in heterozygous or homozygous state from inbred strain reference standards.

### **2.2.3 Evaluation of disease-related symptoms in aged mice**

To assess clinical manifestation of disease, we produced initial cohorts of 58, 79 and 53 transgenic animals and their littermates (C57BL/6Tac, 129/SvEvTac and FVB/NJ backgrounds, respectively) for aging. In routine health checks, we scored the cohorts with observation periods of up to 750 days of age for kyphosis, tremors, hypokinesia and tail rigidity (present/absent). We then recorded the number of animals manifesting at least three of these symptoms simultaneously on three consecutive days; in the case of weight loss of 20% or more the animals were euthanized. The development of symptoms in Tg animals was irreversible. Non-transgenic littermates were also retained for aging analysis (n= 23, 21 and 23 C57BL/6Tac, 129/SvEvTac and FVB/NJ backgrounds, respectively).

### **2.2.4 Isotropic Fractionator**

The isotropic fractionator method for quantifying neuronal loss in tissue samples was performed as previously described with minor modifications (Herculano-Houzel and Lent 2005). Briefly,

perfused and post-fixed brain samples were mechanically dissociated and homogenized in 10 volumes of a solution of 40 mM sodium citrate and 1% Triton X-100. The homogenates were collected, and the homogenizer washed at least twice to collect any residual cells. To visualize nuclei and obtain total cell counts, 20  $\mu$ L of 100  $\mu$ g/mL stock solution of 4',6-diamidino-2-phenylindole (DAPI, Sigma) was added to the cell suspension and the total number of cells was counted (final concentration of DAPI = 0.20  $\mu$ g/ml). Counting was done in a semi-automated manner: pictures of the quadrants were taken (by a QImaging retiga 2000 camera) and a sub-routine software, adjusted to detect fluorescent signals from stained nuclei (InCell Analyzer software, GE-Healthcare), was used for unbiased counting of the cells. All four quadrants in both the upper and lower grids of the hemocytometer were used for counting and the results were averaged. To determine total neuron counts, 1 mL of each cell suspension was removed, washed with PBS, and centrifuged for 10 minutes at 5000 xg. Cells were then incubated in anti-NeuN antibody (1:200; Millipore) for 2 hours followed by incubation in a secondary anti-mouse IgG-Alexa-Fluor 594 for one hour (1:200; Millipore). Cells were then counted with a hemocytometer using a Nikon eclipse 90i microscope and the percentage of NeuN-stained nuclei was recorded. Total cell numbers and neuronal numbers were then calculated by multiplying the number of cells/mL by the final volume.

### **2.2.5 Quantification of phosphorylated and total Tau protein**

Brain samples were homogenized 10% w/v in 2% sarkosyl phosphate-buffered saline containing 1% protease inhibitor cocktail (Sigma, St. Louis, MO). Total protein concentration in samples was determined by Bicinchoninic Acid assay (Pierce). Twenty  $\mu$ g total protein from each sample was loaded and electrophoresed on a 10% Tris-tricine SDS-PAGE gel. Western blotting was then performed on samples as described below.

### **2.2.6 Extraction of phosphorylated Tau protein**

Fractions of brain were prepared as previously described (Sahara, DeTure et al. 2013). Briefly, tissues were homogenized in 10 volumes of Tris-buffered saline [TBS: 50 mM Tris/HCl (pH 7.4), 274 mM NaCl, 5 mM KCl, 1% protease inhibitor mixture, 1% phosphatase inhibitor cocktail (Sigma) and 1 mM phenylmethylsulfonyl fluoride (PMSF)]. The homogenates were then centrifuged at 27,000  $\times g$  for 20 min at 4°C to obtain supernatant (“SUP1”) and pellet fractions. The pellet was then re-suspended in five volumes of high salt/sucrose buffer [0.8 M NaCl, 10% sucrose, 10 mM Tris/HCl, (pH 7.4), 1 mM EGTA, and 1 mM PMSF] and centrifuged at 27,000  $\times g$  for 20 min at 4°C. The supernatants obtained from this step were collected and incubated with sarkosyl (1% final concentration; Sigma) for one hour at 37°C, followed by centrifugation at 150,000  $\times g$  for one hour at 4°C to obtain salt and sarkosyl-extractable (“SUP3”) and sarkosyl-insoluble (“P3”) fractions. The P3 pellet was re-suspended in TE buffer [10 mM Tris/HCl (pH 8.0), 1 mM EDTA] to a volume equivalent to half of that of the brain specimens used to produce brain homogenates.

### **2.2.7 Western blots**

Western blotting was performed as described previously (Towbin, Staehelin et al. 1979, Murakami, Paitel et al. 2006). Samples were prepared in loading buffer containing SDS and 2-mercaptoethanol and boiled for 10 minutes. They were then electrophoresed on 10% Tris-tricine gels using a BioRad system and transferred to polyvinyl difluoride (PVDF; Millipore) membranes (wet transfer) and blots were then blocked with 5% skim milk in 1xTBS-0.1% Tween 20 for one hour at room temperature and incubated with primary antibodies at 4°C overnight. CP13 (detecting phosphorylated Ser202), CP27 (detecting total human Tau protein) and PHF1 (detecting phosphorylated S396 and Serine 404) antibodies (kind gifts from Dr. Peter Davies, Albert Einstein College of Medicine) were used at 1/500 dilution, while ET3 (detecting 4R Tau residues 273-288) from the same source was used at 1/250 dilution. Membranes were subsequently incubated with secondary antibody (BioRad) at 1/10000 for one hour at room temperature and visualized using enhanced chemiluminescence (ECL, Pierce). Anti-actin antibody (Sigma) was used for quantification blots (1/2000 dilution).

### **2.2.8 Trypsin digestion of sarkosyl-insoluble Tau extracts**

Sarkosyl insoluble fractions (P3) were subjected to trypsin digestion as previously described (Guo, Narasimhan et al. 2016, Taniguchi-Watanabe, Arai et al. 2016) with some modifications. Briefly, reactions were set up using 2-5 ug of P3 fraction (depending on the immunoblot signal intensity observed in non-digested P3 sample) with 1/25 parts sequencing grade trypsin (Pierce) (Except for a few experiments where the the trypsin ratio was different, and the actual ratio is stated in methods). After 30 minutes of incubation at 37°C, the reaction was stopped by addition of sample buffer and boiling for 10 minutes. Samples were then resolved on NuPAGE Novex 4-12% gradient gels and prepared for immunoblotting. ET3 antibody was used for detection of Tau fragments.

### **2.2.9 Immunohistochemistry:**

Each specimen was fixed by immersion in neutral-buffered 10% formalin. Samples were subsequently dehydrated, and paraffin embedded. 6µm sagittal sections were rehydrated and endogenous peroxidase activity was blocked by treatment with 3% hydrogen peroxide for six minutes. After washes, sections were incubated overnight with primary antibody anti-Tau (1:200; ThermoFisher), AT8 (1:200, Thermofisher), MC1 (1:100, Peter Davies), CP27, RZ3 and PHF1 (all at 1:200, Peter Davies), visualized with horseradish peroxidase using the DAKO ARK™ kit according to the manufacturer's instructions. Sections were counterstained using Mayer's hematoxylin, dehydrated and cover-slipped with permanent mounting medium. For Thioflavin-S-staining, following de-paraffination and rehydration, slices were immersed in 0.3% potassium permanganate for five minutes, and the reaction was quenched in a solution containing 1% potassium metabisulfite and 1% oxalic acid. Slices were then immersed in a 0.05% Thioflavin S solution for 30 min. Then the slides were differentiated in 80% alcohol, incubated in phosphate buffer for 30 minutes and counterstained with propidium iodine before mounting. For classification of pathology types, AT8-immunostained sagittal sections 0.72mm lateral to the midline were assessed: a scheme was devised based upon recurring patterns of deposition occurring in 113 brains from aged Tg animals. This scheme was then formalized (See Fig. 5)

and then brains were inspected by one or two further observers blind to the original designations to confirm classification of a given sample. A fraction of the brain samples did not achieve a consensus classification (“other”) because of the coincident appearance of two or more patterns, or because of different morphologies or because there was no AT8 staining.

#### **2.2.10 Homogenate and lysate preparation:**

Hemi-sectioned transgenic mouse brains were stored at  $-80^{\circ}\text{C}$  prior to homogenization. Frozen brains were placed onto a chilled metal block on dry ice and were transected coronally at the level of the midbrain to separate caudal and rostral brain sections (see also Fig. 15). Sections were placed in 1 mL PBS prepared with protease inhibitor tablet (Roche) and were sonicated using a probe sonicator (Omni Sonic Ruptor 400) at 30% pulse/30% power, 20 times, 10-second cycles. The resulting homogenates were centrifuged at  $10,000 \times g$  for 15 minutes at  $4^{\circ}\text{C}$ . and supernatants used for subsequent steps (Sanders, Kaufman et al. 2014). Clone 1, Clone 9, and Clone 10 lysates were prepared as described previously (Sanders, Kaufman et al. 2014). Cell pellets were lysed in 0.1% Triton-X/PBS solution plus protease inhibitor cocktail (“Complete”, Roche) and were clarified with sequential five-minute  $500 \times g$  and  $1000 \times g$  spins. Protein concentrations in brain homogenates and cell lysates were measured by Bradford assay (Bio-Rad) and were normalized to  $5 \mu\text{g}/\mu\text{L}$  and stored at  $-80^{\circ}\text{C}$  until use.

#### **2.2.11 Negative stain electron microscopy:**

Aliquots ( $5 \mu\text{L}$ ) of sarkosyl-insoluble P3 fractions were loaded onto freshly glow-discharged 400 mesh carbon coated copper grids (Electron Microscopy Sciences) and adsorbed for  $\sim 1$  minute. Next, the grids were washed with  $50 \mu\text{L}$  each of 0.1 M and 0.01 M ammonium acetate respectively and negatively stained with  $2 \times 50 \mu\text{L}$  of freshly filtered 2% uranyl acetate. After drying, the grids were examined with a Tecnai G20 transmission electron microscope (FEI Company) using an acceleration voltage of 200 kV. Electron micrographs were recorded with an Eagle 4k x 4k CCD camera (FEI Company). The morphology of individual Tau filaments was

readily visible and classified into "straight filaments", "coiled filaments", and "twisted ribbon-like filaments".

#### **2.2.12 Cell culture:**

Clone 1 cells (monoclonal HEK293 cells stably expressing Tau RD P301L/V337M-YFP, described previously (Sanders, Kaufman et al. 2014)), were cultured in Dulbecco's modified Eagle's medium (Gibco) supplemented with 10% fetal bovine serum (HyClone), 1% penicillin/streptomycin (Gibco), and 1% Glutamax (Gibco). Cells were maintained and passaged in 10 cm dishes at 37°C, 5% CO<sub>2</sub>, in a humidified incubator.

#### **2.2.13 Transduction of homogenates into Clone 1 cells:**

Clone 1 cells were plated at 100,000 cells/well in 24-well plates. 18 hours later, cells were transduced with brain homogenates or cell lysates packaged into liposomes. Liposomes were prepared as follows: 100 µg of clarified homogenate was combined with OptiMEM (Gibco) to a final volume of 50 µL. 48 µL OptiMEM and 2 µL lipofectamine-2000 (Invitrogen) were then added to the OptiMEM/lysate mixture to a final volume of 100 µL. After a 15-minute incubation, liposome preparations were added to the cells. 18 hours later, cells were washed, trypsinized, and re-plated into 6-well plates. At confluency (96 hours following the original lysate transduction), cells were passaged onto coverslips in 24-well plates. 120 hours following transduction, cells were fixed with 3% PFA, washed once with PBS and stained with DAPI (1:1000 diluted from 1 mg/mL stock) in 0.1% Triton-X/PBS for 10 minutes. DAPI solution was replaced with PBS and coverslips were mounted using ProLong Gold Antifade Reagent (Life Technologies) and sealed with nail polish. Prior to imaging, mounted coverslips were stored at 4°C.

#### **2.2.14 Confocal analysis of seeded Clone 1 cells:**

Confocal microscopy was performed using a Zeiss LSM 780 PASCAL system coupled to a Zeiss Axiovert 200M microscope. A pinhole size of 0.8  $\mu\text{m}$  was used for the collection of all images. The imager was blinded to the identity of the samples to avoid bias in selection of representative fields of cells.

### **2.2.15 Data analysis**

Departures from normal distribution were checked using the Kolmogorov-Smirnov (K-S) goodness of fit test. A general linear model of factorial ANOVA (Statistical Package for Social Sciences, SPSS v.22, Inc. Chicago), with genotype, line/genetic background as between subject factors, or repeated measures analysis of variance (RMANOVA) with the type of cell count (total cell and neuronal counts) as within subject factors were used to analyze the data. Eta squared ( $\eta^2$ ) was used to estimate the effect size, i.e. the proportion of variance associated with each of the main effects and interactions. Bonferroni adjustment of  $\alpha$  level (MODLSD Bonferroni t-tests, SPSS v22) was applied in multiple planned comparisons. In the case when data represented discrete category measures on a nominal scale and did not meet the assumption of parametric statistics, a  $\chi^2$  test of independence was used to test for homogeneity between the groups.

### **2.2.16 Trypsin digestion of sarkosyl-insoluble Tau extracts and in-gel analysis:**

Sarkosyl insoluble fractions (P3) were subjected to trypsin digestion as previously described (Bondulich, Guo et al. 2016, Taniguchi-Watanabe, Arai et al. 2016) with some modifications. Reactions were set up on 5  $\mu\text{g}$  of protein from a P3 fraction depending on the protein concentration of the samples with sequencing grade trypsin (Pierce), with trypsin/protein ratio adjusted for 1/25 (unless stated otherwise). After 30 min of incubation at 37°C, the reaction was stopped by addition of sample buffer and boiled for 10 min. Samples were western blotted using ET3 antibody. For in-gel digestion of sarkosyl-insoluble material, each lane of trypsin-digested P3 material was separated into strips. The samples were transferred to a round bottom 96 well

plate and 150  $\mu$ L of destaining solution (50 mM ammonium bicarbonate, 50% acetonitrile) were added into each well. The plate was incubated for 10 min at 37°C. The solution was removed from the wells and the destaining step was repeated 3-4 times. The solution was removed and replaced by acetonitrile. The samples were incubated again at 37°C until the gel bands became white. The remaining acetonitrile was removed, and the samples were dried at 37°C for 10 min. The samples were rehydrated with 175  $\mu$ L of reducing solution (100 mM ammonium bicarbonate and 5 mM  $\beta$ -mercaptoethanol) and incubated for 30 min at 37°C. After that, the reducing solution was removed and 175  $\mu$ L of alkylating solution (10 mg/mL of iodoacetamide and 100 mM ammonium bicarbonate) were added. Samples were incubated for 30 min at 37°C. The gel bands were subsequently washed with 175  $\mu$ L of 100 mM ammonium bicarbonate and incubated for 10 min at 37°C. The samples were then incubated for 10 min at 37°C in acetonitrile. Once the gel pieces became white, acetonitrile was removed, and the samples were dried at 37°C for 10 min. The protein samples were then digested with 50  $\mu$ L of digestion buffer (50 mM ammonium bicarbonate and 20 ng/ $\mu$ L of trypsin, Promega inc.). The solutions containing tryptic peptides were transferred to a V-bottom 96-well plate. Tryptic peptides were further extracted from the gel with 2% acetonitrile and 1% formic acid followed by incubation at 37°C for 1 h. The extraction was repeated using 50% acetonitrile and 0.5% formic acid followed by incubation at 37°C for 1 h. The samples were freeze-dried under vacuum overnight. The peptides recovered from some of the wells were combined to generate a total of 8 fractions. The eight fractions covered between 250 and 75 kDa (F1), 75 to 60 kDa (F2), 60 to 50 kDa (F3), 50 to 37 kDa (F4), 37 to 25 kDa (F5), 25 to 20 kDa (F6), 20 to 15 kDa (F7) and 15 to 8 kDa (F8). The samples were resuspended in 0.2% formic acid before analysis by LC-MS/MS.

### **2.2.17 Mass spectrometry:**

Peptides were analyzed using a nanoflow-HPLC (Thermo Scientific EASY-nLC 1000 System) coupled to the Q-Exactive (Thermo Fisher Scientific) mass spectrometer. A trap column (5  $\mu$ m, 100  $\text{\AA}$ , 100  $\mu$ m x 2 cm, Acclaim PepMap 100 nanoViper C18; Thermo Fisher Scientific) and an analytical column (3  $\mu$ m, 300  $\text{\AA}$ , 75  $\mu$ m x 15 cm, PepMap RSLC C18; Thermo Fisher Scientific) were used for the reverse phase separation of the peptide mixture. Peptides were eluted over a

linear gradient over the course of 90 min from 0% to 95% acetonitrile in 0.2% formic acid. Data analysis was performed using ProteinDiscoverer (v1.4.1.14) software against a Tau mouse wt sequence and the Tau P301L mutant (sequences downloaded from <https://www.uniprot.org/uniprot/P10637>). Search parameters included two missed trypsin cleavages, a precursor mass tolerance of 10 ppm, a fragment mass tolerance of 0.01 Da, carbamidomethylation of Cys (static modification), and oxidation of Met and Deamidation of Asn and Gln (dynamic modifications). A decoy database search was performed to evaluate the false-positive rates. The strict target false discovery rate was set at 0.01 and the relaxed FDR was set at 0.05. Results reported include only the peptides identified at medium and high confidence.

### **2.2.18 Dephosphorylation of phospho-tau by lambda phosphor-protein phosphatase (lambda PP):**

To dephosphorylate the phospho-tau protein species, 10 ug of total protein from soluble brain fraction (SUP1) was incubated with 0.2 ug of lambda PP at 37°C for 2 hours. To minimize the possibility of protein degradation by naturally present proteases in brain homogenate, 1 ul of 10X protease inhibitor cocktail was added to each reaction. The reaction volume was then set up to 10 ul. Finally, the reaction was stopped by addition of sample buffer and boiling at 95°C for 10 minutes.

## **2.3 RESULTS**

### **2.3.1 Genetic profiles and Tau expression in sublines of TgTau<sup>P301L</sup> mice.**

After a series of backcrosses of a TgTauP301L founder stock (**Fig. 2.1A**) genomic DNA from an individual of each inbred derivative sub-line (C57BL/6Tac, 129/SvEvTac or FVB/NJ) was analyzed in a genome-wide 384 single nucleotide polymorphism (SNP) array versus reference standards. For the tested samples, the "call rate" for scoring polymorphisms on the array was between 98.2% and 99.7% (**Table 2.1**) with the positions of the residual unscored SNPs not being shared by the three inbred derivatives. For called loci each Tg subline yielded 99.2% or higher values for being a homozygous or heterozygous match to SNPs in the reference genome (**Table 2.1**); these data indicate incipient congenic status for the 129/SvEvTac and C57BL/6Tac

sublines and congenic status for the FVB/NJ sub-line (99.87% match, 99.9% desired). For 21 scored variations from the inbred strain reference standards, only two SNP variants were shared by different backgrounds: (i) VF at position Chr01-26 in Tg mice versus VV expected in the 129/SvEvTac and FVB reference samples (where V and F refer to the two fluorescent dyes used for tagging allele-specific oligonucleotides) and (ii) VF in Tg mice instead of FF at position Chr07-05 in 129/SvEvTac and C57BL/6 versus reference samples. Overall, these data confirm matching between the three inbred Tg sublines with respect to reference genomic DNAs and that residual distinctions are dispersed across the mouse genome in chromosomes 1, 5, 7 and 14.

The parental Tg line was notable for a low level of transgene expression (previously estimated at 1.7x endogenous); to verify that this parameter was unaltered by the series of back-crosses, we quantitated western blot analyses on brain material of young, 90-day old mice from the three inbred sublines, to measure levels of total tau (i.e., endogenous tau plus human tau) (**Fig. 2.1B**). Considering transgene-encoded tau measured with an anti-human tau CP27 antibody, we did not detect significant differences in steady-state expression levels (**Fig. 2.1C**) between the three genetic derivatives. While histological analysis with CP27 antibody specific for human tau was not above background for non-Tg mice (as anticipated), similar patterns of dispersed immunoreactivity were present in each of the congenic or incipient congenic derivatives (**Fig. 2.1D**). These data are compatible with the broad pattern of neuronal expression associated with the parental Syrian hamster prion protein gene (Kretzschmar, Prusiner et al. 1986) and seen in other Tg lines made with the cos.Tet expression vector derived from this gene (Scott, Groth et al. 1993, Chishti, Yang et al. 2001).

Derivative line	Backcrosses (gender)	# SNP assays	Call Rate (%)	% match to reference		
				Overall	Full	Half
129/SvEvTac	12 (M)	384	98.2	99.2 <sup>a</sup>	98.4	1.6
FVBN/J	11 (F)	384	98.7	99.9 <sup>b</sup>	99.7	0.3
C57BL/6Tac	8 (M)	384	99.7	98.6 <sup>c</sup>	99.2	0.8

**Table 2-1. Single Nucleotide Polymorphism (SNP) profiling of congenic and incipient congenic lines.**

<sup>a</sup>distinctions from reference genome located at positions chr 01-26, chr 07-05, 7-19 and chr 14-05; <sup>b</sup>distinctions from reference genome located at position chr 01-26; <sup>c</sup>distinctions from reference genome located at positions chr 01-05, chr 05-19, and 14-03. "Full" indicates a homozygous match to reference, "half", a heterozygous match to reference.

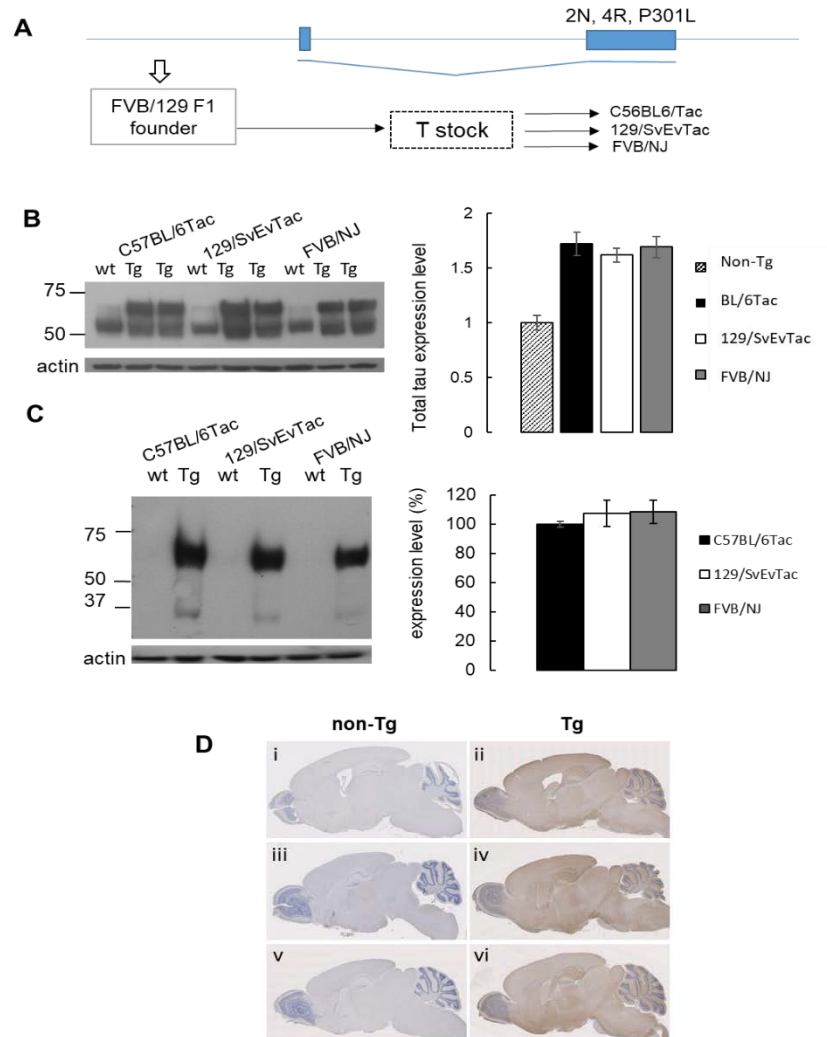


**Figure 2-1. Total human Tau and total phosphorylated Tau in 3 congenic strains of TgTauP301L mice.**

A schematic of the cosmid transgene and derivation of a founder Tg line (open arrow). A Toronto breeding stock (T, indicated by dashed square) was used to generate three inbred derivatives. In panels b and c, brain homogenates of Tg mice from all 3 congenic strains and controls were analyzed for total Tau and total human Tau expression levels using western blot. **B** A representative blot showing total Tau expression in Tg mice of all congenic strains and control animals. Graph represents relative expression levels of total Tau normalized to actin loading control and then compared to control non-Tg mice  $n=2$  Tg sample per inbred stain with values for non-Tg sample pooled from the three strains and assigned the value "1.0". Antibody is DA9:1/500). TgTau<sup>P301L</sup> mice have ~ 1.7X Tau expression level (1.77, 1.61, 1.69 for C57BL/6Tac, 129/SvEvTac and FVB/NJ respectively) compared to controls. **C** A representative blot showing total human Tau expression level in Tg mice and controls. Graph represents total human Tau expression levels in transgenic mice of all 3 congenic strains ( $n=3$  each) normalized to C57BL/6Tac (100%; antibody CP27, 1/500). **D** Total human Tau distribution (CP27) in brain of Tg mice (280-324 days old) from C57BL/6Tac (ii), 129/SvEvTac (iv) and FVB/NJ (vi) backgrounds, with corresponding non-Tg animals shown in panels i, iii and v.

We next analyzed fractionated brain samples in all three genetic backgrounds to determine relative levels of hyperphosphorylated Tau species (64-68 kDa) in a standard procedure to yield TBS-extractable (SUP1), salt and sarkosyl-extractable (SUP3) and sarkosyl-insoluble (P3) fractions. **Figure 2.2** shows western blots of fractionated brains of Tg mice at 90 and 240 days of age versus non-Tg littermates (“WT”). Using the CP13 antibody, an antibody that also detects endogenous mouse Tau species, at 90 days, the P3 fraction was not populated with phosphorylated Tau species in any of the three genetic backgrounds. This situation altered at a 240-day time point wherein the human transgene encoded species became visible in the P3 fraction of each subline. Thus, an accumulation of insoluble Tau species was apparent comparing 90 and 240-day time-points in asymptomatic mice of all three genetic backgrounds.

### **2.3.2 Neurologic symptoms and Tau species in aged Tg mice.**

Tg mice were scrutinized for neurological signs of disease as they approached and entered their second year of life, with the presence of three simultaneous signs of disease required for a score. Using initial cohorts of 58, 79 and 53 transgenic animals (C57BL/6Tac, 129/SvEvTac and FVB/J backgrounds, respectively) surviving over 240 days and observation periods of up to 750 days, all three genetic backgrounds presented with signs of neurologic disease (**Fig. 2.3**), albeit with incomplete penetrance (34.4%, 20.2% and 28.3%, respectively). Symptomatic presentation occurred in a different manner from progressive age-related losses scored in non-Tg littermates (and documented from large-scale breeding studies of inbred strains (Russell 1975)). Mean elapsed times for onset of symptoms (days)  $\pm$  SD corresponded to  $543.8 \pm 123.4$ ,  $582.4 \pm 74.6$  and  $509.8 \pm 96$  for Tg lines maintained on C57BL/6Tac, 129/SvEvTac and FVB/NJ genetic backgrounds and were not different between groups ( $\chi^2(2) = 5.5$ ,  $p = 0.06$ ).

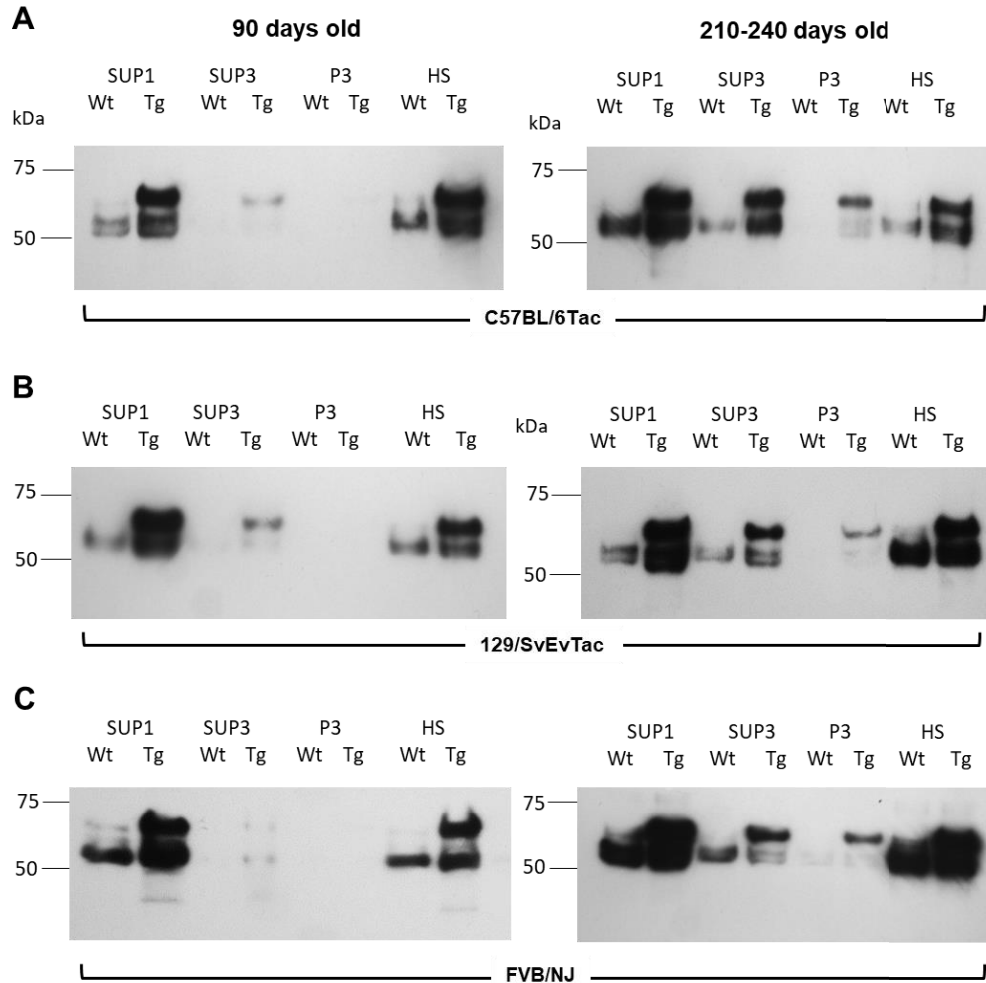


**Figure 2-2. Presence of phosphorylated Tau species in fractionated brain of 90- and 240-days old mice from 3 genetic backgrounds.**

Half brains of TgTau<sup>P301L</sup> mice and non-Tg littermate controls were subjected to fractionation and presence of phosphorylated Tau species were investigated in different fractions. Samples from three inbred strains were obtained from mice that were euthanized at 90 and 210-240 days of age, as indicated. **A)** C57BL/6Tac, **B)** 129/SvEvTac, and **C)** FVB/NJ. In each case, 10 µg of total protein was separated by gel electrophoresis and immunoblotted. Antibody: CP13 (1/500; phosphoserine 202). SUP= Supernatant and P= pellet fractions.

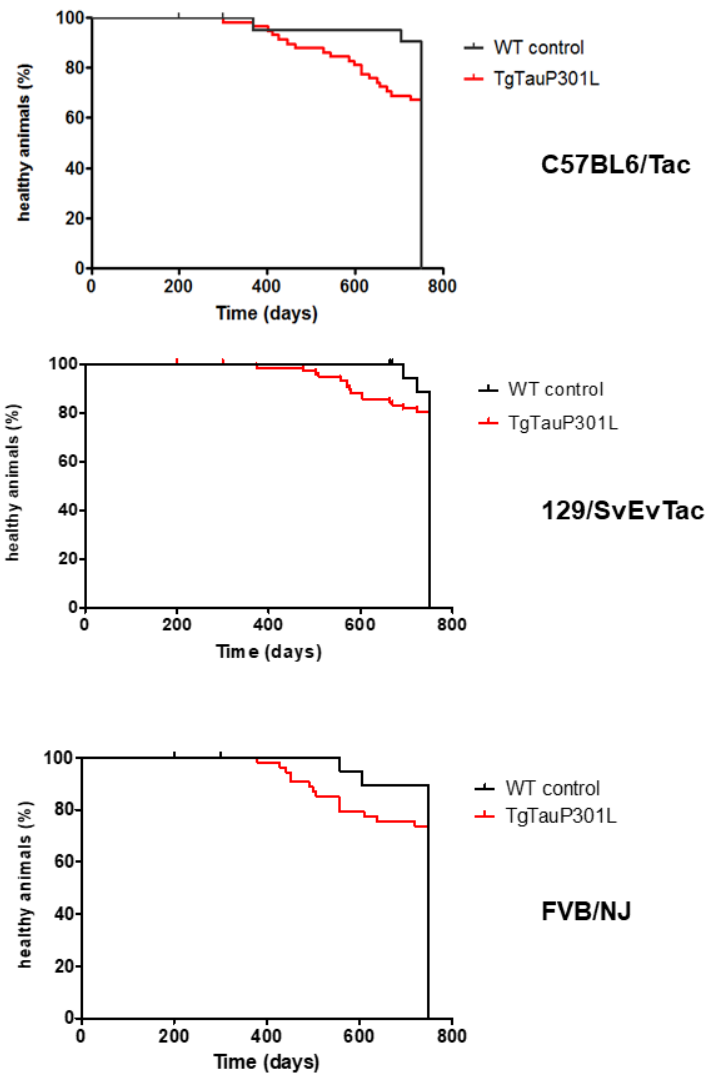


**Figure 2-3. Appearance of disease-associated symptoms in TgTauP301L mice three genetic backgrounds.**

Time points when disease-associated symptoms were apparent in animals are presented alongside the performance of non-Tg littermates. Survival curves of non-Tg littermates of Tg animals are represented as well. The symptoms recorded for Tg animals are specific for them and none of the non-Tg littermates manifest such symptoms. Non-Tg animals live up to ca. 750 days, however a few animals succumb to natural deaths or have health problems (such as dermatitis or eye infection), requiring euthanasia to be performed. The number of cohort sizes for each group (n) are represented within each graph. All sample groups were terminated at 750 days.

### 2.3.3 Quantification of neuronal loss in aged TgTau<sup>P301L</sup> mice.

Earlier characterization of TgTau<sup>P301L</sup> mice in the Okayama cohort demonstrated brain atrophy in 540 days old animals, loss of CA1 and CA2 neurons and thinning of the CA3 cell layer (Murakami, Paitel et al. 2006). We investigated this issue in the newer iterations of this model using the isotropic fractionator technique (Herculano-Houzel, von Bartheld et al. 2015), a quantitative method reported as having similar accuracy to unbiased stereology (Miller, Balaram et al. 2014, Herculano-Houzel, von Bartheld et al. 2015). We used a total of 42 aged mice from all three congenic lines for this purpose: 14 of FVB/NJ line (7 nTg (4♂/3♀) and 7 Tg (3♂/4♀)), 14 of 129SvEv (7 nTg (3♂/4♀) and 7 Tg (5♂/2♀)), and 14 of C57BL/6 line (7 nTg (4♂/3♀) and 7 Tg (5♂/2♀)). The average age was  $547.8 \pm 13.2$ ,  $711.4 \pm 5.7$ , and  $658.7 \pm 15.1$  days for the FVB/NJ, 129/SvEvTac, and C57BL/6Tac cohorts, respectively. The distribution of age ranges of 129 and B6 lines was normal, but it was negatively skewed towards older age range (skewness = -0.243) for the FVB line ( $D(14) = 0.243$ ,  $p < 0.05$ , K-S one-sample test). The comparison of the age between the strains (genetic background), genotype and sex revealed significant strain effect ( $F(2,30) = 40.8$ ,  $p < 0.001$ ) with no other factors and interactions being significant at  $\alpha = 0.05$ . *Post hoc* comparisons revealed that 129 mice were older than C57BL/6Tac ( $p < 0.05$ ), and both C57BL/6Tac and 129/SvEvTac were older than FVB/NJ ( $p < 0.001$ , MODLSD Bonferroni t-tests). Next, we compared the weights of hemi-brains used for the quantification of neurons. The comparison revealed no differences due to strain, genotype or gender sex (data not shown). Also, none of second and third order interactions between the factors was significant at  $\alpha = 0.05$ . To avoid potential bias in the analyses of cell and neuronal counts between strains and genotypes due to existing subtle (not significant) differences in age ranges and brain weights, we investigated the relationships between age and brain weight, and total cell and neuronal cell counts. Since neither bivariate Pearson nor partial correlations, the latter controlling for the strain effects, revealed significant associations between the two independent variables and total cell or neuronal counts (data not shown), we did not include the age or brain weight as covariates in the analyses. Also, since the representations of males and females in some strain and genotype cohorts was small (2-3 mice per cell in most cases) and the preliminary data screen analyses revealed no significant effects of sex or interactions involving sex, we pooled that data across gender. Overall analysis of total cell and neuronal counts revealed a significant genotype effect

( $F(1,36) = 20.6$ ,  $p < 0.001$ ,  $\eta^2 = 0.36$ , RMANOVA), cell type count ( $F(1, 36) = 2330.7$ ,  $p < 0.001$ ,  $\eta^2 = 0.99$ ), and cell type count by genotype interaction ( $F(1, 36) = 12.5$ ,  $p = 0.001$ ,  $\eta^2 = 0.26$ ). None of the other factors or interactions were significant at  $\alpha = 0.05$ . *Post hoc* analysis revealed no significant strain effects or strain by cell type interaction for non-transgenic and TgTau<sup>P301L</sup> mice (data not shown), indicating that the significant genotype effect was due to the differences in the cell number between nTg and TgTau<sup>P301L</sup> mice, and not being affected by the strain of the line or interactions involving strain (**Fig. 2.4**).

Analysis of total cell counts revealed no significant effects of strain, transgenotype or the interaction between the factors (data not shown). However, there was a significant transgenotype effect ( $F(1, 36) = 44.9$ ,  $p < 0.001$ ,  $\eta^2 = 0.56$ ), with TgTau<sup>P301L</sup> mice having overall fewer neurons than their non-Tg littermates ( $85.4 \pm 2.4$  versus  $108.3 \pm 2.4$  per gram of brain wet weight, respectively). The average number of neurons per gram of brain weight, detected by means of counting NeuN positive nuclei (which is a nucleus marker specific to neuronal cells), is presented in **Fig. 2.4**. The comparison between the genotypes within each genetic background revealed a consistent finding that TgTau<sup>P301L</sup> mice had significantly lower number of neurons ( $t(12) = 2.3$ ,  $p < 0.05$ ,  $t(12) = 4.6$ ,  $p = 0.001$ , and  $t(9) = 6.3$ ,  $p < 0.001$  for C57BL/6Tac, 129/SvEvTac and FVB/NJ backgrounds, respectively (degrees of freedom for FVB mice were adjusted due to inequality of variances). Thus, on average, the three genetic backgrounds did not affect the degree of neuronal loss manifested by aged TgTau<sup>P301L</sup> mice. It is noteworthy to mention that the number of total brain cells as well as neurons obtained from non-Tg mice is in close proximity with previously reported values in laboratory mice (*Mus musculus*) (Herculano-Houzel, Mota et al. 2006, Brautigam, Steele et al. 2012).

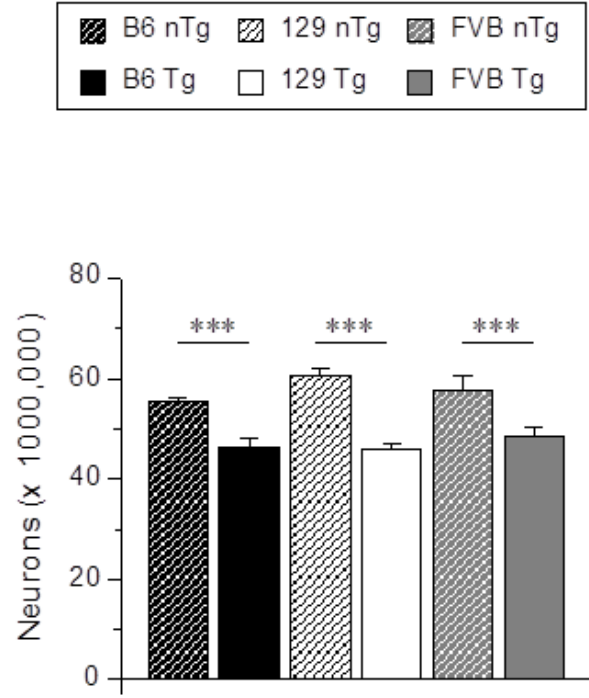


**Figure 2-4. Quantification of neurons in whole brain of aged TgTauP301L and non-Tg littermate mice.**

Total number of neurons in TgTau<sup>P301L</sup> and non-transgenic mice. \*\*\* p < 0.001. n=7 for all genotypes.

### 2.3.4 Heterogeneity in Tau pathologies.

We next used histological analysis to see if the performance of the three inbred Tg derivative lines diverged as they aged. For this purpose, we used the AT8 anti-Tau antibody, a reagent highlighted in a consensus meeting for the diagnosis of FTD (Mott, Dickson et al. 2005) and also used in the characterization of Tau strains in inoculation experiments (Kaufman, Sanders et al. 2016)). Regarding Tg mice sampled in the range of 450-758 days of age, heterogeneity was manifest in several effects. From a sample of 113 AT8-positive aged TgTau<sup>P301L</sup> mice, we encountered heterogeneities in deposition (**Table 2.2**). Of these, 84 brains were provisionally classified as belonging to one of five different categories, as scored by independent observers (**Fig. 2.5-2.9**). The five categories were present in each genetic background, with the exception of Class V, which lacked an example from FVB/NJ mice. To assess if the predominant categories (I-III) might represent different steps in a synchronous process, we examined their average ages of onset but here no pair-wise comparisons for sample groups >5 within the same inbred strain type reached significance (**Table 2.2**). Pooled across genetic backgrounds categories I-III were represented by both genders in a 1:15 ratio (32 females, 37 males).

The features that formed the basis of this classification scheme are detailed in the following manner. **Class I** has striatal staining that includes mature NFT's in the caudate and GFT's in the hippocampal formation (**Fig. 2.5**). Cortical staining is minimal. **Class II**: this is the most common class, representing close to half of the animals examined, having predominance of pathology in the frontal cortex but with staining in this area being augmented in other animals with striatal and hippocampal staining (as per Class I) and eventually encompassing all ventral brain areas (**Fig. 2.6**). This pattern of deposition resembles mice in our first description of the TgTau<sup>P301L(T)</sup> line (Murakami, Paitel et al. 2006). **Class III**: this manifestation is defined by immunoreactivity in the pons and/or medulla occurring in addition to Class II reactivity (**Fig. 2.7**). **Class IV** represents a caudal pattern of deposition with rostral areas spared (**Fig. 2.8**) while in **Class V** animals this pattern is augmented by numerous GFTs in the molecular layer of the hippocampus (**Fig. 2.9**). Amongst mouse brains which did not fit within these classes, several exhibited strikingly focal patterns of deposition with the rest of the brain completely spared; five such patterns of focal deposition in corpus callosum, the retrosplenial area, the locus coeruleus,

the inferior colliculus and the cerebellar white matter tract are presented in **Fig. 2.10**. Beyond AT8 antibody, we used conformation, phospho, and sequence dependent antibodies (MC1, PHF1, CP27 and RZ3) to re-examine brain sections from the five canonical classes (**Fig 2.11-2.27**). These analyses yielded generally similar results, albeit with a tendency for MC1 to yield superior signals in brain stem pathologies.

<sup>a</sup> Genetic background (n ♀, ♂)	<sup>b</sup> Pathology Class				
	average age in days ± SD (n ♀, ♂)				
	I	II	III	IV	V
<b>C57BL/6Tac</b> (44,35)	<sup>c</sup> 603 ± 96 (5,6)	<sup>c</sup> 612 ± 65 (9,9)	<sup>c</sup> 611 ± 70 (24,10)	526 ± 42 (4,7)	609 ± 55 (2,3)
<b>129/SvEvTac</b> (48,53)	597 ± 97 (3,2)	<sup>d</sup> 600 ± 84 (8,13)	<sup>d</sup> 628 ± 81 (25,25)	546 ± 38 (7,4)	597 ± 72 (5,9)
<b>FVB/NJ</b> (34,29)	<sup>c</sup> 526 ± 65 (5,13)	<sup>c</sup> 571 ± 73 (5,5)	<sup>c</sup> 601 ± 88 (12,6)	513 ± 72 (9,3)	510 ± 56 (3,2)
<b>Trypsin-resistance pattern (n/N)</b>	A (3/6)	A (7/8)	B (6/7)	C (4/4)	C (2/2)

**Table 2-2. Pathology classes were based upon the location of AT8 antibody immunostaining.**

<sup>a</sup>C57BL/6Tac age-range = 451-758 days; 129/SvEvTac age-range = 466-733 days; FVB/NJ age-range = 451-678 days. Aged animals lacking pathology are not included in this Table but are described in the main text. <sup>c,d,e</sup> All pair-wise comparisons of mean age within a genetic background n.s. For trypsin-resistant pattern, n= number of animals presenting that pattern and N= number of all samples processed from that specific class. The inbred strain distribution of mice trypsin resistant core patterns A, B or C was 7, 13, 11 (n=31) for C57BL/6Tac, 129/SvEvTac and FVB/NJ, respectively. One sample each from classes I, II and III had no detectable signal while 4 animals with unclassified patterns of focal Tau deposition had trypsin-resistant signature of pattern C. \* 2/6 mice had trypsin-resistant signature of pattern C.

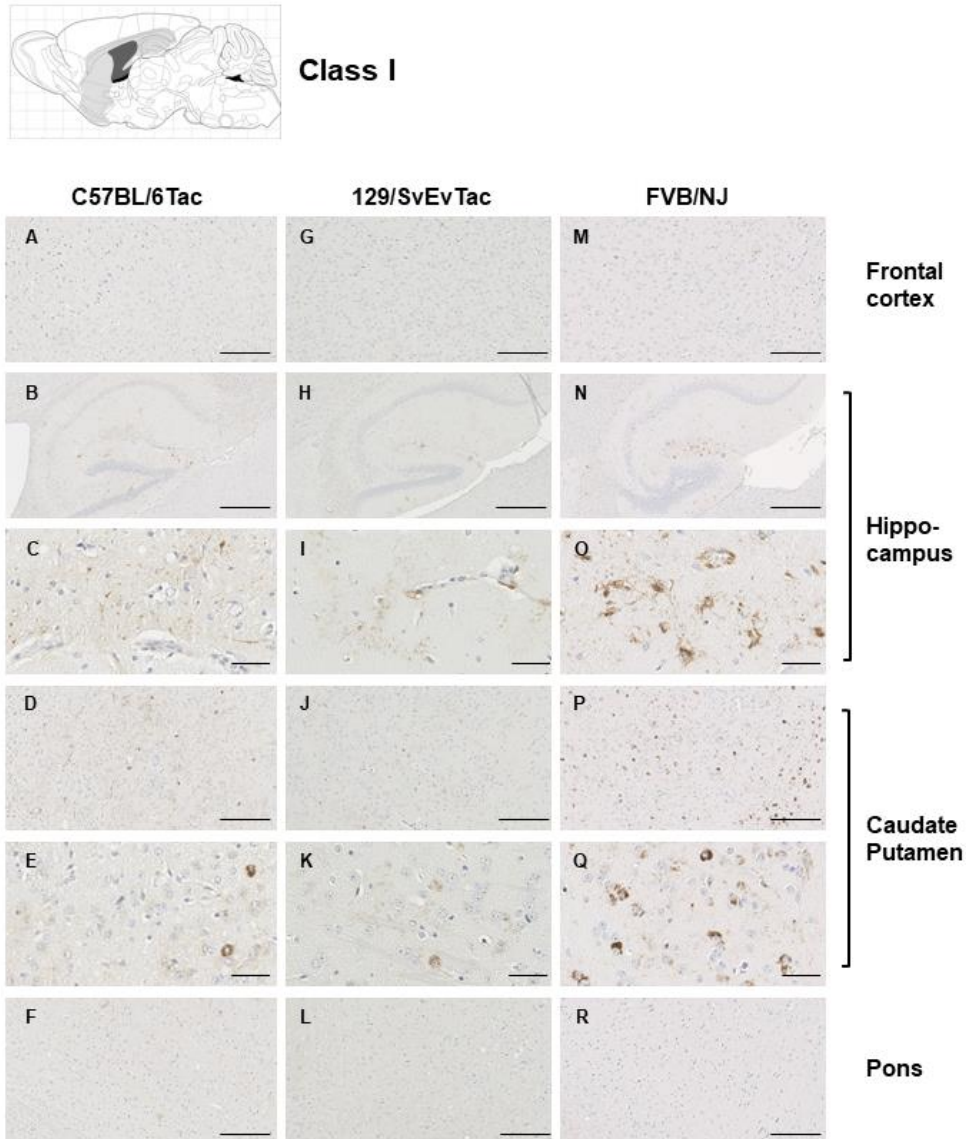


**Figure 2-5. Class I Tau pathology.**

Immunostaining with the phosphorylation-dependent anti-Tau antibody AT8 in the brain of TgTau mice illustrating the different patterns of deposition. Three different genetic backgrounds are represented C57BL/6J (panels A to F); 129/SvEvTac (panels G to L) and FVB/NJ (panels M to R). Several structures characteristic of the pattern of deposition are shown: while the frontal cortex is negative (panels A, G, M), the hippocampus (“Hpc”, panels B, C, H, I, N, O) exhibits GFT’s and occasional NFT’s, the caudate putamen (D, E, J, K, P, Q) exhibits NFT’s while the Pons (panels F, L, R) is negative for immunostaining.

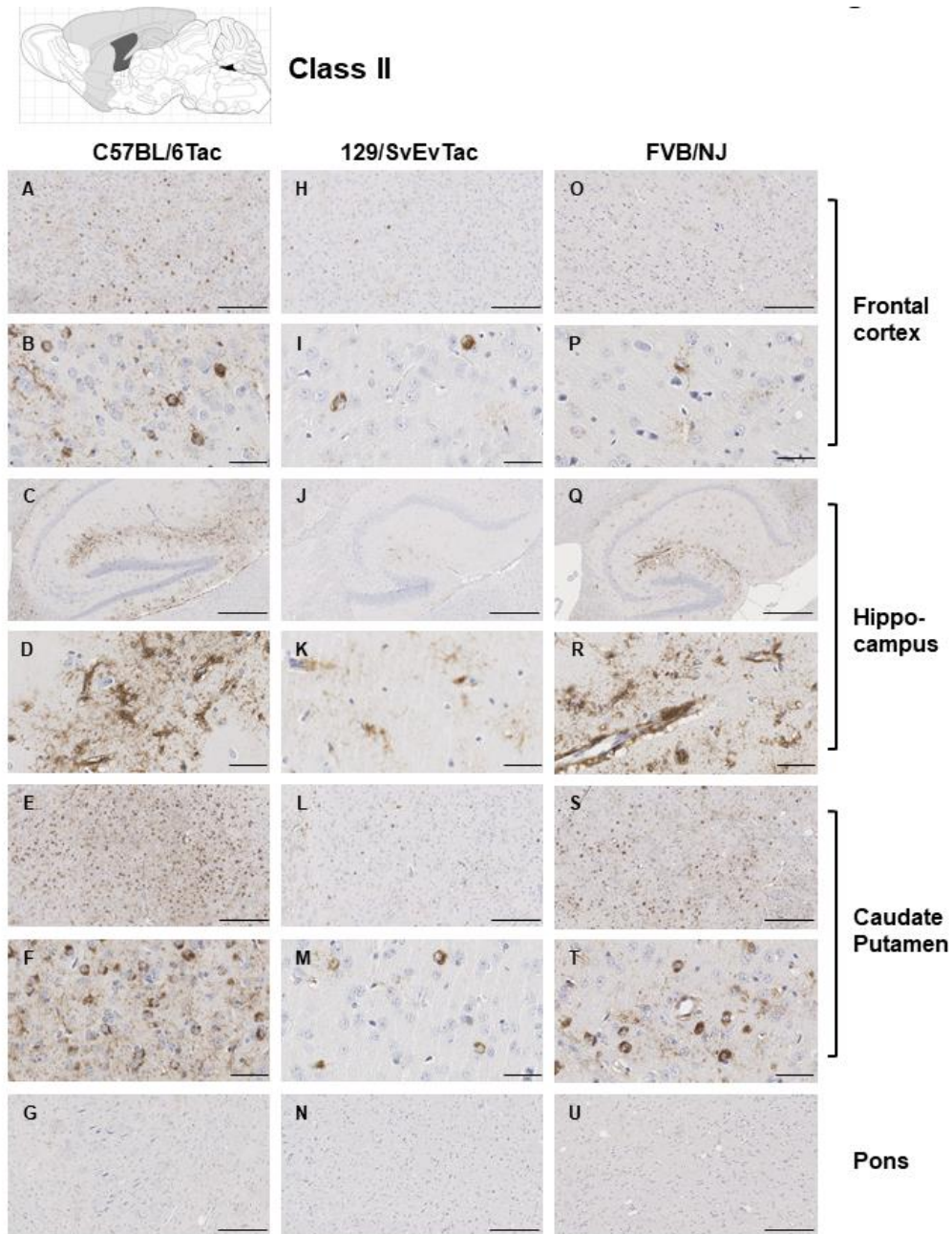


**Figure 2-6. Class II Tau pathology.**

Three different genetic backgrounds have been studied with AT8 antibody as per Fig. 4. In distinction to class I there is staining in the cortex corresponding to NFT's and GFT's (A, H, O, B, I, P) but like class I has staining in hippocampus (panels C, J, Q, D, K and R) and caudate putamen (panels E, L, S, F, M, T), with the pons being spared (G, N, U). Scale bar = 500  $\mu$ m for panels C, J and Q. Scale bar = 250  $\mu$ m for panels A, E, G, H, L, N, O, S and U. Scale bar = 50  $\mu$ m for panels B, D, F, I, K, M, P, R and T.

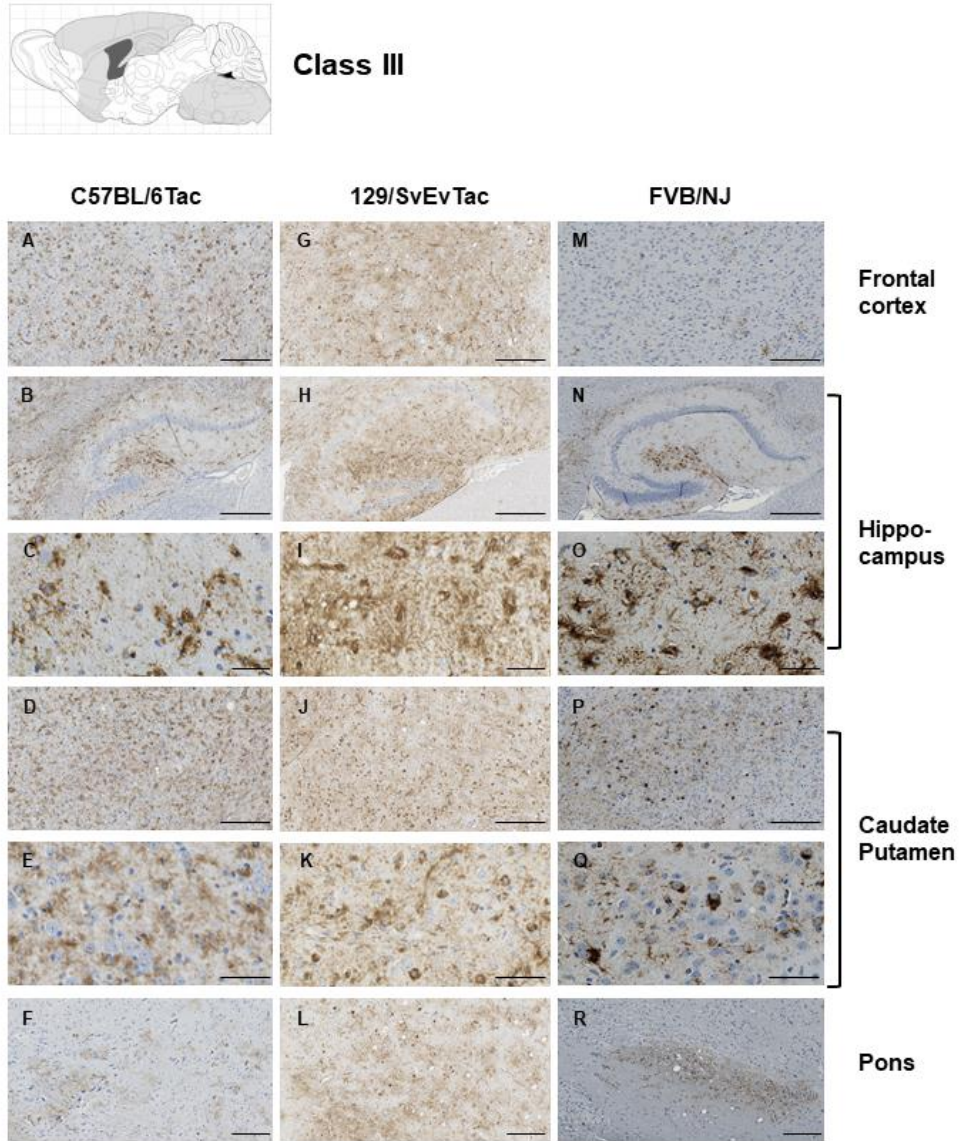


**Figure 2-7. Class III Tau pathology.**

Different genetic backgrounds and anatomical structures have been studied with AT8 antibody as per Fig. 4. The distinction from class I and II is the involvement of the pons (F, L, R). Scale bar = 500  $\mu\text{m}$  for panels B, H, and N. Scale bar = 250  $\mu\text{m}$  for panels A, D, F, G, J, L, M, P, and R. Scale bar = 50  $\mu\text{m}$  for panels C, E, I, K, O, and Q.

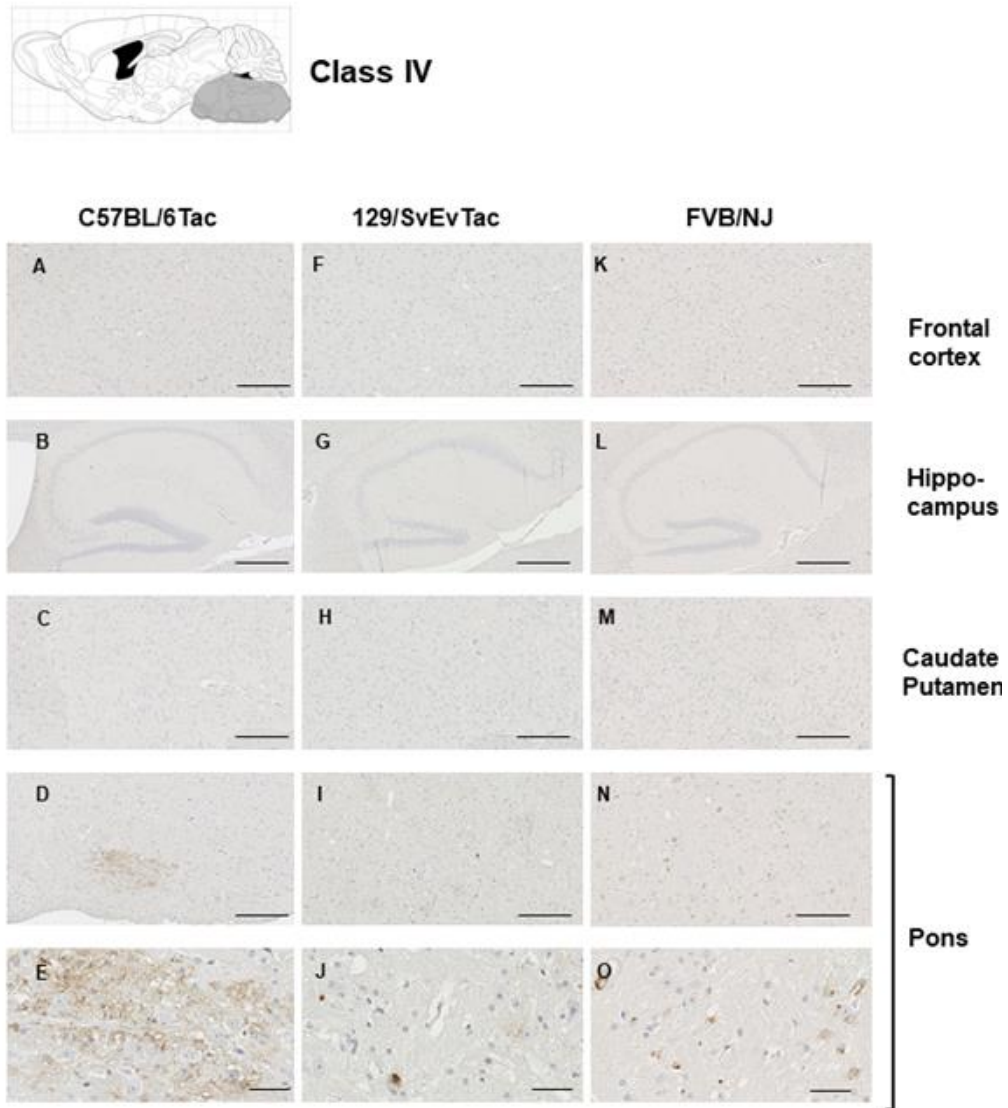


**Figure 2-8. Class IV Tau pathology.**

Different genetic backgrounds and anatomical structures have been studied with AT8 antibody as per Fig. 4. In contrast to classes I-III, immunostaining is restricted to the pons (D, E, I, J, N, O). Scale bar = 500  $\mu$ m for panels B, G, and L. Scale bar = 250  $\mu$ m for panels A, C, D, F, H, I, K, M, and N. Scale bar = 50  $\mu$ m for panels E, J, and O. Cells presented in panel J exhibit vacuoles.

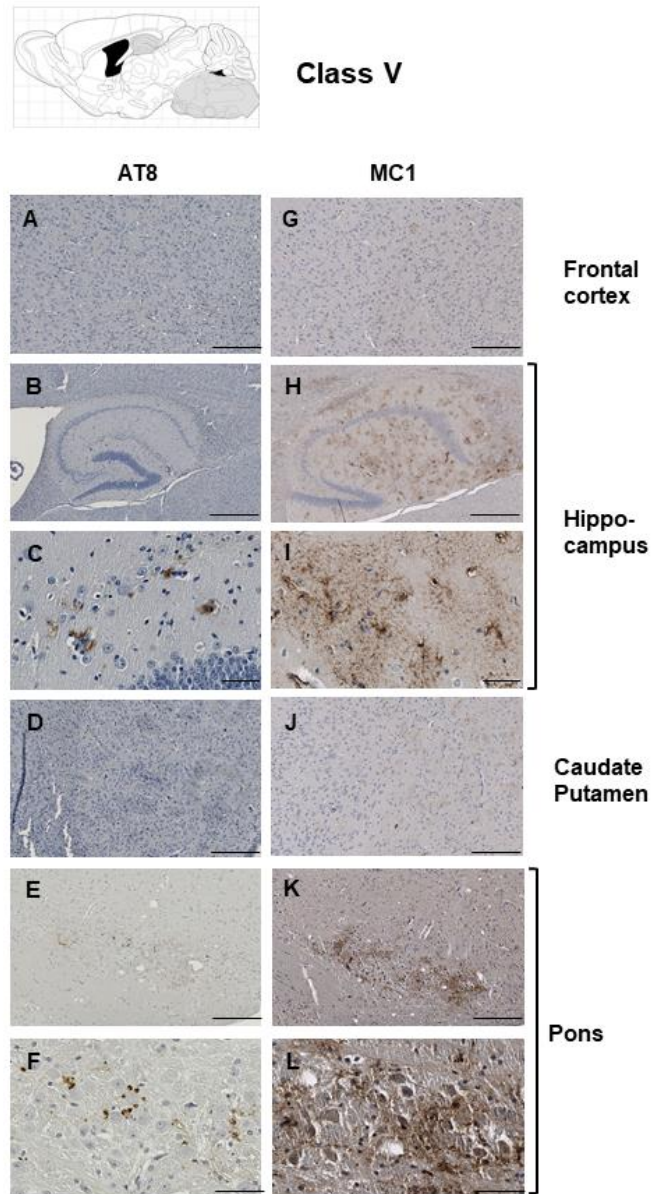


**Figure 2-9. Class V Tau pathology.**

Class V comprised the rarest class of pathology. Three out of four occurrences were in the 129/SvEvTac background and a single mouse from this background is represented with AT8 or MC1 staining. In contrast to class IV, immunostaining encompasses the hippocampus (B, C, H, I). Scale bar = 500  $\mu\text{m}$  for panels B, and H. Scale bar = 250  $\mu\text{m}$  for panels A, D, E, G, J, and K. Scale bar = 50  $\mu\text{m}$  for panels C, F, I, and L.

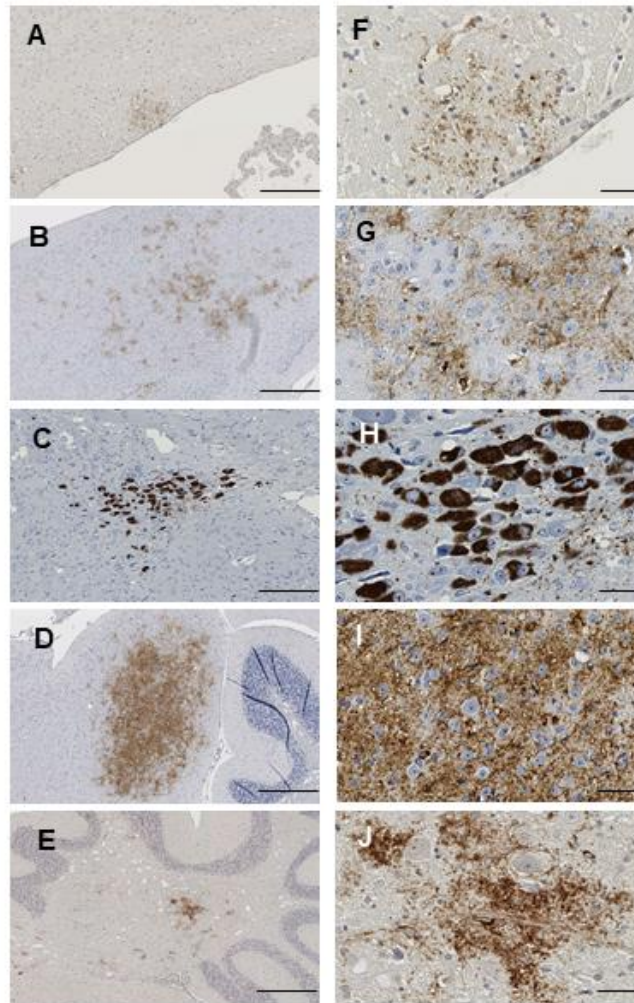


**Figure 2-10. Focal staining in aged TgTauP301L mice.**

Representative images of focal immunostaining of sagittal brain sections analyzed with AT8 antibody. Corpus callosum (panels A, F), retrosplenial areas (panels B, G), Locus coeruleus (panels C, H), inferior colliculus (panels D, I) and cerebellar fiber tracts (panels E, J) are presented. Scale bar = 250  $\mu\text{m}$  for panels A, B, C, D, and E. Scale bar = 50  $\mu\text{m}$  for panels F, G, H, I and J.

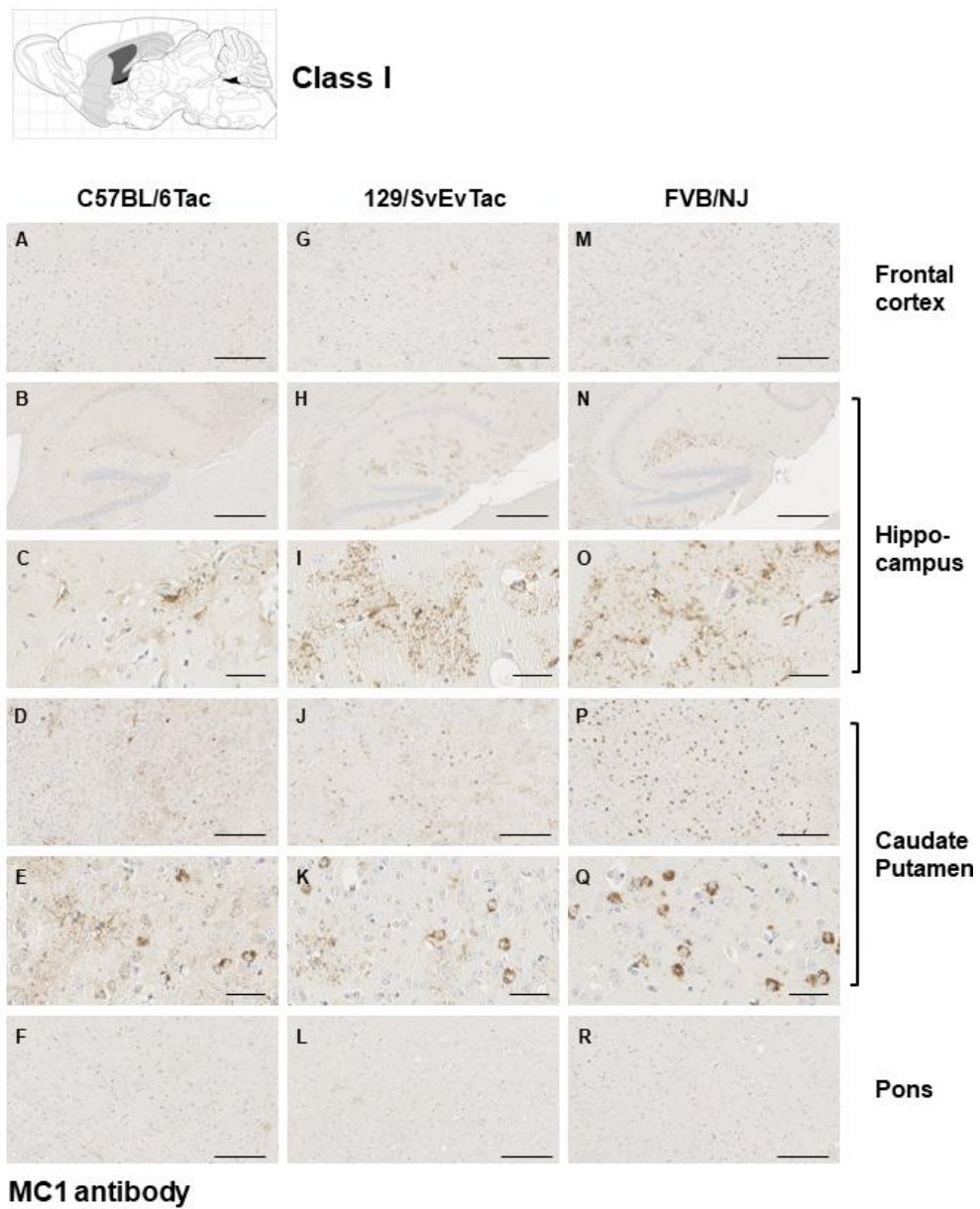


**Figure 2-11. MC1 staining in class I mice.**

This figure represents the counterparts of Fig 2.5. stained with MC1, which is a conformational antibody. The same pattern of pathology is observed in animals of the same class and no new patterns of pathology could be detected by using a different antibody.

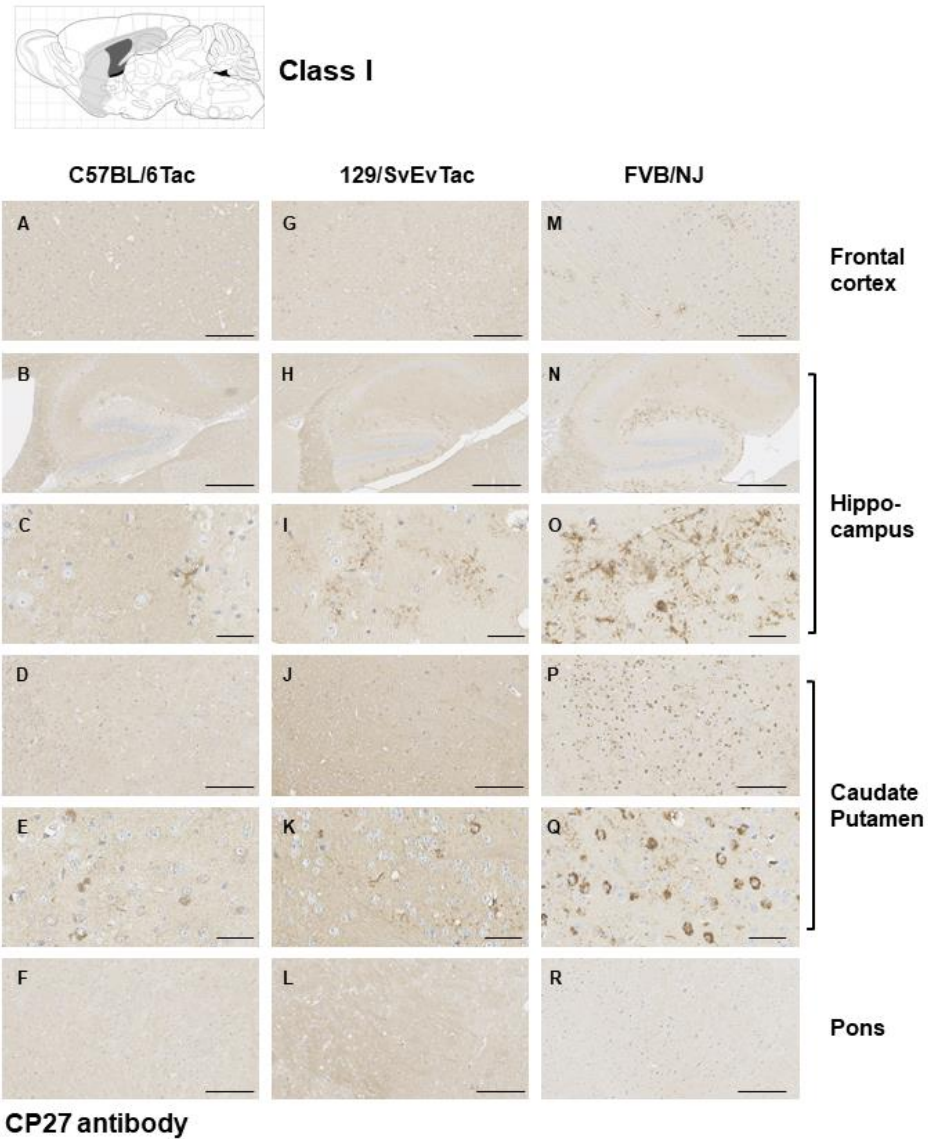


**Figure 2-12. CP27 staining in class I mice.**

This figure represents the counterparts of Fig 2.5. stained with CP27, which is an anti-human tau antibody with its epitope in N-terminal region. The same pattern of pathology is observed in animals of the same class and no new patterns of pathology could be detected by using a different antibody.

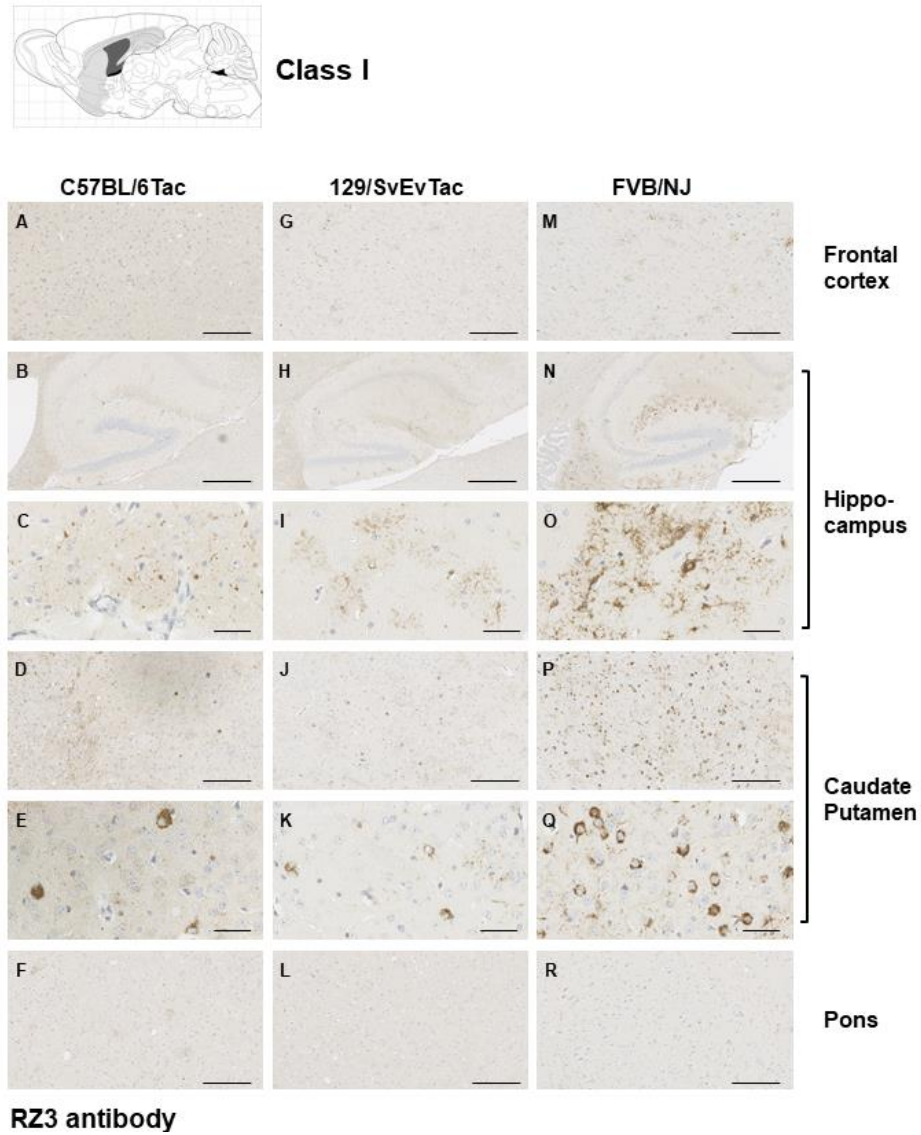


**Figure 2-13. RZ3 staining in class I mice.**

This figure represents the counterparts of Fig 2.5. stained with RZ3, which is an anti phospho-tau antibody. The same pattern of pathology is observed in animals of the same class and no new patterns of pathology could be detected by using a different antibody.

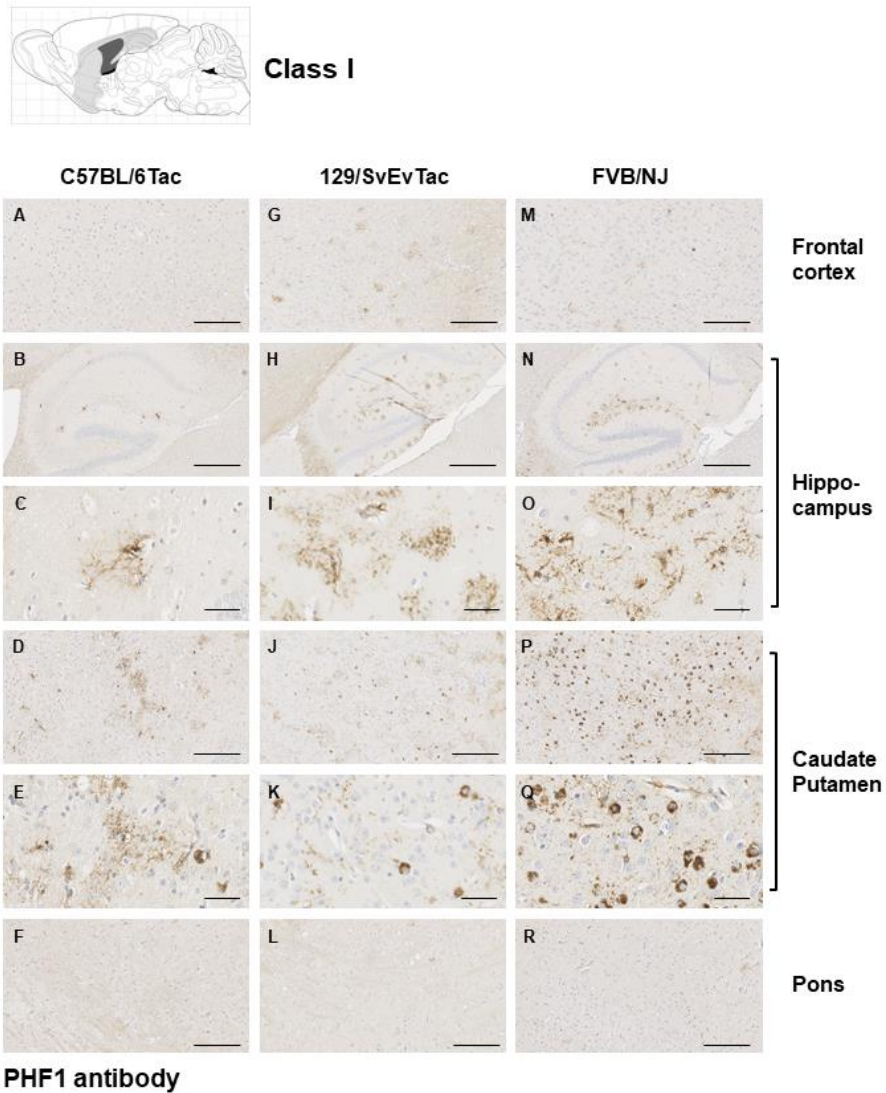


**Figure 2-14. PHF1 staining in class I mice.**

This figure represents the counterparts of Fig 2.5. stained with PHF1, which is phospho-tau specific antibody. The same pattern of pathology is observed in animals of the same class and no new patterns of pathology could be detected by using a different antibody.

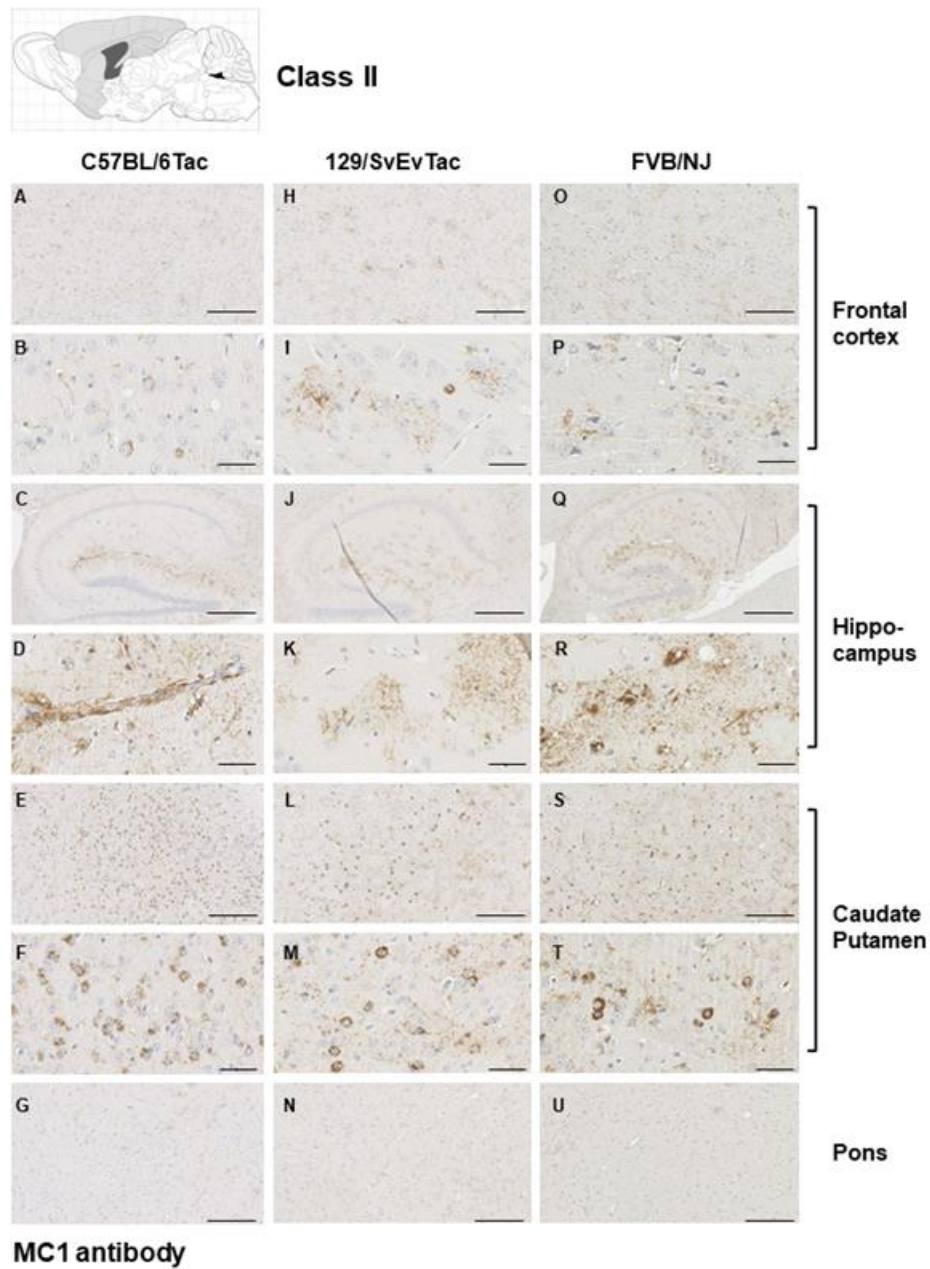


**Figure 2-15. MC1 staining in Class II mice.**

This figure represents the counterparts of Fig 2.6. stained with MC1, which is a conformational antibody. The same pattern of pathology is observed in animals of the same class and no new patterns of pathology could be detected by using a different antibody.

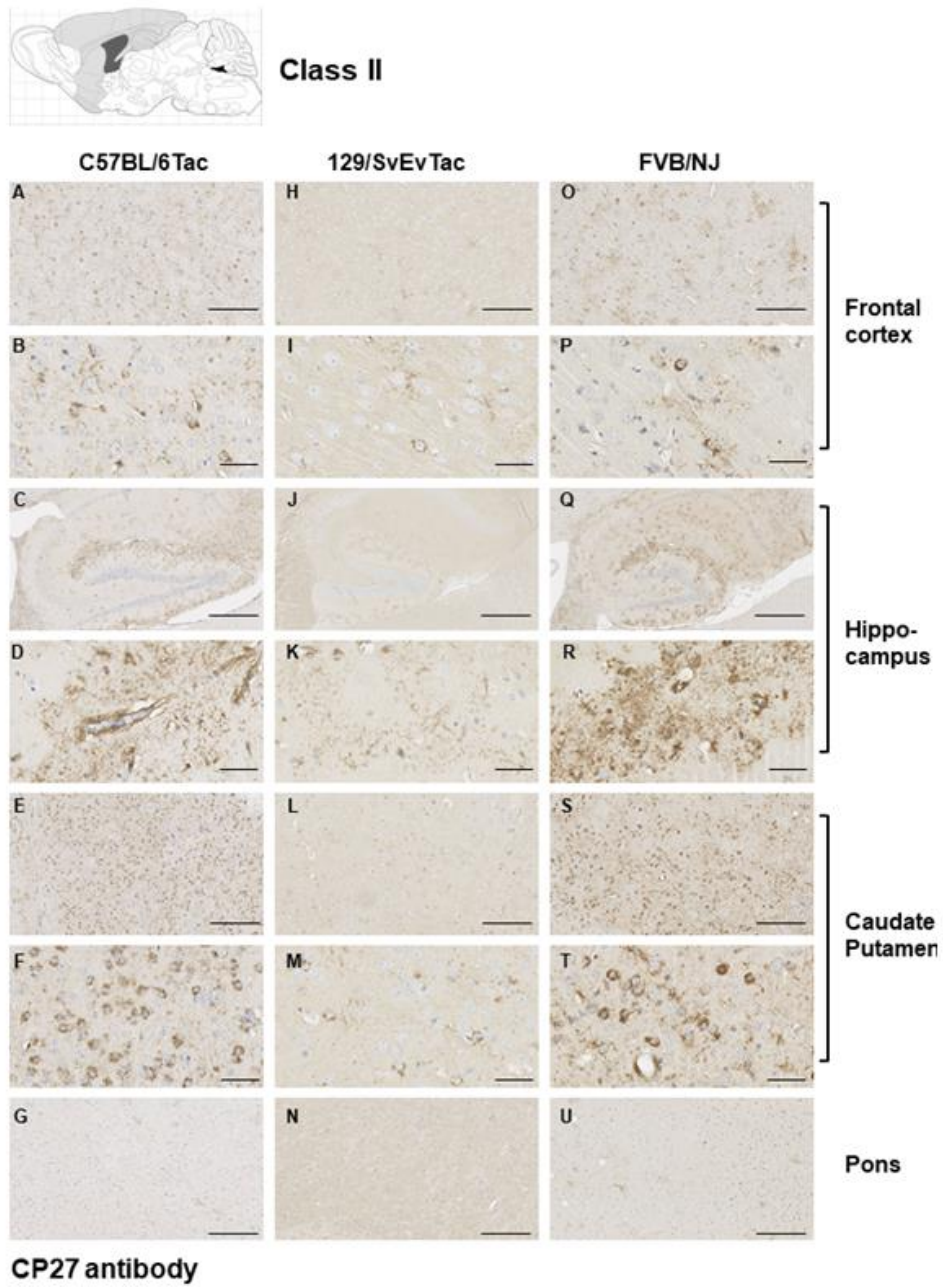


**Figure 2-16. CP27 staining in class II mice.**

This figure represents the counterparts of Fig 2.6. stained with CP27, which is an anti-human tau antibody with its epitope in N-terminal region.

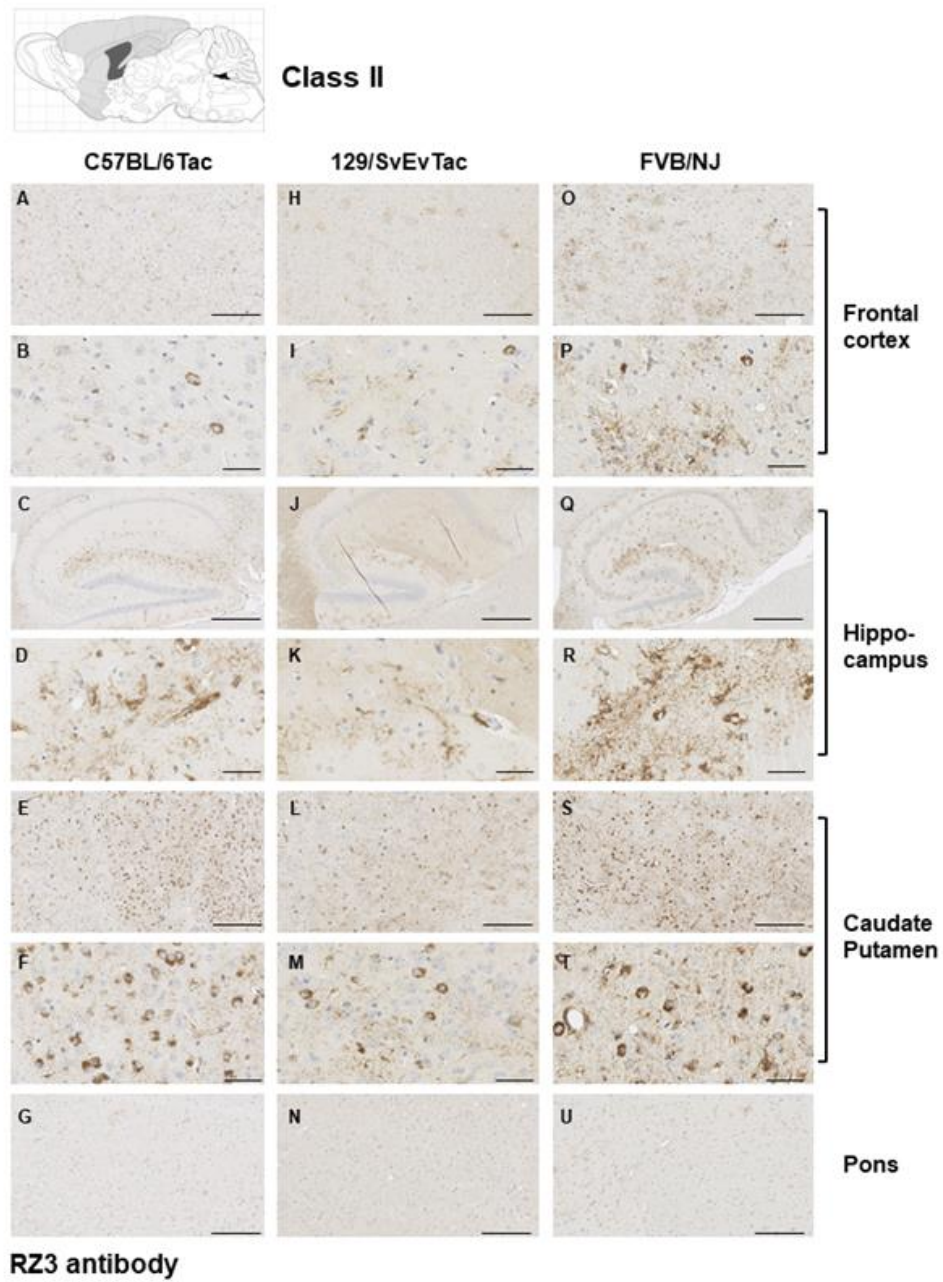


**Figure 2-17. RZ3 staining in class II mice.**

This figure represents the counterparts of Fig 2.6. stained with RZ3, which is an anti phospho-tau antibody.

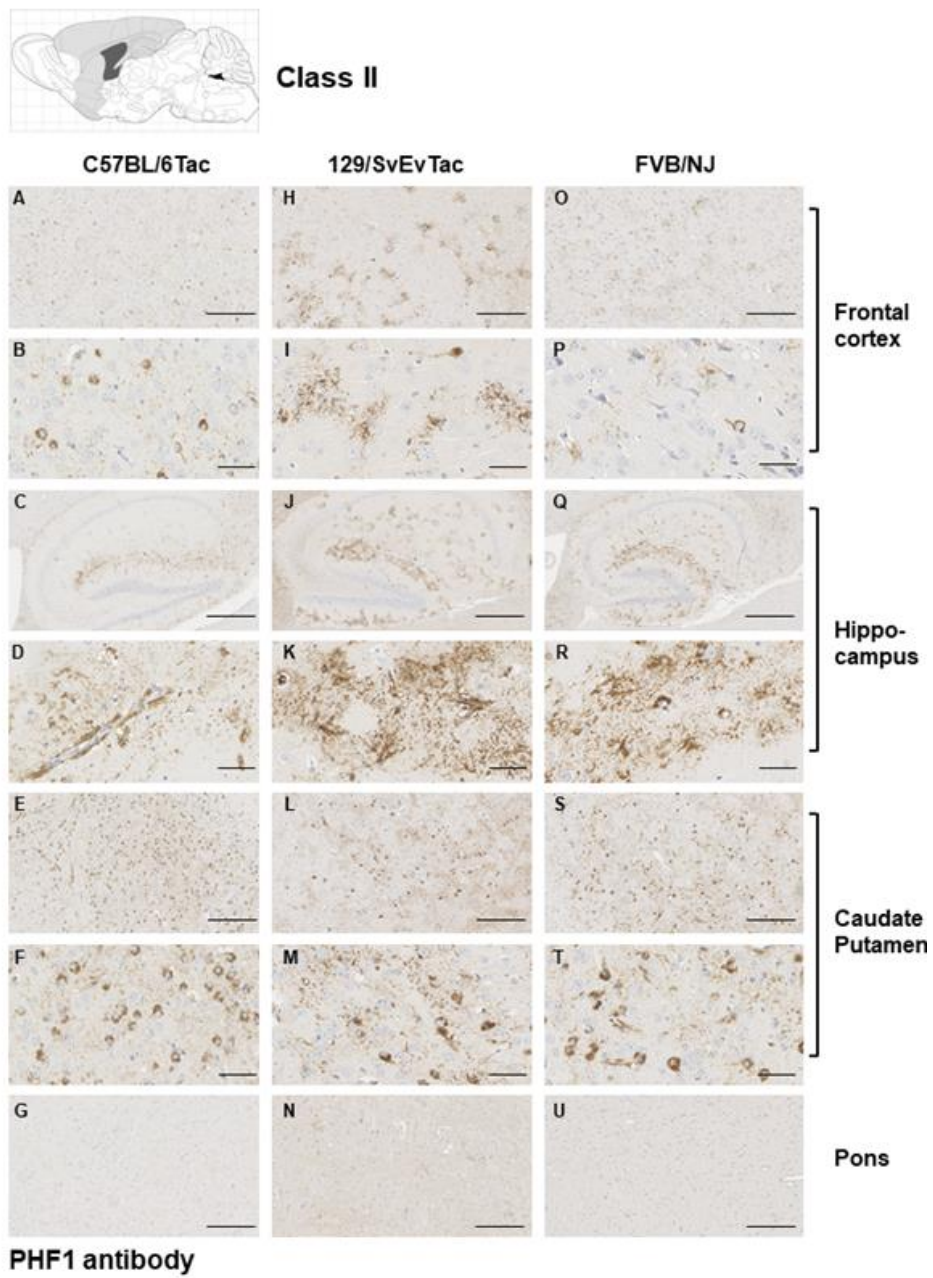


**Figure 2-18. PHF1 staining in class II mice.**

This figure represents the counterparts of Fig 2.6. stained with PHF1, which is an anti phospho-tau antibody. The same pattern of pathology is observed in animals of the same class and no new patterns of pathology could be detected by using a different antibody.

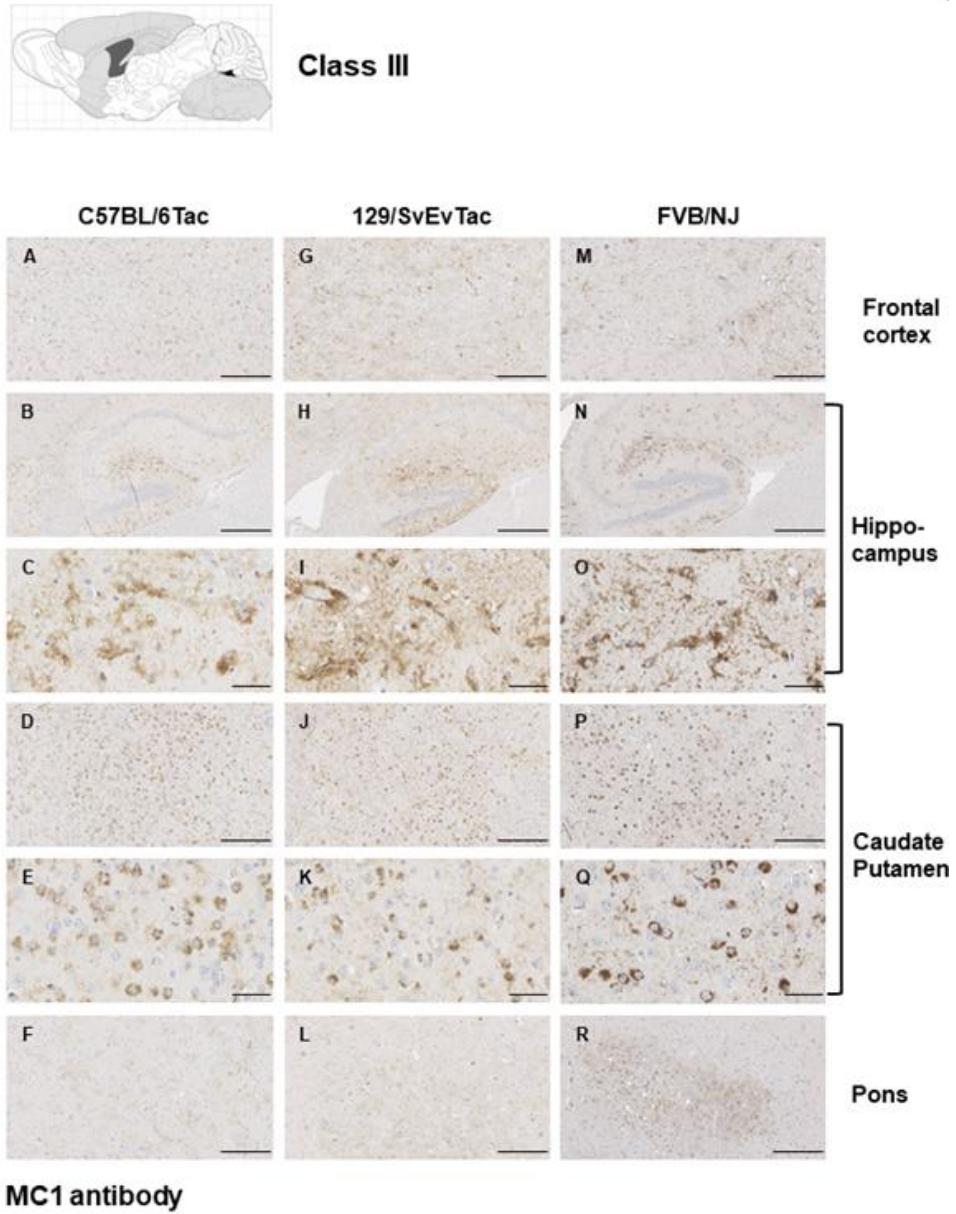


**Figure 2-19. MC1 staining in class III mice.**

This figure represents the counterparts of Fig 2.7. stained with MC1, which is a conformational antibody. The same pathology pattern is observed in animals of the same class and no new patterns of pathology could be detected by using a different antibody.

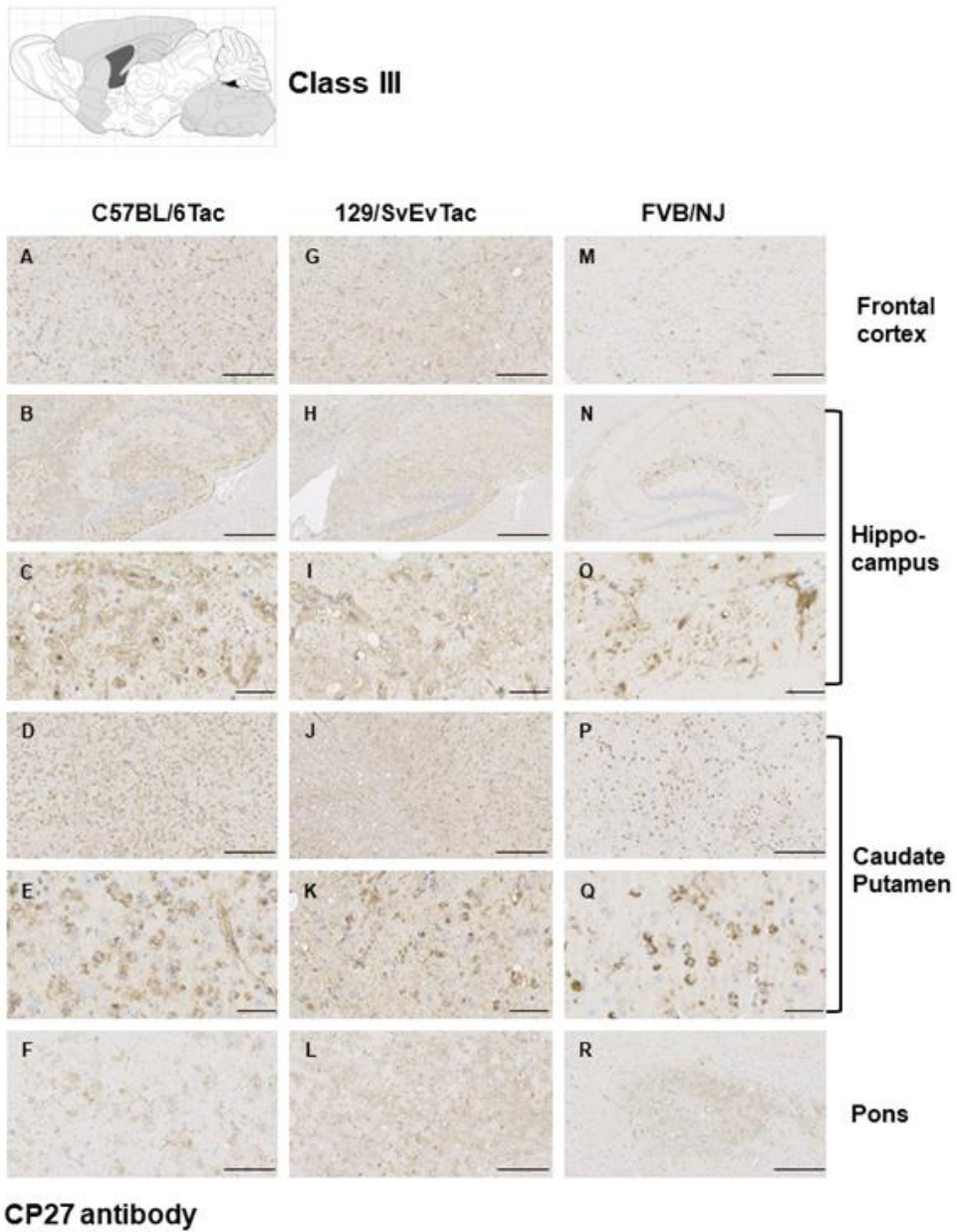


**Figure 2-20. CP27 staining in class III mice.**

This figure represents the counterparts of Fig 2.7. stained with CP27, which is an anti-human tau antibody with its epitope in N-terminal region.

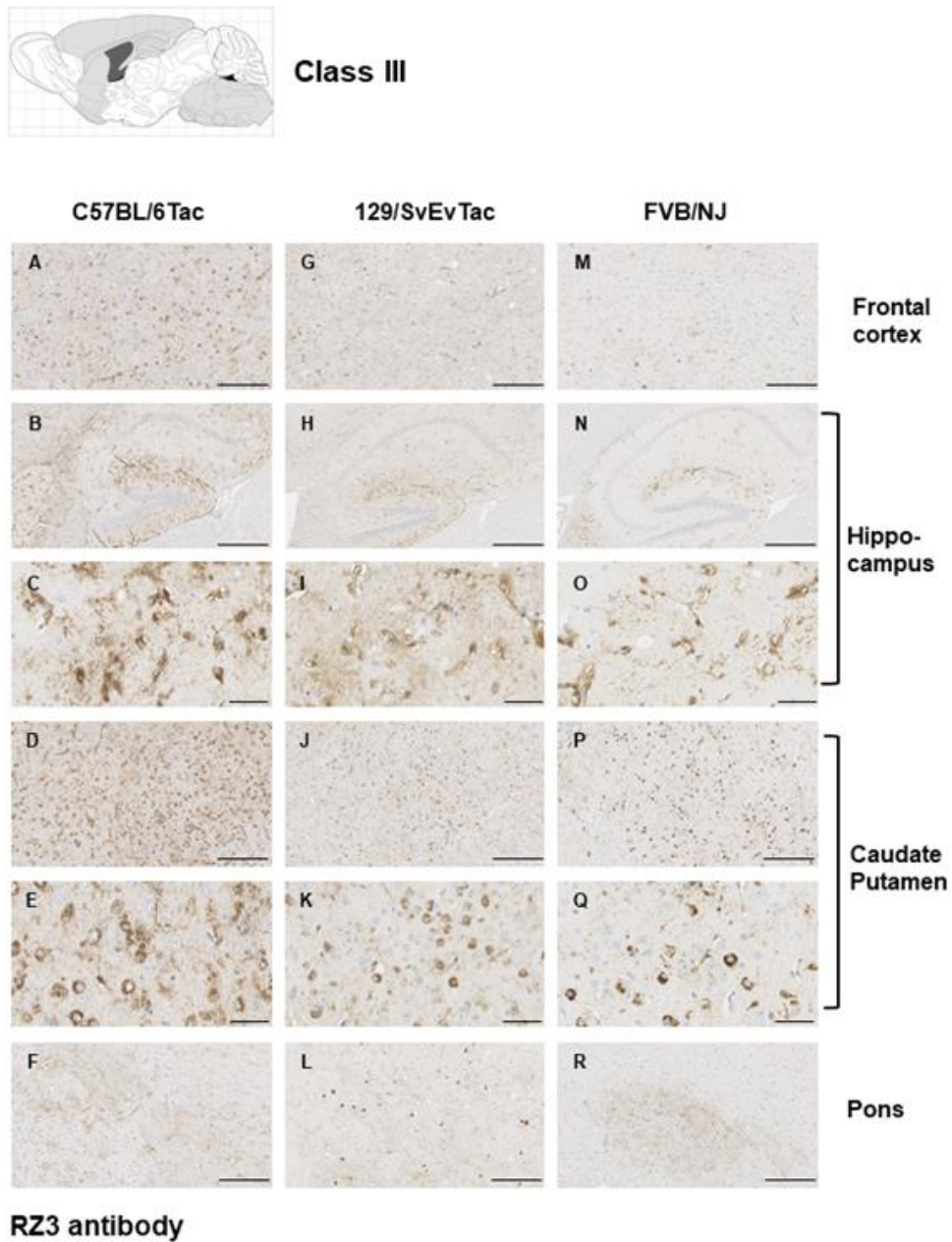


**Figure 2-21. RZ3 staining in class III mice.**

This figure represents the counterparts of Fig 2.7. stained with RZ3, which is an anti phospho-tau antibody. The same pathology pattern is observed in animals of the same class and no new patterns of pathology could be detected by using a different antibody.

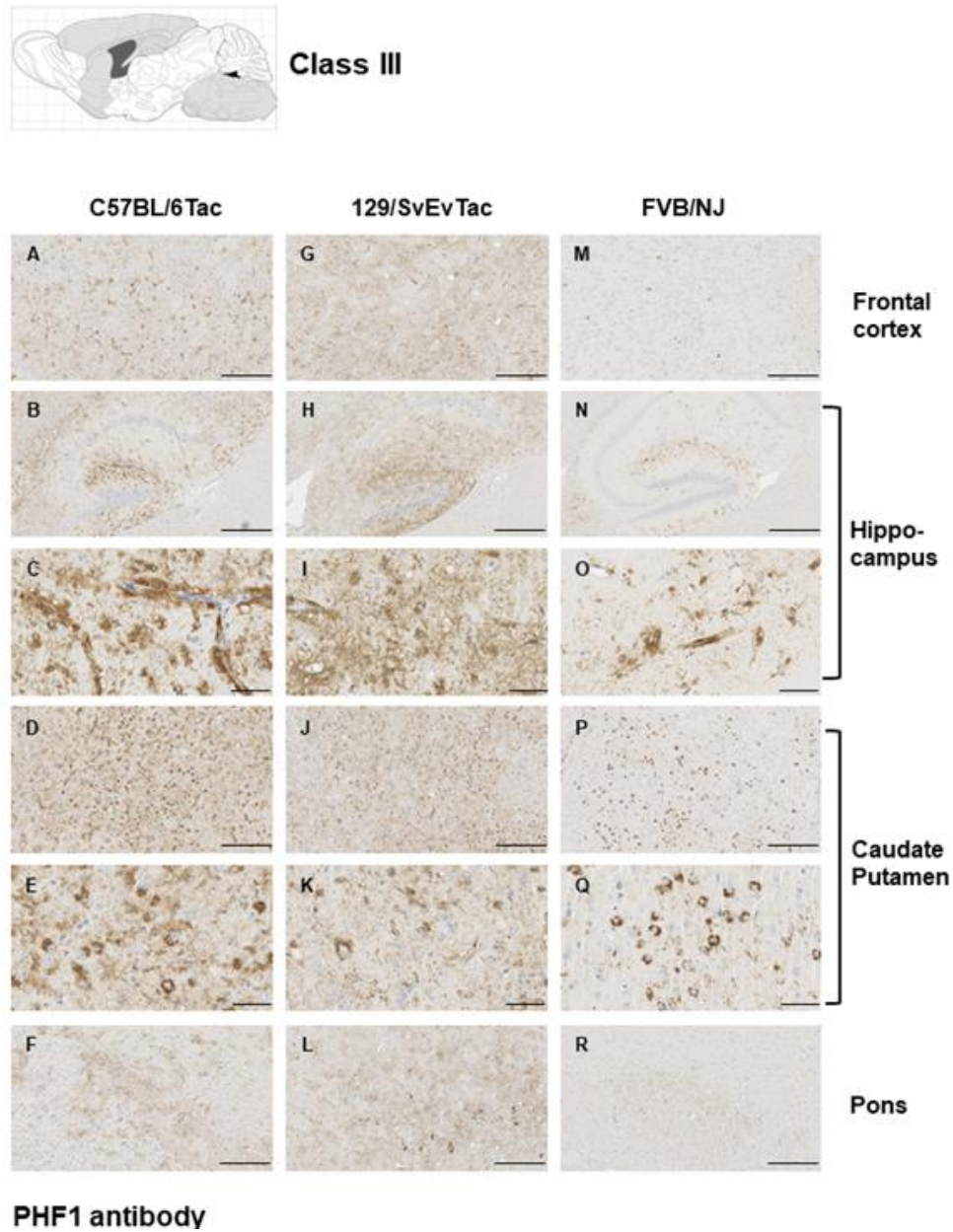


**Figure 2-22. PHF1 staining in Class III mice.**

This figure represents the counterparts of Fig 2.7. stained with PHF1, which is phospho-tau specific antibody. The same pathology pattern is observed in animals of the same class and no new patterns of pathology could be detected by using a different antibody.

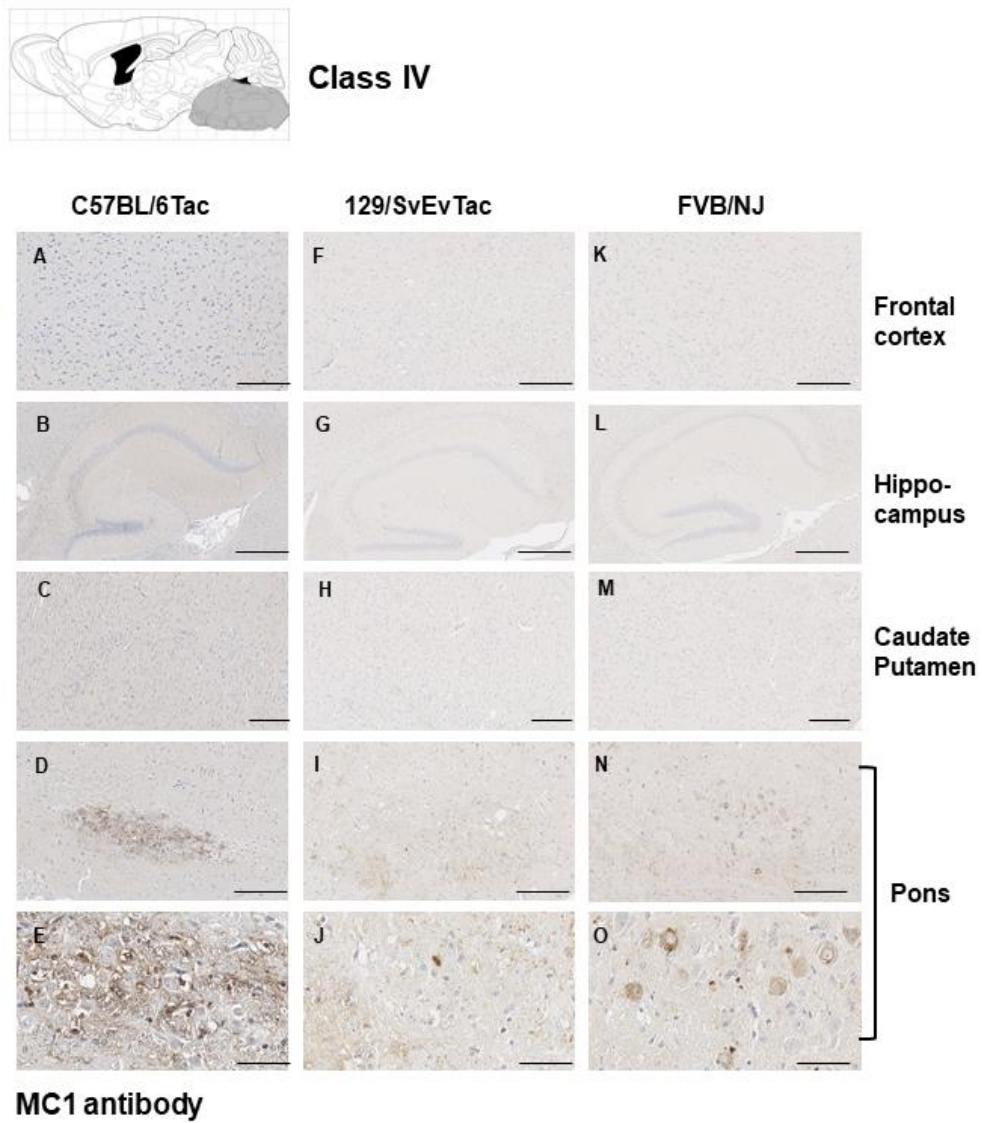


**Figure 2-23. MC1 staining in class IV mice**

This figure represents the counterparts of Fig 2.8. stained with MC1, which is a conformational antibody. The same pathology pattern is observed in animals of the same class and no new patterns of pathology could be detected by using a different antibody.

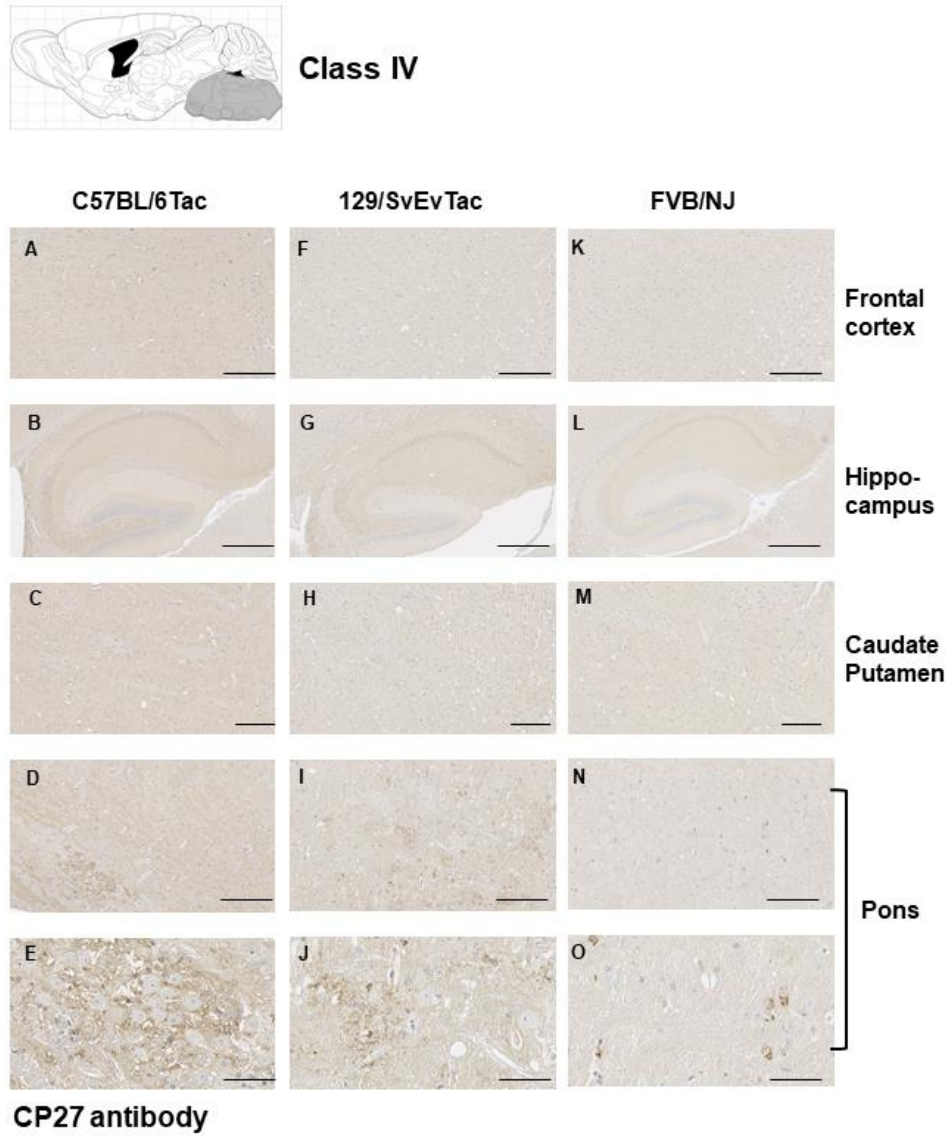


**Figure 2-24. CP27 staining in class IV mice.**

This figure represents the counterparts of Fig 2.8. stained with CP27, which is an anti-human tau antibody with its epitope in N-terminal region.

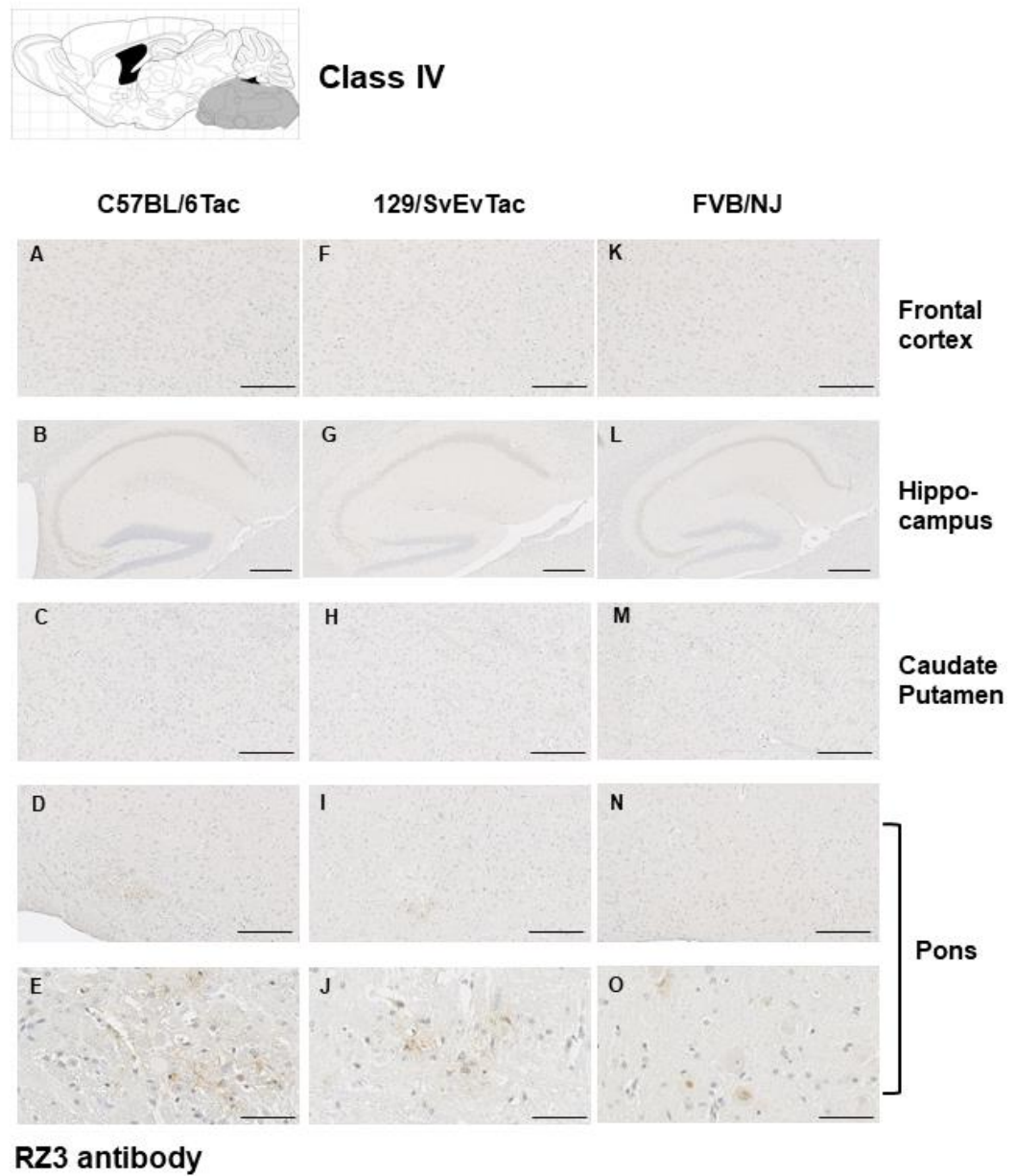


**Figure 2-25. RZ3 staining in class IV mice.**

This figure represents the counterparts of Fig 2.8. stained with RZ3, which is an anti phospho-tau antibody. The same pathology pattern is observed in animals of the same class and no new patterns of pathology could be detected by using a different antibody.

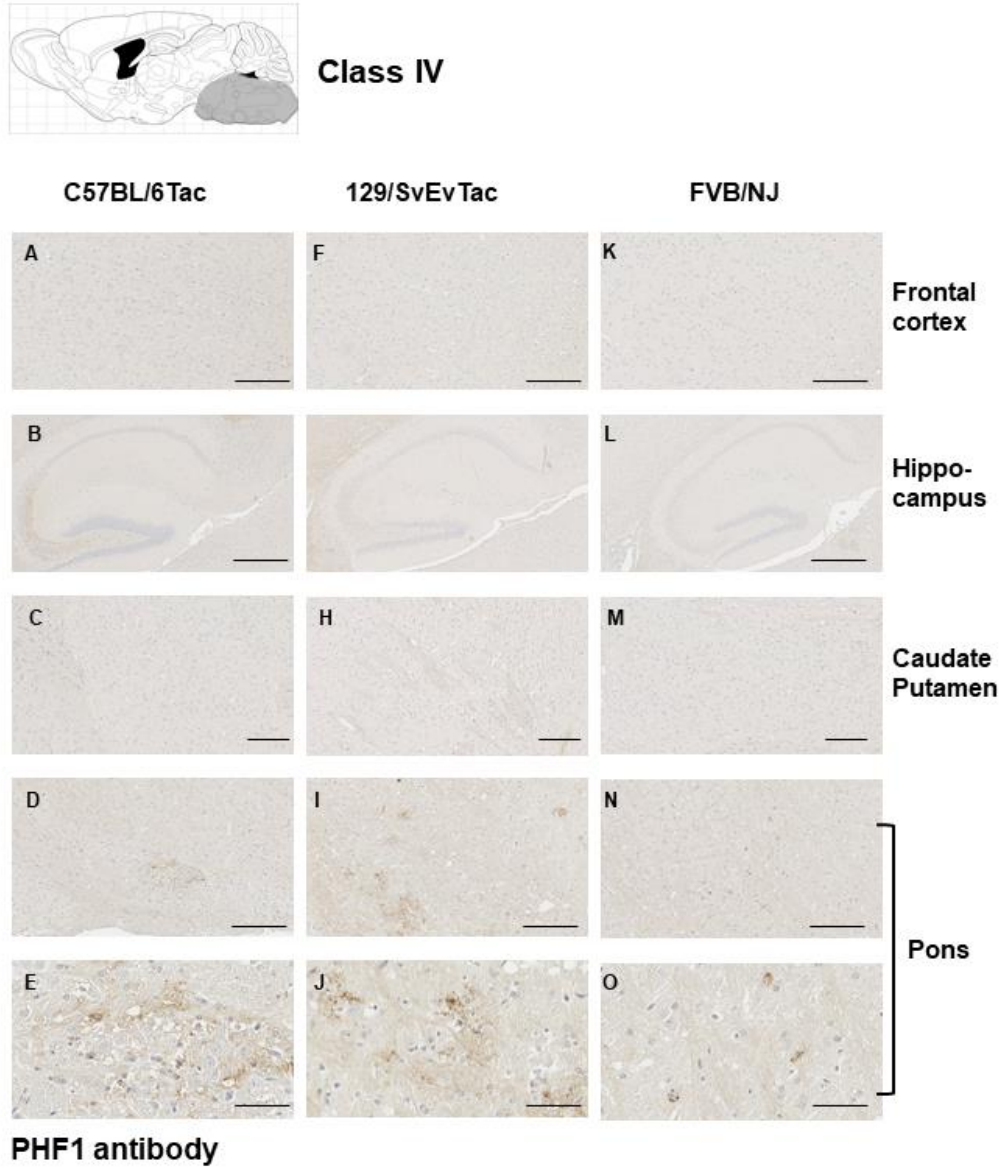


**Figure 2-26. PHF1 staining in class IV mice.**

This figure represents the counterparts of Fig 2.8. stained with PHF1, which is phospho-tau specific antibody. The same pathology pattern is observed in animals of the same class and no new patterns of pathology could be detected by using a different antibody.

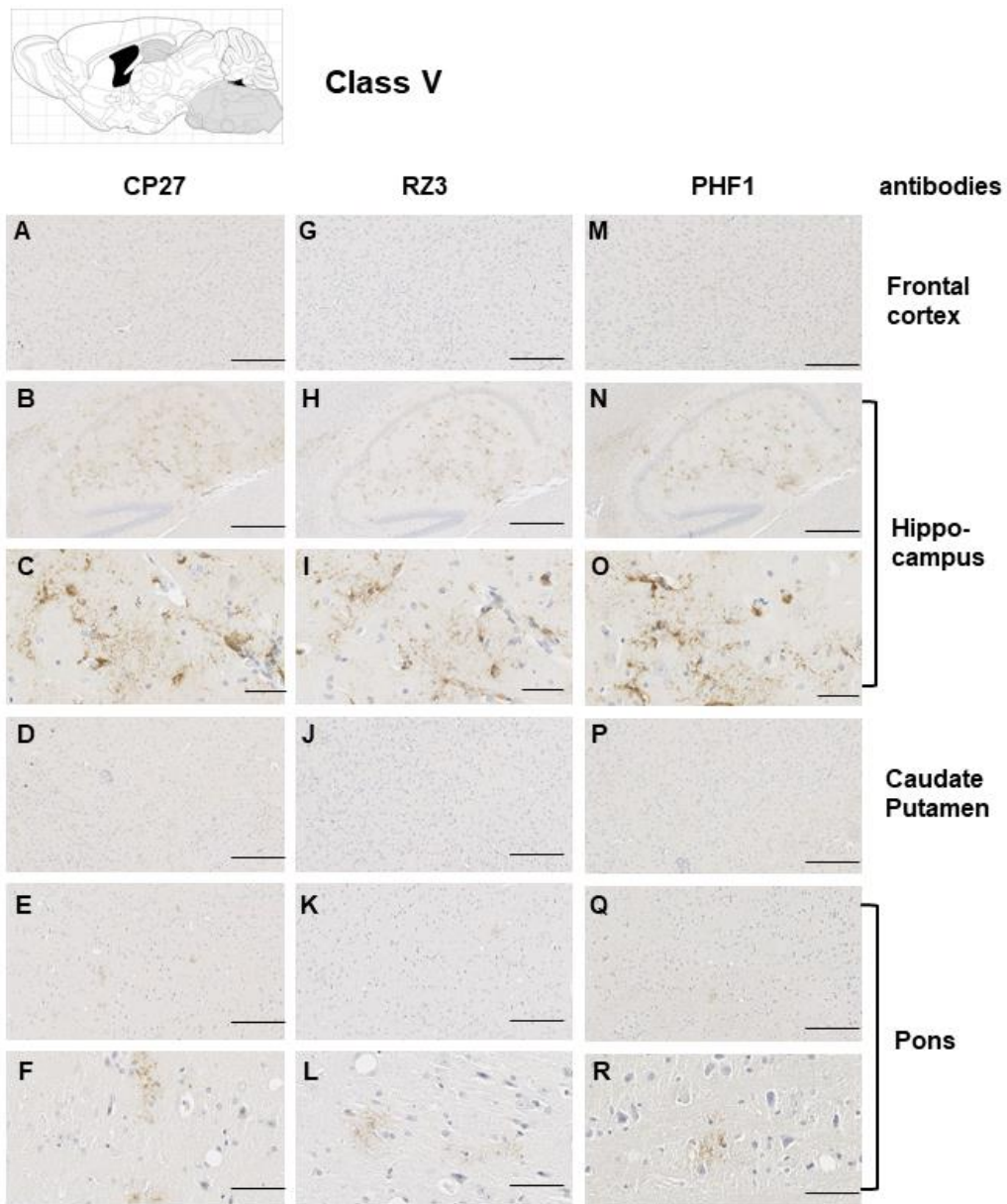


**Figure 2-27. CP27, RZ3 and PHF1 staining in class V mice.**

This figure represents a counterpart of Fig. 2.9 stained with CP27, RZ3 and PHF1 antibodies.

### 2.3.5 Variable Tau pathology versus transgene expression effects.

Given the aforementioned heterogeneities in pathology, we performed further analyses to assess potential relationships to hypothetical variations in transgene expression. While dispersed patterns of transgene expression are visible at low magnification (**Fig.2.1D**), we examined areas that defined pathology classes or were prone to focal pathology (**Fig. 2.5-2.10**), to see if they were prone to corresponding hotspots of transgene expression. Using human-specific CP27 antibody to assess transgene expression in young animals, this type of relationship did not prove to be the case (**Fig.2.28, A-J**), with dispersed immunostaining visible in these neuroanatomical areas. Secondly, we noted that Tau pathology was incompletely penetrant in aged animals; a lack of AT8-positive Tau pathology was apparent in about one quarter of all TgTau<sup>P301L</sup> mice examined (32/145, range 451 to 758 days). Pathology-negative animals were present in each of the three genetic backgrounds as follows: 13/41 C57BL/6Tac Tg mice, average age  $\pm$  SD = 614  $\pm$  91 days; 7/36 129SvEv/Tac Tg mice average age 636  $\pm$  33 days and 12/39 FVB/NJ Tg mice, average age 555  $\pm$  58 days. However, this lack of pathology was not due to lack of transgene expression, as assessed by western blot analysis of the other brain hemisphere of animals assessed for AT8 immunostaining (**Fig.2.29**); indeed, the aged Tg mice with no discernible pathology had immunoblot signals greater than their young counterparts. Both of these analyses argue against a crucial rate-limiting effect of transgene expression.

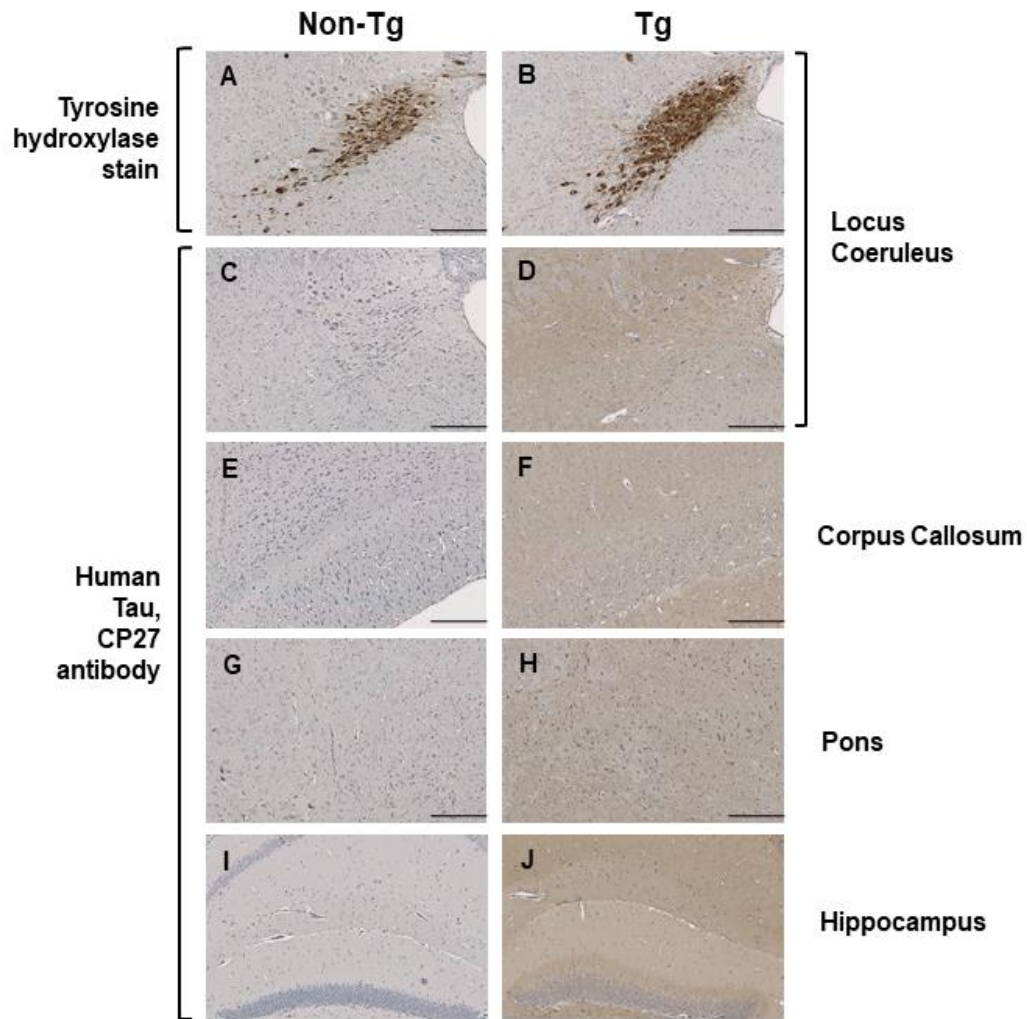


**Figure 2-28. Transgene-encoded human Tau is not expressed in a focal pattern in areas subject to focal staining in aged mice.**

Neuroanatomical areas prone to focal deposition in aged Tg mice were assessed before the onset of AT8-positive immunostaining. A, B, non-Tg and TgTau<sup>P301L</sup> mouse (C57BL6/Tac background, ages 355 and 309 d, respectively) stained for tyrosine hydroxylase antibody in the locus coeruleus. The remaining panels indicate sections from different brain areas from non-Tg mice and Tg mice stained with using CP27 antibody, with Tg mice not exhibiting focal patterns of staining. All scale bars = 250  $\mu$ m.

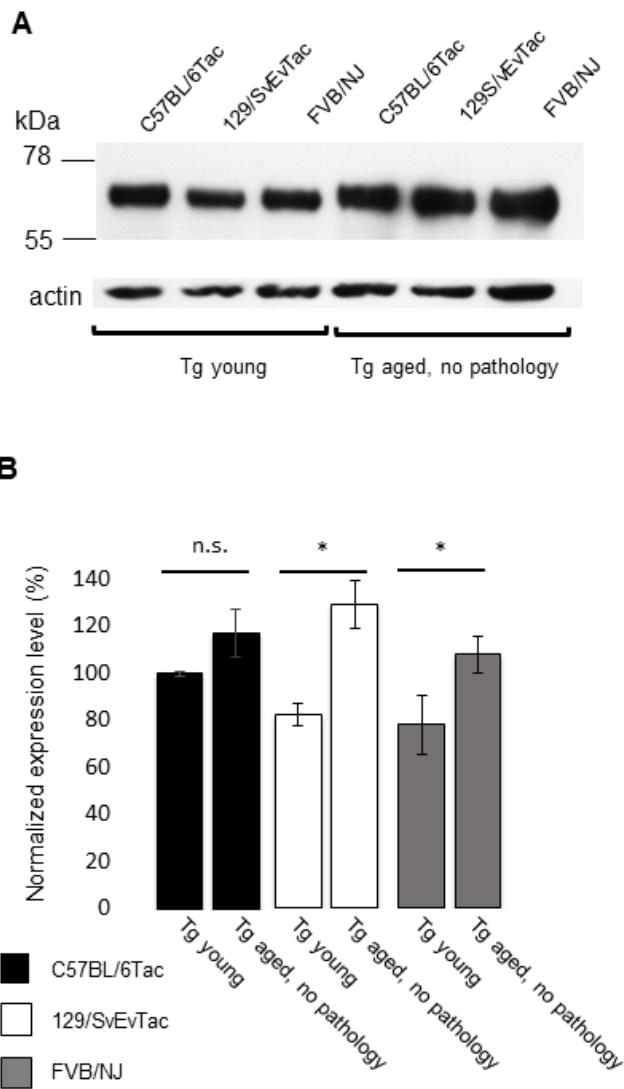


**Figure 2-29. Presence of Tau protein in aged Tg animals with negative pathology.**

A) Matching hemibrains of aged animals found lacking AT8 immunostaining (lanes 4-6, ages 723, 608, and 604 d respectively) were processed for western blot analysis and probed with antibody alongside young Tg mice (lanes 1-3, 66, 84 and 58d, respectively). Actin re-probe (lower panel) indicates similar sample loadings. B) represents densitometric analyses of the blot data expressed normalized to actin and adjusted to C57BL/6Tg (“100%”). Aged pathology negative Tg mice had more, rather than less, Tau than their young counterparts from the same inbred strain background, this reaching significance for the 129/SvEvTg and FVB/NJ backgrounds.

### 2.3.6 Biochemical analyses of Tau species in Different Pathology Classes.

Fractionation procedure presented in Fig.2.1 were used to assess alterations in Tau species in Tg mice of each of the three inbred backgrounds in their second year of life (**Fig.2.30** , **Fig.2.31**; range 466-732d), examining Class I, Class II and Class IV animals. These analyses with CP13 antibody confirmed the presence of phosphorylated Tau, especially 64-68 kDa species, in all brain fractions (SUP1, SUP3, and P3). There was a continuing trend in all three genetic backgrounds for insoluble Tau to accumulate in pellet 3 (P3) fractions of aged Tg mice versus mice at 240 days (**Fig.2.30 A-C**, **Fig.2.2**). Comparing amongst these aged animals, the yield of insoluble/soluble Tau (P3:SUP3) increased between Class I and II, with Class IV being significantly lower than either ( $p < 0.01$ ); **Fig.2.30 D**). A further distinction from brain lysates of 240 days old mice was the presence of both lower and higher molecular weight bands in mice with class I and class II pathology; this was manifest in all three backgrounds (**Fig. 2.30 A-C**). The lower molecular weight species may be due to fragmentation (as observed in FTL D-MAPT, as well as AD patients' brains (Wang, Biernat et al. 2007, Delobel, Lavenir et al. 2008, Garcia-Sierra, Mondragon-Rodriguez et al. 2008)) while the higher molecular weight species with mobility above full-length transgene encoded Tau in Class I and Class II P3 samples were inferred to represent SDS-resistant aggregates. To investigate the possibility of oligomeric species further, the supernatant of P1 samples (SUP1) was subject to brief ultracentrifugation and the concentrated samples analyzed on denaturing gels (**Fig.2.30 E**). For three out of four Class I and Class II samples, signals were seen at a mobility slower than a 100kDa  $M_r$  marker. Conversely, such signals were absent from equivalent Class IV samples, even upon extended autoradiographic exposure. Probing of P3 fractions with CP13 total tau and PHF phospho-Tau antibodies revealed overlapping signatures for Classes I and II mice, albeit with different relative intensities for putative fragmented species (in the range 30-50 kDa) for CP13 vs. PHF1 analyses (**Fig. 2.32**). Class IV animals presented with weaker, less complex signals that in two cases included prominent species at 50 and 25kDa.

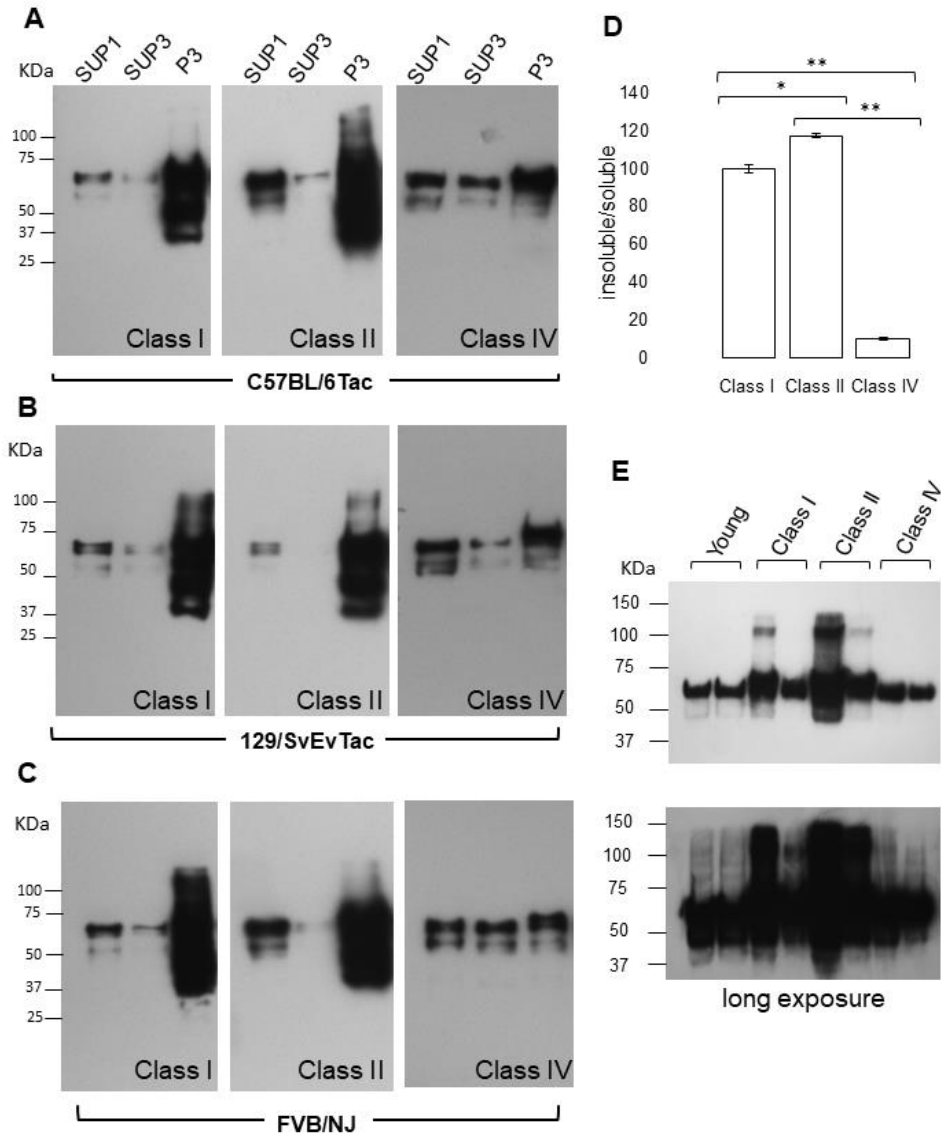


**Figure 2-30. Insoluble Tau species in the brains of aged TgTauP301L mice.**

Fractionated brains comprising supernatant pellet 1 (SUP1), supernatant pellet 3 (SUP3), and pellet 3 (P3) of aged TgTau<sup>(P301L)</sup> mice were analyzed by western blot analysis. One example of Class I, II and IV is shown for each genetic background. **A** C57BL/6Tac mice at ages 587, 732, and 530 days left to right **B**, 129/SvEvTac at ages 662, 592, and 466 days left to right, and **C** FVB/NJ mice at ages 646, 658, and 639 days left to right. For all samples, 10  $\mu$ g of total protein was loaded on the gel.

Antibody: CP13 (1/500; phosphoserine 202). SUP= Supernatant, and P= pellet fractions. **D** P3/S3 ratios of animals presented in A-C. Ratios were pooled across strain backgrounds. Class I vs. II  $p=0.020$ ; I vs IV,  $p=0.08$ ; II vs, IV,  $p= 0.003$ . **E** SUP1 fraction of animals with classes I, II and IV pathology to show the presence of oligomeric species in the soluble extract, antibody: CP27 (1/500).

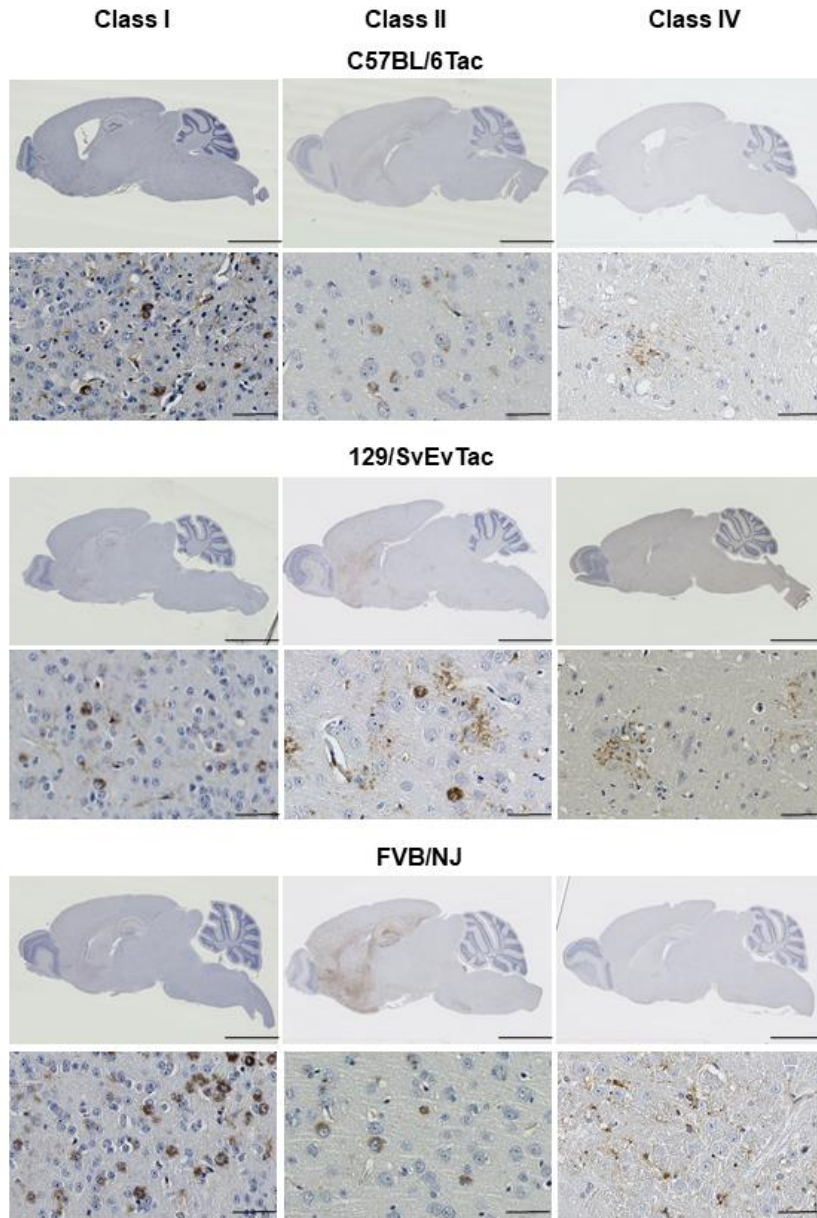
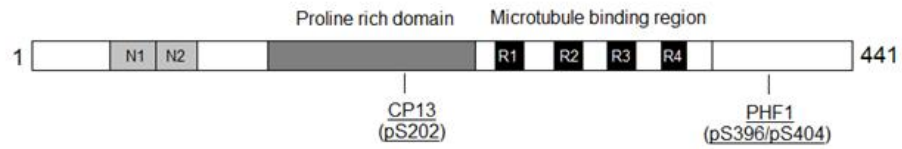
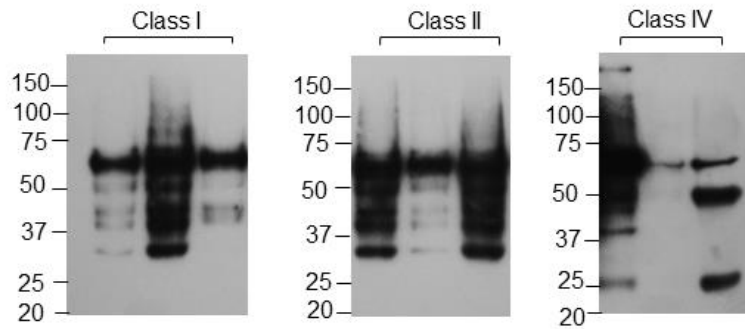


**Figure 2-31. Pathology in aged Tg mice assessed for insoluble Tau species.**

These data represent the counterparts (other hemi-brains) of the animals assessed for insoluble Tau species in Fig 2.30; pathology class and genetic background are annotated. Scale bars for low power views = 2.5mm, high power views = 50  $\mu$ m.



### CP13



### PHF1

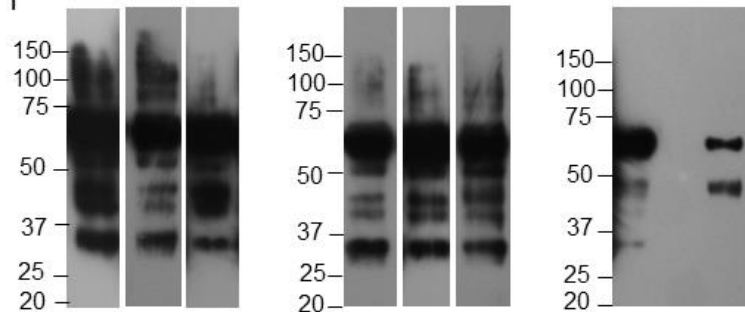


**Figure 2-32. Undigested P3 fraction assessed with CP13 and PHF1 antibodies.**

A schematic of antibody epitopes is presented. Blot represents P3 fraction from 3 animals of classes I, II and IV. Class I mice at ages 587, 662, and 646 days left to right, class II animals at ages 735, 592, and 658 days left to right, and class IV mice at ages 530, 466, and 639 days left to right. For both blots, 5  $\mu$ g of total protein was loaded on the gel. Antibody: CP13 (1/500) and PHF1 (1/500).

We next performed trypsin digestions on P3 fractions of Classes I-V mice (**Fig.2.33**); these samples were probed with an antibody which has an epitope lying within a previously defined trypsin resistant core, ET3 (Taniguchi-Watanabe, Arai et al. 2016). A portion of digested samples were submitted for in-gel digestion to identify the sequence coverage by LC/MS/MS.

Strikingly, we observed three types of signatures in trypsin-resistant cores:

- i) **Pattern A** consisting of up to three main fragments (**Fig. 2.33 and 2.34 A**). Peptide signatures corresponding to 37, 24, and 20.8 kDa bands were as follows respectively (residues 212-406, 212-438 and 212-406), hence suggesting that the 37 kDa band was SDS-resistant dimer of the 20 kDa fragment.
- ii) **Pattern B** consisting of four fragments; A 25 kDa band, followed by a faint 20 kDa band, and then 18 and 12 kDa fragments (**Fig. 2.33 and 2.34 B**). Peptide signatures corresponding to these fragments are presented in **Fig 2.34 B**.
- iii) **Pattern C** with the least complex banding pattern of trypsin resistant core consisting only of two bands (50 and 25 kDa fragments). Peptide signatures obtained from these fragments suggested that the 50 kDa band was in fact SDS-resistant dimers of the 25 kDa fragment (**Fig.2.34 C**)

Generally, trypsin-resistant cores in our TgTau mice were more N-terminally extended than those reported for MAPT cases (181-406, 212-406 as well as 164-395 and 212-395, versus 260-406, 260-395) (Taniguchi-Watanabe, Arai et al. 2016). The finding of seemingly related Class I/II and Class III signatures and yet distinct Class IV and V signatures was reiterated in analyses of undigested P3 samples probed with CP13 and PHF1 antibodies (**Fig.2.32**). Also, in these analyses either with or without trypsin treatment, Class IV animals often yielded weaker signals than those obtained for Classes I and II and III.

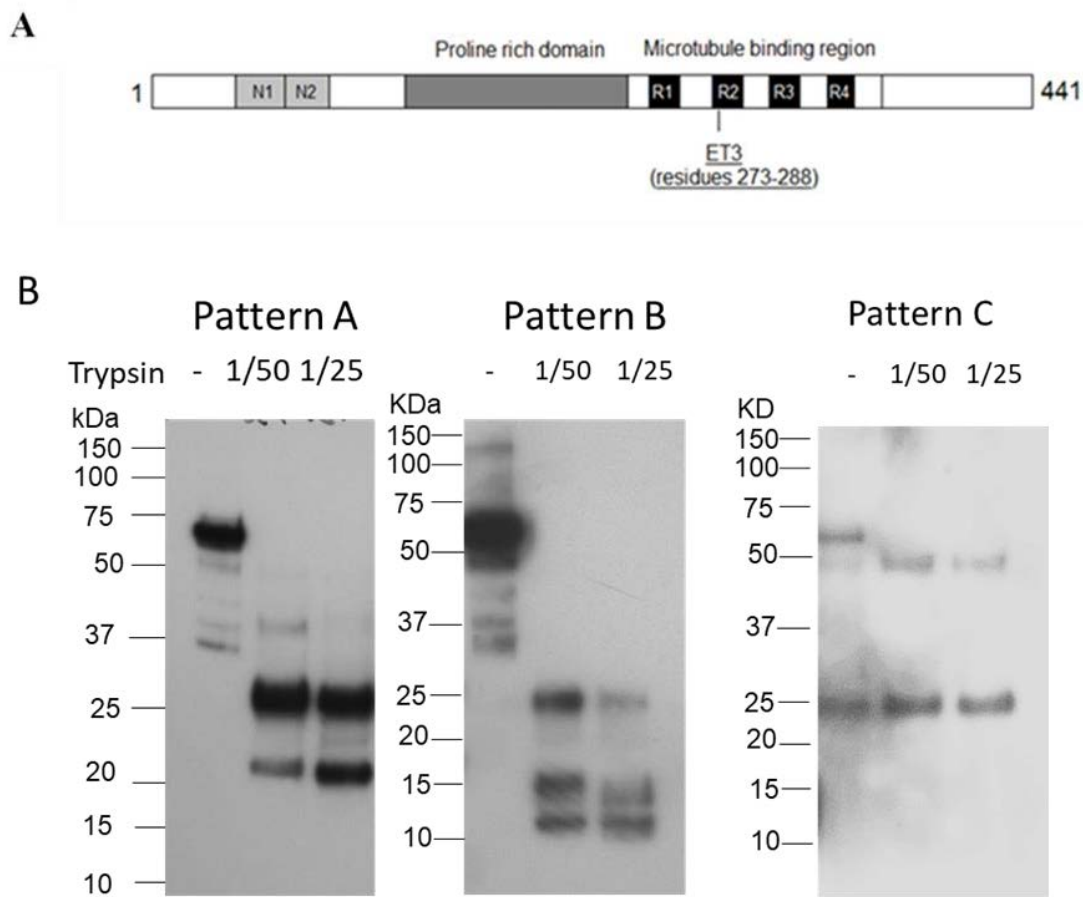


**Figure 2-33. Trypsin-resistance of sarkosyl-insoluble Tau fractions.**

A) A schematic of ET3 antibody epitope is presented. **B)** 10 ug of P3 fractions from animals of different classes were subjected to increasing concentration of trypsin for digestion (1/50 and 1/25 for enzyme/protein ratio) and analyzed by western blotting. The banding patterns in samples are represented before and after trypsin-digestion. Three patterns (A-C) of trypsin resistant cores were detected in the mice. ET3 anti-Tau (4R specific, residues 273-288) was used to detect Tau fragments at 1/250 dilution.

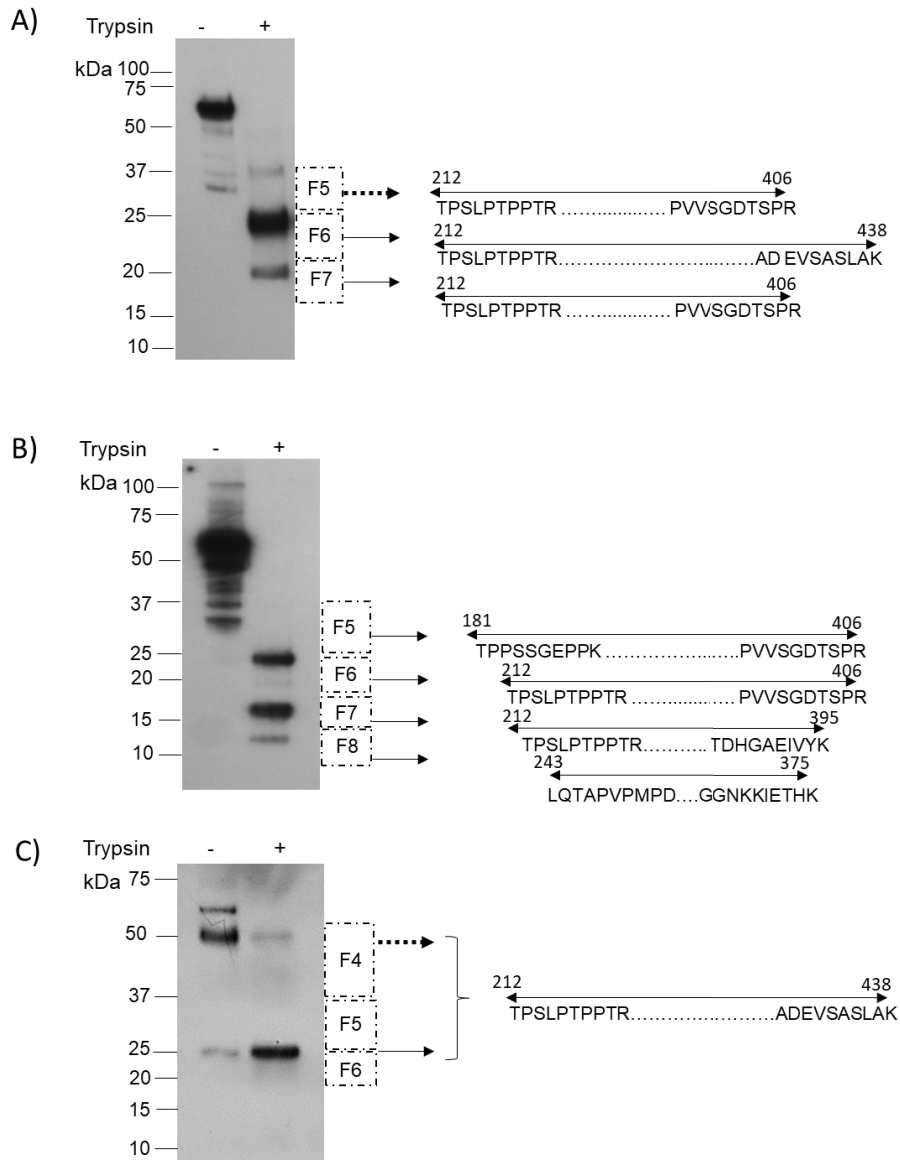


**Figure 2-34. The protein sequence of trypsin-resistant core of TgTauP301L mice identified by LC/MS/MS.**

The sequence of the fragments identified in each pattern are presented. The dashed squares represent fractions of the gel each fragment was detected in, with the fraction number mentioned in each square. The dashed lines indicate cases where the fragment mass did not agree with the electrophoresis mobility size suggesting presence of SDS-resistant dimers A) A representative blot from pattern A of trypsin-resistance, with detected fragments, B) A representative blot from pattern B of trypsin-resistance, with detected fragments and C) A representative blot from pattern C of trypsin-resistance, with the identified fragment.

### 2.3.7 Electron microscopic analysis of Tau filaments.

We next analyzed the ultrastructure of individual Tau filaments in the P3 fractions (**Fig. 2.35**). Negatively stained Tau filaments were readily apparent in most of the P3 fractions available for electron microscopy (**Table 2.3**). The morphology of individual Tau filaments fell into three recognizable types: straight filaments (**Fig. 2.35 A**), coiled filaments (**Fig. 2.35 B**), and twisted ribbon-like filaments (**Fig. 2.35 C**). Only a few filaments could not be assigned to one of these three types due to overlapping particles or poor staining (not shown). In all samples, the straight filaments were the dominant type, coiled filaments were most noted amongst Class I samples, while twisted ribbon-like filaments were rare in all samples (**Table 2.3**). Despite loading equal amounts of total protein from fraction P3 on the grids, the number of observed filaments was disproportionately lower in all Class IV samples, and these samples were abundant in amorphous non-fibrillar particles. These observations suggest that only a lesser fraction of the tau protein in Class IV was in fibrillar form as compared to Classes I and II.

### 2.3.8 Seeding activity in brains from aged Tau<sup>P301L</sup> mice.

Lastly, we asked whether the different patterns of deposition in individual mice were due to structurally distinct self-propagating Tau amyloid conformers or "strains" (strains used here in the sense of prion effects). Previously, a monoclonal cell culture model was developed that could differentiate Tau strains based on inclusion morphology (Sanders, Kaufman et al. 2014). These recipient cells (Clone 1) stably express the Tau repeat domain ("RD", amino acids 244-372 of the longest 441 amino acid 2N,4R isoform) fused to YFP. At baseline, Tau RD exists as soluble monomer. However, upon addition of exogenous aggregates or seeds, cells rapidly convert to an accumulation of a fibrillar state, which propagates itself stably to daughter cells over months of culture. In this paper, two recombinant fibrillar Tau-derived strains (Clone 9 and Clone 10) were extensively characterized. Consistent with earlier results, addition of Clone 1 lysate did not seed aggregation (**Fig.2.36 A**). However, Clone 9 and Clone 10 lysate seeded aggregation in the majority of cells and produced characteristic inclusion morphologies—Clone 9, nuclear speckles (**Fig.2.36 B**); Clone 10, an ordered juxtannuclear inclusion (**Fig.2.36 C**). Using rostral and caudal

samples derived from a total of six mice classified as having Class I, Class II or Class IV pathology, we tested seeding capacity. All 12 TgTau<sup>P301L</sup> mouse brain samples seeded inclusion formation (**Fig.2.37, A-L**), with a similar signature featuring large deposits of Tau tangles with few nuclear deposits; these inclusions thus differed from those associated with Clone 9 and Clone 10. We conclude that a single Tau species predominates in these seeding assays, irrespective of the location and intensity of Tau deposition. In terms of strain identity, out of a previously defined panel of 18 possible Tau strains deriving from diverse source materials (recombinant Tau fibrils, cell lines, human brain material from different Tauopathies, mouse brain material), the signature morphology from TgTau<sup>P301L</sup> mice most closely resembled a strain isolate called DS6 (Kaufman, Sanders et al. 2016). Interestingly DS6 derives from a homogenate of a P301S Tau Tg mouse brain (Yoshiyama, Higuchi et al. 2007). We conclude that seeding activity does not necessarily correspond with areas of Tau immunostaining.

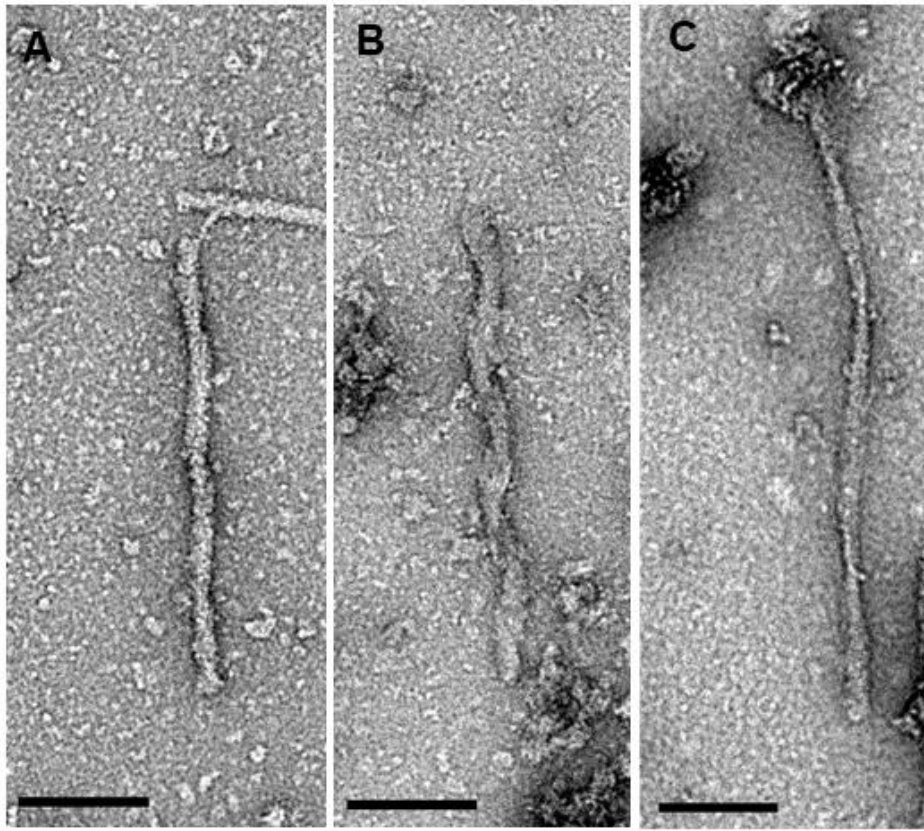


**Figure 2-35. Negative stain electron microscopy of insoluble Tau fractions.**

The morphology of individual Tau filaments was readily discernible and three separate filament types were observed: straight filaments (A), coiled filaments (B), and twisted ribbon-like filaments (C). Scale bars = 100 nm.

Mouse lines	Pathology Class I				Pathology Class II				Pathology Class IV			
	N	Filament Types			N	Filament Types			N	Filament Types		
		Straight Filament	Coiled Filament	Twisted Ribbon-like Filament		Straight Filament	Coiled Filament	Twisted Ribbon-like Filament		Straight Filament	Coiled Filament	Twisted Ribbon-like Filament
C57BL/6	2	39	35	1	2	189	0	0	2	6	0	0
		52%	47%	1%		100%	0%	0%		100%	0%	0%
129SvEv	1	22	0	1	1	55	0	0	3	23	0	0
		96%	0%	4%		100%	0%	0%		100%	0%	0%
FVB/NJ	2	21	0	0	3	121	1	0	3	14	0	0
		100%	0%	0%		99%	1%	0%		100%	0%	0%

**Table 2-3. Categorization of individual Tau filaments according to pathology classification and genetic background.**

Negative stain electron microscopy was used to distinguish the different morphologies of isolated Tau filaments (**Fig.2.35**). Filaments numbers were totaled for animals of the same Class and inbred strain type. N, number of animals analyzed.

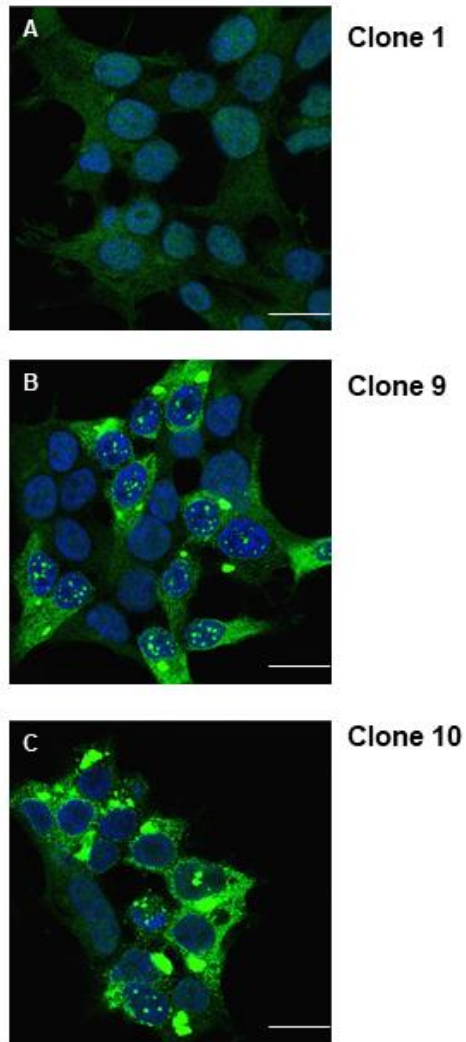


**Figure 2-36. Clones used for fluorescence microscopy assays.**

Clone 1 (negative control) lysate never seeds inclusions, whereas Clone 9 and Clone 10 seed the formation of aggregates with distinctive morphologies.

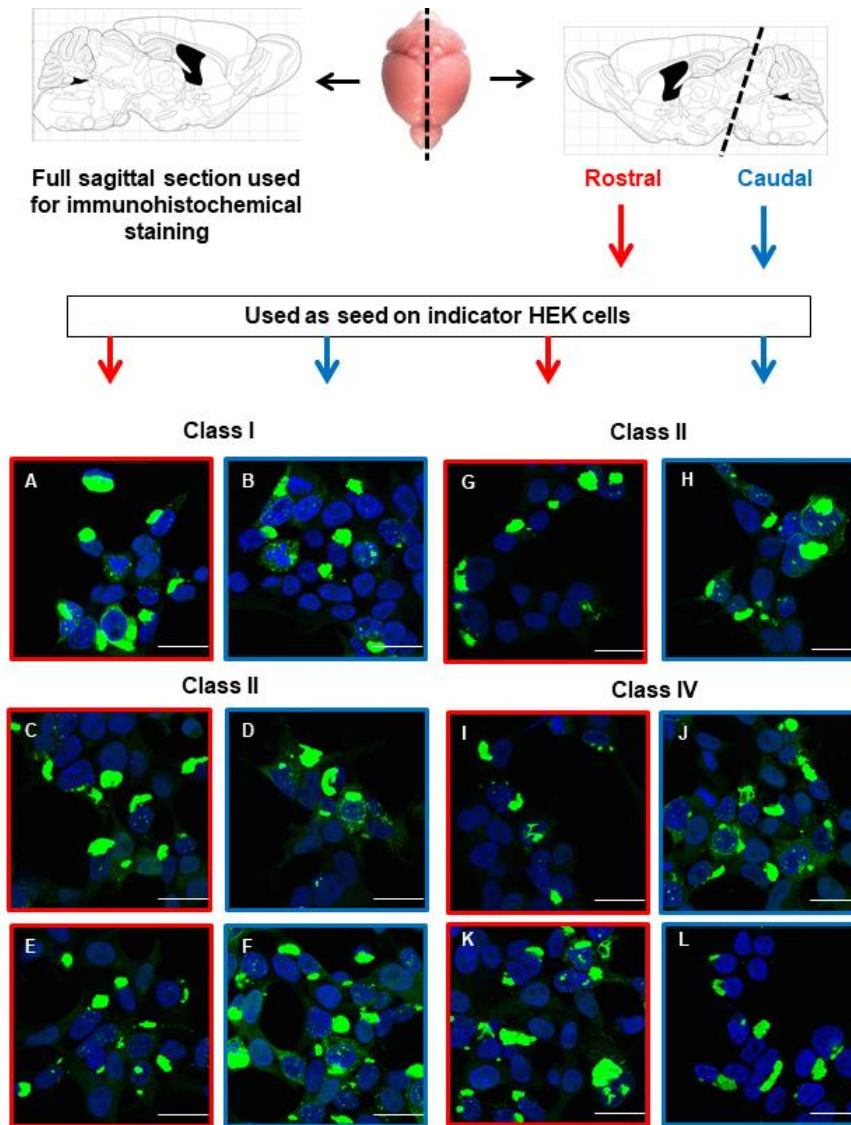


**Figure 2-37. Assessment of Tau strains in a cell-based seeding assay.**

Upper panel: Mouse brains have been cut sagittally with the right hemispheres fixed in formalin for further processing and embedding in paraffin and for use in immunohistochemistry. Left hemispheres were cut transversally according to the diagram (dashed line). Each rostral or caudal portion was then homogenized and used as a seed on cell cultures as described. Lower panels represent the fluorescent micrographs obtained from seeding assays with rostral (red border) or caudally derived (blue border) derived homogenates. When transduced into Clone 1 cells, which express Tau RD-YFP but lack aggregates, all homogenates seed morphologically indistinguishable Tau inclusions, which feature tangles of filamentous Tau (panels A-L). These inclusions are morphologically distinct from those seeded by Clone 9 (nuclear speckles) and Clone 10 (ordered inclusion) lysates (see Fig. 2.36).

### **2.3.9 Presence of a 25 kDa fragment in the soluble fraction of TgTau<sup>P301L</sup> mice suggest potential cleavage of tau by calpain.**

Upon assessment of the soluble fraction (SUP1) obtained from TgTau mice, we noticed the presence of a 25 kDa fragment of tau. To ensure the molecular weight of this fragment is not misrepresented due to phosphorylation of tau protein, we dephosphorylated all samples by lambda PP (**Fig.2.38 A**). The aforementioned 25 kDa fragment was detectable by both human specific and total tau antibodies (**Fig.2.38 B**). Further analysis revealed that this fragment accumulates as the animals age and is mostly abundant in SUP1 fractions from animals of +500 days old. Despite the heterogeneity amongst samples in the amount of this fragment, no significant difference was observed between animals of different classes or genetic background (**Fig 2.38 C**).

We next applied epitope mapping experiments, as well as LC/MS/MS analysis to identify the protein sequence of this fragment. Interestingly, epitope mapping experiments suggested that both N and C-terminal regions of human tau are present in this fragment, albeit far N-terminal regions were less abundant and the signal intensity obtained in western blot was much weaker than that of obtained from C-terminal antibodies. MS/MS analysis provided the same results; in all samples peptides corresponding to the C-terminal region of the protein were consistently present, however in 50% of the samples some N-terminal peptides were detectable as well (**Fig.2.39**). These results proposed that the fragment we had identified was the product of a cleavage event in the middle of the full-length tau protein (ca. 50 kDa), hence consisting of two approximately 25 kDa fragments. The low signal intensity from far N-termini peptides suggest that the N-terminal half of the molecule is less stable than the C-terminal fragment. We searched for known proteases that could cleave tau protein in the similar manner and found calpain as a potential candidate. We also identified calpain subunits amongst protein interactors of the aforementioned 25 kDa fragment. We next asked whether murine tau can be subjected to the same cleavage, and thus tested a few non-Tg mice SUP1 for the presence of the same fragment. A 25 kDa fragment was present in non-Tg mice, albeit without the heterogeneity observed in our TgTau animals. (**Fig. 2.38 D**)

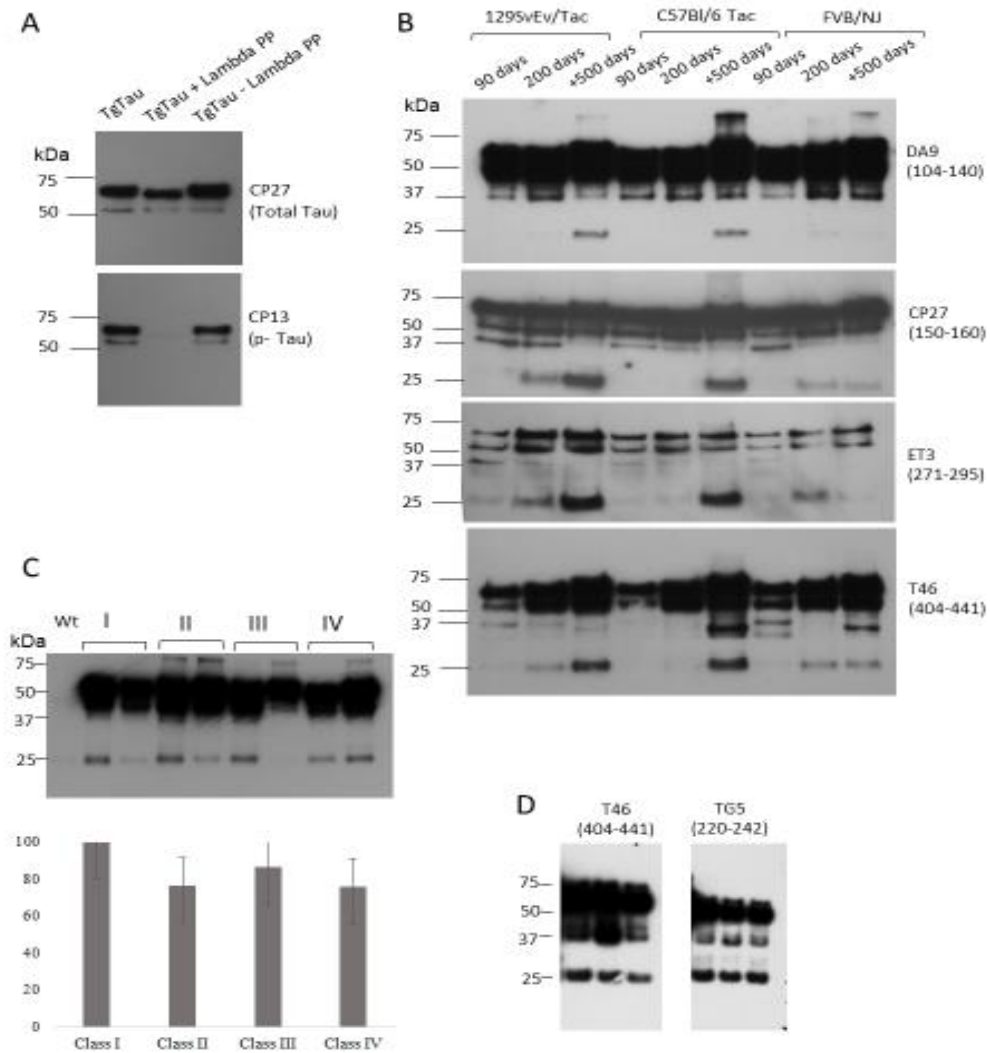
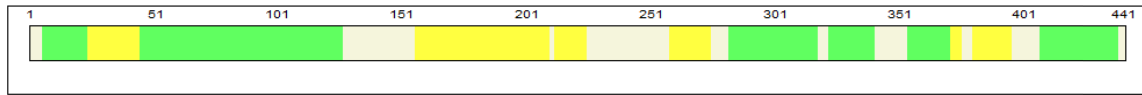


**Figure 2-38. The 25 kDa fragment in the soluble fraction of TgTauP301L mice.**

A) Dephosphorylation of tau by Lambda PP results in elimination of P-tau dependent antibodies' detection (CP13 here). B) epitope mapping of the 25 kDa band with different antibodies. The residues the antibody detect on 2N4R tau are presented in parentheses, C) The 25 kDa is present in all classes of pathology, albeit with vast heterogeneity (p-value > 0.5). D) A similar 25 kDa fragment is detectable in soluble fraction of aged non-Tg mice, yet without heterogeneity in its levels.

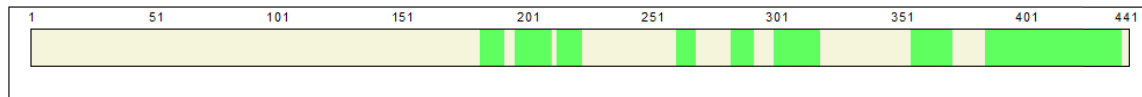
A

MAEPRQEFEV MEDHAGTYGL GDRKDQGGYT MHQDQEGDTD AGLKESPLQT PTEDGSEEPG SETSDAKSTP TAEDVTAPLV DEGAPGKQAA AQPHTIPEG TTAEAGIGD  
 TPSLEDEAAG HVTQARMVSK SKDGTGSDDK KAKGADGKTK IATPRGAAPP GQKQANATR IPAKTPPAPK TPPSSGEPPK SGDRSGYSSP GSPGTPGSR S RTPSLPTPT  
 REPKKVAVVR TPPKSPSSAK SRLQTAPVPM PDLKNVSKI GSTENLKHQP GGGKVQIINK KLDLSNVQSK CGSKDNIKHV LGGGSVQIVY KPVDLRSVTS KCGSLGNIHH  
 KPGGGQVEVK SEKLDKFRDV QSKIGSLDNI THVPGGGNKK IETHKLFRE NAKAKTDHGA EIVYKSPVVS GDTSPRHLSN VSSTGSIDMV DSPQLATLAD EVSASLARQG  
 L



B

MAEPRQEFEV MEDHAGTYGL GDRKDQGGYT MHQDQEGDTD AGLKESPLQT PTEDGSEEPG SETSDAKSTP TAEDVTAPLV DEGAPGKQAA AQPHTIPEG TTAEAGIGD  
 TPSLEDEAAG HVTQARMVSK SKDGTGSDDK KAKGADGKTK IATPRGAAPP GQKQANATR IPAKTPPAPK TPPSSGEPPK SGDRSGYSSP GSPGTPGSR S RTPSLPTPT  
 REPKKVAVVR TPPKSPSSAK SRLQTAPVPM PDLKNVSKI GSTENLKHQP GGGKVQIINK KLDLSNVQSK CGSKDNIKHV LGGGSVQIVY KPVDLRSVTS KCGSLGNIHH  
 KPGGGQVEVK SEKLDKFRDV QSKIGSLDNI THVPGGGNKK IETHKLFRE NAKAKTDHGA EIVYKSPVVS GDTSPRHLSN VSSTGSIDMV DSPQLATLAD EVSASLARQG  
 L



C

MAEPRQEFEV MEDHAGTYGL GDRKDQGGYT MHQDQEGDTD AGLKESPLQT PTEDGSEEPG SETSDAKSTP TAEDVTAPLV DEGAPGKQAA AQPHTIPEG TTAEAGIGD  
 TPSLEDEAAG HVTQARMVSK SKDGTGSDDK KAKGADGKTK IATPRGAAPP GQKQANATR IPAKTPPAPK TPPSSGEPPK SGDRSGYSSP GSPGTPGSR S RTPSLPTPT  
 REPKKVAVVR TPPKSPSSAK SRLQTAPVPM PDLKNVSKI GSTENLKHQP GGGKVQIINK KLDLSNVQSK CGSKDNIKHV LGGGSVQIVY KPVDLRSVTS KCGSLGNIHH  
 KPGGGQVEVK SEKLDKFRDV QSKIGSLDNI THVPGGGNKK IETHKLFRE NAKAKTDHGA EIVYKSPVVS GDTSPRHLSN VSSTGSIDMV DSPQLATLAD EVSASLARQG  
 L

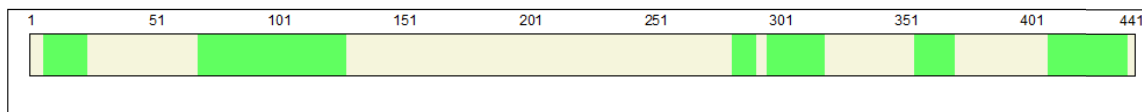


**Figure 2-39. In-gel digestion and LC/MS/MS of the 25 kDa fragment in SUP1 of TgTauP301L mice.**

A) A representative sequence coverage of the full-length tau. This was checked in each processed sample as a control. B) A representative sequence coverage results obtained from the 25 kDa fragment consists of the C-terminal region of human tau protein, consistent with data obtained from epitope mapping (Fig.2.38). C) In 50% of the samples some N-terminal peptides were detected (regions detectable by N-terminal antibodies such as DA9 in Fig.2.38 B).

## 2.4 DISCUSSION

### 2.4.1 Phenotypic variation and classes in P301L Tauopathy.

Our earlier studies defined a degree of diversity in cognitive and pathology phenotypes in a P301L mouse model (Murakami, Paitel et al. 2006) and we have now sought to understand these phenomena within the framework of an extended study. New derivative sublines of TgTau<sup>P301L</sup> mice were created in three distinct inbred backgrounds, and, while uniform responses were recorded in some criteria, neuropathological diversity was certainly not extinguished. Rather, the larger cohorts of animals produced for study allowed us to perceive both recurrent patterns (classes of pathology) or variations (animals either falling outside of the classification scheme with focal pathologies or completely lacking pathology) that we had not previously appreciated. Collectively, these data pose a number of overlapping questions that include a) the nature of operational parameters that distinguish this study from other studies, b) the mechanistic origin(s) of histopathological heterogeneity that includes stereotypic and variant, focal events, c) the possible role of "spreading effects", d) the possible role of Tau "strains" and e) the possible relationships to clinical variations amongst patients with the same *MAPT* mutations.

### 2.4.2 Signatures of uniform expression and protein misfolding in TgTau<sup>P301L</sup> mice.

Operationally, the paradigm described here is markedly different from using specialized promoters or stereotaxic injections of misfolded Tau to produce local effects (de Calignon, Polydoro et al. 2012, Liu, Drouet et al. 2012, Iba, McBride et al. 2015, Stancu, Vasconcelos et al. 2015). But how might focal effects originate, and could they relate to the transgene system? Besides special chemical attributes of the 2N, 4R Tau isoform of human Tau, several factors may allow the accretion of diverse, focal pathology. First, the ability to accumulate Tau in neurons or astrocytes or oligodendrocytes (Murakami, Paitel et al. 2006), perhaps reflecting a low-level of "leaky" non-neuronal expression from the hamster PrP gene promoter or the trafficking of nascent, misformed Tau from neurons to astrocytes (Moser 1995). Second, the level of transgene expression (1.7X endogenous) may be fortuitous, allowing us to perceive focal events in a slow

pathogenic cascade with most alterations occurring in the last 40% of the animals' natural lifespan (using the aforementioned figure that 750 days of age represents 95% or greater of natural lifespan for inbred mouse strains that are not prone to neoplasias). These events cannot be scored in models with 1x expression such as P301L knock-in mice that have a latent underrepresentation of neuronal mitochondria but lack CNS pathology (Gilley, Seereeram et al. 2012, Rodriguez-Martin, Pooler et al. 2016), or might be difficult to discern in TgTau mice with overexpression, e.g. up to 13x in widely-used rTg4510 mice with loss of 23% of CA1 hippocampal neurons evident within the first third of a lifespan (Santacruz, Lewis et al. 2005). In the studies here, the TgTau<sup>P301L</sup> transgene array is co-expressed with endogenous mouse *Mapt* and therefore approximates to the human situation with dominant *MAPT* mutations co-expressed with a WT allele. Misfolded human Tau species may be interacting with endogenous mouse Tau protein (Ando, Leroy et al. 2011) but this would be a systematic effect and other studies have indicated that use of a *Mapt*<sup>0/0</sup> background blunts rather than exacerbates Tau toxicity (Wegmann, Maury et al. 2015). Although epigenetic effects can affect neurobiological endpoints, mechanistically these derive from DNA and histone methylation modulating transcription (Labrie, Pai et al. 2012) and the Tau transgene insertion site would need to be posited as a target for modification. In practice, the levels of Tau expression do not decrease with age in TgTau<sup>P301L</sup> mice and do not seem to be a limiting variable for the development of Tau pathology, as shown by pathology-negative but transgene-expressing mice. Instead, broadly homogeneous expression in a rostral/caudal plane (**Fig. 2.1D**), as driven by the cos.Tet vector (Scott, Köhler et al. 1992) is consistent with position-independent, pan-neuronal expression of transgene-encoded mRNA observed in other uses of this vector (Prusiner, Scott et al. 1990, Scott, Groth et al. 1993, Citron, Westaway et al. 1997); in this case it produces a comparatively uniform level of Tau substrate considered in a neuroanatomical sense (**Fig. 2.1, 2.2**) that may be conducive to scoring age-related events that cause focal deposition. Other studies failed to reveal hotspots of transgene expression (**Fig. 2.28**), again speaking against a rate-limiting role for expression of full-length 2N, 4R Tau.

Foci can frequently initiate as astrocytic plaques in the molecular layers of the Hpc and the subiculum. In the pons, events can occur in the Raphe nuclei and superior olivary complex. In the striatum, foci occur as tangles and astrocytic plaques. Rarer events portrayed in **Fig.2.27** include the locus coeruleus and also the retrosplenial cortex (both known to capable of

supporting the DS6 strain of misfolded Tau (Kaufman, Sanders et al. 2016) - see below). Other animals fell outside of this classification scheme by having focal pathologies and yet other animals has no discernible Tau deposition. As the three inbred derivatives of Tg founder each approach genetic homogeneity and are different from each other (apart from the chromosome region flanking the insertion site and some non-syntenic blocks of DNA), there are strong indications that genetic effects do not underpin the pathologies that, instead, appear to define heterogeneous and possibly stochastic events. In this respect, our data parallel studies where FVB/129 versus C57BL/6NTac genetic backgrounds minimally altered the presentation of Tau pathology in rTg4510 Tau mice with a P301L mutation (Bailey, Howard et al. 2014).

### **2.4.3 Tau proteolysis, classes of Pathology and Tau spreading.**

Tau could be subjected to several proteolysis events, some of which can make significant contributions to its aggregation and deposition in brain (Quinn, Corbett et al. 2018). A 24 kDa fragment of tau derived from calpain proteolysis accumulates in Tg601 mouse model in an age-dependant manner (Matsumoto, Motoi et al. 2015). Calpain-generated tau fragments have been detected in AD and FTD human patients (Chun and Johnson 2007, Chen, Liu et al. 2018). This fragment is more prone to aggregation than full length tau and could recruit the full length molecule into the seeded aggregates (Chun and Johnson 2007). We detected a similar fragment in the soluble fraction of our aged TgTau mice (**Fig.2.38**). Moreover, the trypsin-resistant core in all animals (all three patterns) consisted of C-terminal region which is present in this fragment (**Fig.2.34**). The fact that a similar band is present in aged non-Tg mice suggest that calpain cleavage of tau to generate this C-terminal fragment could be a consequence of aging (**Fig.238 D**). However, it is not clear why human tau in our TgTau mice show vast heterogeneity in being processed by calpain. Whether this fragmentation is the cause or consequence of tau spreading and aggregation and most importantly formation of distinct classes of pathology requires further work and investigations.

When Tau attains abnormal forms, and becomes fragmented in older animals (as per **Fig.2.30 A-C**), this may facilitate template-directed folding and neuroanatomical “spreading” in a prion-like manner (Clavaguera, Bolmont et al. 2009, Iba, Guo et al. 2013, Clavaguera, Hench et al. 2015,

Peeraer, Bottelbergs et al. 2015) to produce a larger field of pathology. Hence, deposition in animals with higher burden of pathology could reflect the sum total of early initiating events plus subsequent events derived from spreading. Given the involvement of adjacent fields, Classes I, II and III could be interpreted to represent sequential invasion of neuroanatomic areas from an initial focus, but the scenario with specific classes synchronized to specific chronological ages is excluded as these classes have indistinguishable average onset within an inbred strain and between each other (**Table 2.1**). In this respect, our data differ from analyses of compound Tg mice comprised of PS19 Tg mice (1N, 4R isoform) with a frontotemporal dementia mutation (P301S) (Yoshiyama, Higuchi et al. 2007) crossed with PDAPP A $\beta$ -depositing mice (Games, Adams et al. 1995); the majority of these animals represented predictable progression between the ages of 4, 8 and 11 months from stages referred to as I/II, III/IV and V/VI (Hurtado, Molina-Porcel et al. 2010). Cortical deposition was present in all stages and some analogies to the Braak staging scheme for sporadic AD were also noted (Braak and Braak 1991, Braak and Braak 1995, Hurtado, Molina-Porcel et al. 2010). On the other hand, for TgTau<sup>P301L</sup> mice, if initiating focal events were to start at different ages in different animals, then a predictable progression from Class I->II->III promoted by "spreading" becomes plausible. In this scenario, two animals assigned to different classes - I and III, for example - could nonetheless share the same chronological age. A kinship between events in Class I and Class II mice is also suggested by biochemical analyses of Tau species (**Figs.2.30, 2.31, 2.32, Table 2.3**). With regards to seeded growth as a necessary step in neuroanatomical spread, it is notable that brain material taken from older animals has seeding capacity in a fluorescent assay (**Fig.2.36** and discussed further below). The low level of transgene expression in TgTau<sup>P301L</sup> mice must limit the substrate concentration for templated refolding and in this sense, may be the key mechanistic variable to dictate "slow motion" pathogenesis and hence the ability to capture focal pathologies before spreading.

#### **2.4.4 Pathological heterogeneity and Tau strains.**

For protein-mediated effects, templated growth of heterogeneous misfolded protein conformers might cause heterogeneity in neurobiological endpoints, a concept pioneered for prion infections. Prion strains involve differently misfolded forms of the cellular prion protein (Bessen 1995,

Collinge and Clarke 2007) and prior analyses have suggested the existence of Tau "strains" in human brain material (Sanders, Kaufman et al. 2014, Clavaguera, Hench et al. 2015). However, the inventory of covalent modifications to Tau is complex, including alternative splicing of N-terminal sequences and/or microtubule binding repeat exons, truncation, phosphorylation at up to 85 sites, O-glycosylation and acetylation (Wang and Mandelkow 2016). This complexity in covalent structure thereby imposes constraints upon interpreting Tau strain phenomena as an exclusive basis for pathological heterogeneity. Here we used a transgene construct with no alternative exonic splicing and used seeding assays and biochemical profiling to begin to address this issue.

Although the cellular assay for seeding was positive from Tg mouse-derived material and can detect up to 18 distinct Tau signatures (Sanders, Kaufman et al. 2014, Kaufman, Sanders et al. 2016), we obtained only one signature from animals with rostral or caudal Tau deposition (i.e. Classes I, II or IV; **Fig.2.37**). This particular signature resembled the isolate designated DS6 derived from P301S mice (Yoshiyama, Higuchi et al. 2007, Kaufman, Sanders et al. 2016). Of note, DS6 produces deposits in many brain regions after inoculation (Kaufman, Sanders et al. 2016), an observation compatible with the DS6-like seeding activity within TgTau<sup>P301L</sup> animals populating different brain regions. In our experiments seeding activity was unrelated to the presence of AT8 immunostaining and it is unclear whether dispersed oligomeric species (Tai, Wang et al. 2014, Shammass, Garcia et al. 2015) contribute to the seeding activity because these species were not readily detected in Class IV animals (**Fig.2.30 D**). However, widespread seeding activity with little relationship to protein deposition assessed by light microscopy clearly parallels results using a templating assay for mice expressing a mutant form of PrP (Alibhai, Blanco et al. 2016). Seeding activity is known to occur in early Braak stages of Alzheimer's Disease (Furman, Vaquer-Alicea et al. 2017) and given the observation of seeding before immunopositivity in TgP301S mice (Kaufman, Thomas et al. 2017) it is possible that seeding activity arises early in the life of TgTau<sup>P301L</sup> mice.

What about other signatures that might relate to Tau strain phenomena? Using EM to examine P3 samples we observed a predominant morphology of straight filaments, irrespective of class type (**Table 2.3**), similar to other analyses (Götz, Chen et al. 2001). But in some other respects Class IV animals did differ from Classes I and II. The P3 fractions had the fewest observable

straight filaments per ug of protein, generally less net immunoblot signal, different immunoblot quality as assessed with three antibodies and different signature after trypsin digestion (Figs.2.32, 2.34; Table 2.3). Some of these qualitative different properties may derive from a fundamentally different (lowered) propensity of misfolded Tau in Class IV animals to aggregate. In sum, TgTau<sup>P301L</sup> mice clearly harbor at least three and perhaps up to four variants of Tau. One variant is detected in the seeding assay (this is present in all classes and is also present in brain areas without immunostaining), while three more variants are detected by trypsin digestion. In the absence of divergent data from seeding assays or true breeding of biochemical properties in serial transmissions experiments we cannot formally conclude that variants reflect the creation of new Tau strains; however, this is a straightforward explanation of the current data.

#### **2.4.5 Origins of variegated Tau pathology in inbred mice.**

The quantitative and qualitative differences in Tau species between the pathology Classes are unequivocally striking and they do beg the question of origination. Genesis of Tau seeding activity may be amenable to study in the congenic models presented here but beyond this, the macroscopic assemblies detected with anti-Tau antibodies represent independent and perhaps more biologically impactful events. Weaker/stronger AT8 reactivity in TgTau<sup>P301L(T)</sup> mice was associated with lesser/greater amounts of insoluble Tau and better/worse performance in the conditioned taste aversion (CTA) assay for memory function (Murakami, Paitel et al. 2006). Although CTA assays were not undertaken for the current cohorts, the correlation between Tau aggregation/deposition, synaptic dysfunction and frank cognitive impairment is well established (Bondareff, Mountjoy et al. 1989, Bierer, Hof et al. 1995, Braak and Braak 1995, Hochgrafe, Sydow et al. 2013, Brier, Gordon et al. 2016, Schwarz, Yu et al. 2016). Hence a more pertinent question is "how can heterogeneity occur in aged brains, given the genetic constraints, the absence of extraneous pathogens and the regulated housing conditions?". While the performance of other mouse models with indolent Tau deposition remains to be assessed, the question about heterogeneity is underscored by the benchmark of human case material, where phenotypic variation exists in human FTLT-MAPT kindreds, and can be present even within families harboring the exact same mutation in codon 301 (Foster, Wilhelmsen et al. 1997, Clark, Poorkaj

et al. 1998, Bird, Nochlin et al. 1999, Mirra, Murrell et al. 1999, van Swieten, Stevens et al. 1999, Kobayashi, Mori et al. 2002, Yasuda, Nakamura et al. 2005).

Decreases in quality control processes affecting protein maturation, turnover and clearance might facilitate the appearance of abnormal Tau species that can then go on to initiate a cascade of accumulation (Nixon 2013, Tarasoff-Conway, Carare et al. 2015, Myeku, Clelland et al. 2016) but the associated molecular and cellular pathways may be generic in scope - for example being present in immortalized mammalian cells and conserved in yeast - and not tailored to different neuroanatomical regions. Also, the proteostatic machinery of cells in a given neuroanatomical region might be anticipated to be similar between animals of the same age and genetic background. We therefore posit that external insults to the aging CNS - especially those that could act with asymmetry with respect to neuroanatomy - are the missing links needed to understand variegated Tau pathology. In principle, these insults/parameters could include: mechanical aspects of the blood supply such as focal alterations in the blood-brain barrier or hyper-vascularization, blood constituents such as hormones/cytokines/nutrients/toxins, as well as blood-borne cells that can patrol the CNS, such as microglia. Xenobiotics, such as metabolites from microbiota and variations in the microbiota themselves might also warrant consideration (Borroni, Ferrari et al. 2014, Mayer, Knight et al. 2014, Mayer, Tillisch et al. 2015, Radford, Morsch et al. 2015, Mather and Harley 2016, Sampson, Debelius et al. 2016, Erdo, Denes et al. 2017). Here, the involvement of caudal brain structures (**Figs. 2.8-2.10, 2.28**) that include inputs from the enteric nervous system and hence the digestive tract, illustrate a subset of these possibilities. Overall, we deduce that the initiating parameters that determine presence/absence of focal pathologies lie beyond the information stored in the mouse nuclear genome and beyond the internal CNS connectivity that allows Tau spreading (Clavaguera, Hench et al. 2015). The congenic models described here with indolent changes in pathology constitute experimental platforms to define and push stochastic, rate-limiting steps in pathogenesis in the aging mammalian brain. Understanding stochastic events in TgTau<sup>P301L</sup> mice may be useful in understanding sporadic events that feature in the common idiopathic forms of dementia.

## 2.6 CONCLUSIONS.

In our first description of a TgTauP301L transgenic line, onset of clinical disease differed between Tg colonies maintained at different laboratory sites. Additionally, some heterogeneity also existed within cohorts of age matched Tg mice of the same colony with regards to levels of insoluble tau and memory function [12]. Given that phenotypic variation occurs in patients carrying the same P301L mutation [1, 14-17], we extrapolated that the TgTauP301L line might be manifesting a related biological effect. Here we considered two views to account for this phenotypic heterogeneity; the action of genetic modifier loci versus a role for stochastic cell biological events and/or environmental inputs. To explore these hypotheses a founder stock designated TgTauP301L(T) was used to make three inbred derivatives. Phenotypic variations were not eliminated by this maneuver and different classes of pathologic variation were observed; these were shared between (and independent of) the three inbred genetic backgrounds, suggesting the action of extrinsic disease modifiers. Moreover, distinct molecular signatures for three pathology classes following trypsin digestion of detergent-insoluble material strongly suggest the *de novo* formation of different Tau strains. Thus, heterogeneous factors affecting the genesis of abnormal Tau species may be amenable to discovery using the inbred models described here.

**Chapter 3: Quaternary structure changes for PrP<sup>Sc</sup>  
predate PrP<sup>C</sup> down-regulation and neuronal death  
during progression of experimental scrapie disease**

### 3.1 Introduction.

Prion diseases are fatal neurodegenerative diseases in humans and animals with the common feature of misfolding and aggregation of the cellular prion glycoprotein (PrP<sup>C</sup>) to protease resistant “Scrapie” prion protein (PrP<sup>Sc</sup>). (Bolton, McKinley et al. 1982, Carlson, Westaway et al. 1989, Prusiner 1991). The pathogenesis of prion diseases is associated with a progressive accumulation of PrP<sup>Sc</sup> molecules. Interestingly, prion diseases with different incubation periods share a relatively long sub-clinical stage during which levels of infectious titre do not grow exponentially, but instead reach a maximum (Dickinson 1979). Although the molecular mechanism of this plateau effect, as well as the process through which the subsequent exit to overt clinical disease occurs are debated, previous work suggests that a decrease in PrP<sup>C</sup> protein levels at pre-clinical stages of the disease could be of importance in controlling pathogenesis (Mays, Kim et al. 2014, Mays, van der Merwe et al. 2015).

The notion that different conformational states of PrP<sup>Sc</sup> exist amongst distinct prion strains is well-established (Safar, Wille et al. 1998, Tanaka, Chien et al. 2004, Bartz 2016). Also, historically, detergent-insoluble protease-resistant PrP<sup>Sc</sup> species have been defined as the major neurotoxic species and linked directly to disease pathogenesis (Meyer, McKinley et al. 1986, Hughes and Halliday 2017). However, accumulating experimental evidence obtained from different analytical methods suggests complexities exist even within the confines of one strain with regards to the structural heterogeneity and hints at the presence of different PrP<sup>Sc</sup> assemblies with distinct biochemical, biophysical and toxicological characteristics (Meyer, McKinley et al. 1986, Simoneau, Rezaei et al. 2007, Igel-Egalon, Bohl et al. 2019, Igel-Egalon, Laferrière et al. 2019). Thus some studies suggest the presence of a broader spectrum of PrP<sup>Sc</sup> species with distinct biochemical characteristics and neurotoxicity features at different timepoints during the disease development (Simoneau, Rezaei et al. 2007, Hughes and Halliday 2017); the species with conformational characteristics distinct from the material detected at terminal stages of the disease may be responsible for triggering the cascade of events contributing to pathogenesis and neurotoxicity in the brain (Kim, Haldiman et al. 2011, Mays, van der Merwe et al. 2015, Foliaki, Lewis et al. 2018). Here we have investigated biochemical transitions of PrP<sup>C</sup> molecules using fractionation under minimally denaturing conditions, in a mouse model of prion disease (RML) at different timepoints during disease progression. We assessed neural and non-neural cell

populations, as well as histological changes of the brain, at the same timepoints to unravel the correlation between PrP<sup>Sc</sup> species detected at each timepoint and the processes of disease pathogenesis.

## **3.2 Experimental procedures.**

### **3.2.1 Animals:**

All animals were maintained in ventilated racks (Tecniplast, Green Line) and fed irradiated chow (LabDiets, 5053). They were housed with a 12 hr/12 hr light/dark cycle. Cage environmental enrichment comprised 5 cm diameter plastic tubes and nesting material ("Nestlets", Ancare Inc.). Mice were inoculated at 3 to 6 weeks of age with 50 µl 1% w/v brain homogenate containing mouse-adapted scrapie (RML). For the collection of brains for analysis by the isotropic fractionator technique and metabolomic studies, animals were anesthetized by isoflurane inhalation, perfused with 25 mL phosphate saline, the brain was quickly extracted, and one half brain was stored at 4% phosphate-buffered paraformaldehyde (PFA). The other half brain was snap-frozen and kept at -80°C until being processed for metabolic analysis. For immunohistochemistry and western blot analysis, animals were sacrificed by cervical dislocation, the brain was removed and cut sagittally; one half brain was fixed in Carnoy's fixation solution (Metha-Carn) (Puchtler, Waldrop et al. 1970) for immunohistochemistry analysis and the other half was snap-frozen and kept at -80°C until being processed for western blot experiments. All protocols were in accordance with the Canadian Council on Animal Care (CCAC) and were approved by the Animal Care and Use Committee at the University of Alberta (AUP00000357).

### **3.2.2 Brain homogenization:**

Half brains were weighed and homogenized in ddH<sub>2</sub>O with glass Dounce homogenizers, to make 10% brain homogenates (w/w). Aliquots of solution were prepared and kept at -80°C for further analysis.

### **3.2.3 Quantification of brain cells using Isotropic fractionator:**

The isotropic fractionator method for quantifying neuronal loss in tissue samples was performed as previously described with minor modifications (Herculano-Houzel and Lent 2005, Eskandari-Sedighi, Daude et al. 2017). Briefly, perfused and post-fixed brain samples were mechanically dissociated and homogenized in 10 volumes of a solution of 40 mM sodium citrate and 1% Triton X-100. The homogenates were collected, and the homogenizer was washed at least twice to collect any residual cells. To visualize nuclei and obtain total cell counts, 20  $\mu$ L of 100  $\mu$ g/mL stock solution of 4',6-diamidino-2-phenylindole (DAPI, Sigma) was added to the cell suspension and the total number of cells were counted (final concentration of DAPI was 0.20  $\mu$ g/ml) using disposable hemocytometers (inCYTO). Counting was done in a semi-automated manner: pictures of the quadrants were taken using an InCell 2000 analyzer, and a sub-routine software, adjusted to detect fluorescent signals from stained nuclei (InCell Analyzer software, GE-Healthcare), was used for unbiased counting of the cells. All four quadrants in both the upper and lower grids of the hemocytometer were used for counting and the results were averaged. To determine total neuron counts, 1 mL of each cell suspension was removed, washed with PBS, and centrifuged for 10 minutes at 5000xg. Cells were then incubated with neuronal cell specific nucleus marker, NeuN, antibody (1:200; rabbit polyclonal, Millipore) for two hours followed by incubation in a secondary anti-rabbit IgG-Alexa-Fluor 594 for one hour (1:200; Invitrogen). Cells were then counted in the same semi-automated manner described earlier. The percentage of NeuN-stained nuclei was recorded. Total cell numbers and neuronal numbers were then calculated by multiplying the number of cells/mL by the final volume.

### **3.2.4 Immunohistochemistry:**

Sagittal sections were fixed in Carnoy's fixative solution and embedded in paraffin. Hematoxylin and Eosin (H and E) staining was done as previously described (Mercer, Daude et al. 2018). For immunodetection, slices were heated to 121°C in 10 mM citrate buffer and allowed to cool to room temperature. Staining for PrP<sup>Sc</sup> was then accomplished by treatment with formic acid and 4 M guanidine thiocyanate before an overnight incubation with biotinylated SAF83 (Cayman Chemicals). GFAP immunodetection was accomplished by subsequent incubation in 3% peroxide and overnight incubation with a biotinylated primary antibody cocktail (BD Biosciences; 556330), as well as counterstaining with Mayer's hematoxylin.

### **3.2.5 Western Blotting:**

Western blotting was performed as described previously (Towbin, Staehelin et al. 1979). Samples were prepared in loading buffer containing SDS and 2-mercaptoethanol and boiled for 10 min. They were then electrophoresed on 10% bis-tris precast gels (Invitrogen) using an Invitrogen system and transferred to polyvinyl difluoride (PVDF; Millipore) membranes (wet transfer). Blots were then blocked with 5% skim milk in 1xTBS-0.1% Tween 20 for one hour at room temperature and incubated with primary antibodies at 4 °C overnight (except for blots prepared for detection with Sha31 (Spibio) antibody, where no blocking was done and blots were directly incubated with antibody in 1xTBS-0.5% Tween 20). To assess inflammation markers and synaptic density antibodies against Iba1(Waco), TREM2 (Abcam) and synaptophysin (Sigma-Aldrich) were used at concentrations recommended by the manufacturer.

### **3.2.6 Data Analysis:**

Histology and western blot data were analyzed using ImageJ software (NIH). For quantification of histology data, we used trainable Weka (Waikato Environment for Knowledge Analysis) segmentation and ImageJ (Arganda-Carreras, Cardona et al. 2015). Briefly, a probability map was

created for each histology experiment by a training set that was chosen from 5 control images and prion infected animals (RML). The trained map was then applied to the samples and the measured values were then quantified in ImageJ.

### **3.2.7 Proteinase-K digestion:**

For Proteinase-K (PK) digestion of crude brain homogenates, 10 µg of brain homogenate was incubated with PK (New England Biolabs) for 1 hour at 37°C. The reaction was then stopped by addition of Pefabloc (Sigma). Samples were then boiled with SDS-sample buffer and electrophoresed on 4-12% NuPAGE gels.

For PK digestion of fractions obtained from AF4, we incubated equal volumes from each fraction with 20 µg/ml of PK. Since protein concentration in fraction samples were way lower than detection limits of bicinchoninic acid (BCA) protein assay kit, and to make sure we have equal amount of protein in all samples, we added total of 20 µg bovine serum albumin (BSA) to each fraction. Reactions were then adjusted to the same volume for all samples and they were incubated with PK for 1 hour at 37°C. The reaction was then stopped by addition of Pefabloc. Samples were then boiled with SDS-sample buffer and ran on gel.

### **3.2.8 Asymmetric Flow field-flow fractionation (AF4):**

Brain homogenates (10% w/v) were solubilized by adding an equal volume of solubilization buffer (50 mM HEPES pH 7.4; 300 mM NaCl; 10 mM EDTA; 4% (w/v) dodecyl-β-D-maltoside (Sigma)) and incubated for 45 min on ice. Sarkosyl (N-lauryl sarcosine; Fluka) was added to a final concentration of 2% and incubated on ice for 30 min. The samples were then centrifuged (20,000xg, 10 min) at 4°C. The supernatants were collected, and 350 µg of total protein were subjected to asymmetrical flow field-flow fractionation on an AF2000 Postnova system using phosphate-buffered saline solution pH 7.4 containing 0.05% sodium dodecyl sulfate (SDS) as the running buffer. The fractionation channel was 26.5 cm in length and 350µ m in height, constructed with a trapezoidal spacer of maximal width 21 mm at the inlet, and lined with a 10-

kDa cut-off polyethersulphone membrane at the accumulation wall. Samples were focused for 4 min and then eluted at a channel flow rate of 0.5 mL/min with constant cross-flow for the first 10 min, decreasing from 1.5 to 0.35 mL/min in the following 15 min, from 3.5 to 0 mL/min in the next 30 min, and running with no cross-flow for the last 10 min. A slot pump was run at 0.3 mL/min to concentrate the samples before they passed through the detectors. Fractions of 0.2 mL were collected. Static and dynamic light scattering measurements were carried out on an in-line DAWN HELEOS II detector (Wyatt Technology) and the data collected and analyzed using ASTRA analysis software (version 6.0).

### **3.2.9 Expression and Purification of mouse PrP:**

A codon-optimized synthetic gene corresponding to full length mouse PrP (moPrP23-231; allelic type *Prnp<sup>a</sup>*), was obtained as previously described (Cortez, Kumar et al. 2013). *Escherichia coli* BL21 (DE3) cells harboring this plasmid were grown in LB media plus 100 µg/mL ampicillin at 37 °C. Protein expression was induced with addition of 1 mM isopropyl-1-thio-β-D-galactopyranoside. Bacteria cells were then pelleted and resuspended in lysis buffer (8 M urea, 10 mM Tris, 100 mM Na<sub>2</sub>PO<sub>4</sub>, pH 8.0) and sonicated with digital sonifier (Branson 450 digital sonifier) using a microtip at 30% amplitude for 10 cycles of 30 sec. Cell debris were removed by centrifugation at 6000xg and the supernatant was loaded in a nickel-nitrilotriacetic acid column (ThermoFisher). Contaminants were removed using 5 column volumes of 8M urea, 10 mM Tris, 100 mM Na<sub>2</sub>PO<sub>4</sub> and 50 mM imidazole (pH 6.3). The His-tagged prion protein was eluted using 8M urea, 10 mM Tris, 100 mM Na<sub>2</sub>PO<sub>4</sub> and 500 mM imidazole (pH 4.5). The collected sample was then subjected to HPLC for further purification (C4 Vydac preparative column). Aliquots of 8 mL of sample were injected and then eluted using a gradient of acetonitrile (ACN) (20-60%) and 0.1% trifluoroacetic acid in 60 min. The protein eluting at 35-38% ACN was collected, lyophilized, and stored at -80 °C.

### **3.2.10 Real-time quaking-induced conversion (RT-QuIC) assay:**

Recombinant PrP (moPrP) was solubilized in 6 M guanidine hydrochloride (GdnHCl) solution. This was then diluted in RT-QuIC buffer (20 mM sodium phosphate pH 7.4; 130 mM NaCl; 10 mM EDTA; 0.002% SDS) to a final protein concentration of 0.2 mg/mL (and residual 0.2 M GdnHCl). Reactions were seeded with 2  $\mu$ L of 10% solubilized brain homogenate in a final volume of 180  $\mu$ L/well. The aggregation reactions were carried out in 96-well plates (Costar 3610) sealed with thermal adhesive film (08-408-240; Fisherbrand). The samples were incubated in the presence of 10 mM thioflavin T (ThT) at 42 °C with cycles of 1 min shaking (700 rpm double orbital) and 1 min rest. ThT fluorescence measurements (450+/210 nm excitation and 480+/210 nm emission; bottom read) were recorded every 60 minutes. There were three technical replicates for each sample per experiment.

## **3.3 Results:**

### **3.3.1 Quantitative and qualitative changes in brain cell populations during the course of infection with the RML scrapie prion isolate**

Isotropic fractionation is a non-stereological method to quantify different cell populations in the brain based on counting isolated nuclei following detergent lysis of cell membranes, and its accuracy has been verified by cross-referencing to other techniques (Collins, Young et al. 2010, Brautigam, Steele et al. 2012, Bahney and von Bartheld 2014, Repetto, Monti et al. 2016, Ngwenya, Nahirney et al. 2017); we took advantage of this method to determine the number of cells in the brain at different timepoints in RML inoculated animals, as well as in matched controls.

Assessments of neural and non-neural cell populations at different timepoints indicated a significant increase in total brain cells (i.e total number of nuclei as stained with DAPI) at 120 days post-inoculation (DPI), followed by a significant decrease at 150 DPI (**Fig.1 A**). Analyses of the NeuN antibody-positive population of nuclei revealed significant neuronal loss at terminal stage of the disease (150 DPI). In contrast, the non-neural cell population trended to an increase,

starting from 90 DPI and reaching significance at 120 DPI (**Fig.1 B and C**). In parallel to these measurements we observed a significant decrease in body weight of the RML-infected mice, however the wet weight of brains showed no significant changes in any of the cohorts thus excluding this parameter as a confound for data interpretation (**Fig.1 D and E**). Due to the current lack of lineage-specific nuclear markers for any of the non-neuronal cell populations in the brain (i.e., analogous to the use of NeuN for identifying nuclei derived from neurons), we could not distinguish individual cell lineages amongst the non-neuronal cell cohort. However, prior reports indicate microgliosis and astrogliosis initiating at pre-clinical stages of prion diseases (Hwang, Lee et al. 2009, Alibhai, Blanco et al. 2016) and the results here from the isotropic fractionator analyses are potentially compatible with these data.

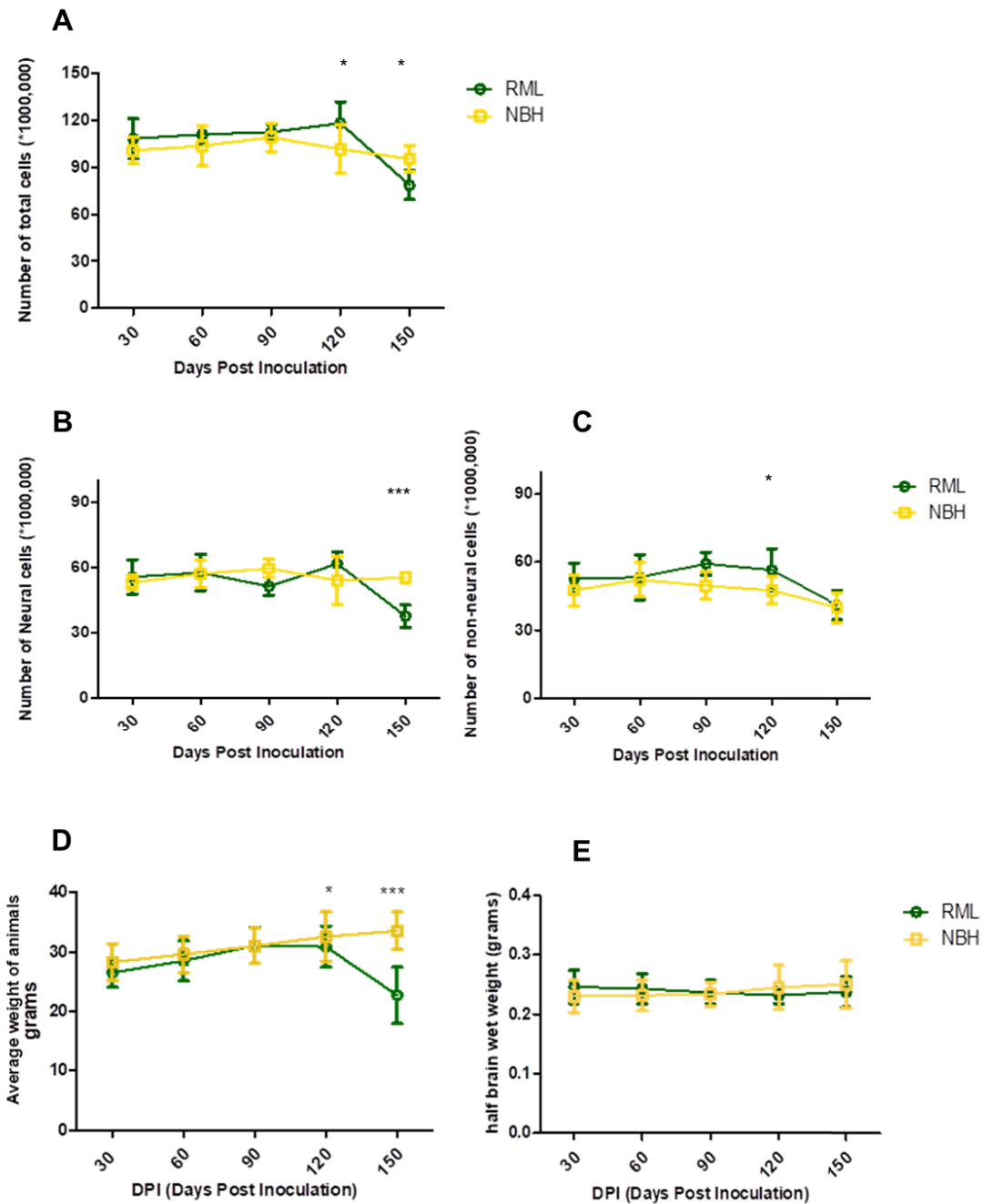
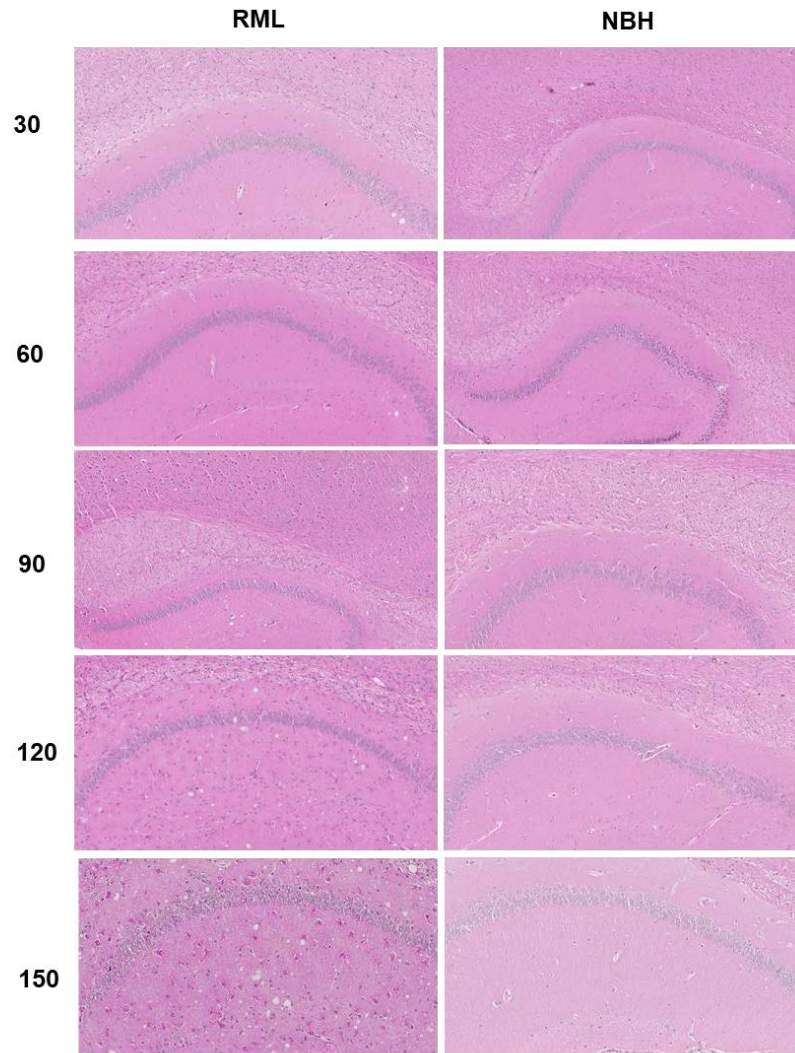


**Figure 3-1. Quantification of brain cells by isotropic fractionator**

**A)** Quantification of total brain cells indicate significantly higher number of cells at 120 DPI and a significant decrease at the number of cells at 150 DPI in RML-inoculated animals **B)** Quantification of neuronal cells in brain indicate a significant decrease in the number of neurons at 150 DPI in RML-inoculated animals **C)** Quantification of non-neuronal cell population suggest a trend towards increase at 90 DPI, and a significantly higher number of cells at 120 DPI in RML-inoculated animals **D)** Monitoring weight changes of NBH and RML-infected animals indicates a significant decrease in animal weight at 120 and 150 DPI in RML-inoculated mice **e)** No significant difference was detected in brain wet weight amongst NBH and RML inoculated animals. Data obtained from 5 animals were averaged per group in each timepoint. Error bars represent SD. (p-values \*  $\leq 0.05$ , \*\*  $\leq 0.01$  and \*\*\*  $\leq 0.001$ )

### 3.3.2 Timing of pathological changes in the brain

To understand the correlation between the molecular transition of PrP and disease progression, we monitored the development of clinical signs and assessed changes to the brain tissue by histology (**Fig. 2-4**). We analyzed the vacuolation (by H&E staining), PK-resistant PrP accumulation and glial fibrillary acidic protein (GFAP) expression at different timepoints during disease progression. We observed the first clinical signs (weight loss, low activity, tail rigidity, kyphosis and hypokinesia) in RML-inoculated mice at around 90-100 DPI (around 60% of incubation period) similar to previous reports (Hwang, Lee et al. 2009). Moreover, the combination of histology and immunoblotting experiments point to discernible changes in the brain of RML-inoculated animals at 90 DPI and thereafter (**Fig. 2-5**).



**B**

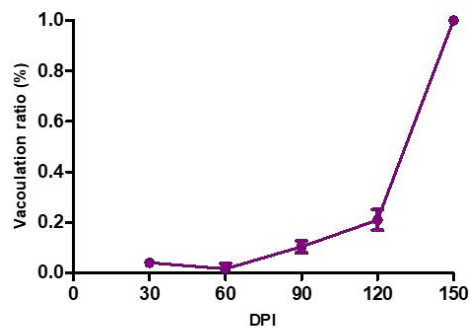


**Figure 3-2. H and E staining of brain sections from RML and NBH inoculated animals at different timepoints during disease progression.**

**A)** A section of the brain consisting of hippocampus and part of the cerebral cortex are presented. Vacuoles are first noticeable at 90 DPI **B)** Quantification of H & E staining by Weka image segmentation and ImageJ. The values obtained at terminal-stage were adjusted to 1 and the rest of the timepoints were normalized relative to that. Error bars represent SD (n=2).

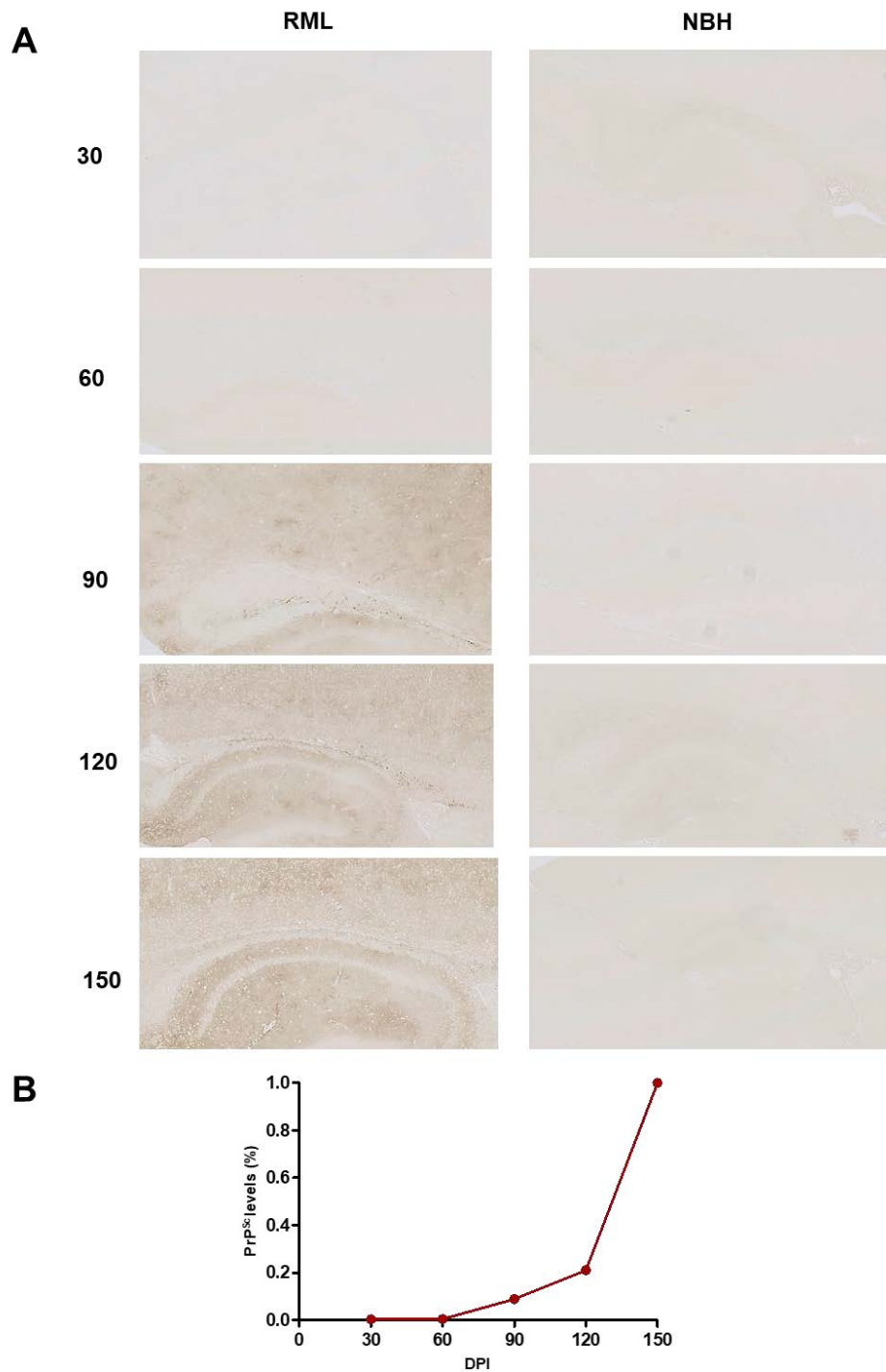


**Figure 3-3. PrP<sup>Sc</sup> immunostaining of brain sections from RML and NBH inoculated animals at different timepoints**

**A)** A section of the brain consisting of hippocampus and part of the cerebral cortex are presented. PK-resistant PrP is first noticeable at 90 DPI **B)** Quantification of PrP immunostaining by ImageJ. The values obtained at terminal-stage were adjusted to 1 and the rest of the timepoints were normalized relative to that. Error bars represent SD (n=2).

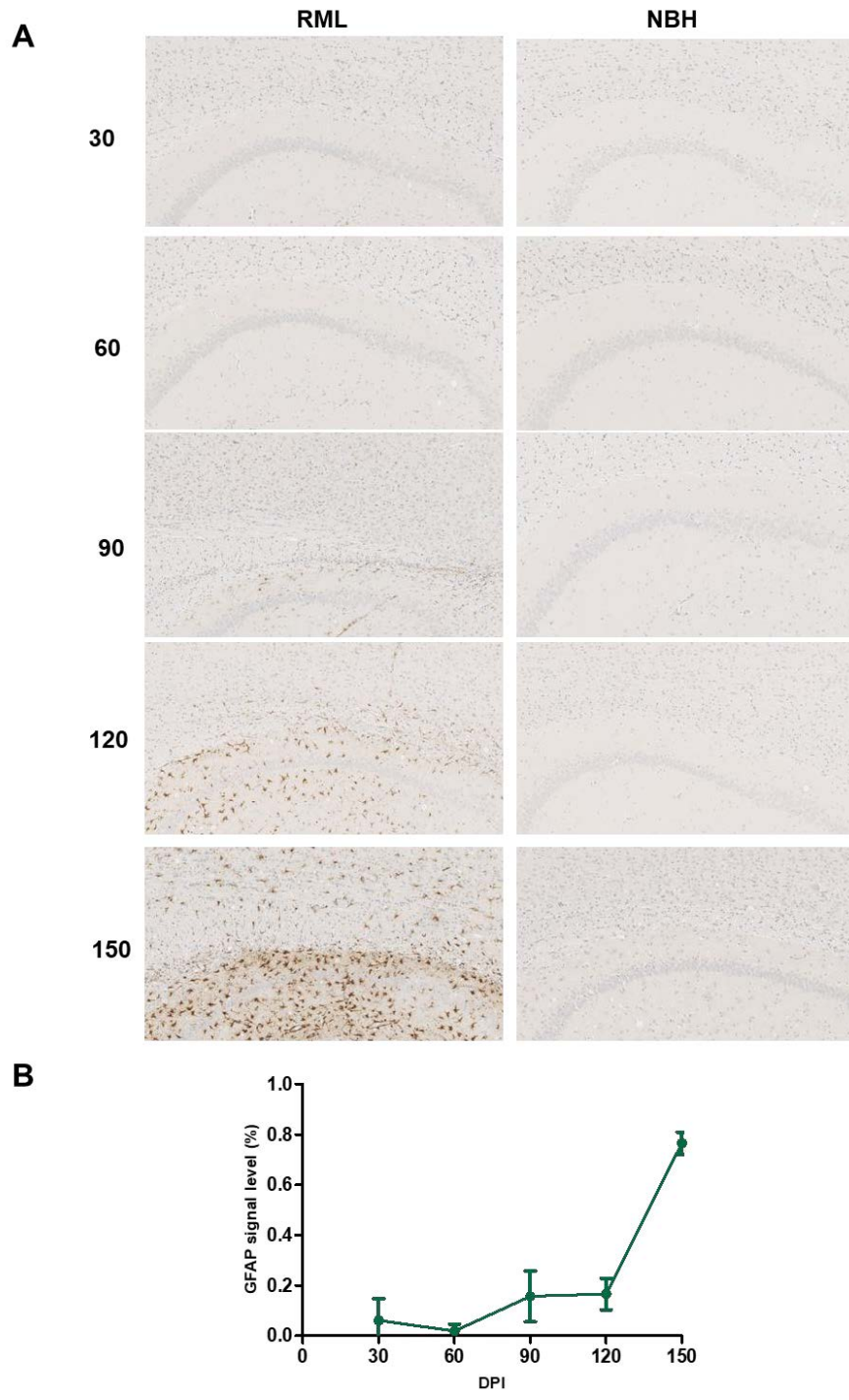


**Figure 3-4. GFAP immunostaining of brain slices from RML and NBH inoculated animals**

**A)** A section of the brain consisting of hippocampus and part of the cerebral cortex are presented. Increased GFAP immunoreactivity is first noticeable at 90 DPI **B)** Quantification of GFAP immunostaining by ImageJ. Error bars represent SD (n=2).

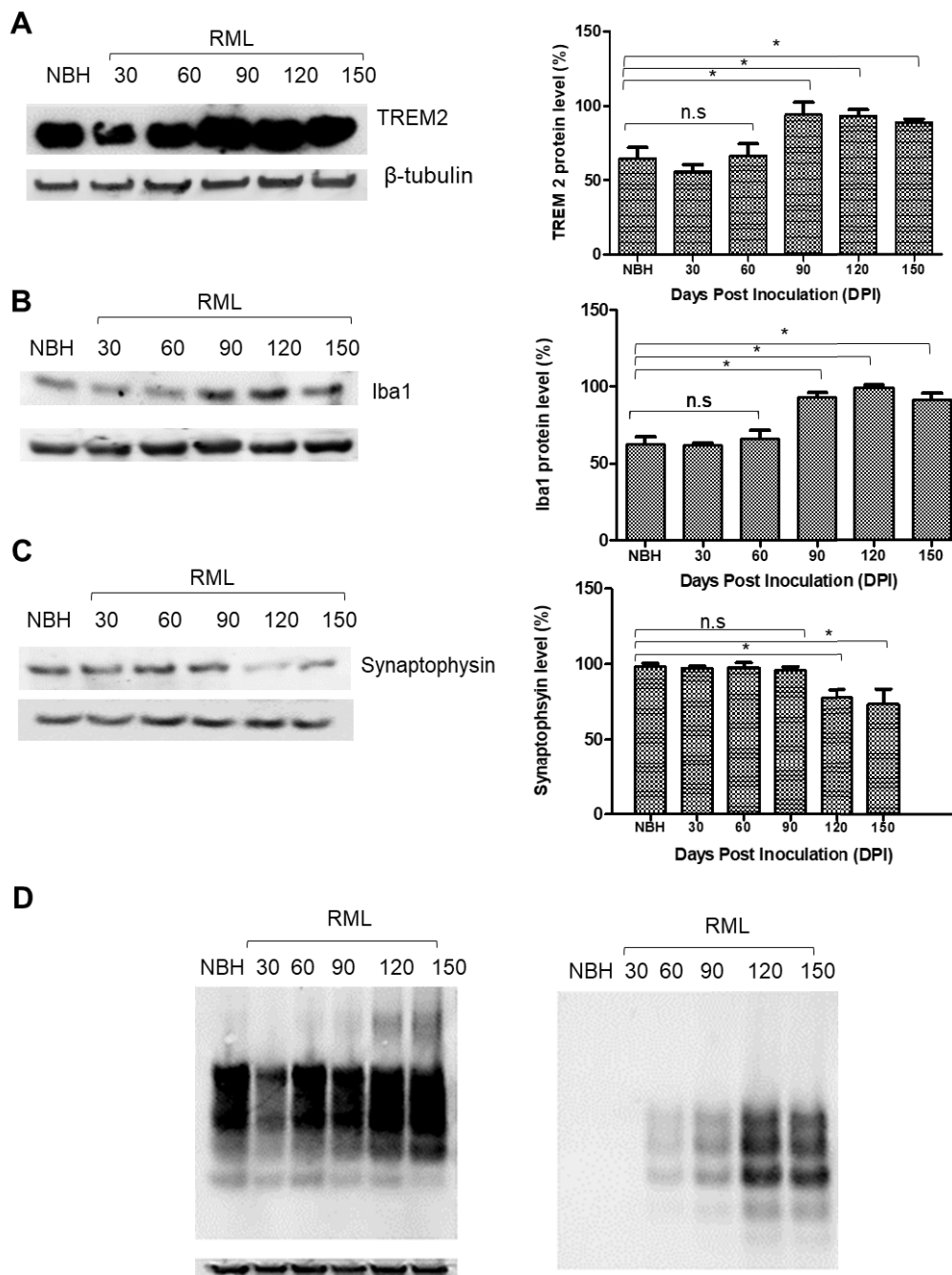


**Figure 3-5. Assessment of inflammatory and synaptic health markers' changes at different timepoints during disease progression.**

A) Immunoblotting of TREM2 protein in solubilized brain homogenate of RML-inoculated animals. A sample from NBH-inoculated animal at 150 DPI was used as the control. B) Immunoblotting of Iba1 protein in solubilized brain homogenate of RML-inoculated animals, C) Immunoblotting of synaptophysin protein in solubilized brain homogenate of RML-inoculated animals. D) Immunoblotting of total PrP (left) and PK-resistant PrP (right) in solubilized brain homogenate of RML-inoculated animals. Quantification of the blots were done by ImageJ. Data represent average of 2 repeats. Error bars represent SD (n=3). \* indicates p-value  $\leq$  0.05.

### 3.3.3 Molecular transitions of PrP: decrease at PrP<sup>C</sup> levels and presence of high-molecular-weight species at early stages of the disease

To understand the evolution of PrP forms during disease progression, we used asymmetric flow field-flow fractionation (AF4), a flow-based separation method for isolation of macromolecules based on hydrodynamic radius. Solubilization conditions for processing brain homogenate were optimized to ascertain the presence of all PrP assemblies, including less-soluble PrP<sup>Sc</sup> aggregates, within the final sample. To this end the buffer contained 4% dodecyl- $\beta$ -D-maltoside and 2% sarkosyl (Wroblewski, Burlot et al. 1978, Tao, Liu et al. 2010, Tixador, Herzog et al. 2010, Laferrière, Tixador et al. 2013, Chisnall, Johnson et al. 2014).

First, to assess PrP<sup>C</sup> protein levels in RML-infected animals, we quantified PrP<sup>C</sup> protein levels in fractionated brains of RML-infected animals at different timepoints (**Fig.6**). Interestingly, we detected a decrease in PrP<sup>C</sup> protein levels at pre-clinical stages of the disease; this trend began at 90 DPI, and by 120 DPI there was an approximately 25% reduction in PrP<sup>C</sup> levels, which then further decreased at 150 DPI to 38% (**Fig. 6**). The profile of this decrease and the absolute percentage values were notably similar to a study using different methodologies (Mays, Kim et al. 2014). Secondly, regarding the high-molecular weight assemblies of PrP, a comparison of PrP size range in NBH-inoculated and RML-inoculated animals suggests that assemblies of PrP with R<sub>H</sub> values within the range of 10-100 nm are mostly absent in healthy conditions (**Fig.7 A and B**). This range of assemblies in RML-infected animals would consist of at least 23 PrP monomers (**Table 1**). We next investigated the presence of high-molecular weight species at all timepoints in RML-inoculated animals and detected the first signs of such assemblies at 60 DPI (equivalent to 40% of the disease incubation period) (**Fig.7**). The distribution of multimeric assemblies detected at 60 DPI is different from either NBH-inoculated or RML-inoculated animals at 30 DPI, but is similar to that of terminal-stage RML mice (albeit with lower signal intensity); the columns corresponding to R<sub>H</sub> values of 5-10 nm are slightly higher than that of NBH-inoculated animals, and there is generally a rise in signal for species with R<sub>H</sub> values above 10 nm, with the highest peaks at 10-20 nm and 40-70 nm. This observation is in agreement with

our data from PK-digestion of total brain homogenate, indicating the presence of PK-resistant PrP<sup>Sc</sup> at this timepoint (**Fig. 5D**).

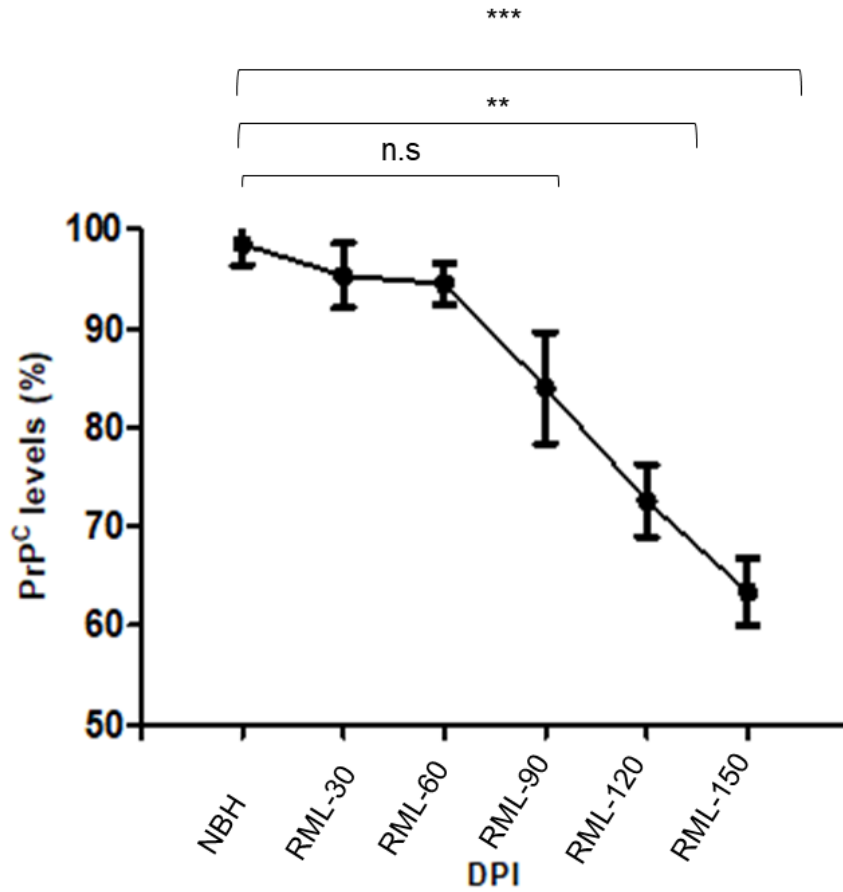


**Figure 3-6. PrP<sup>C</sup> levels in brain homogenate of RML-inoculated animals at different timepoints**

Protein levels were quantified by adding the values from fractions corresponding to PrPC (obtained from fractionation of brains from NBH-inoculated mice). There is a trend towards decrease at 90 DPI, and a significant reduction at 120 and 150 DPI (20% and 30% respectively). Data represent average of 2 repeats. Error bars represent SD (n=2). \*\* indicates p-value  $\leq 0.01$

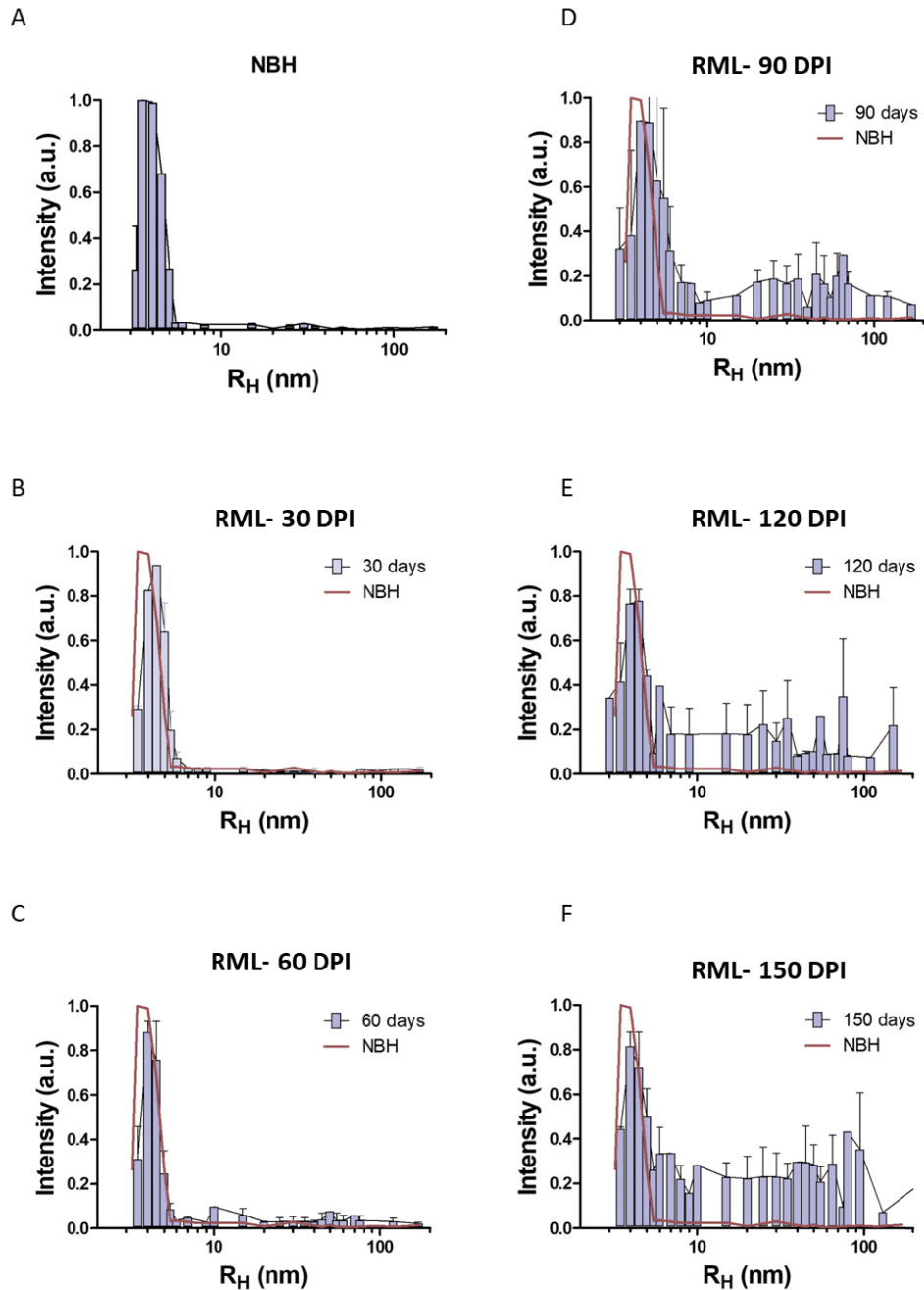


**Figure 3-7. AF4 analysis of solubilized brain homogenate of RML-infected animals at different timepoints during disease progression.**

**A)** A representative graph from fractionated brain of a NBH-inoculated animal at 150 DPI, **B)** fractionated brain of RML-inoculated mice sacrificed at 30 DPI, **C)** 60 DPI, **D)** 90 DPI, **E)** 120 DPI, **F)** and terminal stage (150 DPI). Data represent average of 2 repeats. Error bars represent SD (n=2).

<b>R<sub>H</sub> (nm ± SD)</b>	<b>Number of PrP monomers in the complex (Full length)</b>
<b>2.6 (± 0.05)</b>	<b>(PrP)<sub>1</sub> - monomer</b>
<b>3.5 (± 0.52)</b>	<b>(PrP)<sub>2</sub> – dimer</b>
<b>7 (± 0.62)</b>	<b>(PrP)<sub>10</sub> – decamer</b>
<b>10 (± 0.85)</b>	<b>(PrP)<sub>23</sub>-mer</b>
<b>20 (± 1.55)</b>	<b>(PrP)<sub>115</sub>-mer</b>
<b>40 (± 6.16)</b>	<b>* (PrP)<sub>550</sub></b>
<b>70 (± 10.63)</b>	<b>* (PrP)<sub>2000</sub></b>

**Table 3-1. Full-length PrP molecules per oligomer as a function of R<sub>H</sub>**

PrP particle R<sub>H</sub> values and correlated number of PrP monomers present in each particle was calculated by Zetasizer Software 7.11. These calculations were done based on the molecular weight of PrP<sup>C</sup> which is 32kDa. The particle shape is presumed as spherical for all these calculations. The measured values for very high-molecular weight assemblies (presented with \*) are not as reliable since these particles probably consist of protofibrils and fibrils

### 3.3.4 Polymeric assemblies of PrP have distinct protease resistance characteristics

Our initial assessment of PK-resistant PrP<sup>Sc</sup> performed on supernatants from a 20,000xg sedimentation of brain homogenate revealed PK-resistant PrP<sup>Sc</sup> material from 60 DPI onwards (**Fig. 5D**). To probe the biochemical characteristics of these assemblies, we investigated the PK-resistance of soluble brain homogenates subsequent to their fractionation under the mild denaturing conditions of AF4 fractionation, i.e. using dodecyl- $\beta$ -D-maltoside and sarkosyl detergents but lacking exposure to thermal denaturation or use of chaotropic agents (Wroblewski, Burlot et al. 1978, Tao, Liu et al. 2010, Chisnall, Johnson et al. 2014). Interestingly, we observed that PK-resistant PrP assemblies manifested similar patterns of distribution regardless of the timepoint (**Fig. 8**). A comparison of total brain homogenate and PK-digested AF4 fractions suggest that the very first polymers of PK-resistant PrP<sup>Sc</sup> assemblies appear at fraction #28 (corresponding to assemblies of c.a. 15 nm R<sub>H</sub> and predicted to be composed of ~100 PrP monomers).

Next, to characterize the seeding potential of PrP<sup>Sc</sup> assemblies from different timepoints, we assessed the seeding capacity of solubilized brain homogenate from different timepoints by RT-QuIC. Brain homogenates of RML-inoculated animals from 90 DPI, 120 DPI and 150 DPI timepoints showed seeding activity in this assay (**Fig. 9**). Conversely, the seeding potential of PrP<sup>Sc</sup> species at 60 DPI fell below the threshold of this assay configuration; from dilution series performed on 150 DPI brain homogenates, this threshold for positivity lies 100x below the amount present at this last timepoint. A similar distinction between 60 and 90DPI timepoints was noted using a standard scrapie cell assay to titrate prion infectivity (as discussed below; (Mays, Kim et al. 2014, Mays, van der Merwe et al. 2015))

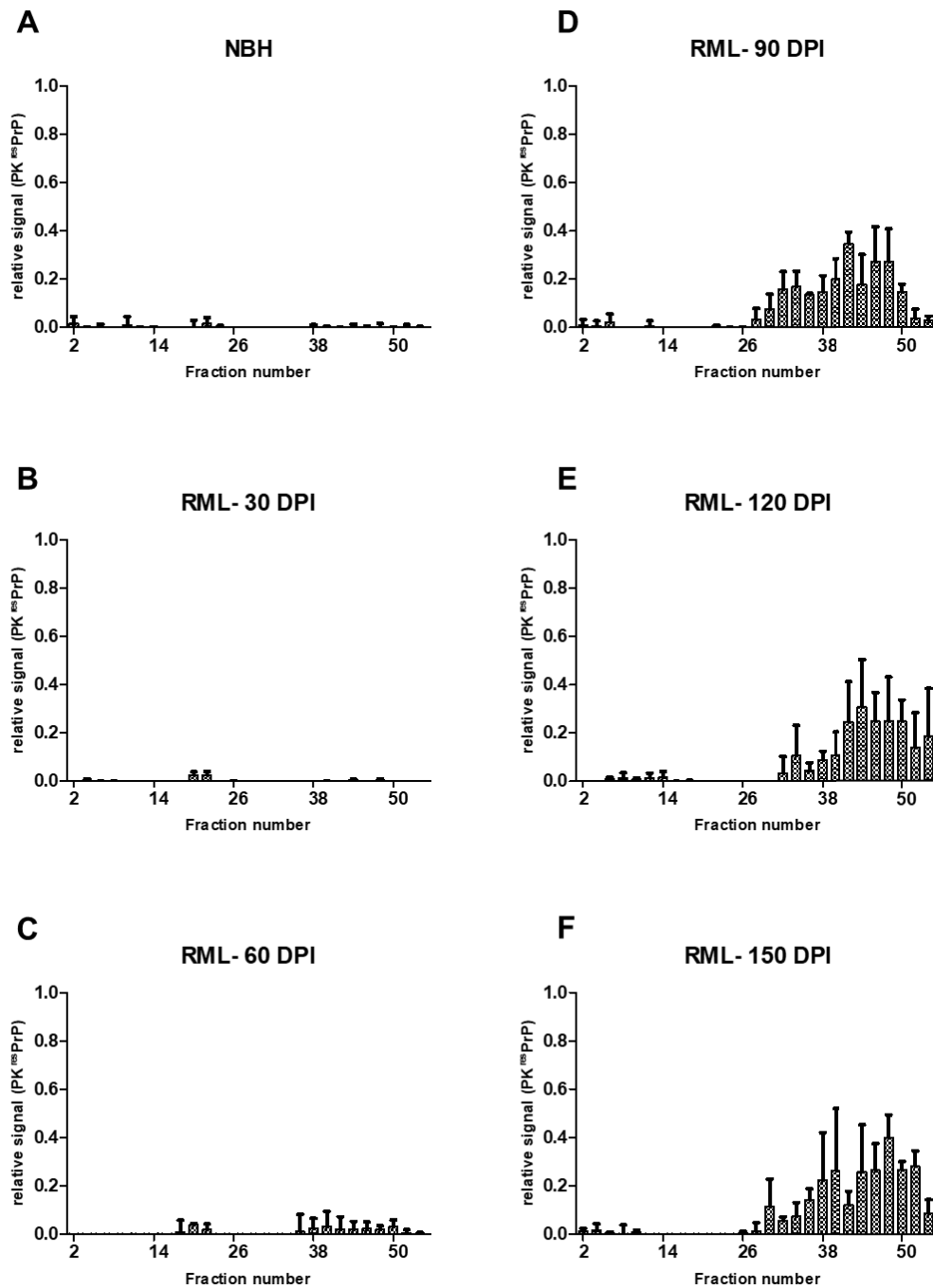


**Figure 3-8. PK-resistant PrP<sup>Sc</sup> in fractionated brain of RML-inoculated animals at different timepoints**

A) digested fractionated brain of a NBH-inoculated animal at 150 DPI, B) PK-digested fractionated brain of RML-inoculated mice sacrificed at 30 DPI, C) 60 DPI, D) 90 DPI, E) 120 DPI and F) and terminal stage (150 DPI). Data represent average of 2 repeats. Error bars represent SD (n=2).

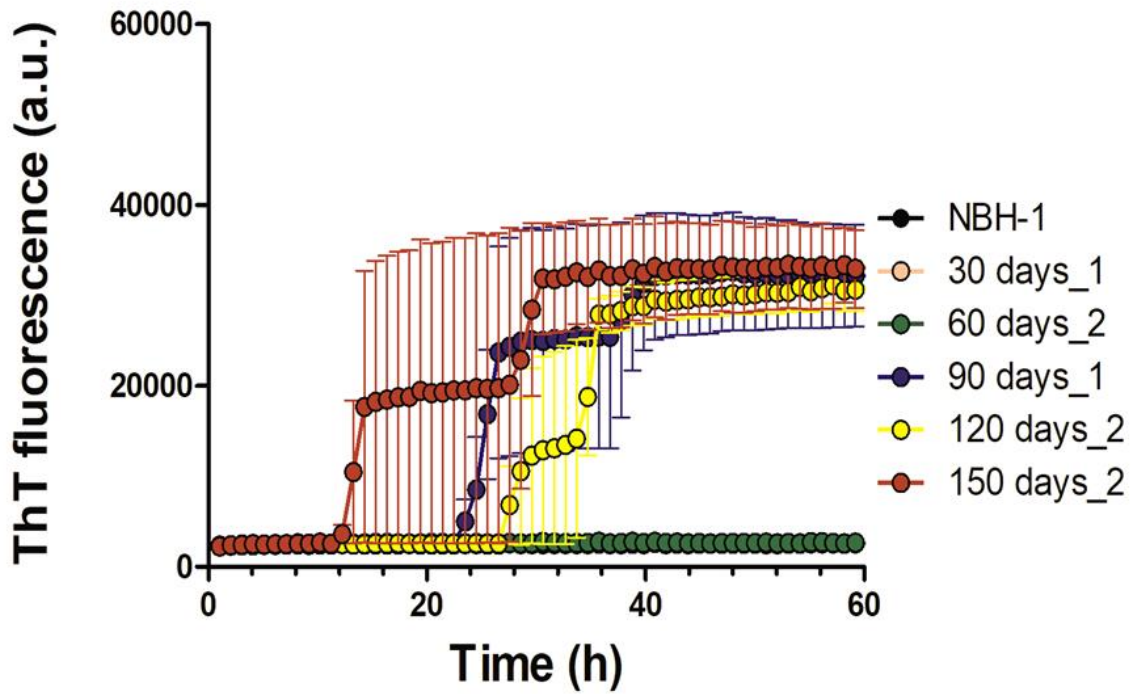


**Figure 3-9. Seeding activity of total brain homogenate of RML-inoculated animals at different timepoints**

For each assay 2  $\mu$ l of 10% brain homogenate was used to assess the seeding potential of PrP species present in each timepoint. Data represents average of 5 repeats. Error bars represent SEM (n=3).

### 3.4 Discussion:

#### 3.4.1 Downregulation of the cellular prion protein precedes neuronal loss

In prion diseases, there is an extended sub-clinical phase during which the infectivity titre, as well as the PrP<sup>Sc</sup> levels, remain constant (Dickinson 1979, Bartz 1999). This effect can be observed in our fractionation assay as well, where the net amount of high-molecular weight assemblies of PrP is relatively constant at 90-120 DPI timepoints (**Fig. 7 d-f**). An early and important hypothesis in the field proposed that this extended incubation period is due to a limited number of replication sites in the host, which with the benefit of hindsight can be equated with levels of PrP<sup>C</sup>, the obligatory substrate for the production of PrP<sup>Sc</sup> (Dickinson 1979, Westaway, Goodman et al. 1987, Bartz 2016). Subsequently, data from native velocity gradient fractionation and conformation-dependent immunoassays defined a progressive fall in levels of PrP<sup>C</sup> and the PrP-like, GPI-anchored shadoo protein (Sho) at pre-symptomatic stages of prion diseases; these data offer a simple explanation for the plateau in titre levels during the disease incubation period (Mays, Coomaraswamy et al. 2014, Mays, Kim et al. 2014, Mays, van der Merwe et al. 2015).

Our results using AF4 fractionation indicate that PrP<sup>C</sup> protein levels trend downwards starting at 90 DPI and reached a significant decrease by 120 DPI (-25% at 120 DPI and -35% at 150 DPI). The profile of these data is strikingly similar to data obtained from different cohorts of RML-infected animals analyzed by entirely different methods (velocity gradient sedimentation and conformation dependent immunoassay). Moreover, the absolute numerical values for each timepoint (-24% at 120 DPI and -37% at 150 DPI; (Mays, Kim et al. 2014)) are also strikingly similar, speaking to robustness. Since we observed no significant decrease in the number of neuronal cells until the last timepoint in our experiment (150 DPI), and while neuronal loss could be partially responsible for dropped PrP<sup>C</sup> levels at this terminal stage, we conclude that falling PrP<sup>C</sup> levels in pre-clinical disease are not necessarily due to cell loss and may require an alternative explanation. These data align with previous observations suggesting that the pre-clinical phase of disease features a controlled depletion of the substrate (PrP<sup>C</sup>), as well as the PrP-like shadoo protein (but not of other control proteins) and perhaps reflects a protective physiological response (Watts, Stöhr et al. 2011, Westaway, Genovesi et al. 2011, Mays, Kim et

al. 2014, Mays, van der Merwe et al. 2015). Within the pre-clinical phase, changes in neuro-inflammatory markers were amongst the earliest changes noted in the brain (**Fig.3 and Fig. 5 A and B**). Based on our observations, inflammation preceded other events such as synaptic damage. The notion that non cell-autonomous events that involve activation of the innate immune system might relate to PrP<sup>C</sup> downregulation may be worthy of investigation.

### **3.4.2 Molecular transition of prion protein and formation of prion assemblies is initiated at early stages of the disease**

Despite the early recognition that PK-resistant PrP<sup>Sc</sup> molecules correlate strongly with infectious titre, growing evidence points at the role of PK-sensitive PrP<sup>Sc</sup> assemblies formed at preliminary stages of the disease in triggering pathogenesis (Silveira, Raymond et al. 2005, Hwang, Lee et al. 2009, Bourgoignon, Spiers et al. 2018, Foliaki, Lewis et al. 2019).

We took advantage of asymmetric flow field-flow fractionation to study the molecular transition of PrP. AF4 has higher resolution and reproducibility than similar techniques used for the fractionation of PrP aggregates, such as density gradient centrifugation, and can be run under better controlled conditions (Giddings 1966, Silveira, Hughson et al. 2006, Hawe, Romeijn et al. 2012). In addition, AF4 can separate a wide range of particles within a complex sample (from few nanometers to several micrometers) in the same run. The combination of these points makes AF4 particularly useful for studying aggregated PrP species.

While PK-resistant PrP<sup>Sc</sup> species appear at 90 DPI in immunohistochemistry assays, western blot analysis of solubilized brain homogenate first detects PK-resistant material at 60 DPI. This seeming discrepancy might reflect differences in sensitivity and detection limits of the two techniques (Alibhai, Blanco et al. 2016). Fractionation experiments also identify medium to high molecular weight assemblies of PrP starting from 60 DPI. These assemblies consist of mostly PK-sensitive species, but there are some PK-resistant species detected in fractions that must be composed of higher molecular weight particles. However, (RT-QuIC) analyses failed to document that PrP<sup>Sc</sup> species at 30 and 60 DPI timepoints possessed seeding activity at 10<sup>-3</sup> dilution, which was the highest input concentration used in our assay. These data align with a report where purified PK-resistant PrP<sup>Sc</sup> from inoculated animals sampled at different timepoints using the same RML

agent (and using a PK concentration of 20  $\mu\text{g/ml}$ ) were subjected to quantitative RT-QuIC and wherein material from 30 and 60 DPI did not manifest seeding activity (Shi, Mitteregger-Kretzschmar et al. 2013). Furthermore, entirely analogous results (i.e., 90 DPI being positive, 60 DPI being negative) were also obtained using an *in vivo* test, the standard scrapie cell assay (SSCA;) to measure infectious activity propagated within susceptible L929 cells (Mahal, Baker et al. 2007, Mays, Kim et al. 2014, Mays, van der Merwe et al. 2015). These two studies perhaps mitigate against trivial explanations of sensitivity thresholds and indicate, instead, that there qualitative, intrinsic changes in the nature of PrP conformers at the disease midpoint. Indeed, it has been proposed that prion assemblies at early stage of disease consist of two populations with distinct quaternary structures (Igel-Egalon, Laferrière et al. 2019). In the current study, a comparison of PK-digested fractionated brain homogenate from all timepoints indicate that in our model, polymers of 100-mer PrP or larger are the ones that manifest PK-resistance. The fact that smaller assemblies of PrP ( $R_H$  less than 15 nm) do not show PK-resistance at any stage during disease progression (even at terminal stage where there is high abundance of PrP assemblies with different size and  $R_H$  values), suggests that the relative PK-sensitivity of assemblies that elute in fractions less than 15 nm is not a function of abundance, but is indeed due to the intrinsic structural characteristics of the aforementioned assemblies.

**Chapter 4: Cell and molecular studies on proteolytic processing of an octarepeat mutant allele of prion protein with increased C2 fragmentation, PrPS3**

## 4.1 Introduction

Similar to most proteins in living organisms, cellular prion protein (PrP<sup>C</sup>) can go through several post translational modification (PTM) events, one of which is proteolytic processing. So far, there are at least 4 different identified endoproteolytic events that PrP<sup>C</sup> can go through:  $\alpha$ -cleavage,  $\beta$ -cleavage,  $\gamma$ -cleavage and shedding (**Figure 4.1**, also briefly reviewed in chapter 1). Despite being identified for quite some time now, mechanistic details of most of these proteolytic processing events are mainly unclear (Altmeppen, Puig et al. 2012, Altmeppen, Prox et al. 2013, McDonald, Dibble et al. 2014).

A member of “a disintegrin-and-metalloproteinase” (ADAM) family of proteases, ADAM10 was proposed to be in charge of  $\alpha$ -cleavage of PrP<sup>C</sup> (Vincent, Paitel et al. 2001). However, overexpression, knocking down or knocking out ADAM10 have failed to eliminate C1-fragmentation in cell and animal models (Endres, Mitteregger et al. 2009, Taylor, Parkin et al. 2009, Altmeppen, Prox et al. 2011). Other members of ADAM family of proteases (ADAMs 8, 9, 17) have been reported to influence  $\alpha$ -cleavage in different tissues, but the actual protease in charge of this event is yet to be identified (Altmeppen, Puig et al. 2012). On the other hand, the story is even more complicated for  $\beta$ -cleavage of PrP<sup>C/Sc</sup>. The N-terminal region of PrP<sup>C</sup> can interact with several ions, including copper (Cu<sup>2+</sup>) through the H residues of the octapeptide repeat region (OR), which is composed of five tandem repeats of PHGGGWGQ sequence. PrP<sup>C</sup> can hence interact with different numbers of Cu<sup>2+</sup> ions (up to 5) through OR. It is established that the unstructured N-terminal region can obtain different conformations depending on the number of Cu<sup>2+</sup> ions interacting with OR, and each of these conformations have distinct biophysical and biochemical characteristics (Chattopadhyay, Walter et al. 2005). Primarily, it was believed that  $\beta$ -cleavage of PrP<sup>C</sup> occurs through reactive oxygen species (ROS) generated by the binding of copper ions (Cu<sup>2+</sup>) to the OR region of PrP molecule at around residue 90 (which is a G residue in humans, and Q in mice (McMahon, Mangé et al. 2001, Pushie and Vogel 2008, Watts, Huo et al. 2009). But, since a fragment of PrP with similar molecular weight and sequence is overtly generated during prion infection, a series of pharmacological and genetic approaches were used to identify the protease in charge of this event in prion-infected cells. Interestingly, it was found that C2 fragment of PrP<sup>Sc</sup> was produced by calpains, Ca<sup>2+</sup>-regulated, cytoplasmic cysteine proteases (Yadavalli, Guttman et al. 2004). However, another study in SH-SY5Y cells suggested that C2-

fragmentation does not depend on calpains, and inhibition of calpain proteases did not affect this process, while chemical induction of oxidative stress positively affected C2 fragmentation (Watt, Taylor et al. 2005). Moreover, results from this study indicated that the  $\beta$ -cleavage of PrP<sup>C</sup> under physiological conditions occur at cell surface, and the generated C2 fragment is soluble and PK-sensitive (Watt, Taylor et al. 2005). Later on, reports from a different group suggested that there is vast heterogeneity amongst different prion infected cells and tissues in C2-fragmentation of PrP<sup>Sc</sup>, (Dron, Moudjou et al. 2010). This group also reported major decrease in C2-fragmentation of lysosome-impaired cells, and cells treated with cathepsin inhibitors, hence concluding that C2-fragmentation of PrP<sup>Sc</sup> is indeed a proteolytic processing event, but it relies on acidic hydrolases (such as cathepsin family of proteases) rather than calpains (Dron, Moudjou et al. 2010).

The last few reports are just a few examples of the discrepancy in the field about the biochemical details of PrP  $\beta$ -cleavage. One major challenge in studying this processing event is its lower abundance under physiological conditions than C1 cleavage, which makes tracking down significant changes in the level of generated fragments rather difficult (Gu, Verghese et al. 2003, Mangé, Béranger et al. 2004). As a result, induction of overt C2-fragmentation would be considered a reasonable solution to tackle down this issue. Since  $\beta$ -cleavage is increased during prion infection, a popular approach has been studying C2-fragmentation in prion infected cells or animal models (Chen, Teplow et al. 1995, Jiménez-Huete, Lievens et al. 1998). But this approach has its own caveats, with the main one being the extensive dissimilarities amongst an infected cell or tissue and a healthy one. Moreover, PrP<sup>C</sup> and PrP<sup>Sc</sup> are clearly not identical molecules, and hence can be targeted by different interactors and biochemical pathways that would vastly differ (Rutishauser, Mertz et al. 2009, Watts, Huo et al. 2009, Didonna 2013). It is thus not surprising to see contradictory results when comparing C2-fragmentation of PrP<sup>C</sup> with that of PrP<sup>Sc</sup> (Watt, Taylor et al. 2005, Dron, Moudjou et al. 2010, Altmeppen, Puig et al. 2012). Consequently, development of a more reliable model that could mimic C2-fragmentation of PrP under physiological conditions could potentially provide a new platform for studying this complex biochemical event.

Our lab had previously generated a prion protein (PrP) allele with specific amino acid substitutions within the OR region to mimic the compact conformation of PrP<sup>C</sup> that can bind only one copper ion per OR (Lau, McDonald et al. 2015). This specific allele is named PrPS3. Surprisingly,

transfection of rabbit kidney cells (RK13) cells with PrPS3 constructs resulted in overt C2-fragment production, and this observation was repeated *in vivo* with brain tissue from lab mice expressing this specific PrP allele (Lau, McDonald et al. 2015). A couple of observations strongly suggested that C2-fragmentation of PrPS3 is in fact a proteolytic processing event; First, expression of PrPS3 construct in other cell lines (HEK293T, SH-SY5Y, N2a and SMB-PS) did not result in overt C2 fragment production, suggesting that some specific protease in RK13 cells is in charge of this event. Moreover, a series of experiments modulating the baseline levels of  $\text{Cu}^{2+}$  in media by adding chelators or metals failed to alter C2 formation by the PrPS3, hence contradicting the hypothesis that ROS are in charge of C2-fragmentation. (Lau, McDonald et al. 2015). In accordance with these results, we have hypothesized that C2-cleavage in PrPS3 is a proteolytic process with at least one protease (or a group of proteases) involved, and that the protease(s) responsible for C2-cleavage in PrPS3 can potentially cleave related sites in wt PrP, but with lower efficiency.

This chapter presents data obtained from a series of experiments designed towards understanding the cell and molecular biology of  $\beta$ -cleavage, using PrPS3 allele as a model.

Since data from previous experiments have indicated that PrPS3 and PrPS3F88W do not behave differently regarding in cells, I have conducted all the experiments presented in this chapter on PrPS3F88W (which is detectable by 12B2, an antibody that detects the N-terminal of prion protein and cannot detect PrPS3 due to the amino acid substitution at residue 88). However, to avoid complications, I will be referring to the PrPS3F88W construct and protein as PrPS3 in this chapter.

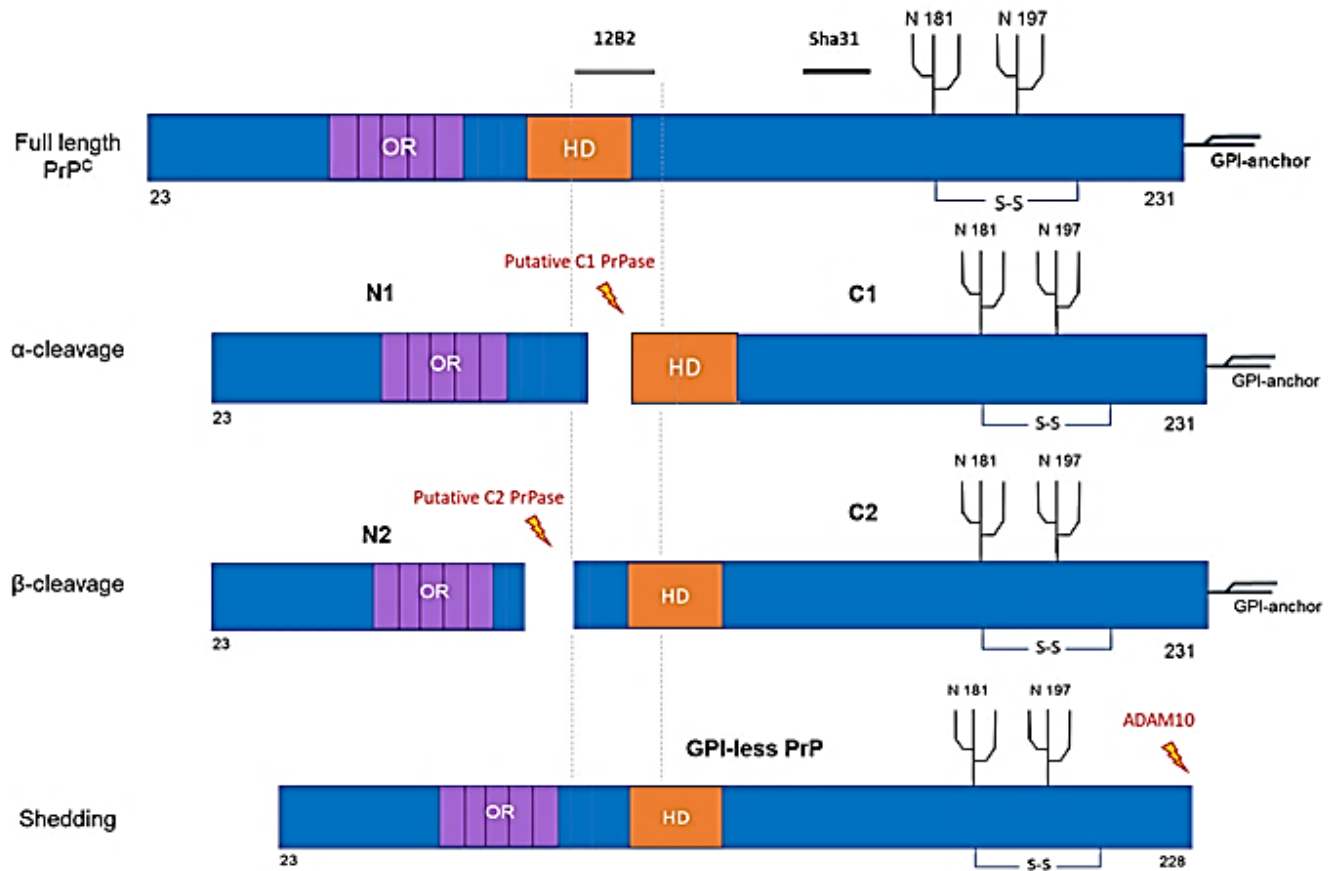


**Figure 4-1. A schematic of different major fragmentation events, (alpha and beta cleavage as well as shedding) that target PrP<sup>C</sup> with generated fragments. All residue numbering on based on mouse PrP<sup>C</sup>**

The fragments generated upon each processing event are distinct in entailing different domains of the protein. And hence each generated fragment can behave differently in both health and disease conditions. The epitopes of 12B2 and Sha31, the two antibodies used in the experiments discussed in this chapter are presented in the schematic. C1 fragment generated by alpha cleavage can not be detected buy 12B2, while full length protein and C2 fragment can both be detected.

## **4.2 Experimental Procedures**

### **4.2.1 Cell Culture**

Rabbit kidney epithelial (RK13) cells were maintained in Dulbecco's modified Eagle's medium (DMEM; Invitrogen) supplemented with 10% foetal bovine serum (FBS; Invitrogen) and penicillin/streptomycin (Invitrogen) at 37°C and 5% CO<sub>2</sub> levels. Cells of approximately 80-90% confluency were transfected using Lipofectamine 2000 (Invitrogen), according to the manufacturer's instructions. RK13 cells with stable expression of PrPWt, PrPS1, PrPS3 and PrPS3F88W (generated and described previously by our lab (Lau, McDonald et al. 2015) ) were also used in experiments presented in this chapter.

### **4.2.2 Cell treatment with Cyclohexamide**

Previously seeded RK13 cells were transfected with pbud-gftp-Wt and pbud-gfp-S3F88W plasmid constructs generated previously in the lab (Lau, McDonald et al. 2015). After 24 hours, cells were treated with 100 µg/ml cycloheximide solution in ddH<sub>2</sub>O (CHX) for 3,6 and 9 hours. Control cells were treated with equivalent volume of ddH<sub>2</sub>O for 9 hours. Cells were then lysed with RIPA buffer containing 1% protease inhibitor cocktail (complete). The lysates were treated with PNGase F (New England Biolabs) according to manufacturer's protocol and ran on 10% SDS-PAGE for further analysis.

### **4.2.3 Cell treatment with lysosomotropic agents (ammonium chloride and chloroquine)**

Previously seeded RK13 cells were transfected with pbud-gftp-PrPWt and pbud-gfp-PrPS3F88W plasmid constructs generated previously in the lab (Lau, McDonald et al. 2015). After 24 hours, cells were treated with 50 µM ammonium chloride (NH<sub>4</sub>Cl) or chloroquine (CQ) for 24 hours. Control cells were treated with equivalent volume of ddH<sub>2</sub>O for 24 hours. Cells were then lysed with RIPA buffer containing 1% protease inhibitor cocktail (complete). The lysates were treated

with PNGase F (New England Biolabs) according to manufacturer's protocol and ran on 10% SDS-PAGE for further analysis.

#### **4.2.4 Acridine Orange assay**

Cells were plated in a 6-well plate 24 hours before experiment. Cells were treated with 5  $\mu\text{g/ml}$  Acridine Orange (A3568, Life Technology) at 37°C for 15 minutes and washed with PBS for three times. To evaluate the effect of  $\text{NH}_4\text{Cl}$  on vesicle pH, cells were treated with different concentrations of  $\text{NH}_4\text{Cl}$  for 24 hours before acquisition of fluorescent images. Illuminated by 488-nm laser beam, the red fluorescence indicates acidity while the green fluorescence indicates alkalinity (Li, Ji et al. 2016).

#### **4.2.5 Cell treatment with thapsigargin**

Previously seeded RK13 cells were transfected with pbud-gftp-Wt and pbud-gfp-S3F88W plasmid constructs generated previously in the lab (Lau, McDonald et al. 2015). After 24 hours, cells were treated with 0.5 or 1  $\mu\text{M}$  thapsigargin for 24 hours. Control cells were treated with equivalent volume of ddH<sub>2</sub>O for 24 hours. Cells were then lysed with RIPA buffer containing 1% protease inhibitor cocktail (complete). The lysates were treated with PNGase F (New England Biolabs) according to manufacturer's protocol and ran on 10% SDS-PAGE for further analysis.

#### **4.2.6 Plasmid constructs**

We had previously created a GPI-anchorless PrP (PrP.S232term) plasmid by replacing S232 with a stop codon (Drisaldi, Coomaraswamy et al. 2004). We took advantage of this previously generated construct to create a GPI-anchorless form of S3 PrP. Briefly, we digested pcDNA3.PrP.S3 and pcDNA3.PrP.S232term constructs with *PciI*, and to avoid recirculation of the pcDNA3.PrP.S3 fragment, we treated it with shrimp alkaline phosphatase. This was then

followed by gel extraction (Qiagen) of obtained fragments and ligation of two *PciI*-digested fragments together to generate pcDNA3.PrP.S3.S232term. The ligation products were then transformed into competent DH5alpha *E. coli* and the plasmids were extracted from resultant colonies (Qiagen Spin Miniprep Kit) and plasmids were confirmed by sequencing.

#### 4.2.7 Cell conditioned media preparation

To generate cell conditioned media (CCCM), cells were transferred to “a modification of Eagle's minimum essential medium” (optiMEM) and incubated at 37°C (5% CO<sub>2</sub> levels) for 24 hours. The media was then collected and concentrated 4X using filter centrifugation (Millipore). To minimize protein degradation in CCCM, protease inhibitor cocktail tablets (mini-complete) were added to each sample, and samples were kept in -80°C freezer until further processed.

#### 4.2.8 *In vitro* proteolysis of recombinant PrPS3

To assess the effect of broad-range chemical inhibitors on proteolytic processing of recombinant PrPS3, we designed an *in vitro* assay. Briefly, Wt RK13 cells were lysed by sonication in PBS containing 0.05% triton-X100. The lysate was clarified by spinning at 1000Xg for 6 minutes, and the clarified suspension was incubated with 3 ug recombinant PrPS3 at 37°C (or 4°C in case of controls) for 1 hour. A portion of recPrPS3 was incubated with HAP cell (Horizon Discovery Ltd.) lysate which is a human-derived cell line with *PRNP* gene knocked out as the negative control.

To test the effect of protein inhibitors, Complete tablets (Sigma) constituting of several broad-range protease inhibitors targeting serine, cysteine, and metalloproteases were used. Alternatively, a second set of protease inhibitor cocktail (Roche) was used to inhibit the proteolytic reaction. The composition of Roche inhibitor cocktail was as follow:

**Antipain:** targeting papain, trypsin, cathepsin A and B, **Bestatin:** targeting amino peptidases, **Chymostatin:** targeting  $\alpha$ -,  $\beta$ -,  $\gamma$ ,  $\delta$ -chymotrypsin, **E-64:** targeting cysteine proteases, **Leupeptin:** targeting serine and cysteine proteases, **Pepstatin:** targeting aspartate proteases

**Phosphoramidon:** targeting metallo-endopeptidases, specifically thermo-lysine, **Pefabloc® SC:** targeting serine proteases, **EDTA:** targeting metalloproteases **Aprotinin:** targeting serine proteases.

At the end of the assay, the reaction was stopped by addition of sample buffer and boiling the samples at 95°C for 10 minutes. 1/10 of the reaction was run on SDS-PAGE for further analysis.

#### **4.2.9 De-glycosylation of prion protein by PNGase-F**

Briefly, 10-20 µg of protein samples were denatured by adding “denaturation buffer” provided by the manufacturer and incubation at 95°C for 10 minutes. The sample was then cooled down, and sufficient amount of NP40 and de-glycosylation buffer (provided in the kit by the manufacturer) were added to the solution. Finally, each reaction was incubated with 0.2 µl of the enzyme overnight at 37°C.

#### **4.2.10 Western blotting**

Western blotting was performed as described previously (Towbin, Staehelin et al. 1979). Samples were prepared in loading buffer containing SDS and 2-mercaptoethanol and boiled for 10 min. They were then electrophoresed on 10% bis-tris precast gels (Invitrogen) using an Invitrogen system and transferred to polyvinyl difluoride (PVDF; Millipore) membranes (wet transfer). Blots were then blocked with 5% skim milk in 1xTBS-0.1% Tween 20 for one hour at room temperature and incubated with primary antibodies at 4 °C overnight (except for blots prepared for detection with Sha31 (Spi-Bio Inc; 1/30,000) antibody, where no blocking was done and blots were directly incubated with antibody in 1X TBS-0.5% Tween 20).

#### **4.2.11 Capillary western blotting (WES)**

Capillary western blotting was performed as described previously (Castle, Daude et al. 2019). Cell lysates were diluted using a proprietary sample buffer (ProteinSimple) when required. 5X Fluorescent Master Mix was added to each sample to provide a denaturing and reducing environment (final concentrations of 1% (v/v) SDS and 40 mM DTT). Samples were then incubated at 95 °C for 5 min. Four microliters of each sample were loaded into the top-row wells of plates preloaded with proprietary electrophoresis buffers designed to separate proteins of 12–230 kDa. Subsequent rows of the plate were filled with blocking buffer (antibody diluent 2), primary and secondary antibody solutions, chemiluminescence reagents, and wash buffer according to the manufacturer's instructions. Primary antibodies were Sha31 anti-PrP (Spi-Bio Inc., A03213, raised in mice, diluted 1:10,000) and anti- $\beta$ -tubulin (Novus Biologicals, NB600-936, raised in rabbits, diluted 1:200 or 1:400), that were subsequently diluted in antibody diluent 2 provided by supplier. Secondary antibodies were anti-mouse secondary HRP conjugate and anti-rabbit secondary HRP conjugate. Plates and capillaries were then loaded into a Wes machine, and assays were performed using the standard 12- to 230-kDa separation range protocol that was introduced upon release of version 4.1.7 of the accompanying Compass software, except that the separation time was changed to 30 min from the default 25 min. Compass reports data as spectra of chemiluminescence signals versus apparent MW. The software determines apparent MWs by mapping ladder peaks to capillary positions and using the signals from fluorescently labeled protein standards of known MW (present in the 5X Master Mix; Novus) to adjust for any differences in migration among capillaries. Peak area calculations were performed by the Compass software using the default Gaussian method. Compass was also used to generate artificial lane view images from the spectra. Visual adjustment to lane view images was performed solely using the brightness/contrast slider within the software.

## **4.3 Results**

### **4.3.1 Fragments of prion protein have different half-lives**

Fragments of a protein could have distinct biochemical characteristics in comparison to the full-length molecule. One of the parameters that could change upon proteolytic processing of a protein

is the half-life of newly generated fragments. Our analysis on the half-life of different fragments of PrPWt and PrPS3 molecules indicate that both C1 (in PrPWt and PrPS3) and C2 fragments (in PrPS3) have longer half lives in comparison to the full-length molecule (**Figure 4.2**). In both PrPWt and PrPS3, C1 fragment seems to have the longest stability with 34.5% decrease in signal intensity after 9 hours of CHX treatment. C2 in PrPS3 is the next stable fragment with a 36% decrease in its amount after 9 hours of CHX treatment. Full length PrPWt and PrPS3 both have the least stability, with only 16% of the molecule present at 9-hours timepoint.

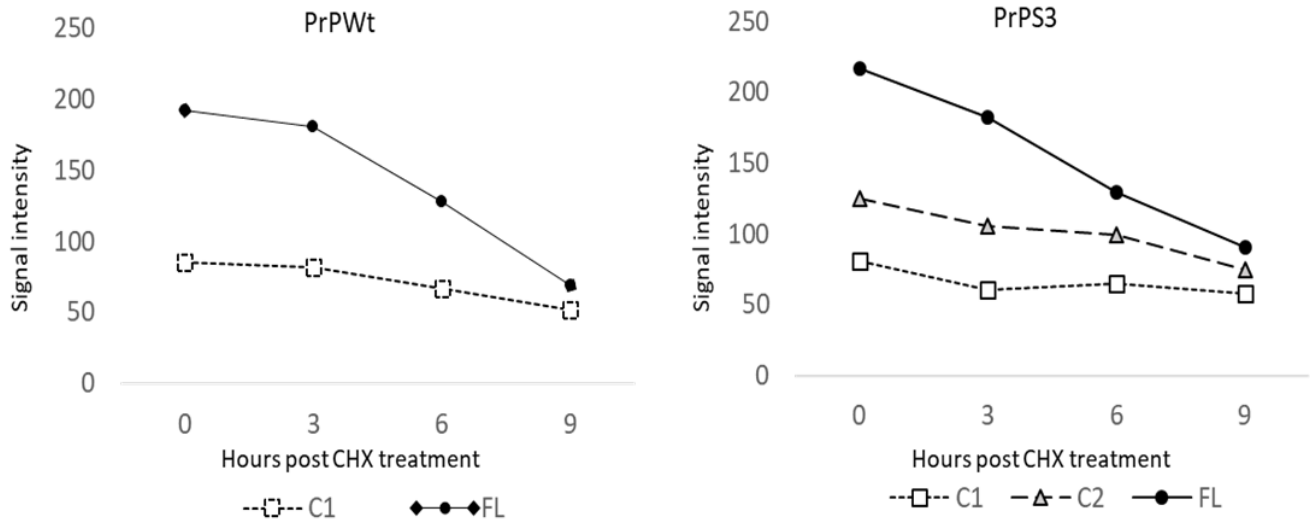


**Figure 4-2. Cyclohexamide (CHX) treatment of cells expressing PrPWt or PrPS3**

CHX treatment results in inhibition of protein synthesis, and hence the half-life of previously generated proteins can be measured. Herein, full length PrP in both PrPWt and PrPS3 expressing cells has the shortest half-life (84% decrease in signal after 9 hours of CHX treatment), while C1 fragment has the longest half life (only 34.5% decrease after 9 hours of CHX treatment). The C2-fragment generated in PrPS3 expressing cells has slightly shorter half life than the C1 fragment (36% decrease after 9 hours of CHX treatment).

### 4.3.2 C2-fragmentation of PrPS3 can be inhibited by protease inhibitors *in vitro*

Previous work by our lab has provided multiple evidence in support of the idea that C2-fragmentation in our PrPS3 model is driven by a protease. However, to further confirm this hypothesis, we tested the effect of two different protease inhibitor cocktails on recombinant PrPS3F88W processing by RK13 cell lysate in an *in vitro* assay. As discussed earlier in this chapter, the reason we used PrPS3F88W in this experiment was due to the difference of residue 88 between PrPS3 (which has F in position 88) and PrPS3F88W; presence of a tryptophan in position 88 is necessary for the detection of full length prion protein or its C-terminal fragments by antibody 12B2.

Incubation of recombinant PrPS3 with RK13 cell lysate results in generation of a 20 kDa band, which is the same molecular weight as C2 fragment detected in PrPS3F88W *ex vivo* and *in vivo*. The aforementioned fragment can be detected by Sha31, a C-terminal antibody epitope: YEDRYRE, amino acid 145–152), as well as the N-terminal antibody 12B2, that can detect C2 fragment. However, the fragment is missing in samples where PrPS3F88W is incubated with other cell lysates, or in samples where protease inhibitor cocktails are added to the RK13 cell lysate (**Fig. 4.3. A and B**). This observation further supports the idea that a protease that is present in RK13 cells is in charge of processing PrPS3F88W to generate the aforementioned C2 fragment.

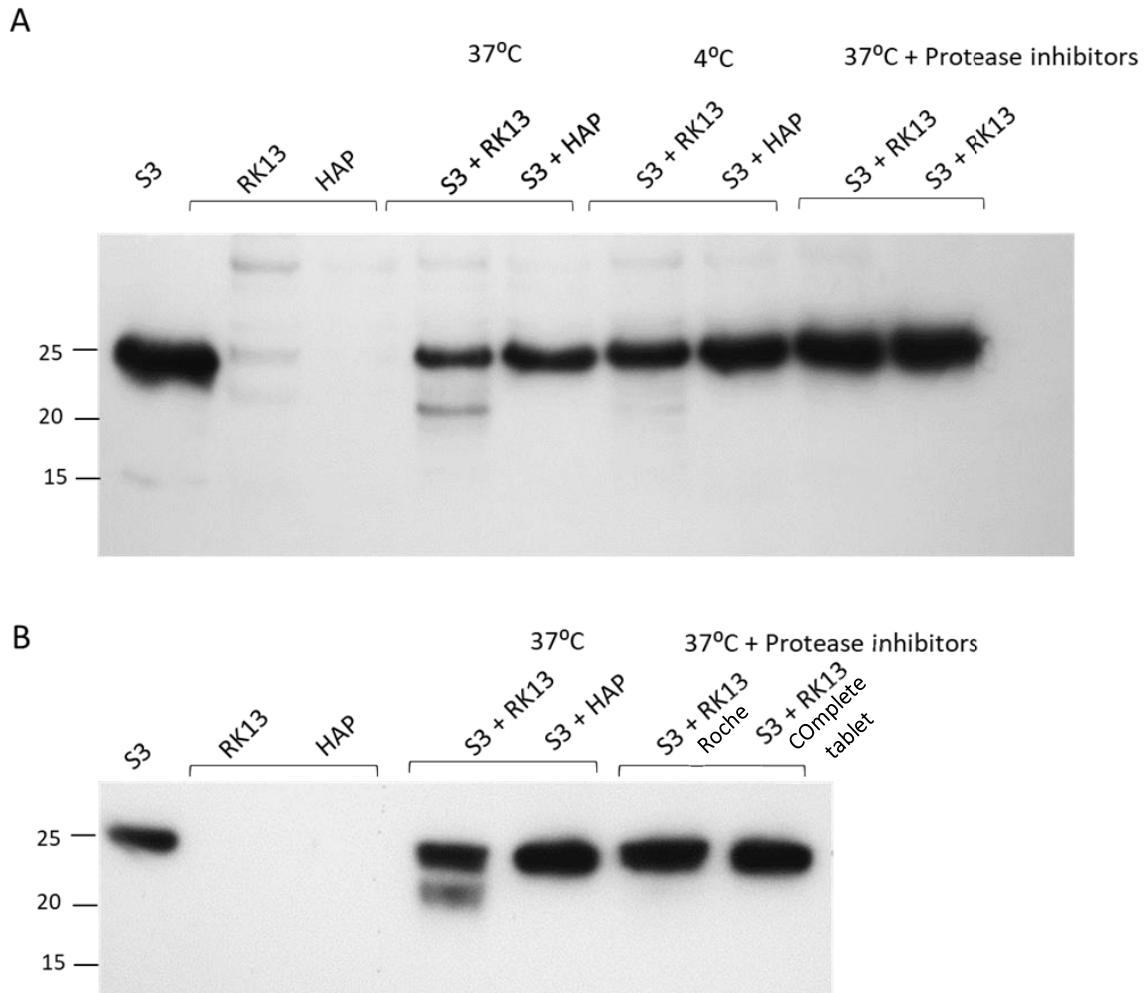


**Figure 4-3. Inhibition of C2-fragmentation of recPrPS3 by cell lysate by addition of protease inhibitors *in vitro*.**

**A)** RecPrPS3 treated with RK13 cell lysate presents an approximately 20 kDa fragment detectable by the C-terminal antibody Sha31. **B)** The same samples blotted with 12B2 antibody that can detect C2 but not C1 fragment (check fig 4.1)

### **4.3.3 Inhibition of lysosomal proteolysis does not have an impact on C2-fragmentation of PrPS3**

Previous reports indicate that inhibition of lysosomal pathway protein degradation could not stop C2 fragmentation (Yadavalli, Guttman et al. 2004). To further assess the effect of lysosomal pathway inhibition on C2 generation in PrPS3 expressing cells, we treated the cells with lysomotropic agents NH<sub>4</sub>Cl and Chloroquine. Neither of these chemical inhibitors of lysosomal hydrolases could inhibit or reduce C2 generation in PrPS3 expressing cells (**Fig.4.4**).

### **4.3.4 Induction of endoplasmic reticulum-stress does not affect C2-fragmentation**

To investigate whether manipulating endoplasmic reticulum (ER) could have any effect on PrP processing occur in, we treated RK13 cells expressing PrPWt and PrPS3 with a classic ER-stress inducer thapsigargin for 24 hours. This treatment resulted in under-glycosylation of PrPS3 and PrPWt (**Fig.4.5 A**), which indicates successful induction of ER stress by the treatment (Trombetta and Parodi 2003, Xu and Ng 2015). However, we observed no changes in C1 or C2 fragmentation of PrP in any of the treated cells. We hence conclude that since disturbing ER homeostasis did not have any significant effect on C2 fragmentation in PrPS3 expressing cells, it is unlikely that this proteolytic processing occurs in this organelle (**Fig 4.5 B-D**).



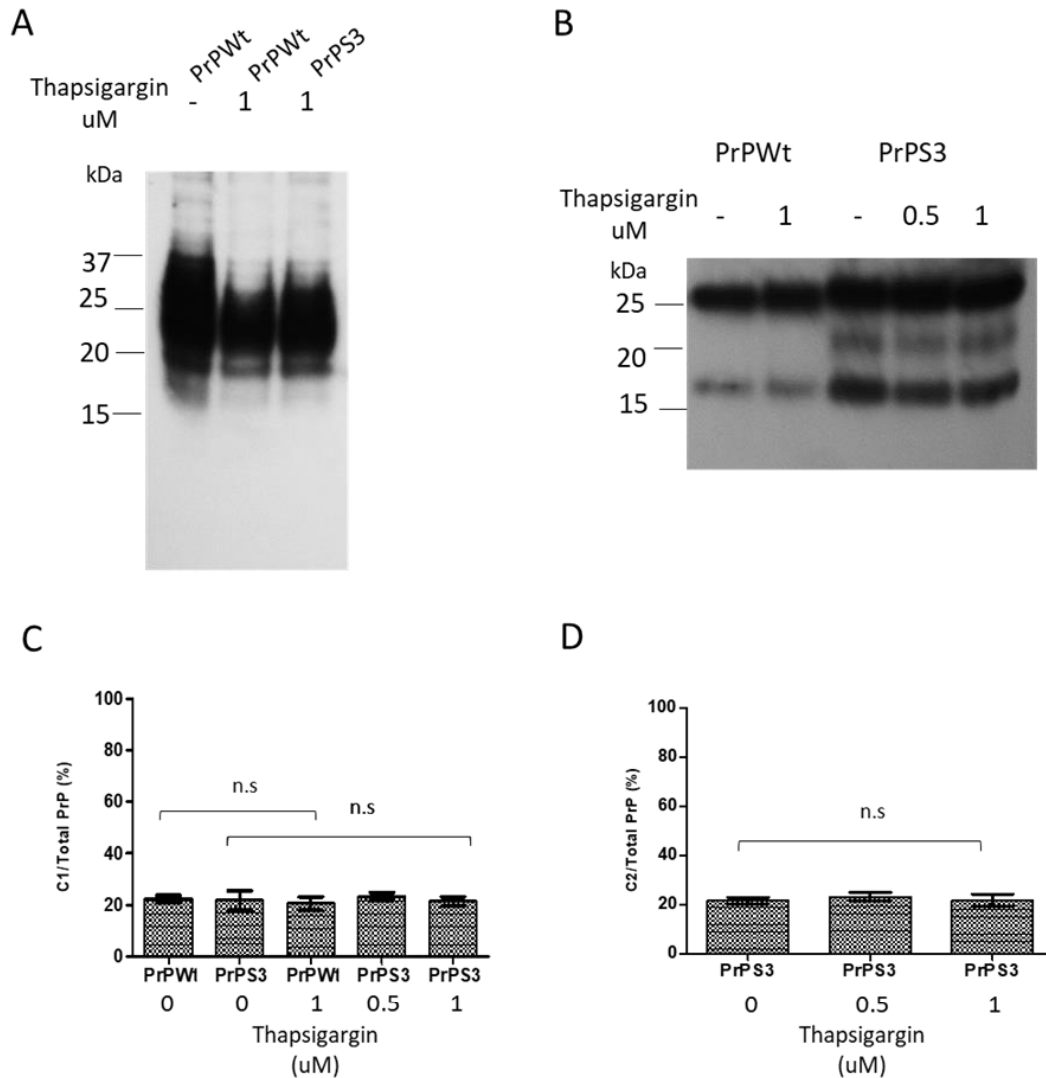


**Figure 4-5. Induction of ER stress with thapsigargin did not affect C1 or C2 fragmentation in PrPWt or PrPS3 expressing cells.**

**A)** Thapsigargin treatment and induction of ER-stress results in underglycosylation of PrP molecules. **B)** Induction of ER-Stress does not have a significant impact on C1 or C2 fragmentation in neither of the PrPWt and PrPS3 expressing cells. **C)** Quantification of C1 fragmentation in both PrPWt and PrPS3. **D)** Quantification of C2 fragmentation in PrPS3

#### 4.3.5 Absence of GPI-anchor affects both C1 and C2 fragmentation of both prion protein alleles, PrPWt and PrPS3

We next investigated the impact of GPI-anchorage of PrPS3 and PrPWt on their proteolytic processing. As reported previously, removal of GPI-anchor had a huge impact on both PrPWt and PrPS3 glycosylation, mostly due to the fact that  $\Delta$ GPI-PrPWt and  $\Delta$ GPI-PrPS3 take less time to transit the secretory pathway and hence do not get as heavily glycosylated as the GPI-anchored proteins (Walmsley, Watt et al. 2009, Oliveira-Martins, Yusa et al. 2010).

To analyze the impact of GPI-anchor removal on C1 and C2 processing of PrPWt and PrPS3, we analyzed both natural and de-glycosylated cell lysates of GPI-anchored and  $\Delta$ GPI PrPWt or PrPS3 expressing cells. Since absence of GPI anchor results in release of the prion protein into extracellular environment, we also collected and analysed the conditioned media (CCM) of cells expressing  $\Delta$ GPI-PrPWt or  $\Delta$ GPI-PrPS3. Interestingly, we observed a significant decrease in C1 fragment levels in the cell lysate of both  $\Delta$ GPI-PrPWt and  $\Delta$ GPI-PrPS3 expressing cells. The overt C2 fragmentation of PrPS3 had also disappeared in  $\Delta$ GPI-PrPS3 cells. The C1 fragment missing in cell lysates, had re-appeared in the CCM of both  $\Delta$ GPI-PrP alleles. However, the C2-fragment in CCM of  $\Delta$ GPI-PrPS3 was still significantly less than what was observed in PrPS3 cell lysates. The combination of these results unravels a few important points about proteolytic processing of prion protein in our models (**Fig.4.6**).

First,  $\alpha$ -cleavage of both PrP alleles was inhibited by absence of GPI anchor in the cell lysates. However, the secreted prion proteins in CCM still presented the C1-fragment in levels comparable to what was observed in GPI-anchored proteins. These results suggest that although PrP association with plasma membrane is necessary for  $\alpha$ -cleavage throughout the secretory pathway, the protease or proteases in charge of this event could still process the  $\Delta$ GPI protein secreted into the extracellular environment. Hence, it is fair to conclude that the protease (or proteases) in charge of  $\alpha$ -cleavage in our model is a membrane (or membrane-associated) protein, and despite being quite efficient (30-40% of total PrP signal corresponds to C1 fragment), this enzymatic reaction needs some time to occur. Second,  $\beta$ -cleavage in our PrPS3 model requires GPI-anchorage of the substrate molecule and removal of the GPI anchor in  $\Delta$ GPI-PrPS3 cells results in elimination of the overt generation of the C2 fragment both in cell lysate and CCM.

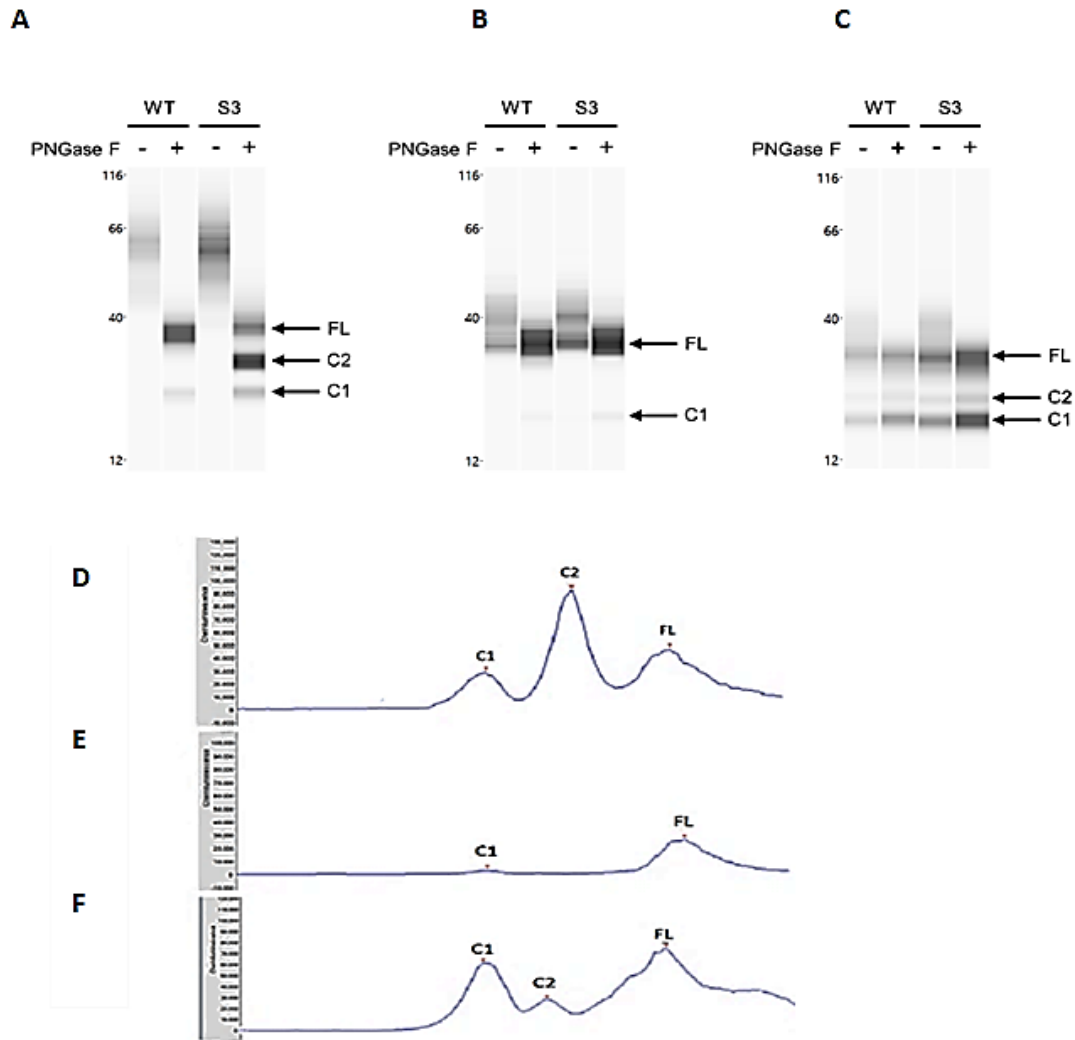


**Figure 4-6. Absence of GPI anchor impacts C1 and C2 fragmentation of both PrPWt and PrPS3 alleles.**

**A)** Blot view of the WES data from PrPS3 and PrPWt molecules. **B)** Blot view of the WES data from cell lysate of GPI-anchorless PrPWt and PrPS3 proteins. **C)** Blot view of the WES data from conditioned media of GPI-anchorless PrPWt and PrPS3. **D-F)** Representative graph view of the samples PrPS3 cell lysate, GPI-less PrPS3 cell lysate and GPI-less PrPS3 conditioned media respectively. This is the format of data in capillary western blot system.

## 4.4 Discussion

Proteolytic processing of PrP<sup>C</sup> is considered an important post-translation modification event that can target this protein; These processing events result in generation of distinct fragments with different half-lives (**Fig. 4.1**) or unique bioactive features (Altmeyden, Puig et al. 2012). In addition, the long hydrophobic stretch (residues 106-126), characterized as amyloidogenic, which is believed to play a critical role in the conformational change of PrP<sup>C</sup> to PrP<sup>Sc</sup> could be affected differently depending on the type of processing event that targets the protein (Prusiner, Scott et al. 1998, Mangé, Béranger et al. 2004). And hence, alternative processing of the prion protein could have a remarkable influence on PrP<sup>Sc</sup> replication in course of prion diseases.

Despite the debate about metal catalyzed hydrolysis versus enzymatic catalysis of protein scission, accumulating data suggest that proteases probably do play a major role in  $\beta$ -cleavage of PrP<sup>C/Sc</sup> (Watt, Taylor et al. 2005, Dron, Moudjou et al. 2010, Lau, McDonald et al. 2015). Our group had previously generated a synthetic PrP allele named PrPS3 that has amino acid substitutions at OR region and goes through overt C2-fragmentation. Using PrPS3 as a model, we have tried to elucidate some cellular and biological details of C2-fragmentation under physiological conditions. Data from previous experiments had ruled out the role of Cu<sup>2+</sup> ions in overt C2 production of PrPS3-expressing RK13 cells. Herein, we observed that addition of protease inhibitor cocktails to RK13 cell lysate fully eliminated C2-fragmentation of recPrPS3 in our *in vitro* assay, further confirming the direct role of proteases in this event.

A critical aspect of proteolytic processing which could provide valuable information about the potential proteases involved in the process is the cellular compartment in which the proteolysis occurs. To learn more about the location of C2-fragmentation of PrPS3, we assessed the impact of this PrP molecule's association with different organelles and cell compartments on its proteolysis. Our results suggest that lysosomal hydrolases, or ER-associated proteases are unlikely to be involved in C1 or C2 fragmentation, while membrane localization had a huge impact on proteolytic processing of both PrPWt and PrPS3 (**Fig.4.6**). This is in agreement with previous reports on the effect of GPI-anchor, and cell-surface localization of PrP<sup>C</sup> on its processing to generate both C1 and C2 fragments (McMahon, Mangé et al. 2001, Mangé, Béranger et al. 2004, Watt, Taylor et al. 2005, Oliveira-Martins, Yusa et al. 2010). A valuable point from these experiments, is the similarity of PrPS3 and PrPWt in their behavior. Regarding protein half-life, full length PrPS3 has

similar half-life as full length PrPWt, and the half-life of C1 fragment in both alleles is quite similar as well (**Fig 4.2**). Moreover, both PrP molecules behave comparably regarding their response to manipulation of different cell compartments. Although PrPS3 was reported to have similar cell surface accessibility, and internalization kinetics as PrPWt, these observations further confirm that PrPS3 goes through the similar cellular routes (such as secretory pathway, or internalization and recycling) as PrPWt, thus supporting the idea that PrPS3 could be a good model to study prion protein proteolytic processing (Lau, McDonald et al. 2015).

We had initially hypothesized that C2-cleavage in PrPS3 is a proteolytic event with at least one protease (or a group of proteases) involved, and that the protease(s) responsible for C2-cleavage in PrPS3 can potentially cleave related sites in PrPWt, but with less efficiency. Based on the results presented in this chapter, we conclude that C2-fragmentation of PrPS3 is indeed a protease-dependent event and is eliminated in the presence of chemical protease inhibitors. Moreover, the GPI-anchorage of full-length molecule is critical for its proper processing to generate both C1 and C2 fragments. The fact that PrPS3 and PrPWt behave the same in several experiments in our hand, and C1-fragmentation is quite identical in these two PrP molecules suggest that PrPS3 is an allele with enhanced C2-cleavage and the protease in charge of this event can potentially target PrPWt as well. However, further experiments are required to confirm this hypothesis.

## **Chapter 5: Conclusions and Future directions**

## 5.1 Generation and validation of *in vivo* and *ex vivo* models for studying protein misfolding diseases

Neurodegenerative diseases caused by misfolded protein species are becoming a rising matter globally. Similar to other human diseases, understanding the detailed molecular mechanism of protein misfolding and its contribution to disease pathogenesis is the key point to designing and generation of successful, mechanism-based therapeutics. Several unique features of this class of disorders such as a) the dynamic nature of proteins involved, b) the vast heterogeneity of misfolded protein species in disease conditions and c) complex multi-dimensional mechanisms of toxicity of misfolded protein species, have caused huge challenges in studying them (Sweeney, Park et al. 2017, Swearingen 2018). Generation of well-founded *in vivo* and *ex vivo* models, that can recapitulate the disease as it occurs in human kindreds, is considered a promising approach towards establishment of solid platforms for studying the mechanism of disease in complex, yet controllable systems (Janus and Welzl 2010).

The projects presented in this thesis have focused on development and validation of models for studying different aspects of protein misfolding diseases. The conclusive remarks from each project, as well as the future directions will be discussed next.

## 5.2 Distinct conformers of tau in FTL D-MAPT animal model

Tg.Tau(P301L)23027 mice have low expression of the longest form of human tau protein, 2N4R with P301L mutation, under the control of the Syrian hamster *Prnp* promoter which restricts the transgene expression to neuronal cells. The relatively low expression level of tau protein in these mice (1.7X WT littermates) in comparison to other animal models, which have up to 16X higher tau protein expression level than WT animals, is a unique feature of the TgTau mice (Denk and Wade-Martins 2009). These mice show neuronal loss, memory deficiency, and NFT-like pathology in the brain, at very late stages of life (Murakami, Paitel et al. 2006). Interestingly, there is heterogeneity amongst age-matched Tg animals in tangle-like pathology, as well as tau fragmentation, and some biochemical characteristics of tau protein extracted from the brain. Our biochemical assessment of brain-extracted tau from different classes of pathology suggest the presence of multiple tau conformers or strains. The fact that transgenic mice expressing a mutant

tau protein that causes a well-characterized genetic tauopathy in humans present different strains is quite interesting, since so far presence of various strains of a misfolded protein have only been associated with different diseases (Kaufman, Sanders et al. 2016). These findings are provocative since similar phenotypic variations have been reported in human kindreds carrying the same mutation (Foster, Wilhelmsen et al. 1997, Mirra, Murrell et al. 1999). Hence, our model may have recapitulated the disease as it occurs in humans and can possibly be used as a platform to elucidate the molecular mechanism of phenotypic variations observed in patients.

Previously, the heterogeneity observed in sporadic protein misfolding diseases, such as sporadic AD have been correlated with the presence of distinct strains (Cohen, Appleby et al. 2016). But so far there has been no report on the presence of multiple strains or conformers of an individual protein in a genetic neurodegenerative disease (Kaufman, Sanders et al. 2016). To unravel the biochemical details of disease pathogenesis in these mice, two major points shall be addressed.

### **5.2.1 *De novo* generation of tau strains**

Regarding protein misfolding field, strains are isolates that generate distinct phenotypes in identical hosts, and hence there is no attribution to genetic variability in their existence (Colby and Prusiner 2011). *In vivo* conditions such as increased concentration of the specific protein of interest (for example by its overexpression), mutations that destabilize the native form and enhance the protein's misfolding and aggregation, formation of amyloid-prone segments through cleavage of the native form or presence of different isoforms of the protein, or failure of the cellular protein quality control (proteostasis) can all partially contribute to protein misfolding and formation of the primary seeds (Jucker and Walker 2013, Morales, Callegari et al. 2015). However, the biochemical and cellular conditions that promote formation of different conformers of misfolded proteins are still mostly ambiguous.

A potential way to further unravel the biophysical and biochemical mechanisms of *de novo* formation of strains in P301L tau would be structural analysis of different fibril morphologies. These set of experiments could provide an input towards the conformation of tau monomers within each conformer. Next step could then be performance of aggregation assays on recombinant P301L tau protein *in vitro*. These experiments could help us understand whether the

formation of different conformers is due to the intrinsic characteristics of P301L tau or are there any other environmental conditions (such as PTMs or cell-specific conditions) and interactors (such as chaperone molecules) involved in this phenomenon.

Finally, it is important to investigate whether the tau strains identified in TgTauP301L mice are stable and maintain their distinct phenotypes upon isolation *in vivo*. This could be analyzed by serial passaging of the brain-derived tau extracts obtained from animals of distinct classes into young TgTauP301L and humanized transgenic mice expressing all 6 isoforms of human tau on a knock-out background ( TgMAPT ) mice. The answer to these questions could provide fundamental perspectives regarding the stability and transmissibility of the tau strains in these mice.

### **5.2.2 Tau fragmentation and aggregation: the cause or a side effect?**

Several reports have indicated that stepwise proteolysis of aggregated tau species could liberate pro-aggregating fragments that could act as seeds to initiate aggregation of the full-length molecule. Tau fragmentation could hence be considered a consequence of clearance of the abnormally modified protein (Wang, Biernat et al. 2007, Wang, Martinez-Vicente et al. 2009). (Wang, Biernat et al. 2007).and Previous reports have indicated that the 24 kDa, calpain cleaved tau fragment is prone to aggregation and could act as a seed to recruit FL-tau into aggregated state (Chun and Johnson 2007, Matsumoto, Motoi et al. 2015).

P301L is a prone-to-aggregation mutant form of tau protein and has been reported to form aggregates in several *in vivo* models (Jicha, Rockwood et al. 1999, Sahara, Lewis et al. 2002, Lee, Kenyon et al. 2005). This hence raises the question about the impact of tau fragmentation on P301L aggregation. Potential future experiments could assess aggregation efficiency of P310Ltau in the presence and absence of the calpain-cleaved 24 kDa tau fragment *ex vivo*. Moreover, knocking down calpain proteases in TgTauP301L could also provide helpful information regarding the role of the calpain-generated C-terminal fragment of tau in disease pathogenesis. Another informative piece of experiment would be analysis of FTL D-MAPT human tissues for the presence of this specific fragment.

Finally, next steps in further validation of our TgTauP301L mouse model would be assessment and comparison of samples obtained from human cases with these mice. Presence of any biochemical similarities amongst human samples and mouse derived material would further suggest these animals can provide a promising platform to study and elucidate the phenotypic variances in FTLD-MAPT patients and potentially open up some horizons towards understanding the molecular mechanism of *de novo* strain formation in sporadic protein misfolding diseases of the nervous system.

### **5.3 Molecular evolution of PrP<sup>Sc</sup> during prion disease progression**

Data obtained from the project presented in chapter 3 strongly suggest that in accordance with previous reports, early-onset PrP<sup>C</sup> downregulation at pre-clinical stages of prion diseases is not due to neuronal loss (Mays, van der Merwe et al. 2015).

The molecular pathways responsible for initiating this event are yet to be identified. It is possible that early-onset events in the brain such as inflammation and activation of brain-resident immune cells (microglia) are involved in this event. Future experiments could study detailed cell signaling events in a mixed-culture system, and investigate the pathways activated upon prion infection of the cells.

Moreover, the comparative analysis amongst native brain homogenate fractions and PK-digested ones indicate that PK-digestion at any timepoint during disease progression selects for a specific subpopulation of PrP<sup>Sc</sup> assemblies with similar biophysical characteristics. The RT-QuIC data hint at the high seeding activity of these species, although this could be further investigated in future experiments where representative fractions from each subpopulation at different timepoints are used as seeding material in RT-QuIC. If PK-resistant species are the ones with highest seeding activity, only fractions corresponding to this group of PrP<sup>Sc</sup> assemblies should have high response in the assay, even at timepoints close to the terminal stage of the disease.

We also propose that disease-related events such as inflammation and pathological changes in brain are triggered by PK-sensitive oligomers of PrP<sup>Sc</sup> and the PK-resistant subpopulations that have active seeding potential are responsible for misfolded protein replication and its distribution throughout the brain.

## 5.4 PrPS3 as a model to study proteolytic processing of cellular prion protein (PrP<sup>C</sup>)

In Chapter 4 of this thesis, the overt C2 production in a PrP allele with amino-acid substitutions at OR region was further explored. The primary goal in this study was to verify whether the C2-fragmentation of PrPS3 is an enzymatic event. The experiments with broad-range protease inhibitor cocktail suggest that proteases are involved in this event. However, for future directions more detailed analysis with chemical protease inhibitors is required to unravel more information about the biochemistry of this proteolytic processing event.

Understanding the detailed molecular and biochemical mechanism of proteolytic processing of PrPS3 could help us learn more about processing of PrP<sup>C</sup> and PrP<sup>Sc</sup>. Results from previous studies as well as data obtained from the experiments presented in this chapter suggest that aside from overt C2 production, PrPS3 is indeed quite similar to PrPWt especially regarding its cellular localization and half life (Lau, McDonald et al. 2015). Although it is still too early to conclude that the processing event that targets PrPS3 is identical to the  $\beta$ -cleavage of PrP<sup>C</sup>, current data propose PrPS3 as a potentially good candidate model for studying  $\beta$ -cleavage, which is a processing event that happens at very low concentrations in the Wt allele. However, further assessment is required to verify the similarity of the C2 fragment produced from PrPS3 and the C2 fragment generated in PrPWt. The identified protease in charge of C2-fragmentation of PrPS3, should indeed be capable of processing PrPWt in the same manner, albeit with lower affinity and efficiency.

### 5.4.1 The importance of PrP<sup>C</sup> proteolytic processing in prion diseases

Aside from the generation of bioactive products under physiological condition, proteolytic processing of PrP<sup>C</sup> can have a huge impact in case of prion diseases as well. Depending on the type of processing that targets full length PrP<sup>C</sup>, distinct fragments with different conversion capabilities will be generated. For example, It is well-established that the longest product generated by  $\alpha$ -cleavage of PrP<sup>C</sup>, C1, cannot misfold to PrP<sup>Sc</sup> (Jiménez-Huete, Lievens et al. 1998), and it has been reported to inhibit fibrilization of the full length molecule *in vitro* (Campbell, Gill et al. 2013). At the same time, the neurotoxic domain of PrP<sup>C</sup>, which is critical

for its conversion to PrP<sup>Sc</sup> remains intact in C2 fragment (Altmeppen, Puig et al. 2012). Inhibition of PrP<sup>Sc</sup> formation by manipulating proteolytic processing of full length PrP<sup>C</sup> during disease could hence be a promising therapeutic approach which requires characterization of enzymology and cell biology of these fragmentation events. The protease in charge of PrP<sup>Sc</sup> fragmentation could thus be targeted for inhibition in prion disease cell and animal models to analyze its impact on disease pathogenesis.

The discovery of prions as proteinaceous infectious particles began to open a new perspective for polymeric misfolded protein assemblies as stable carriers of structural information (Colby and Prusiner 2011). This concept has evolved throughout the years, and today the concept of “prion” has been applied to many proteins other than the cellular prion protein, including tau. (Peggion, Sorgato et al. 2014). But it must be taken into consideration that despite some commonalities (discussed in section 1.8 of this thesis), tau protein and prion protein have their distinctions; tau protein is cytoplasmic with 6 different isoforms (with regulated ratios in the brain). Disturbances in isoform ratios have been reported in several pathological conditions (Sanders, Kaufman et al. 2016). Although this specific point is unlikely to contribute to strain formation in our mouse model, its impact on formation of distinct tau conformers in different tauopathies is well established (Woerman, Aoyagi et al. 2016). Moreover, tau goes through several post translation modifications (PTMs), some of which (such as phosphorylation and proteolytic processing) could heavily affect pathological conversion of the molecule. The cellular prion protein, however, is expressed into the secretory pathway and has no alternative splicing events for the gene coding region.

In conclusion, the concept of “prion strains” is by nature one of the most complicated aspects of prion diseases. But the numerous differences amongst the basic conditions of tau protein and the prion protein suggest that this concept is potentially even more complicated in case of tau protein, and there are several fundamental aspects that should be considered upon studying misfolded tau conformers.

## Cumulative Bibliography

- Aguzzi, A., M. Heikenwalder and M. Polymenidou (2007). "Insights into prion strains and neurotoxicity." Nature reviews Molecular cell biology **8**(7): 552.
- Ahn, A. C., M. Tewari, C.-S. Poon and R. S. Phillips (2006). "The limits of reductionism in medicine: could systems biology offer an alternative?" PLoS medicine **3**(6): e208.
- Alibhai, J., R. A. Blanco, M. A. Barria, P. Piccardo, B. Caughey, V. H. Perry, T. C. Freeman and J. C. Manson (2016). "Distribution of Misfolded Prion Protein Seeding Activity Alone Does Not Predict Regions of Neurodegeneration." PLoS Biol **14**(11): e1002579.
- Altmeppen, H. C., J. Prox, B. Puig, F. Dohler, C. Falker, S. Krasemann and M. Glatzel (2013). "Roles of endoproteolytic  $\alpha$ -cleavage and shedding of the prion protein in neurodegeneration." The FEBS journal **280**(18): 4338-4347.
- Altmeppen, H. C., J. Prox, B. Puig, M. A. Kluth, C. Bernreuther, D. Thurm, E. Jorissen, B. Petrowitz, U. Bartsch and B. De Strooper (2011). "Lack of a-disintegrin-and-metalloproteinase ADAM10 leads to intracellular accumulation and loss of shedding of the cellular prion protein in vivo." Molecular neurodegeneration **6**(1): 36.
- Altmeppen, H. C., B. Puig, F. Dohler, D. K. Thurm, C. Falker, S. Krasemann and M. Glatzel (2012). "Proteolytic processing of the prion protein in health and disease." American journal of neurodegenerative disease **1**(1): 15.
- Amadoro, G., M. T. Ciotti, M. Costanzi, V. Cestari, P. Calissano and N. Canu (2006). "NMDA receptor mediates tau-induced neurotoxicity by calpain and ERK/MAPK activation." Proceedings of the National Academy of Sciences **103**(8): 2892-2897.
- Ando, K., K. Leroy, C. Heraud, Z. Yilmaz, M. Authelet, V. Suain, R. De Decker and J. P. Brion (2011). "Accelerated human mutant tau aggregation by knocking out murine tau in a transgenic mouse model." Am J Pathol **178**(2): 803-816.
- Araki, K. and K. Nagata (2011). "Protein folding and quality control in the ER." Cold Spring Harbor perspectives in biology **3**(11): a007526.
- Arganda-Carreras, I., A. Cardona, V. Kaynig and J. Schindelin (2015). Trainable weka segmentation <http://fiji.sc>, Trainable\_Weka\_Segmentation.
- Avila, J., J. J. Lucas, M. Perez and F. Hernandez (2004). "Role of tau protein in both physiological and pathological conditions." Physiological reviews **84**(2): 361-384.
- Azevedo, F. A., L. R. Carvalho, L. T. Grinberg, J. M. Farfel, R. E. Ferretti, R. E. Leite, W. J. Filho, R. Lent and S. Herculano-Houzel (2009). "Equal numbers of neuronal and nonneuronal cells make the human brain an isometrically scaled-up primate brain." Journal of Comparative Neurology **513**(5): 532-541.
- Bahney, J. and C. S. von Bartheld (2014). "Validation of the isotropic fractionator: comparison with unbiased stereology and DNA extraction for quantification of glial cells." Journal of neuroscience methods **222**: 165-174.
- Bailey, R. M., J. Howard, J. Knight, N. Sahara, D. W. Dickson and J. Lewis (2014). "Effects of the C57BL/6 strain background on tauopathy progression in the rTg4510 mouse model." Mol

Neurodegener **9**: 8.

Bartz, J. C. (1999). "Analysis of TSE interspecies transmission and molecular investigations of strain variability."

Bartz, J. C. (2016). "Prion strain diversity." Cold Spring Harbor perspectives in medicine **6**(12): a024349.

Bessen, R. A., Kocisko, D.A., Raymond, G.J., Nandan, S., Lansbury, P.T., and Caughey, B. (1995). "Non-genetic propagation of strain-specific properties of scrapie prion protein." Nature **375**: 698-700.

Bhak, G.-B., Y.-J. Choe and S.-R. Paik (2009). "Mechanism of amyloidogenesis: nucleation-dependent fibrillation versus double-concerted fibrillation." BMB reports **42**(9): 541-551.

Bierer, L. M., P. R. Hof, D. P. Purohit, L. Carlin, J. Schmeidler, K. L. Davis and D. P. Perl (1995). "Neocortical neurofibrillary tangles correlate with dementia severity in Alzheimer's disease." Arch Neurol **52**(1): 81-88.

Bird, T. D., D. Nochlin, P. Poorkaj, M. Cherrier, J. Kaye, H. Payami, E. Peskind, T. H. Lampe, E. Nemens, P. J. Boyer and G. D. Schellenberg (1999). "A clinical pathological comparison of three families with frontotemporal dementia and identical mutations in the tau gene (P301L)." Brain **122** ( Pt 4): 741-756.

Bolton, D. C., M. P. McKinley and S. B. Prusiner (1982). "Identification of a protein that purifies with the scrapie prion." Science **218**(4579): 1309-1311.

Bondareff, W., C. Q. Mountjoy, M. Roth and D. L. Hauser (1989). "Neurofibrillary degeneration and neuronal loss in Alzheimer's disease." Neurobiol Aging **10**(6): 709-715.

Bondulich, M. K., T. Guo, C. Meehan, J. Manion, T. Rodriguez Martin, J. C. Mitchell, T.

Hortobagyi, N. Yankova, V. Stygelbout, J. P. Brion, W. Noble and D. P. Hanger (2016). "Tauopathy induced by low level expression of a human brain-derived tau fragment in mice is rescued by phenylbutyrate." Brain.

Borroni, B., F. Ferrari, D. Galimberti, B. Nacmias, C. Barone, S. Bagnoli, C. Fenoglio, I. Piaceri, S. Archetti, C. Bonvicini, M. Gennarelli, M. Turla, E. Scarpini, S. Sorbi and A. Padovani (2014). "Heterozygous TREM2 mutations in frontotemporal dementia." Neurobiol Aging **35**(4): 934 e937-910.

Bourgognon, J.-M., J. G. Spiers, H. Scheiblich, A. Antonov, S. J. Bradley, A. B. Tobin and J. R. Steinert (2018). "Alterations in neuronal metabolism contribute to the pathogenesis of prion disease." Cell Death & Differentiation **25**(8): 1408.

Braak, H. and E. Braak (1991). "Neuropathological staging of Alzheimer-related changes." Acta Neuropathol **82**(4): 239-259.

Braak, H. and E. Braak (1995). "Staging of Alzheimer's disease-related neurofibrillary changes." Neurobiol Aging **16**(3): 271-278; discussion 278-284.

Brautigam, H., J. W. Steele, D. Westaway, P. E. Fraser, P. H. St George-Hyslop, S. Gandy, P. R. Hof and D. L. Dickstein (2012). "The isotropic fractionator provides evidence for differential loss of hippocampal neurons in two mouse models of Alzheimer's disease." Molecular neurodegeneration **7**(1): 58.

Brier, M. R., B. Gordon, K. Friedrichsen, J. McCarthy, A. Stern, J. Christensen, C. Owen, P. Aldea, Y. Su, J. Hassenstab, N. J. Cairns, D. M. Holtzman, A. M. Fagan, J. C. Morris, T. L. Benzinger and B. M. Ances (2016). "Tau and Abeta imaging, CSF measures, and cognition in Alzheimer's disease." Sci Transl Med **8**(338): 338ra366.

Brion, J. P., K. Ando, C. Heraud and K. Leroy (2010). "Modulation of tau pathology in tau transgenic models." Biochem Soc Trans **38**(4): 996-1000.

Brizzee, K. (1973). Quantitative histological studies on aging changes in cerebral cortex of rhesus monkey and albino rat with notes on effects of prolonged low-dose ionizing irradiation in the rat. Progress in brain research, Elsevier. **40**: 141-160.

Bruce, A. J., W. Boling, M. S. Kindy, J. Peschon, P. J. Kraemer, M. K. Carpenter, F. W. Holtsberg and M. P. Mattson (1996). "Altered neuronal and microglial responses to excitotoxic and ischemic brain injury in mice lacking TNF receptors." Nature medicine **2**(7): 788.

Buée, L., T. Bussièrre, V. Buée-Scherrer, A. Delacourte and P. R. Hof (2000). "Tau protein isoforms, phosphorylation and role in neurodegenerative disorders." Brain Research Reviews **33**(1): 95-130.

Cairns, N. J., E. H. Bigio, I. R. Mackenzie, M. Neumann, V. M.-Y. Lee, K. J. Hatanpaa, C. L. White, J. A. Schneider, L. T. Grinberg and G. Halliday (2007). "Neuropathologic diagnostic and nosologic criteria for frontotemporal lobar degeneration: consensus of the Consortium for Frontotemporal Lobar Degeneration." Acta neuropathologica **114**(1): 5-22.

Campbell, I. L., C. R. Abraham, E. Masliah, P. Kemper, J. D. Inglis, M. Oldstone and L. Mucke (1993). "Neurologic disease induced in transgenic mice by cerebral overexpression of interleukin 6." Proceedings of the National Academy of Sciences **90**(21): 10061-10065.

Campbell, L., A. C. Gill, G. McGovern, C. M. Jalland, J. Hopkins, M. A. Tranulis, N. Hunter and W. Goldmann (2013). "The PrPC C1 fragment derived from the ovine A136R154R171 PRNP allele is highly abundant in sheep brain and inhibits fibrillisation of full-length PrPC protein in vitro." Biochimica et Biophysica Acta (BBA)-Molecular Basis of Disease **1832**(6): 826-836.

Carlson, G. A., D. Westaway, S. J. DeArmond, M. Peterson-Torchia and S. B. Prusiner (1989). "Primary structure of prion protein may modify scrapie isolate properties." Proceedings of the National Academy of Sciences **86**(19): 7475-7479.

Castle, A. R., N. Daude, S. Gilch and D. Westaway (2019). "Application of high-throughput, capillary-based Western analysis to modulated cleavage of the cellular prion protein." Journal of Biological Chemistry **294**(8): 2642-2650.

Castle, A. R. and A. C. Gill (2017). "Physiological functions of the cellular prion protein." Frontiers in molecular biosciences **4**: 19.

Chattopadhyay, M., E. D. Walter, D. J. Newell, P. J. Jackson, E. Aronoff-Spencer, J. Peisach, G. J. Gerfen, B. Bennett, W. E. Antholine and G. L. Millhauser (2005). "The octarepeat domain of the prion protein binds Cu (II) with three distinct coordination modes at pH 7.4." Journal of the American Chemical Society **127**(36): 12647-12656.

Chen, H.-H., P. Liu, P. Auger, S.-H. Lee, O. Adolfsson, L. Rey-Bellet, J. Lafrance-Vanasse, B.

A. Friedman, M. Pihlgren and A. Muhs (2018). "Calpain-mediated tau fragmentation is altered in Alzheimer's disease progression." Scientific reports **8**(1): 1-15.

Chen, S. G., D. B. Teplow, P. Parchi, J. K. Teller, P. Gambetti and L. Autilio-Gambetti (1995). "Truncated forms of the human prion protein in normal brain and in prion diseases." Journal of Biological Chemistry **270**(32): 19173-19180.

Chishti, M. A., D. S. Yang, C. Janus, A. L. Phinney, P. Horne, J. Pearson, R. Strome, N. Zuker, J. Loukides, J. French, S. Turner, G. Lozza, M. Grilli, S. Kunicki, C. Morissette, J. Paquette, F. Gervais, C. Bergeron, P. E. Fraser, G. A. Carlson, P. S. George-Hyslop and D. Westaway (2001). "Early-onset amyloid deposition and cognitive deficits in transgenic mice expressing a double mutant form of amyloid precursor protein 695." J Biol Chem **276**(24): 21562-21570.

Chisnall, B., C. Johnson, Y. Kulaberoglu and Y. W. Chen (2014). Insoluble protein purification with sarkosyl: facts and precautions. Structural Genomics, Springer: 179-186.

Chu, C. T. (2019). "Mechanisms of selective autophagy and mitophagy: Implications for neurodegenerative diseases." Neurobiology of disease **122**: 23-34.

Chun, W. and G. Johnson (2007). "The role of tau phosphorylation and cleavage in neuronal cell death." Front Biosci **12**(733): e56.

Citron, M., D. Westaway, W. Xia, G. A. Carlson, T. Diehl, G. Levesque, K. Johnson-Wood, M. Lee, P. Seubert, A. Davis, D. Kholodenko, R. Motter, R. Sherrington, B. Perry, H. Yao, R. Strome, I. Lieberburg, J. Rommens, S. Kim, D. Schenk, P. Fraser, StGeorge-Hyslop and D. Selkoe (1997). "Mutant presenilins of Alzheimer's Disease increase production of 42-residue amyloid b-protein in both transfected cells and transgenic mice." Nature Medicine **3**: 67-72.

Clark, L. N., P. Poorkaj, Z. Wszolek, D. H. Geschwind, Z. S. Nasreddine, B. Miller, D. Li, H. Payami, F. Awert, K. Markopoulou, A. Andreadis, I. D'Souza, V. M. Lee, L. Reed, J. Q. Trojanowski, V. Zhukareva, T. Bird, G. Schellenberg and K. C. Wilhelmsen (1998). "Pathogenic implications of mutations in the tau gene in pallido-ponto- nigral degeneration and related neurodegenerative disorders linked to chromosome 17." Proc Natl Acad Sci U S A **95**(22): 13103-13107.

Clavaguera, F., T. Bolmont, R. A. Crowther, D. Abramowski, S. Frank, A. Probst, G. Fraser, A. K. Stalder, M. Beibel, M. Staufenbiel, M. Jucker, M. Goedert and M. Tolnay (2009). "Transmission and spreading of tauopathy in transgenic mouse brain." Nat Cell Biol **11**(7): 909-913.

Clavaguera, F., J. Hench, M. Goedert and M. Tolnay (2015). "Invited review: Prion-like transmission and spreading of tau pathology." Neuropathol Appl Neurobiol **41**(1): 47-58.

Cleveland, D. W., S.-Y. Hwo and M. W. Kirschner (1977). "Physical and chemical properties of purified tau factor and the role of tau in microtubule assembly." Journal of molecular biology **116**(2): 227-247.

Cohen, M., B. Appleby and J. G. Safar (2016). "Distinct prion-like strains of amyloid beta implicated in phenotypic diversity of Alzheimer's disease." Prion **10**(1): 9-17.

Colby, D. W. and S. B. Prusiner (2011). "De novo generation of prion strains." Nature Reviews Microbiology **9**(11): 771-777.

Colby, D. W. and S. B. Prusiner (2011). "Prions." Cold Spring Harbor perspectives in biology **3**(1): a006833.

Collinge, J. and A. R. Clarke (2007). "A general model of prion strains and their pathogenicity." Science **318**(5852): 930-936.

Collins, C. E., N. A. Young, D. K. Flaherty, D. C. Airey and J. H. Kaas (2010). "A rapid and reliable method of counting neurons and other cells in brain tissue: a comparison of flow cytometry and manual counting methods." Frontiers in neuroanatomy **4**: 5.

Cortez, L. M., J. Kumar, L. Renault, H. S. Young and V. L. Sim (2013). "Mouse prion protein polymorphism phe-108/val-189 affects the kinetics of fibril formation and the response to seeding evidence for a two-step nucleation polymerization mechanism." Journal of Biological Chemistry **288**(7): 4772-4781.

Crusio, W. E., D. Goldowitz, A. Holmes and D. Wolfer (2009). "Standards for the publication of mouse mutant studies." Genes Brain Behav **8**(1): 1-4.

Dawson, H. N., A. Ferreira, M. V. Eyster, N. Ghoshal, L. I. Binder and M. P. Vitek (2001). "Inhibition of neuronal maturation in primary hippocampal neurons from  $\tau$  deficient mice." Journal of cell science **114**(6): 1179-1187.

de Calignon, A., M. Polydoro, M. Suarez-Calvet, C. William, D. H. Adamowicz, K. J. Kopeikina, R. Pitstick, N. Sahara, K. H. Ashe, G. A. Carlson, T. L. Spire-Jones and B. T. Hyman (2012). "Propagation of tau pathology in a model of early Alzheimer's disease." Neuron **73**(4): 685-697.

Delobel, P., I. Lavenir, G. Fraser, E. Ingram, M. Holzer, B. Ghetti, M. G. Spillantini, R. A. Crowther and M. Goedert (2008). "Analysis of tau phosphorylation and truncation in a mouse model of human tauopathy." Am J Pathol **172**(1): 123-131.

Denk, F. and R. Wade-Martins (2009). "Knock-out and transgenic mouse models of tauopathies." Neurobiology of aging **30**(1): 1-13.

Di Scala, C., N. Yahi, S. Boutemour, A. Flores, L. Rodriguez, H. Chahinian and J. Fantini (2016). "Common molecular mechanism of amyloid pore formation by Alzheimer's  $\beta$ -amyloid peptide and  $\alpha$ -synuclein." Scientific reports **6**: 28781.

Dickey, C. A., A. Kamal, K. Lundgren, N. Klosak, R. M. Bailey, J. Dunmore, P. Ash, S. Shoraka, J. Zlatkovic and C. B. Eckman (2007). "The high-affinity HSP90-CHIP complex recognizes and selectively degrades phosphorylated tau client proteins." The Journal of clinical investigation **117**(3): 648-658.

Dickinson, A. (1979). "The scrapie replication-site hypotheses and its implications for pathogenesis." Slow transmissible diseases of the nervous system **2**: 13-31.

Didonna, A. (2013). "Prion protein and its role in signal transduction." Cellular & Molecular Biology Letters **18**(2): 209.

Dobson, C. M. (2003). "Protein folding and misfolding." Nature **426**(6968): 884-890.

Drisaldi, B., J. Coomaraswamy, P. Mastrangelo, B. Strome, J. Yang, J. C. Watts, M. A. Chishti, M. Marvi, O. Windl and R. Ahrens (2004). "Genetic Mapping of Activity Determinants within Cellular Prion Proteins N-TERMINAL MODULES IN PrPC OFFSET PRO-APOPTOTIC

ACTIVITY OF THE DOPPEL HELIX B/B' REGION." Journal of Biological Chemistry **279**(53): 55443-55454.

Dron, M., M. Moudjou, J. Chapuis, M. K. F. Salamat, J. Bernard, S. Cronier, C. Langevin and H. Laude (2010). "Endogenous proteolytic cleavage of disease-associated prion protein to produce C2 fragments is strongly cell-and tissue-dependent." Journal of Biological Chemistry **285**(14): 10252-10264.

Dujardin, S., M. Colin and L. Buée (2015). "Invited review: animal models of tauopathies and their implications for research/translation into the clinic." Neuropathology and applied neurobiology **41**(1): 59-80.

Endres, K., G. Mitteregger, E. Kojro, H. Kretzschmar and F. Fahrenholz (2009). "Influence of ADAM10 on prion protein processing and scrapie infectiosity in vivo." Neurobiology of disease **36**(2): 233-241.

Erdo, F., L. Denes and E. de Lange (2017). "Age-associated physiological and pathological changes at the blood-brain barrier: A review." J Cereb Blood Flow Metab **37**(1): 4-24.

Eskandari-Sedighi, G., N. Daude, H. Gapeshina, D. W. Sanders, R. Kamali-Jamil, J. Yang, B. Shi, H. Wille, B. Ghetti and M. I. Diamond (2017). "The CNS in inbred transgenic models of 4-repeat Tauopathy develops consistent tau seeding capacity yet focal and diverse patterns of protein deposition." Molecular neurodegeneration **12**(1): 72.

Fivenson, E. M., S. Lautrup, N. Sun, M. Scheibye-Knudsen, T. Stevnsner, H. Nilsen, V. A. Bohr and E. F. Fang (2017). "Mitophagy in neurodegeneration and aging." Neurochemistry international **109**: 202-209.

Foliaki, S. T., V. Lewis, D. I. Finkelstein, V. Lawson, H. A. Coleman, M. Senesi, A. M. T.

Islam, F. Chen, S. Sarros and B. Roberts (2018). "Prion acute synaptotoxicity is largely driven by protease-resistant PrPSc species." PLoS pathogens **14**(8): e1007214.

Foliaki, S. T., V. Lewis, A. M. T. Islam, L. J. Ellett, M. Senesi, D. I. Finkelstein, B. Roberts, V. A. Lawson, P. A. Adlard and S. J. Collins (2019). "Early existence and biochemical evolution characterise acutely synaptotoxic PrPSc." PLoS pathogens **15**(4): e1007712.

Foster, N. L., K. Wilhelmsen, A. A. Sima, M. Z. Jones, C. J. D'Amato and S. Gilman (1997). "Frontotemporal dementia and parkinsonism linked to chromosome 17: a consensus conference. Conference Participants." Ann Neurol **41**(6): 706-715.

Foster, N. L., K. Wilhelmsen, A. A. Sima, M. Z. Jones, C. J. D'Amato, S. Gilman and C. Participants (1997). "Frontotemporal dementia and parkinsonism linked to chromosome 17: a consensus conference." Annals of neurology **41**(6): 706-715.

Friedhoff, P., M. von Bergen, E.-M. Mandelkow and E. Mandelkow (2000). "Structure of tau protein and assembly into paired helical filaments." Biochimica et Biophysica Acta (BBA)-Molecular Basis of Disease **1502**(1): 122-132.

Frost, B. and M. I. Diamond (2010). "Prion-like mechanisms in neurodegenerative diseases." Nature Reviews Neuroscience **11**(3): 155.

Furman, J. L., J. Vaquer-Alicea, C. L. White, 3rd, N. J. Cairns, P. T. Nelson and M. I. Diamond (2017). "Widespread tau seeding activity at early Braak stages." Acta Neuropathol **133**(1): 91-

100.

Games, D., D. Adams, R. Alessandrini, R. Barbour, P. Berthelette, C. Blackwell, T. Carr, J. Clemens, T. Donaldson, F. Gillespie and et al. (1995). "Alzheimer-type neuropathology in transgenic mice overexpressing V717F beta-amyloid precursor protein [see comments]." Nature **373**(6514): 523-527.

Garcia-Sierra, F., S. Mondragon-Rodriguez and G. Basurto-Islas (2008). "Truncation of tau protein and its pathological significance in Alzheimer's disease." J Alzheimers Dis **14**(4): 401-409.

Giddings, J. C. (1966). "A new separation concept based on a coupling of concentration and flow nonuniformities." Separation Science **1**(1): 123-125.

Gilley, J., K. Ando, A. Seereeram, T. Rodríguez-Martín, A. M. Pooler, L. Sturdee, B. H. Anderton, J.-P. Brion, D. P. Hanger and M. P. Coleman (2016). "Mislocalization of neuronal tau in the absence of tangle pathology in phosphomutant tau knockin mice." Neurobiology of aging **39**: 1-18.

Gilley, J., A. Seereeram, K. Ando, S. Mosely, S. Andrews, M. Kerschensteiner, T. Misgeld, J.-P. Brion, B. Anderton and D. P. Hanger (2012). "Age-dependent axonal transport and locomotor changes and tau hypophosphorylation in a "P301L" tau knockin mouse." Neurobiology of aging **33**(3): 621. e621-621. e615.

Gilley, J., A. Seereeram, K. Ando, S. Mosely, S. Andrews, M. Kerschensteiner, T. Misgeld, J. P. Brion, B. Anderton, D. P. Hanger and M. P. Coleman (2012). "Age-dependent axonal transport and locomotor changes and tau hypophosphorylation in a "P301L" tau knockin mouse." Neurobiol Aging **33**(3): 621 e621-621 e615.

Glaser, J. R. and E. M. Glaser (2000). "Stereology, morphometry, and mapping: the whole is greater than the sum of its parts." Journal of chemical neuroanatomy **20**(1): 115-126.

Goedert, M. and M. G. Spillantini (2011). "Pathogenesis of the tauopathies." Journal of Molecular Neuroscience **45**(3): 425.

Golub, V. M., J. Brewer, X. Wu, R. Kuruba, J. Short, M. Manchi, M. Swonke, I. Younus and D. S. Reddy (2015). "Neurostereology protocol for unbiased quantification of neuronal injury and neurodegeneration." Frontiers in aging neuroscience **7**: 196.

Götz, J., F. Chen, R. Barmettler and R. M. Nitsch (2001). "Tau filament formation in transgenic mice expressing P301L tau." J Biol Chem **276**(1): 529-534.

Gotz, J., N. Deters, A. Doldissen, L. Bokhari, Y. Ke, A. Wiesner, N. Schonrock and L. M. Ittner (2007). "A decade of tau transgenic animal models and beyond." Brain Pathol **17**(1): 91-103.

Green, E. L. (1966). *Biology of the Laboratory Mouse*. New York, McGraw-Hill: 11-22.

Gu, Y., S. Verghese, R. S. Mishra, X. Xu, Y. Shi and N. Singh (2003). "Mutant prion protein-mediated aggregation of normal prion protein in the endoplasmic reticulum: implications for prion propagation and neurotoxicity." Journal of neurochemistry **84**(1): 10-22.

Guillot-Sestier, M.-V., C. Sunyach, C. Druon, S. Scarzello and F. Checler (2009). "The  $\alpha$ -secretase-derived N-terminal product of cellular prion, N1, displays neuroprotective function in vitro and in vivo." Journal of Biological Chemistry **284**(51): 35973-35986.

Guo, J. L., S. Narasimhan, L. Changolkar, Z. He, A. Stieber, B. Zhang, R. J. Gathagan, M. Iba, J. D. McBride, J. Q. Trojanowski and V. M. Lee (2016). "Unique pathological tau conformers from Alzheimer's brains transmit tau pathology in nontransgenic mice." J Exp Med **213**(12): 2635-2654.

Guo, T., W. Noble and D. P. Hanger (2017). "Roles of tau protein in health and disease." Acta neuropathologica **133**(5): 665-704.

Halliday, M. and G. R. Mallucci (2014). "Targeting the unfolded protein response in neurodegeneration: a new approach to therapy." Neuropharmacology **76**: 169-174.

Hanger, D. P., B. H. Anderton and W. Noble (2009). "Tau phosphorylation: the therapeutic challenge for neurodegenerative disease." Trends in molecular medicine **15**(3): 112-119.

Harada, A., K. Oguchi, S. Okabe, J. Kuno, S. Terada, T. Ohshima, R. Sato-Yoshitake, Y. Takei, T. Noda and N. Hirokawa (1994). "Altered microtubule organization in small-calibre axons of mice lacking tau protein." Nature **369**(6480): 488.

Hardy, J. (1999). Pathways to primary neurodegenerative disease. Mayo Clinic Proceedings, Elsevier.

Hawe, A., S. Romeijn, V. Filipe and W. Jiskoot (2012). "Asymmetrical flow field-flow fractionation method for the analysis of submicron protein aggregates." Journal of pharmaceutical sciences **101**(11): 4129-4139.

Henriksen, K., Y. Wang, M. G. Sørensen, N. Barascuk, J. Suhy, J. T. Pedersen, K. L. Duffin, R. A. Dean, M. Pajak and C. Christiansen (2013). "An enzyme-generated fragment of tau measured in serum shows an inverse correlation to cognitive function." PLoS One **8**(5).

Herculano-Houzel, S. (2011). The isotropic fractionator: a fast, reliable method to determine numbers of cells in the brain or other tissues. Neuronal Network Analysis, Springer: 391-403.

Herculano-Houzel, S. (2016). The human advantage: a new understanding of how our brain became remarkable, MIT Press.

Herculano-Houzel, S. and R. Lent (2005). "Isotropic fractionator: a simple, rapid method for the quantification of total cell and neuron numbers in the brain." Journal of Neuroscience **25**(10): 2518-2521.

Herculano-Houzel, S., D. J. Messeder, K. Fonseca-Azevedo and N. A. Pantoja (2015). "When larger brains do not have more neurons: increased numbers of cells are compensated by decreased average cell size across mouse individuals." Frontiers in neuroanatomy **9**: 64.

Herculano-Houzel, S., B. Mota and R. Lent (2006). "Cellular scaling rules for rodent brains." Proceedings of the National Academy of Sciences **103**(32): 12138-12143.

Herculano-Houzel, S., C. S. von Bartheld, D. J. Miller and J. H. Kaas (2015). "How to count cells: the advantages and disadvantages of the isotropic fractionator compared with stereology." Cell and tissue research **360**(1): 29-42.

Herculano-Houzel, S., C. S. von Bartheld, D. J. Miller and J. H. Kaas (2015). "How to count cells: the advantages and disadvantages of the isotropic fractionator compared with stereology." Cell Tissue Res **360**(1): 29-42.

Herculano-Houzel, S. (2014). "The glia/neuron ratio: how it varies uniformly across brain

structures and species and what that means for brain physiology and evolution." Glia **62**(9): 1377-1391.

Hetz, C. and B. Mollereau (2014). "Disturbance of endoplasmic reticulum proteostasis in neurodegenerative diseases." Nature Reviews Neuroscience **15**(4): 233.

Hetz, C. and F. R. Papa (2018). "The unfolded protein response and cell fate control." Molecular cell **69**(2): 169-181.

Hetz, C. and S. Saxena (2017). "ER stress and the unfolded protein response in neurodegeneration." Nature Reviews Neurology **13**(8): 477.

Hochgrafe, K., A. Sydow and E. M. Mandelkow (2013). "Regulatable transgenic mouse models of Alzheimer disease: onset, reversibility and spreading of Tau pathology." FEBS J **280**(18): 4371-4381.

Holzbaur, E. L. (2017). "Dynamics of autophagy and mitophagy in neurons." The FASEB Journal **31**(1 supplement): 402.404-402.404.

Hoover, B. R., M. N. Reed, J. Su, R. D. Penrod, L. A. Kotilinek, M. K. Grant, R. Pitstick, G. A. Carlson, L. M. Lanier and L.-L. Yuan (2010). "Tau mislocalization to dendritic spines mediates synaptic dysfunction independently of neurodegeneration." Neuron **68**(6): 1067-1081.

Hughes, D. and M. Halliday (2017). "What Is Our Current Understanding of PrPSc-Associated Neurotoxicity and Its Molecular Underpinnings?" Pathogens **6**(4): 63.

Hurtado, D. E., L. Molina-Porcel, M. Iba, A. K. Aboagye, S. M. Paul, J. Q. Trojanowski and V. M. Lee (2010). "A {beta} accelerates the spatiotemporal progression of tau pathology and augments tau amyloidosis in an Alzheimer mouse model." Am J Pathol **177**(4): 1977-1988.

Hutton, M., C. L. Lendon, P. Rizzu, M. Baker, S. Froelich, H. Houlden, S. Pickering-Brown, S. Chakraverty, A. Isaacs, A. Grover, J. Hackett, J. Adamson, S. Lincoln, D. Dickson, P. Davies, R. C. Petersen, M. Stevens, E. de Graaff, E. Wauters, J. van Baren, M. Hillebrand, M. Joesse, J. M. Kwon, P. Nowotny, P. Heutink and et al. (1998). "Association of missense and 5'-splice-site mutations in tau with the inherited dementia FTDP-17." Nature **393**(6686): 702-705.

Hwang, D., I. Y. Lee, H. Yoo, N. Gehlenborg, J. H. Cho, B. Petritis, D. Baxter, R. Pitstick, R. Young and D. Spicer (2009). "A systems approach to prion disease." Molecular systems biology **5**(1).

Iba, M., J. L. Guo, J. D. McBride, B. Zhang, J. Q. Trojanowski and V. M. Lee (2013). "Synthetic tau fibrils mediate transmission of neurofibrillary tangles in a transgenic mouse model of Alzheimer's-like tauopathy." J Neurosci **33**(3): 1024-1037.

Iba, M., J. D. McBride, J. L. Guo, B. Zhang, J. Q. Trojanowski and V. M. Lee (2015). "Tau pathology spread in PS19 tau transgenic mice following locus coeruleus (LC) injections of synthetic tau fibrils is determined by the LC's afferent and efferent connections." Acta Neuropathol **130**(3): 349-362.

Igel-Egalon, A., J. Bohl, M. Moudjou, L. Herzog, F. Reine, H. Rezaei and V. Béringue (2019). "Heterogeneity and Architecture of Pathological Prion Protein Assemblies: Time to Revisit the Molecular Basis of the Prion Replication Process?" Viruses **11**(5): 429.

Igel-Egalon, A., F. Laferrière, M. Moudjou, J. Bohl, M. Mezache, T. Knäpple, L. Herzog, F.

Reine, C. Jas-Duval and M. Doumic (2019). "Early stage prion assembly involves two subpopulations with different quaternary structures and a secondary templating pathway." Communications biology **2**(1): 1-13.

Iqbal, K., F. Liu and C.-X. Gong (2016). "Tau and neurodegenerative disease: the story so far." Nature Reviews Neurology **12**(1): 15.

Irwin, D. J. (2016). "Tauopathies as clinicopathological entities." Parkinsonism & related disorders **22**: S29-S33.

Ittner, A., S. W. Chua, J. Bertz, A. Volkerling, J. van der Hoven, A. Gladbach, M. Przybyla, M. Bi, A. van Hummel and C. H. Stevens (2016). "Site-specific phosphorylation of tau inhibits amyloid- $\beta$  toxicity in Alzheimer's mice." Science **354**(6314): 904-908.

Janus, C. and H. Welzl (2010). Mouse models of neurodegenerative diseases: criteria and general methodology. Mouse Models for Drug Discovery, Springer: 323-345.

Jarrett, J. T. and P. T. Lansbury Jr (1993). "Seeding "one-dimensional crystallization" of amyloid: a pathogenic mechanism in Alzheimer's disease and scrapie?" Cell **73**(6): 1055-1058.

Jellinger, K. A. (2010). "Basic mechanisms of neurodegeneration: a critical update." Journal of cellular and molecular medicine **14**(3): 457-487.

Jicha, G. A., J. M. Rockwood, B. Berenfeld, M. Hutton and P. Davies (1999). "Altered conformation of recombinant frontotemporal dementia-17 mutant tau proteins." Neuroscience letters **260**(3): 153-156.

Jiménez-Huete, A., P. M. Lievens, R. Vidal, P. Piccardo, B. Ghetti, F. Tagliavini, B. Frangione and F. Prelli (1998). "Endogenous proteolytic cleavage of normal and disease-associated isoforms of the human prion protein in neural and non-neural tissues." The American journal of pathology **153**(5): 1561-1572.

Jucker, M. (2010). "The benefits and limitations of animal models for translational research in neurodegenerative diseases." Nature medicine **16**(11): 1210.

Jucker, M. and L. C. Walker (2013). "Self-propagation of pathogenic protein aggregates in neurodegenerative diseases." Nature **501**(7465): 45-51.

Kaufman, S. K., D. W. Sanders, T. L. Thomas, A. J. Ruchinkas, J. Vaquer-Alicea, A. M. Sharma, T. M. Miller and M. I. Diamond (2016). "Tau Prion Strains Dictate Patterns of Cell Pathology, Progression Rate and Regional Vulnerability In Vivo." Neuron.

Kaufman, S. K., D. W. Sanders, T. L. Thomas, A. J. Ruchinkas, J. Vaquer-Alicea, A. M. Sharma, T. M. Miller and M. I. Diamond (2016). "Tau prion strains dictate patterns of cell pathology, progression rate, and regional vulnerability in vivo." Neuron **92**(4): 796-812.

Kaufman, S. K., T. L. Thomas, K. Del Tredici, H. Braak and M. I. Diamond (2017). "Characterization of tau prion seeding activity and strains from formaldehyde-fixed tissue." Acta Neuropathol Commun **5**(1): 41.

Kelly, J. W. (2000). "Mechanisms of amyloidogenesis." Nature structural biology **7**(10): 824-826.

Kim, C., T. Haldiman, Y. Cohen, W. Chen, J. Blevins, M.-S. Sy, M. Cohen and J. G. Safar (2011). "Protease-sensitive conformers in broad spectrum of distinct PrPSc structures in sporadic

Creutzfeldt-Jakob disease are indicator of progression rate." *PLoS pathogens* **7**(9): e1002242.

Kobayashi, T., H. Mori, Y. Okuma, D. W. Dickson, N. Cookson, Y. Tsuboi, Y. Motoi, R. Tanaka, N. Miyashita, M. Anno, H. Narabayashi and Y. Mizuno (2002). "Contrasting genotypes of the tau gene in two phenotypically distinct patients with P301L mutation of frontotemporal dementia and parkinsonism linked to chromosome 17." *J Neurol* **249**(6): 669-675.

Kraus, A., B. R. Groveman and B. Caughey (2013). "Prions and the potential transmissibility of protein misfolding diseases." *Annual review of microbiology* **67**: 543-564.

Kretzschmar, H. A., S. B. Prusiner, L. E. Stowring and S. J. DeArmond (1986). "Scrapie prion proteins are synthesized in neurons." *Am. J. Pathol.* **122**: 1-5.

Kulnane, L. S. and B. T. Lamb (2001). "Neuropathological characterization of mutant amyloid precursor protein yeast artificial chromosome transgenic mice." *Neurobiol Dis* **8**(6): 982-992.

Labrie, V., S. Pai and A. Petronis (2012). "Epigenetics of major psychosis: progress, problems and perspectives." *Trends Genet* **28**(9): 427-435.

Laferrière, F., P. Tixador, M. Moudjou, J. Chapuis, P. Sibille, L. Herzog, F. Reine, E. Jaumain, H. Laude and H. Rezaei (2013). "Quaternary structure of pathological prion protein as a determining factor of strain-specific prion replication dynamics." *PLoS pathogens* **9**(10).

Laible, G. (2018). *Production of Transgenic Livestock: Overview of Transgenic Technologies. Animal Biotechnology 2*, Springer: 95-121.

Last, N. B. and A. D. Miranker (2013). "Common mechanism unites membrane poration by amyloid and antimicrobial peptides." *Proceedings of the National Academy of Sciences* **110**(16): 6382-6387.

Lau, A., A. McDonald, N. Daude, C. E. Mays, E. D. Walter, R. Aglietti, R. C. Mercer, S. Wohlgemuth, J. van der Merwe and J. Yang (2015). "Octarepeat region flexibility impacts prion function, endoproteolysis and disease manifestation." *EMBO molecular medicine* **7**(3): 339-356.

Lazarou, M., D. A. Sliter, L. A. Kane, S. A. Sarraf, C. Wang, J. L. Burman, D. P. Sideris, A. I. Fogel and R. J. Youle (2015). "The ubiquitin kinase PINK1 recruits autophagy receptors to induce mitophagy." *Nature* **524**(7565): 309-314.

Lebouvier, T., F. Pasquier and L. Buée (2017). "Update on tauopathies." *Current opinion in neurology* **30**(6): 589-598.

Lee, G., N. Cowan and M. Kirschner (1988). "The primary structure and heterogeneity of tau protein from mouse brain." *Science* **239**(4837): 285-288.

Lee, V. M.-Y., T. K. Kenyon and J. Q. Trojanowski (2005). "Transgenic animal models of tauopathies." *Biochimica et Biophysica Acta (BBA)-Molecular Basis of Disease* **1739**(2-3): 251-259.

Lewis, J., E. McGowan, J. Rockwood, H. Melrose, P. Nacharaju, M. Van Slegtenhorst, K. Gwinn-Hardy, M. Paul Murphy, M. Baker, X. Yu, K. Duff, J. Hardy, A. Corral, W. L. Lin, S. H. Yen, D. W. Dickson, P. Davies and M. Hutton (2000). "Neurofibrillary tangles, amyotrophy and progressive motor disturbance in mice expressing mutant (P301L) tau protein." *Nat Genet* **25**(4): 402-405.

Lewis, V., V. A. Johanssen, P. J. Crouch, G. M. Klug, N. M. Hooper and S. J. Collins (2016).

"Prion protein "gamma-cleavage": characterizing a novel endoproteolytic processing event." Cellular and molecular life sciences **73**(3): 667-683.

Li, C., A. Ebrahimi and H. Schluesener (2013). "Drug pipeline in neurodegeneration based on transgenic mice models of Alzheimer's disease." Ageing Res Rev **12**(1): 116-140.

Li, Z., X. Ji, W. Wang, J. Liu, X. Liang, H. Wu, J. Liu, U. S. Eggert, Q. Liu and X. Zhang (2016). "Ammonia induces autophagy through dopamine receptor D3 and MTOR." PloS one **11**(4): e0153526.

Liu, L., V. Drouet, J. W. Wu, M. P. Witter, S. A. Small, C. Clelland and K. Duff (2012). "Trans-synaptic spread of tau pathology in vivo." PLoS One **7**(2): e31302.

Mahal, S. P., C. A. Baker, C. A. Demczyk, E. W. Smith, C. Julius and C. Weissmann (2007). "Prion strain discrimination in cell culture: the cell panel assay." Proceedings of the National Academy of Sciences **104**(52): 20908-20913.

Mandelkow, E.-M. and E. Mandelkow (2012). "Biochemistry and cell biology of tau protein in neurofibrillary degeneration." Cold Spring Harbor perspectives in medicine **2**(7): a006247.

Mangé, A., F. Béranger, K. Peoc'h, T. Onodera, Y. Frobert and S. Lehmann (2004). "Alpha-and beta-cleavages of the amino-terminus of the cellular prion protein." Biology of the Cell **96**(2): 125-132.

Mather, M. and C. W. Harley (2016). "The Locus Coeruleus: Essential for Maintaining Cognitive Function and the Aging Brain." Trends Cogn Sci **20**(3): 214-226.

Matsumoto, S.-E., Y. Motoi, K. Ishiguro, T. Tabira, F. Kametani, M. Hasegawa and N. Hattori (2015). "The twenty-four kDa C-terminal tau fragment increases with aging in tauopathy mice: implications of prion-like properties." Human molecular genetics **24**(22): 6403-6416.

Mayer, E. A., R. Knight, S. K. Mazmanian, J. F. Cryan and K. Tillisch (2014). "Gut microbes and the brain: paradigm shift in neuroscience." J Neurosci **34**(46): 15490-15496.

Mayer, E. A., K. Tillisch and A. Gupta (2015). "Gut/brain axis and the microbiota." J Clin Invest **125**(3): 926-938.

Mays, C. E., J. Coomaraswamy, J. C. Watts, J. Yang, K. W. Ko, B. Strome, R. C. Mercer, S. L. Wohlgemuth, G. Schmitt-Ulms and D. Westaway (2014). "Endoproteolytic processing of the mammalian prion glycoprotein family." The FEBS journal **281**(3): 862-876.

Mays, C. E., C. Kim, T. Haldiman, J. van der Merwe, A. Lau, J. Yang, J. Grams, M. A. Di Bari, R. Nonno and G. C. Telling (2014). "Prion disease tempo determined by host-dependent substrate reduction." The Journal of clinical investigation **124**(2).

Mays, C. E., J. van der Merwe, C. Kim, T. Haldiman, D. McKenzie, J. G. Safar and D. Westaway (2015). "Prion infectivity plateaus and conversion to symptomatic disease originate from falling precursor levels and increased levels of oligomeric PrP<sup>Sc</sup> species." Journal of virology **89**(24): 12418-12426.

McDonald, A. J., J. P. Dibble, E. G. Evans and G. L. Millhauser (2014). "A new paradigm for enzymatic control of  $\alpha$ -cleavage and  $\beta$ -cleavage of the prion protein." Journal of Biological Chemistry **289**(2): 803-813.

McMahon, H. E., A. Mangé, N. Nishida, C. Créminon, D. Casanova and S. Lehmann (2001).

"Cleavage of the amino terminus of the prion protein by reactive oxygen species." Journal of Biological Chemistry **276**(3): 2286-2291.

Mercer, R. C., N. Daude, L. Dorosh, Z.-L. Fu, C. E. Mays, H. Gapesina, S. L. Wohlgemuth, C. Y. Acevedo-Morantes, J. Yang and N. R. Cashman (2018). "A novel Gerstmann-Sträussler-Scheinker disease mutation defines a precursor for amyloidogenic 8 kDa PrP fragments and reveals N-terminal structural changes shared by other GSS alleles." PLoS pathogens **14**(1): e1006826.

Meyer, R. K., M. P. McKinley, K. A. Bowman, M. B. Braunfeld, R. A. Barry and S. B. Prusiner (1986). "Separation and properties of cellular and scrapie prion proteins." Proceedings of the National Academy of Sciences **83**(8): 2310-2314.

Miller, D. J., P. Balaram, N. A. Young and J. H. Kaas (2014). "Three counting methods agree on cell and neuron number in chimpanzee primary visual cortex." Front Neuroanat **8**: 36.

Miller, D. J., P. Balaram, N. A. Young and J. H. Kaas (2014). "Three counting methods agree on cell and neuron number in chimpanzee primary visual cortex." Frontiers in neuroanatomy **8**: 36.

Miller, D. J., T. Duka, C. D. Stimpson, S. J. Schapiro, W. B. Baze, M. J. McArthur, A. J. Fobbs, A. M. Sousa, N. Šestan and D. E. Wildman (2012). "Prolonged myelination in human neocortical evolution." Proceedings of the National Academy of Sciences **109**(41): 16480-16485.

Mirra, S. S., J. R. Murrell, M. Gearing, M. G. Spillantini, M. Goedert, R. A. Crowther, A. I. Levey, R. Jones, J. Green and J. M. Shoffner (1999). "Tau pathology in a family with dementia and a P301L mutation in tau." Journal of neuropathology and experimental neurology **58**(4): 335-345.

Mirra, S. S., J. R. Murrell, M. Gearing, M. G. Spillantini, M. Goedert, R. A. Crowther, A. I. Levey, R. Jones, J. Green, J. M. Shoffner, B. H. Wainer, M. L. Schmidt, J. Q. Trojanowski and B. Ghetti (1999). "Tau pathology in a family with dementia and a P301L mutation in tau." J Neuropathol Exp Neurol **58**(4): 335-345.

Morales, R., K. Abid and C. Soto (2007). "The prion strain phenomenon: molecular basis and unprecedented features." Biochimica et Biophysica Acta (BBA)-Molecular Basis of Disease **1772**(6): 681-691.

Morales, R., K. Callegari and C. Soto (2015). "Prion-like features of misfolded A $\beta$  and tau aggregates." Virus research **207**: 106-112.

Moser, M., Colello, R.J., Pott, U., and Oesch, B. (1995). "Developmental Expression of the Prion Protein in Glial Cells." Neuron **14**: 509-517.

Mott, R. T., D. W. Dickson, J. Q. Trojanowski, V. Zhukareva, V. M. Lee, M. Forman, V. Van Deerlin, J. F. Ervin, D. S. Wang, D. E. Schmechel and C. M. Hulette (2005). "Neuropathologic, biochemical, and molecular characterization of the frontotemporal dementias." J Neuropathol Exp Neurol **64**(5): 420-428.

Mullen, R. J., C. R. Buck and A. M. Smith (1992). "NeuN, a neuronal specific nuclear protein in vertebrates." Development **116**(1): 201-211.

Murakami, T., E. Paitel, T. Kawarabayashi, M. Ikeda, M. A. Chishti, C. Janus, E. Matsubara, A. Sasaki, T. Kawarai and A. L. Phinney (2006). "Cortical neuronal and glial pathology in

TgTauP301L transgenic mice: neuronal degeneration, memory disturbance, and phenotypic variation." The American journal of pathology **169**(4): 1365-1375.

Murakami, T., E. Paitel, T. Kawarabayashi, M. Ikeda, M. A. Chishti, C. Janus, E. Matsubara, A. Sasaki, T. Kawarai, A. L. Phinney, Y. Harigaya, P. Horne, N. Egashira, K. Mishima, A. Hanna, J. Yang, K. Iwasaki, M. Takahashi, M. Fujiwara, K. Ishiguro, C. Bergeron, G. A. Carlson, K. Abe, D. Westaway, P. St George-Hyslop and M. Shoji (2006). "Cortical neuronal and glial pathology in TgTauP301L transgenic mice: neuronal degeneration, memory disturbance, and phenotypic variation." Am J Pathol **169**(4): 1365-1375.

Myeku, N., C. L. Clelland, S. Emrani, N. V. Kukushkin, W. H. Yu, A. L. Goldberg and K. E. Duff (2016). "Tau-driven 26S proteasome impairment and cognitive dysfunction can be prevented early in disease by activating cAMP-PKA signaling." Nat Med **22**(1): 46-53.

Ngwenya, A., J. Nahirney, B. Brinkman, L. Williams and A. N. Iwaniuk (2017). "Comparison of estimates of neuronal number obtained using the isotropic fractionator method and unbiased stereology in day old chicks (*Gallus domesticus*)." Journal of neuroscience methods **287**: 39-46.

Nixon, R. A. (2013). "The role of autophagy in neurodegenerative disease." Nat Med **19**(8): 983-997.

Nurnberger, J. and M. Gordon (1957). "The cell density of neural tissues: direct counting method and possible applications as a biologic referent." Progress in neurobiology **2**: 100.

Oliveira-Martins, J. B., S.-i. Yusa, A. M. Calella, C. Bridel, F. Baumann, P. Dametto and A. Aguzzi (2010). "Unexpected tolerance of  $\alpha$ -cleavage of the prion protein to sequence variations." PloS one **5**(2): e9107.

Palsson, B. (2000). "The challenges of in silico biology." Nature biotechnology **18**(11): 1147.

Peeraer, E., A. Bottelbergs, K. Van Kolen, I. C. Stancu, B. Vasconcelos, M. Mahieu, H. Duytschaever, L. Ver Donck, A. Torremans, E. Sluydts, N. Van Acker, J. A. Kemp, M. Mercken, K. R. Brunden, J. Q. Trojanowski, I. Dewachter, V. M. Lee and D. Moechars (2015). "Intracerebral injection of preformed synthetic tau fibrils initiates widespread tauopathy and neuronal loss in the brains of tau transgenic mice." Neurobiol Dis **73**: 83-95.

Peggion, C., M. C. Sorgato and A. Bertoli (2014). "Prions and prion-like pathogens in neurodegenerative disorders." Pathogens **3**(1): 149-163.

Phinney, A. L., P. Horne, J. Yang, C. Janus, C. Bergeron and D. Westaway (2003). "Mouse models of Alzheimer's disease: the long and filamentous road." Neurol Res **25**(6): 590-600.

Piovesan, A., F. Antonaros, L. Vitale, P. Strippoli, M. C. Pelleri and M. Caracausi (2019). "Human protein-coding genes and gene feature statistics in 2019." BMC research notes **12**(1): 315.

Planel, E., P. Krishnamurthy, T. Miyasaka, L. Liu, M. Herman, A. Kumar, A. Bretteville, H. Y. Figueroa, W. H. Yu, R. A. Whittington, P. Davies, A. Takashima, R. A. Nixon and K. E. Duff (2008). "Anesthesia-induced hyperphosphorylation detaches 3-repeat tau from microtubules without affecting their stability in vivo." J Neurosci **28**(48): 12798-12807.

Polymenidou, M. and D. W. Cleveland (2012). "Prion-like spread of protein aggregates in neurodegeneration." Journal of Experimental Medicine **209**(5): 889-893.

Prusiner, S., M. Scott, D. Foster, D. Westaway and S. DeArmond (1990). "Transgenic studies implicate interactions between homologous PrP isoforms in scrapie prion replication." Cell **63**: 673-686.

Prusiner, S. B. (1991). "Molecular biology of prion diseases." Science **252**(5012): 1515-1522.

Prusiner, S. B., M. R. Scott, S. J. DeArmond and F. E. Cohen (1998). "Prion protein biology." Cell **93**(3): 337-348.

Puchtler, H., F. S. Waldrop, S. N. Meloan, M. S. Terry and H. Conner (1970). "Methacarn (methanol-Carnoy) fixation." Histochemie **21**(2): 97-116.

Pushie, M. J. and H. J. Vogel (2008). "Modeling by assembly and molecular dynamics simulations of the low Cu<sup>2+</sup> occupancy form of the mammalian prion protein octarepeat region: gaining insight into Cu<sup>2+</sup>-mediated  $\beta$ -cleavage." Biophysical journal **95**(11): 5084-5091.

Quinn, J. P., N. J. Corbett, K. A. Kellett and N. M. Hooper (2018). "Tau proteolysis in the pathogenesis of tauopathies: neurotoxic fragments and novel biomarkers." Journal of Alzheimer's Disease **63**(1): 13-33.

Radford, R. A., M. Morsch, S. L. Rayner, N. J. Cole, D. L. Pountney and R. S. Chung (2015). "The established and emerging roles of astrocytes and microglia in amyotrophic lateral sclerosis and frontotemporal dementia." Front Cell Neurosci **9**: 414.

Repetto, I. E., R. Monti, M. Tropiano, S. Tomasi, A. Arbini, C.-H. Andrade-Moraes, R. Lent and A. Vercelli (2016). "The isotropic fractionator as a tool for quantitative analysis in central nervous system diseases." Frontiers in Cellular Neuroscience **10**: 190.

Rodriguez-Martin, T., A. M. Pooler, D. H. Lau, G. M. Morotz, K. J. De Vos, J. Gilley, M. P. Coleman and D. P. Hanger (2016). "Reduced number of axonal mitochondria and tau hypophosphorylation in mouse P301L tau knockin neurons." Neurobiol Dis **85**: 1-10.

Ross, C. A. and M. A. Poirier (2004). "Protein aggregation and neurodegenerative disease." Nature medicine **10**(7s): S10.

Russell, E. S. (1975). Lifespan and Aging Patterns. Biology of the Laboratory Mouse. G. E.L. New York, Dover Publications: 511-520.

Rutishauser, D., K. Mertz, R. Moos, E. Brunner and T. Rüllicke (2009). "The Comprehensive Native Interactome of a Fully Functional Tagged Prion."

Safar, J., H. Wille, V. Itri, D. Groth, H. Serban, M. Torchia, F. E. Cohen and S. B. Prusiner (1998). "Eight prion strains have PrP Sc molecules with different conformations." Nature medicine **4**(10): 1157-1165.

Sahara, N., M. DeTure, Y. Ren, A. S. Ebrahim, D. Kang, J. Knight, C. Volbracht, J. T. Pedersen, D. W. Dickson, S. H. Yen and J. Lewis (2013). "Characteristics of TBS-extractable hyperphosphorylated tau species: aggregation intermediates in rTg4510 mouse brain." J Alzheimers Dis **33**(1): 249-263.

Sahara, N., J. Lewis, M. DeTure, E. McGowan, D. W. Dickson, M. Hutton and S. H. Yen (2002). "Assembly of tau in transgenic animals expressing P301L tau: alteration of phosphorylation and solubility." Journal of neurochemistry **83**(6): 1498-1508.

Saito, T., Y. Matsuba, N. Mihira, J. Takano, P. Nilsson, S. Itohara, N. Iwata and T. C. Saido

(2014). "Single App knock-in mouse models of Alzheimer's disease." *Nat Neurosci* **17**(5): 661-663.

Sampson, T. R., J. W. Debelius, T. Thron, S. Janssen, G. G. Shastri, Z. E. Ilhan, C. Challis, C. E. Schretter, S. Rocha, V. Gradinaru, M. F. Chesselet, A. Keshavarzian, K. M. Shannon, R. Krajmalnik-Brown, P. Wittung-Stafshede, R. Knight and S. K. Mazmanian (2016). "Gut Microbiota Regulate Motor Deficits and Neuroinflammation in a Model of Parkinson's Disease." *Cell* **167**(6): 1469-1480 e1412.

Sanders, D. W., S. K. Kaufman, S. L. DeVos, A. M. Sharma, H. Mirbaha, A. Li, S. J. Barker, A. C. Foley, J. R. Thorpe, L. C. Serpell, T. M. Miller, L. T. Grinberg, W. W. Seeley and M. I. Diamond (2014). "Distinct tau prion strains propagate in cells and mice and define different tauopathies." *Neuron* **82**(6): 1271-1288.

Sanders, D. W., S. K. Kaufman, B. B. Holmes and M. I. Diamond (2016). "Prions and protein assemblies that convey biological information in health and disease." *Neuron* **89**(3): 433-448.

Santacruz, K., J. Lewis, T. Spires, J. Paulson, L. Kotilinek, M. Ingelsson, A. Guimaraes, M. DeTure, M. Ramsden, E. McGowan, C. Forster, M. Yue, J. Orne, C. Janus, A. Mariash, M. Kuskowski, B. Hyman, M. Hutton and K. H. Ashe (2005). "Tau suppression in a neurodegenerative mouse model improves memory function." *Science* **309**(5733): 476-481.

Schwarz, A. J., P. Yu, B. B. Miller, S. Shcherbinin, J. Dickson, M. Navitsky, A. D. Joshi, M. D. Devous, Sr. and M. S. Mintun (2016). "Regional profiles of the candidate tau PET ligand 18F-AV-1451 recapitulate key features of Braak histopathological stages." *Brain* **139**(Pt 5): 1539-1550.

Scott, M., D. Groth, D. Foster, M. Torchia, S.-L. Yang, S. J. DeArmond and S. B. Prusiner (1993). "Propagation of prions with artificial properties in transgenic mice expressing chimeric PrP genes." *Cell* **73**: 979-988.

Scott, M. R., R. Köhler, D. Foster and S. B. Prusiner (1992). "Chimeric prion protein expression in cultured cells and transgenic mice." *Protein Sci.* **1**: 986-997.

Serio, T. R., A. G. Cashikar, A. S. Kowal, G. J. Sawicki, J. J. Moslehi, L. Serpell, M. F. Arnsdorf and S. L. Lindquist (2000). "Nucleated conformational conversion and the replication of conformational information by a prion determinant." *Science* **289**(5483): 1317-1321.

Shammas, S. L., G. A. Garcia, S. Kumar, M. Kjaergaard, M. H. Horrocks, N. Shivji, E. Mandelkow, T. P. Knowles, E. Mandelkow and D. Klenerman (2015). "A mechanistic model of tau amyloid aggregation based on direct observation of oligomers." *Nat Commun* **6**: 7025.

Shi, S., G. Mitteregger-Kretzschmar, A. Giese and H. A. Kretzschmar (2013). "Establishing quantitative real-time quaking-induced conversion (qRT-QuIC) for highly sensitive detection and quantification of PrP Sc in prion-infected tissues." *Acta neuropathologica communications* **1**(1): 44.

Silveira, J. R., A. G. Hughson and B. Caughey (2006). "Fractionation of Prion Protein Aggregates by Asymmetrical Flow Field-Flow Fractionation." *Methods in enzymology* **412**: 21-33.

Silveira, J. R., G. J. Raymond, A. G. Hughson, R. E. Race, V. L. Sim, S. F. Hayes and B.

Caughey (2005). "The most infectious prion protein particles." *Nature* **437**(7056): 257-261.

Simoneau, S., H. Rezaei, N. Sales, G. Kaiser-Schulz, M. Lefebvre-Roque, C. Vidal, J.-G. Fournier, J. Comte, F. Wopfner and J. Grosclaude (2007). "In vitro and in vivo neurotoxicity of prion protein oligomers." *PLoS pathogens* **3**(8): e125.

Soto, C., L. Estrada and J. Castilla (2006). "Amyloids, prions and the inherent infectious nature of misfolded protein aggregates." *Trends in biochemical sciences* **31**(3): 150-155.

Soto, C. and S. Pritzkow (2018). "Protein misfolding, aggregation, and conformational strains in neurodegenerative diseases." *Nature neuroscience* **21**(10): 1332-1340.

Spillantini, M. G., J. R. Murrell, M. Goedert, M. R. Farlow, A. Klug and B. Ghetti (1998). "Mutation in the tau gene in familial multiple system tauopathy with presenile dementia." *Proc Natl Acad Sci U S A* **95**(13): 7737-7741.

Stalder, A. K., M. J. Carson, A. Pagenstecher, V. C. Asensio, C. Kincaid, M. Benedict, H. C. Powell, E. Masliah and I. L. Campbell (1998). "Late-onset chronic inflammatory encephalopathy in immune-competent and severe combined immune-deficient (SCID) mice with astrocyte-targeted expression of tumor necrosis factor." *The American journal of pathology* **153**(3): 767-783.

Stancu, I. C., B. Vasconcelos, L. Ris, P. Wang, A. Villers, E. Peeraer, A. Buist, D. Terwel, P. Baatsen, T. Oyelami, N. Pierrot, C. Casteels, G. Bormans, P. Kienlen-Campard, J. N. Octave, D. Moechars and I. Dewachter (2015). "Templated misfolding of Tau by prion-like seeding along neuronal connections impairs neuronal network function and associated behavioral outcomes in Tau transgenic mice." *Acta Neuropathol* **129**(6): 875-894.

Stroylova, Y., G. Kiselev, E. Schmalhausen and V. Muronetz (2014). "Prions and chaperones: Friends or foes?" *Biochemistry (Moscow)* **79**(8): 761-775.

Sullivan, P. G., A. J. Bruce-Keller, A. G. Rabchevsky, S. Christakos, D. K. S. Clair, M. P. Mattson and S. W. Scheff (1999). "Exacerbation of damage and altered NF- $\kappa$ B activation in mice lacking tumor necrosis factor receptors after traumatic brain injury." *Journal of Neuroscience* **19**(15): 6248-6256.

Sunyach, C., M. A. Cisse, C. A. Da Costa, B. Vincent and F. Checler (2007). "The C-terminal products of cellular prion protein processing, C1 and C2, exert distinct influence on p53-dependent staurosporine-induced caspase-3 activation." *Journal of Biological Chemistry* **282**(3): 1956-1963.

Swearingen, J. R. (2018). "Choosing the right animal model for infectious disease research." *Animal models and experimental medicine* **1**(2): 100-108.

Sweeney, P., H. Park, M. Baumann, J. Dunlop, J. Frydman, R. Kopito, A. McCampbell, G. Leblanc, A. Venkateswaran and A. Nurmi (2017). "Protein misfolding in neurodegenerative diseases: implications and strategies." *Translational neurodegeneration* **6**(1): 6.

Tacik, P., M. Sanchez-Contreras, M. DeTure, M. E. Murray, R. Rademakers, O. A. Ross, Z. K. Wszolek, J. E. Parisi, D. S. Knopman, R. C. Petersen and D. W. Dickson (2016). "Clinicopathologic heterogeneity in frontotemporal dementia and parkinsonism linked to chromosome 17 (FTDP-17) due to microtubule-associated protein tau (MAPT) p.P301L

mutation, including a patient with globular glial tauopathy." Neuropathol Appl Neurobiol.

Tai, H. C., B. Y. Wang, A. Serrano-Pozo, M. P. Frosch, T. L. Spires-Jones and B. T. Hyman (2014). "Frequent and symmetric deposition of misfolded tau oligomers within presynaptic and postsynaptic terminals in Alzheimer's disease." Acta Neuropathol Commun **2**: 146.

Tanaka, M., P. Chien, N. Naber, R. Cooke and J. S. Weissman (2004). "Conformational variations in an infectious protein determine prion strain differences." Nature **428**(6980): 323-328.

Taniguchi-Watanabe, S., T. Arai, F. Kametani, T. Nonaka, M. Masuda-Suzukake, A. Tarutani, S. Murayama, Y. Saito, K. Arima and M. Yoshida (2016). "Biochemical classification of tauopathies by immunoblot, protein sequence and mass spectrometric analyses of sarkosyl-insoluble and trypsin-resistant tau." Acta neuropathologica **131**(2): 267-280.

Taniguchi-Watanabe, S., T. Arai, F. Kametani, T. Nonaka, M. Masuda-Suzukake, A. Tarutani, S. Murayama, Y. Saito, K. Arima, M. Yoshida, H. Akiyama, A. Robinson, D. M. A. Mann, T. Iwatsubo and M. Hasegawa (2016). "Biochemical classification of tauopathies by immunoblot, protein sequence and mass spectrometric analyses of sarkosyl-insoluble and trypsin-resistant tau." Acta Neuropathol **131**(2): 267-280.

Tao, H., W. Liu, B. N. Simmons, H. K. Harris, T. C. Cox and M. A. Massiah (2010). "Purifying natively folded proteins from inclusion bodies using sarkosyl, Triton X-100, and CHAPS." Biotechniques **48**(1): 61-64.

Tarasoff-Conway, J. M., R. O. Carare, R. S. Osorio, L. Glodzik, T. Butler, E. Fieremans, L. Axel, H. Rusinek, C. Nicholson, B. V. Zlokovic, B. Frangione, K. Blennow, J. Menard, H. Zetterberg, T. Wisniewski and M. J. de Leon (2015). "Clearance systems in the brain-implications for Alzheimer disease." Nat Rev Neurol **11**(8): 457-470.

Taylor, D. R., E. T. Parkin, S. L. Cocklin, J. R. Ault, A. E. Ashcroft, A. J. Turner and N. M. Hooper (2009). "Role of ADAMs in the ectodomain shedding and conformational conversion of the prion protein." Journal of Biological Chemistry **284**(34): 22590-22600.

Taylor, J. P., J. Hardy and K. H. Fischbeck (2002). "Toxic proteins in neurodegenerative disease." Science **296**(5575): 1991-1995.

Tenreiro, S., K. Eckermann and T. F. Outeiro (2014). "Protein phosphorylation in neurodegeneration: friend or foe?" Frontiers in molecular neuroscience **7**: 42.

Tixador, P., L. Herzog, F. Reine, E. Jaumain, J. m. Chapuis, A. Le Dur, H. Laude and V. Beringue (2010). "The physical relationship between infectivity and prion protein aggregates is strain-dependent." PLoS pathogens **6**(4): e1000859.

Towbin, H., T. Staehelin and J. Gordon (1979). "Electrophoretic transfer of proteins from polyacrylamide gels to nitrocellulose sheets: Procedure and some applications." Proc. Natl. Acad. Sci. USA **76**: 4350-4354.

Towbin, H., T. Staehelin and J. Gordon (1979). "Electrophoretic transfer of proteins from polyacrylamide gels to nitrocellulose sheets: procedure and some applications." Proceedings of the National Academy of Sciences **76**(9): 4350-4354.

Trombetta, E. S. and A. J. Parodi (2003). "Quality control and protein folding in the secretory

pathway." Annual review of cell and developmental biology **19**(1): 649-676.

van Swieten, J. C., M. Stevens, S. M. Rosso, P. Rizzu, M. Joesse, I. de Koning, W. Kamphorst, R. Ravid, M. G. Spillantini, Niermeijer and P. Heutink (1999). "Phenotypic variation in hereditary frontotemporal dementia with tau mutations." Ann Neurol **46**(4): 617-626.

Vincent, B., E. Paitel, P. Saftig, Y. Frobert, D. Hartmann, B. De Strooper, J. Grassi, E. Lopez-Perez and F. Checler (2001). "The disintegrins ADAM10 and TACE contribute to the constitutive and phorbol ester-regulated normal cleavage of the cellular prion protein." Journal of Biological Chemistry **276**(41): 37743-37746.

Walker, L. C. and M. Jucker (2015). "Neurodegenerative diseases: expanding the prion concept." Annual review of neuroscience **38**: 87-103.

Walleczek, J. (2006). Self-organized biological dynamics and nonlinear control: toward understanding complexity, chaos and emergent function in living systems, Cambridge University Press.

Walmsley, A. R., N. T. Watt, D. R. Taylor, W. S. S. Perera and N. M. Hooper (2009). " $\alpha$ -cleavage of the prion protein occurs in a late compartment of the secretory pathway and is independent of lipid rafts." Molecular and Cellular Neuroscience **40**(2): 242-248.

Walsh, P., G. Vanderlee, J. Yau, J. Campeau, V. L. Sim, C. M. Yip and S. Sharpe (2014). "The mechanism of membrane disruption by cytotoxic amyloid oligomers formed by prion protein (106–126) is dependent on bilayer composition." Journal of Biological Chemistry **289**(15): 10419-10430.

Wang, J., D. Li, L. J. Dangott and G. Wu (2006). "Proteomics and its role in nutrition research." The Journal of nutrition **136**(7): 1759-1762.

Wang, Y., J. Biernat, M. Pickhardt, E. Mandelkow and E.-M. Mandelkow (2007). "Stepwise proteolysis liberates tau fragments that nucleate the Alzheimer-like aggregation of full-length tau in a neuronal cell model." Proceedings of the National Academy of Sciences **104**(24): 10252-10257.

Wang, Y. and E. Mandelkow (2016). "Tau in physiology and pathology." Nat Rev Neurosci **17**(1): 5-21.

Wang, Y., M. Martinez-Vicente, U. Krüger, S. Kaushik, E. Wong, E.-M. Mandelkow, A. M. Cuervo and E. Mandelkow (2009). "Tau fragmentation, aggregation and clearance: the dual role of lysosomal processing." Human molecular genetics **18**(21): 4153-4170.

Wang, Y. P., J. Biernat, M. Pickhardt, E. Mandelkow and E. M. Mandelkow (2007). "Stepwise proteolysis liberates tau fragments that nucleate the Alzheimer-like aggregation of full-length tau in a neuronal cell model." Proc Natl Acad Sci U S A **104**(24): 10252-10257.

Watt, N. T., D. R. Taylor, A. Gillott, D. A. Thomas, W. S. S. Perera and N. M. Hooper (2005). "Reactive oxygen species-mediated  $\beta$ -cleavage of the prion protein in the cellular response to oxidative stress." Journal of Biological Chemistry **280**(43): 35914-35921.

Watts, J. C., H. Huo, Y. Bai, S. Ehsani, A. Jeon, T. Shi, N. Daude, A. Lau, R. Young and L. Xu (2009). "Interactome analyses identify ties of PrP and its mammalian paralogs to oligomannosidic N-glycans and endoplasmic reticulum-derived chaperones." PLoS pathogens

5(10): e1000608-e1000608.

Watts, J. C., J. Stöhr, S. Bhardwaj, H. Wille, A. Oehler, S. J. DeArmond, K. Giles and S. B. Prusiner (2011). "Protease-resistant prions selectively decrease Shadoo protein." PLoS pathogens **7**(11).

Watts, J. C. and D. Westaway (2007). "The prion protein family: diversity, rivalry, and dysfunction." Biochimica et Biophysica Acta (BBA)-Molecular Basis of Disease **1772**(6): 654-672.

Wegmann, S., E. A. Maury, M. J. Kirk, L. Saqran, A. Roe, S. L. DeVos, S. Nicholls, Z. Fan, S. Takeda, O. Cagsal-Getkin, C. M. William, T. L. Spires-Jones, R. Pitstick, G. A. Carlson, A. M. Pooler and B. T. Hyman (2015). "Removing endogenous tau does not prevent tau propagation yet reduces its neurotoxicity." EMBO J.

Westaway, D., S. Genovesi, N. Daude, R. Brown, A. Lau, I. Lee, C. E. Mays, J. Coomaraswamy, B. Canine and R. Pitstick (2011). "Down-regulation of Shadoo in prion infections traces a pre-clinical event inversely related to PrPSc accumulation." PLoS pathogens **7**(11).

Westaway, D., P. A. Goodman, C. A. Mirenda, M. P. McKinley, G. A. Carlson and S. B. Prusiner (1987). "Distinct prion proteins in short and long scrapie incubation period mice." Cell **51**(4): 651-662.

Westermarck, G. T. and P. Westermarck (2010). "Prion-like aggregates: infectious agents in human disease." Trends in molecular medicine **16**(11): 501-507.

Winklhofer, K. F., J. Tatzelt and C. Haass (2008). "The two faces of protein misfolding: gain- and loss-of-function in neurodegenerative diseases." The EMBO journal **27**(2): 336-349.

Woerman, A. L., A. Aoyagi, S. Patel, S. A. Kazmi, I. Lobach, L. T. Grinberg, A. C. McKee, W. W. Seeley, S. H. Olson and S. B. Prusiner (2016). "Tau prions from Alzheimer's disease and chronic traumatic encephalopathy patients propagate in cultured cells." Proceedings of the National Academy of Sciences **113**(50): E8187-E8196.

Wroblewski, H., R. Burlot and K.-E. Johansson (1978). "Solubilization of *Spiroplasma citri* cell membrane proteins with the anionic detergent sodium lauroyl-sarcosinate (Sarkosyl)." Biochimie **60**(4): 389-398.

Wyss-Coray, T. and L. Mucke (2002). "Inflammation in neurodegenerative disease—a double-edged sword." Neuron **35**(3): 419-432.

Xu, C. and D. T. Ng (2015). "Glycosylation-directed quality control of protein folding." Nature reviews Molecular cell biology **16**(12): 742-752.

Yadavalli, R., R. P. Guttman, T. Seward, A. P. Centers, R. A. Williamson and G. C. Telling (2004). "Calpain-dependent endoproteolytic cleavage of PrPSc modulates scrapie prion propagation." Journal of Biological Chemistry **279**(21): 21948-21956.

Yasuda, M., Y. Nakamura, T. Kawamata, H. Kaneyuki, K. Maeda and O. Komure (2005). "Phenotypic heterogeneity within a new family with the MAPT p301s mutation." Ann Neurol **58**(6): 920-928.

Yoshiyama, Y., M. Higuchi, B. Zhang, S. M. Huang, N. Iwata, T. C. Saido, J. Maeda, T. Suhara, J. Q. Trojanowski and V. M. Lee (2007). "Synapse loss and microglial activation precede tangles

in a P301S tauopathy mouse model." *Neuron* **53**(3): 337-351.

Yu, L., Y. Chen and S. A. Tooze (2018). "Autophagy pathway: cellular and molecular mechanisms." *Autophagy* **14**(2): 207-215.

Zhang, Z., M. Song, X. Liu, S. S. Kang, I.-S. Kwon, D. M. Duong, N. T. Seyfried, W. T. Hu, Z. Liu and J.-Z. Wang (2014). "Cleavage of tau by asparagine endopeptidase mediates the neurofibrillary pathology in Alzheimer's disease." *Nature medicine* **20**(11): 1254.

Zhao, H., M. Klingeborn, M. Simonsson and T. Linné (2006). "Proteolytic cleavage and shedding of the bovine prion protein in two cell culture systems." *Virus research* **115**(1): 43-55.

Zhao, X., L. A. Kotilinek, B. Smith, C. Hlynialuk, K. Zahs, M. Ramsden, J. Cleary and K. H. Ashe (2016). "Caspase-2 cleavage of tau reversibly impairs memory." *Nature medicine* **22**(11): 1268.